UNIVERSIDAD COMPLUTENSE DE MADRID

Facultad de Ciencias Físicas
Departamento de Física Teórica II
(Métodos Matemáticos de la Física)

TESIS DOCTORAL

Ruptura de isoespín y restauración de simetría quiral en gases de mesones ligeros

MEMORIA PARA OPTAR AL GRADO DE DOCTOR

PRESENTADA POR

Ricardo Torres Andrés

Director

Ángel Gómez Nicola

Madrid, 2014

Ruptura de isoespín y Restauración de simetría quiral en gases de mesones ligeros

RUPTURA DE ISOESPÍN Y RESTAURACIÓN DE SIMETRÍA QUIRAL EN GASES DE MESONES LIGEROS

MEMORIA DE TESIS DOCTORAL

PRESENTADA POR

RICARDO TORRES ANDRÉS

BAJO LA DIRECCIÓN DE

ÁNGEL GÓMEZ NICOLA

DEPARTAMENTO DE FÍSICA TEÓRICA II

UNIVERSIDAD COMPLUTENSE

MADRID · AÑO MMXIV

Agradecimientos

Es bien conocido dentro del mundo académico que el camino hacia una tesis doctoral tiene su fin en los agradecimientos. Es lo lógico, lo normal, y además también suena razonable. En mi caso, sin embargo, ha sucedido justo al contrario: empiezo por donde habría de concluir y —pese a que al final la inercia me lleva y todo pasa— esta vez no hay línea recta detrás del muro, y la pared de cristal de todos los días ha dejado de existir.

Intentaré, en la medida de lo posible, que mis agradecimientos no sean una larga lista de asuntos pendientes y diálogos herméticos, aunque es muy probable que todo quede en intento.

La primera parada de este tren de agradecimientos y dedicatorias es para mis padres, Ricardo y Soledad. Han hecho falta unos cuantos años para que el *y química* no fuera parte inseparable de la *física*; pero sin vuestro apoyo, y sin vosotros mismos, nada de esto habría sido posible.

A mis abuelos maternos, Buenaventura y Cándida: gracias por todos los veranos de mi mundo y por estar presentes un poco cada día en cada atardecer. También a mis abuelos paternos, Guillermo y Emilia, a los que —debido a la distancia y a algunas otras circunstancias— no he tenido la suerte de tener a mi lado.

Muchas gracias a mi tía Angelines, a mi tío Vicente y a Víctor Alba, por vuestra compañía y por vuestra ayuda en todo cuanto he podido necesitar.

A veces el agradecimiento a los directores de una tesis tiene un cierto aspecto de obligación, una especie de compromiso tácito adquirido. No es éste el caso: gracias, Ángel, por tu paciencia y comprensión; por tu trabajo sincero y por el tiempo que siempre me has encontrado.

Agradezco también a Ramón Fernández-Álvarez Estrada, Felipe Llanes, José R. Peláez —y a todos aquellos miembros del Grupo de Teorías Efectivas de la *Universidad Complutense* que durante estos años han ayudado a elaborar los proyectos de investigación— su esfuerzo y el tiempo invertido para que muchos otros ha-

yamos tenido la oportunidad de viajar y exponer nuestros trabajos en congresos y reuniones por todo el mundo.

En este sentido creo que trabajar de estancia en el extranjero unos meses ha sido de las más valiosas experiencias que he tenido en estos años: *respirar física* en uno de los sitios punteros de investigación del mundo supuso para mí la oportunidad de recobrar el aliento y las ganas por finalizar esta tesis, ardua lucha conmigo mismo ya por aquel entonces.

A nivel personal —más importante si cabe— me aportó la necesidad de buscarme de nuevo desde dentro y la ocasión de encontrar en mi camino a gente verdaderamente formidable. Me gustaría agradecer la atención que todo el Departamento de Física Nuclear del *Brookhaven National Laboratory* —en especial Rob Pisarski y Raju Venugopalan— me brindó durante mi visita, y gracias —por encima de todo— a Dani y a Miguel, vecinos de *efficiency* y compañeros en el laboratorio, por su inestimable compañía y cercanía durante los meses que coincidimos en *Upton*.

Uno de los mayores logros de esta etapa —sin lugar a dudas el mayor con diferencia— ha sido la oportunidad que he tenido de compartir alegrías, cervezas y alguna que otra pena pasajera con mis colegas de fatigas en el doctorado. Gracias a todos mis compañeros de Teórica I y II por aguantar con paciencia mis altibajos.

Me gustaría también ofrecer un imponderable y especial agradecimiento a Gabriel Álvarez Galindo y Ángela Alera por su siempre pronta disposición a echar una mano, así como a David Gómez-Ullate —casi un compañero más— por su confianza cuando tuve la oportunidad de colaborar con él en docencia, y por las charlas amenas que siempre hemos tenido. Se agradece, David, que no hayas usado armas químicas ni bacteriológicas contra Miguel o contra mí —únicas fuerzas vivas del despacho en los últimos tiempos— a pesar de nuestras interpretaciones musicales vespertinas.

A Fede, *Maestro*, gracias por tantos buenos y *cuánticos* ratos, y por la llave de un montón muy grande de momentos de absoluta felicidad leyendo notas. Mi más profunda gratitud por darme las herramientas para entender que el criterio y el camino son el único equipaje que uno necesita en cualquier viaje. Algún día tu *antídoto* será efectivo para mi mal de *milséis*.

Gracias también a todos mis compañeros del *aula de jazz*: Andrés, Caco, Nano, Quique y Sergio. Todo vuestro tiempo, vuestra entrega con la música y los grandes ratos en el *Félix* han sido baluarte fundamental para haber seguido en esta brecha larga y difícil que al fin termina.

Finalmente, me gustaría expresar mi gratitud a todas aquellas personas cuya presencia misma, opinión o apoyo han activado consciente e inconscientemente mi curiosidad e interés por un montón enorme de cosas bonitas a lo largo de estos

años. Entre ellos: mis compañeros de buceo, escapadas y viajes; mis compañeros de fútbol siete, así como toda la magna y egregia plantilla del club más laureado del Paraninfo. No puedo ni debo olvidar la mención especial a Esther y a Markus: gracias por apoyarme cuando lo he necesitado y por compartir vuestro tiempo conmigo haciendo mucho más llevadero este camino.

Gracias a todos.

Entre Montejo de Tiermes y Madrid
agosto de 2013.

Le mieux est l'ennemi du bien.
François-Marie Arouet

Índice general

Nota sobre la terminología

Escribir una memoria de investigación científica en castellano reporta numerosas satisfacciones: por un lado, escribir en la lengua materna de uno mismo es siempre más cómodo y permite más capacidad de flexionar el significado para otorgar a los escrito una variedad de matices que, personalmente, no podría cubrir escribiendo en cualquier otra lengua. Sin embargo, como en todo, esta elección trae asociada consigo ciertas responsabilidades. De entre ellas, creo que la que más me ha preocupado durante la redacción de esta memoria es el problema de la traducción de términos.

Resulta indudable que, hoy por hoy, el inglés es el idioma en el que se transmite el conocimiento científico en todo el mundo, por lo que no es casual que prácticamente todo el léxico técnico pertenezca a esta lengua. La conveniencia de una traducción literal o, por el contrario, la inclusión desmedida de préstamos plantea un *falso dilema* que los representa como mutuamente excluyentes. A pesar de ello, después de probar las dos opciones —y buscando una suerte de punto medio— he creído conveniente mezclar ambas propuestas. El fundamento de esta decisión reside en el intento de buscar, por un lado, la *familiaridad* del lector con los vocablos anglosajones presentes de manera prácticamente ubicua en la literatura; y, por otro, la homogeneidad con respecto a términos de importancia fundamental en las publicaciones que presento, escritas íntegramente en inglés.

De este modo escribiré Cromodinámica Cuántica, Teoría Quiral de Perturbaciones ó Método de la Amplitud Inversa, por ejemplo, como traducciones literales de *Quantum Chromodynamics*, *Chiral Perturbation Theory* e *Inverse Amplitude Method*, respectivamente; pero mantendré la representación anglosajona a la hora de enunciar las siglas por las que se conocen[1], *vid.*: *QCD*, *ChPT* e *IAM*, así como préstamos de uso consuetudinario como *gauge* o *lagrangiano*. Incluso seguiré conservando el término *workshop* en lugar de hablar de *talleres*.

Con este mismo espíritu tomaré a modo de préstamo muchas otras palabras técnicas, como por ejemplo los números cuánticos de sabor asociados a los quarks[2].

[1] Señalando, por supuesto, su carácter de préstamo mediante el uso de tipografía oblicua.
[2] Palabra que, por ubicua y genuina, respetaré hasta el punto de no poner en cursiva.

Escribiré entonces quark *up*, quark *down* y quark *strange*, en lugar de optar por la traducción literal. Este mismo criterio lo aplicaré al nombre de formalismos y expresiones concretas como *staggered* o *model-independent*, que de otro modo podrían dar una idea no demasiado concreta y desenfocada en relación con la literatura especializada. Como toda regla tiene sus excepciones, a lo largo de la memoria el lector podrá comprobar la presencia de las palabras isoespín, pión, o pionio; e incluso expresiones como *a nivel árbol*, traducción completamente literal del *tree level* inglés.

Reconozco que la justificación que puedo ofrecer para estos casos dista de ser completamente racional o sistemática: las escribo de esta manera a causa de la costumbre, o por alguna conveniencia fonética que será, las más de las veces, fuertemente dependiente del observador.

Quizá la expresión más llamativa —por infrecuente en la literatura técnica actual— sea aquélla de *aforar una simetría global*, en alusión al proceso a través del cual la acción de los elementos de un grupo asociado a una simetría global depende ahora de las coordenadas espacio-temporales. La introducción del campo semántico asociado a *gauge* se basa en una traducción libre de la voz alemana *eichinvarianz* al inglés hecha por H. Weyl a principios del siglo pasado al considerar transformaciones de la métrica dependientes del punto. El intento por respetar el concepto original así como de evitar una castellanización forzada me lleva a creer que, de entre todas las opciones traducidas que he tenido la ocasión de consultar, nuestro *aforar*[3] es una buena manera de referirse al significado que encierra la expresión inglesa *to gauge a group*.

Sirva entonces esta nota como descargo y anuncio de un cierto eclecticismo léxico que espero no conlleve más dificultades que las meramente estéticas.

[3] Según RAE: *ajustar las indicaciones de un instrumento de medida con los valores de una magnitud.*

Lista de publicaciones

La actividad investigadora que se recoge en esta memoria de tesis doctoral ha dado lugar a las siguientes publicaciones en revistas arbitradas:

1. *Isospin breaking quark condensates and chiral perturbation theory.*
   A. Gómez Nicola, R. Torres Andrés.
   Publicado en ***J.Phys.G: Nucl.Part.Phys.*** **39, 015004**.

2. *Isospin breaking and chiral symmetry restoration.*
   A. Gómez Nicola, R. Torres Andrés.
   Publicado en ***Phys. Rev.*** **D83, 076005**.

3. *Thermal masses and scalar susceptibilities.*
   A. Gómez Nicola, R. Torres Andrés.
   Publicado en ***Prog.Part.Nucl.Phys.*** **67, 337-342**.

4. *Chiral restoration and scalar-pseudoscalar partners in QCD.*
   A. Gómez Nicola, R. Torres Andrés.
   Publicado en ***Phys. Rev.*** **D88, 076007**.

Todas ellas han sido directa e íntegramente incluidas en su formato original, y estructuradas en los capítulos de resultados que siguen a continuación. Además, la sección 3.1 del capítulo 3 está formada por el *preprint* con la referencia **ARXIV:1404.2746 [hep-ph]**.

Asimismo, esta investigación también ha dado lugar a la presentación de resultados en diversas conferencias y *workshops*, quedando registrados en las siguientes contribuciones a las actas de los congresos que se citan a continuación:

- *Light scalar susceptibilities and isospin breaking.*
  R. Torres Andres, A. Gomez Nicola.
  AIP Conf. Proc. **1322** (2010) 35.
  Chiral symmetry in hadrons and nuclei.
  Proceedings of Chiral10. Valencia, Spain, June 21-24, 2010.

- *Light scalar susceptibilities and the $\pi^0 - \eta$ mixing.*
  R. Torres Andres, A. Gomez Nicola.
  AIP Conf. Proc. **1343** (2011) 453,
  9th Conference on Quark Confinement and the Hadron Spectrum (Confinement IX).
  30 Aug.-3 Sep. 2010. Madrid, España.

- *Pion masses at finite temperature.*
  R. Torres Andres, A. Gomez Nicola.
  Published in PoS ConfinementX (2012) 190.
  Proceedings of 10th Conference on Quark Confinement and the Hadron Spectrum.
  Munich, Germany, October 8-12, 2012.

1

Introducción

El objetivo de este capítulo es el de ofrecer un breve sustento teórico a los contenidos y técnicas más significativas que han sido utilizados en la elaboración de las publicaciones recogidas en los siguientes capítulos.

He agrupado los puntos a tratar en cuatro secciones pertenecientes a un único capítulo titulado *Interacción Fuerte a baja energía y simetría quiral*. En la primera sección expondré las principales características del espectro de hadrones ligeros tal y como se conoce en la actualidad, junto con las herramientas de clasificación y catalogación que son de uso ubicuo en la física de partículas; así como el patrón de ruptura de la simetría quiral en la Cromodinámica Cuántica (QCD).

Posteriormente señalaré los fundamentos teóricos en los que se basa la Teoría Quiral de Perturbaciones ($ChPT$), y después introduciré los temas fundamentales que constituyen el *leitmotiv* de esta memoria, a saber: la implementación de efectos de ruptura de isoespín y la evolución de éstos a temperatura finita.

A lo largo de estos dos epígrafes expondré, también y de modo breve, distintos métodos usados en la investigación que da lugar a esta memoria en relación con la incorporación de física de resonancias, *i.e.* el llamado Método de la Amplitud Inversa (IAM) y el modelo de acoplo de resonancias de espín 1 al *lagrangiano* quiral.

Interacción Fuerte a bajas energías y simetría quiral

1.1.1 *QCD* a bajas energías y simetría quiral

QCD es, hoy por hoy, la teoría comúnmente aceptada y usada para la descripción a través de campos locales del sector de Interacción Fuerte en el Modelo Estándar.

Durante los años cincuenta se reconocía ya una plétora abundante de hadrones que mostraban —gracias a la aparición de factores de forma en procesos como la dispersión elástica e^+e^-— la existencia de una cierta subestructura en ellos. Sin embargo, la constante de acoplo necesaria para explicar estos procesos a través de una descripción en términos de una Teoría Cuántica de Campos era demasiado alta para permitir una expansión en serie perturbativa al uso. Durante los años setenta, la idea de que existían bloques fundamentales —o quarks— a partir de los que estaban formados todos los hadrones comenzó a ganar adeptos, al menos desde un punto de vista formal y con vistas a la catalogación del espectro de partículas conocido [1, 2].

Hoy en día estos bloques constituyentes son interpretados como grados de libertad físicos de una teoría *gauge* no abeliana renormalizable: la Cromodinámica Cuántica. Esta teoría posee ocho bosones *gauge* vectoriales sin masa correspondientes a cada uno de los ocho generadores del grupo gauge $SU(3)$ de color. En ella los quarks son fermiones de espín $1/2$ que se transforman como los multipletes a los que da lugar la representación fundamental de dicho grupo. Existen seis tipos de quarks o sabores diferentes: *up*, *down*, *strange*, *charm*, *beauty* y *top*, que se transforman como tripletes bajo $SU_C(3)$, aunque los últimos tres son considerados pesados y no juegan un papel relevante en el rango de energías que nos ocupará a lo largo de esta memoria puesto que sus efectos pueden ser desacoplados [3] al estudiar el sector mesónico de baja energía.

QCD se encuentra respaldada ampliamente por evidencias experimentales en procesos de colisiones fuertemente inelásticas hadrón-leptón, producción de hadrones en aniquilación e^+e^- y procesos de tipo *Drell-Yan*[1], e implementa dos características fundamentales de la interacción fuerte, a saber: confinamiento y libertad asintótica.

La libertad asintótica aparece en fenómenos de muy alta energía, donde los

[1] Consultar, por ejemplo [4, 5].

quarks interactúan muy débilmente. Fue descubierta en los años setenta por D. Politzer, F. Wilczek y D. Gross [6–8], cuyos trabajos les valieron el premio Nobel de Física en 2004. La interpretación física de este mecanismo puede efectuarse a través del anti-apantallamiento que se produce debido a la auto-interacción de los gluones, opuesta al apantallamiento provocado por los pares $\bar{q}q$ [9]. Es, por tanto, una propiedad inherente al carácter no abeliano de la teoría.

El confinamiento es el responsable de que a bajas energías los quarks se encuentren ligados formando hadrones. Aunque se han propuesto numerosos escenarios teóricos[2]. todavía no ha sido demostrado analíticamente. Su existencia, sin embargo, es ampliamente aceptada debido a dos razones: hasta el momento, no se han encontrado estados de quarks o gluones libres; y parece aparecer de forma natural en modelos basados en simulación en retículos[3].

QCD presenta —como teoría *gauge* renormalizable en cuatro dimensiones con libertad asintótica [12, 13]— una dependencia en la constante de acoplo, g, respecto a la escala de energías o transferencia de momento. El carácter no abeliano de la teoría es precisamente el que hace que la constante de acoplo tienda a cero a altas energías. A un *loop*, la función β en *QCD* toma la forma

$$\beta(\mu) = \mu \frac{dg(\mu)}{d\mu} = -\frac{g^3}{(4\pi)^2}\left(\frac{11}{3}N_C - \frac{2}{3}N_f\right) + O(g^5), \tag{1.1}$$

donde N_C y N_f representan el número de colores y de sabores en la teoría.

Para $N_C = 3$ y $N_f \leq 16$, la solución de esta ecuación hace que la constante de acoplo vaya como la inversa del logaritmo de la escala de energía cuando ésta tiende a infinito, implementando así la libertad asintótica y permitiendo una expansión en serie de potencias respecto a la constante de acoplo $g(\mu^2)$ para fenómenos de alta energía (alta transferencia de momentos: energías típicas superiores a 1 GeV ó, si se quiere ver de otro modo, distancias cortas de aproximadamente $r < 0.1$ fm).

Cuando la escala de energías decrece, la constante de acoplo aumenta impidiendo un tratamiento perturbativo en potencias de $g(\mu^2)$. Los llamados procesos de baja energía (energías menores de 1 GeV, distancias grandes $r > 1$ fm) son fenómenos con baja transferencia de momento, o que involucran propiedades hadrónicas como la masa, la temperatura, anchuras de resonancia, longitudes de dispersión, etc. en el régimen de baja energía. Han de ser estudiados mediante técnicas no perturbativas, principalmente a través de modelos efectivos que incorporan las simetrías relevantes del *lagrangiano* de *QCD*, o mediante simulaciones en el retículo.

[2] Puede acudirse a [10] para saber más a este respecto.
[3] Consultar [11] para una revisión más pormenorizada de esta cuestión.

Sabor	*up*	*down*	*strange*
Masa	$1.8 - 3.0$ MeV	$4.5 - 5.5$ MeV	$90 - 100$ MeV
Carga	$2/3$	$-1/3$	$-1/3$
Hipercarga	$1/2$	$-1/2$	0

Cuadro 1.1: Valores para la masa [14], carga (en unidades de e^2) e hipercarga de los quarks ligeros y del quark *strange*.

Como ya he comentado anteriormente —en lo que a la dinámica de mesones ligeros se refiere—, es posible *ignorar* en un sentido práctico la existencia de los quarks *charm*, *bottom* y *top*. En esta misma línea práctica, el cuadro 1.1 indica que debido al tamaño de las masas de los quarks ligeros e, incluso, del quark *strange* respecto de la escala típica de energía en *QCD* —que podemos situar de modo informal en el valor $\Lambda_{QCD} \sim 217^{+25}_{-23}$ MeV calculado en [15] usando el esquema $\overline{MS}$ y en la escala de la masa del bosón Z— es posible tratar los valores *físicos* de estas masas como perturbaciones al problema de masa quark nula, también llamado *límite quiral*.

La parte fermiónica del *lagrangiano* de *QCD* en este límite es —omitiendo explícitamente subíndices de color—

$$\mathcal{L}_{\text{L.Q.}} = i\bar{q}\not{D}q, \tag{1.2}$$

donde q es un doblete (triplete) de cuadriespinores de Dirac que contiene los sabores asociados a los quarks en la teoría de dos (tres) sabores, y $D_\mu = \partial_\mu - ig\mathcal{A}_\mu$, es la derivada covariante, que actúa en el espacio de sabor como la identidad e incluye la conexión asociada a los campos de gluones $\mathcal{A}_\mu = \sum_a \frac{\lambda_a}{2}\mathcal{A}_{a,\mu}$ a través del acoplo *gauge* dado por g.

Antes de hablar del grupo quiral, es conveniente descomponer los campos espinoriales asociados a los quarks en sus componentes de quiralidad *right* y *left*, a través de los proyectores quirales P_L y P_R,

$$\psi_L := P_L\psi := \frac{1-\gamma_5}{2}\psi, \qquad \psi_R := P_R\psi := \frac{1+\gamma_5}{2}\psi. \tag{1.3}$$

El *lagrangiano* de *QCD* en el límite quiral no mezcla campos de quarks con quiralidad contraria debido a que $\{\gamma_\mu, \gamma_5\} = 0$, por lo que se tiene

$$\mathcal{L}_{\text{L.Q.}} = i\bar{q}_R\not{D}q_R + i\bar{q}_L\not{D}q_L, \tag{1.4}$$

que es invariante bajo las llamadas *transformaciones quirales* pertenecientes al grupo quiral $SU_L(N_f) \times SU_R(N_f)$, y definidas a través de las siguientes asignaciones globales en el espacio de sabor

$$q_L \mapsto \exp\left(-i\sum_a \theta_L^a \Gamma_a\right) q_L, \qquad q_R \mapsto \exp\left(-i\sum_a \theta_R^a \Gamma_a\right) q_R, \tag{1.5}$$

donde $\Gamma_a \in \{\tau_a, \lambda_a\}$, *i.e.* una matriz de Pauli o de Gell-Mann, dependiendo de que $N_f = 2$ ó $N_f = 3$, respectivamente.

La simetría bajo el grupo quiral da lugar, en virtud del Teorema de Noether, a seis (dieciséis) corrientes conservadas clásicamente[4] definidas a través de

$$J_\mu^{a,L} = \bar{q}_L \gamma_\mu \frac{\Gamma^a}{2} q_L, \quad J_\mu^{a,R} = \bar{q}_R \gamma_\mu \frac{\Gamma^a}{2} q_R, \tag{1.6}$$

que son cantidades conservadas en la evolución, *i.e.*

$$\partial^\mu J_\mu^{a,L} = \partial^\mu J_\mu^{a,R} = 0.$$

Cualquier combinación lineal de corrientes conservadas es también una corriente conservada, de modo que las llamadas corrientes *vectorial* y *axial*

$$\begin{aligned} V_\mu^a &= J_\mu^{a,L} + J_\mu^{a,R} = \bar{q}\gamma_\mu \frac{\Gamma^a}{2} q, \\ A_\mu^a &= J_\mu^{a,R} - J_\mu^{a,L} = \bar{q}\gamma_\mu\gamma_5 \frac{\Gamma^a}{2} q, \end{aligned} \tag{1.7}$$

son también conservadas y se transforman bajo paridad como verdaderos objetos vectoriales y axiales, respectivamente, *i.e.*

$$P : V_\mu^a(\vec{x}, t) \mapsto V_\mu^a(-\vec{x}, t), \tag{1.8}$$

$$P : A_\mu^a(\vec{x}, t) \mapsto -A_\mu^a(-\vec{x}, t). \tag{1.9}$$

Además de las corrientes conservadas asociadas a la invariancia global bajo el grupo quiral que se han analizado anteriormente, existen dos corrientes adicionales vinculadas a la simetría bajo los grupos unitarios de fase global $U_V(1)$ y $U_A(1)$. Resulta, de este modo, que el *lagrangiano* de *QCD* posee una invariancia global clásica bajo

$$SU_L(N_f) \times SU_R(N_f) \times U_V(1) \times U_A(1) \sim U_L(N_f) \times U_R(N_f).$$

Las corrientes conservadas correspondientes son los singletes vectorial y axial-vectorial: $V^\mu = \bar{q}\gamma^\mu q$, que permite —a través de la conservación del número bariónico B— catalogar a los hadrones en mesones ($B = 0$) y bariones ($B = 1$); y $A^\mu = \bar{q}\gamma^\mu\gamma_5 q$, cuyo carácter conservado no se preserva en el proceso de cuantización dando lugar a la anomalía axial bajo $U_A(1)$ [16–19].

¿Qué cambia de todo esto cuando perturbamos el *lagrangiano* en el límite quiral añadiendo las masas de los quarks ligeros? Los quarks adquieren masa de modo explícito a través de un término lineal que da lugar a la mezcla de

[4] Tres (ocho) corrientes por cada grupo $SU(N_f)$.

campos con quiralidad contraria; en efecto, utilizando la notación de multipletes espinoriales

$$\mathcal{L}_{\mathrm{M}} = -\bar{q}\mathcal{M}q = -\bar{q}_L\mathcal{M}q_R - \bar{q}_R\mathcal{M}q_L, \tag{1.10}$$

donde $\mathcal{M} = \mathrm{Diag}\,(m_u, m_d)$ ó $\mathcal{M} = \mathrm{Diag}\,(m_u, m_d, m_s)$, es la matriz de masa de los quarks. Si se analizan nuevamente las variaciones del *lagrangiano* $\mathcal{L}_{\mathrm{L.Q.}} + \mathcal{L}_{\mathrm{M}}$ bajo las transformaciones quirales (1.5) resulta que las divergencias de las corrientes son ahora

$$\partial^\mu V_\mu^a = i\bar{q}\left[\mathcal{M}, \frac{\Gamma^a}{2}\right] q, \tag{1.11}$$

$$\partial^\mu A_\mu^a = i\bar{q}\left\{\frac{\Gamma^a}{2}, \mathcal{M}\right\}\gamma_5\, q, \tag{1.12}$$

es decir, ya no son nulas —no son corrientes exactamente conservadas— sino que son lineales en la masa de los quarks.

Para hacer completo el análisis veamos qué sucede con las cantidades conservadas a través de la invariancia bajo las transformaciones globales correspondientes a los grupos unitarios vectorial y axial.

Para ellas —sin considerar los términos que proceden de la anomalía axial— tenemos

$$\partial^\mu V_\mu = 0, \tag{1.13}$$

$$\partial^\mu A_\mu = 2i\,\bar{q}\,\mathcal{M}\gamma_5\, q. \tag{1.14}$$

A la luz de estos resultados se concluye que la invariancia bajo el grupo quiral sólo es exacta en el límite quiral. Sin embargo, si la matriz de masa es proporcional a la identidad en el espacio de sabor, se tiene $[\Gamma^a, \mathrm{Id}_{\mathrm{N_f}}] = 0$, por lo que la corriente asociada a la simetría bajo el grupo vectorial tiene divergencia nula y es conservada. No sucede lo mismo con la parte asociada a las transformaciones axiales, por lo que resulta que las tres (ocho) corrientes A_μ^a ya no son conservadas y la simetría correspondiente queda rota explícitamente por la masa.

Es evidente que una asunción general de la simetría bajo el grupo vectorial no es demasiado práctica debido a que en el mundo real $m_s >> m_u, m_d$. Sin embargo, considerar que $m_u \approx m_d$ parece ser una buena estrategia de cara a afrontar un análisis fenomenológico general, y no es casual que la mayor parte de los trabajos acerca de propiedades asociadas a mesones ligeros se hagan en este escenario simétrico bajo el grupo vectorial.

La correspondencia con el concepto de espín isotópico en la física nuclear hace que se denomine simetría de isoespín a la invariancia aproximada bajo el grupo vectorial $SU_V(2)$, que resulta ser un subgrupo del grupo quiral completo

en la teoría de tres sabores. Las desviaciones respecto a este escenario deben evaluarse a través de la dinámica de la teoría, pero —debido a que el subgrupo vectorial no puede romperse espontáneamente [20]— deben ser proporcionales al parámetro de ruptura $m_d - m_u$. El análisis de las correcciones a este límite de isoespín en lo tocante al cálculo de condensados de quarks y susceptibilidades quirales escalares será el tema central del capítulo 2.

Hasta ahora hemos incluido sólo la ruptura intrínseca —debida a la diferencia entre las masas de los quarks ligeros— como fuente de ruptura explícita en *QCD*. Sin embargo también la ruptura electromagnética induce una ruptura explícita de la simetría de isoespín, aunque es de naturaleza completamente distinta debido al carácter vectorial de la corriente electromagnética que se acopla a los quarks.

En efecto, la interacción electromagnética se acopla al *lagrangiano* a través de la inclusión del fotón como un campo *gauge* externo[5] en la forma

$$\mathcal{L}_{\mathrm{EM}} = -\bar{q}\,\gamma^{\mu} A_{\mu} Q\, q,$$

donde A_μ es el campo externo del fotón[6]; y $Q = \mathrm{Diag}\,(q_u, q_d)$ para $N_f = 2$, ó $Q = \mathrm{Diag}\,(q_u, q_d, q_s)$ para $N_f = 3$, es la matriz de carga.

El carácter vectorial del acoplo de la interacción electromagnética le hace conectar campos de quarks con la misma quiralidad. La divergencia de las corrientes asociadas a las transformaciones de esta parte del *lagrangiano* bajo el grupo quiral son

$$\partial^{\mu} V_{\mu}^{a} = \bar{q}\left[\frac{\Gamma^a}{2}, Q\right]\gamma^{\mu} A_{\mu}\, q, \tag{1.15}$$

$$\partial^{\mu} A_{\mu}^{a} = \bar{q}\left[\frac{\Gamma^a}{2}, Q\right]\gamma^{\mu} A_{\mu}\gamma_5\, q, \tag{1.16}$$

lo que muestra que si las cargas de los quarks son iguales, *i.e.* $Q \propto \mathrm{Id}_{\mathrm{N_f}}$, entonces la simetría de $\mathcal{L}_{\mathrm{EM}}$ bajo el grupo quiral completo permanece inalterada.

En cualquier otro caso —incluyendo, por supuesto, el caso físico— tanto el subgrupo vectorial como el conjunto de transformaciones axiales quedan rotos explícitamente, haciéndose imposible un análisis estimativo a partir de considerar una simetría aproximada puesto que las diferencias relativas de las cargas de los quarks *up* y *down* son muy diferentes entre sí (ver cuadro 1.1).

Para resumir estos resultados y dar una idea global del estado de la cuestión, analicemos en conjunto el comportamiento de la simetría quiral del *lagrangiano* de *QCD* bajo la inclusión de efectos de ruptura intrínseca y electromagnética.

[5] No trataremos esta cuestión en detalle ahora puesto que se verá con más profusión en el apartado dedicado a la inclusión de fuentes externas en *ChPT*.

[6] A diferenciar del campo *gauge* de los gluones, denotados como $\mathcal{A}_\mu$.

El caso más claro es aquél en el que tanto las masas de los quarks como sus cargas son cero. En este escenario la simetría quiral $SU_V(N_f) \times SU_A(N_f)$ es una simetría exacta del *lagrangiano*. Para el escenario con dos sabores, la inclusión de masas distintas para los quarks ligeros hace que esta simetría se rompa explícitamente. No obstante —debido a la similitud numérica de ambas masas— puede considerarse que la simetría bajo el subgrupo de isoespín se conserva aproximadamente y asumir que las correcciones serán proporcionales a la diferencia $m_d - m_u$, esperando que éstas resulten perturbativamente controlables. Debido a que $m_s \gg m_u, m_d$, la incorporación del sector de extrañeza no nula no permite de modo inmediato considerar una simetría aproximada bajo el subgrupo vectorial $SU_V(3)$, por lo que ha de considerarse este escenario como uno con dos sabores ligeros idénticos y un sabor pesado, $N_f = 2+1$.

Si bien es cierto que hemos dicho que los efectos de carga no rompen la simetría de isoespín siempre que $q_u = q_d$, es evidente que el sistema completo, $\mathcal{L}_{\text{L.Q.}} + \mathcal{L}_{\text{M}} + \mathcal{L}_{\text{EM}}$, pierde esta invariancia siempre que las masas sean diferentes y distintas de cero, por lo que en el caso físico —hacia el que siempre ha de tender todo supuesto teórico— sólo deja margen para considerar que la simetría de isoespín es una buena simetría de la Interacción Fuerte, y a evaluar las correcciones que se derivan del carácter aproximado de esta asunción. Naturalmente, esta hipótesis es mucho más razonable en el caso de dos sabores que en el de tres debido a que la masa del quark *strange* es significativamente mayor que la de cualquiera de los quarks ligeros, induciendo, por ende, correcciones mucho más grandes.

El espectro de hadrones ligeros

Hagamos ahora un pequeño paréntesis para comentar —de forma breve— las propiedades espectroscópicas de los mesones ligeros y aprovechar para catalogarlos haciendo uso de la simetría aproximada $SU_V(3)$ del *lagrangiano* de *QCD*.

Según el modelo quark [1, 2], los mesones son estados ligados formados por un quark y un anti-quark, no necesariamente del mismo sabor. Una clasificación posible se hace atendiendo a su comportamiento bajo paridad (P) y bajo conjugación de carga (C), además de por su momento angular total (J).

Estas cantidades pueden relacionarse con el momento angular orbital (l) y con el espín (s) del par $\bar{q}q'$ a través de

$$\begin{aligned} P &= (-1)^{l+1}, \\ C &= (-1)^{l+s}, \\ |l-s| &\leq J \leq |l+s|, \end{aligned}$$

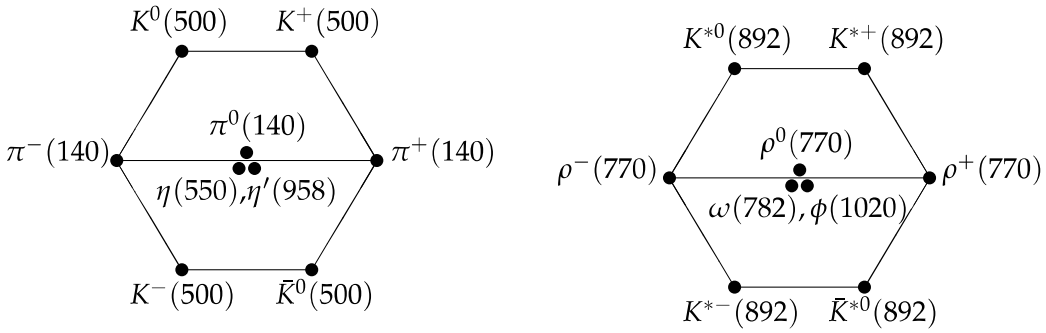

(a) (b)

Figura 1.1: Nonete de mesones pseudoescalares 0^{-+} (a) y vectoriales 1^{--} (b).

donde ha de tenerse en cuenta que s sólo puede valer 1 (espines paralelos) ó 0 (espines anti-paralelos).

Siguiendo este procedimiento, los mesones pueden clasificarse mediante la notación espectroscópica J^{PC}. De este modo se distinguen, por ejemplo, mesones *pseudoescalares* 0^{-+} y *vectoriales* 1^{--} como estados con momento angular orbital $l = 0$; o las excitaciones orbitales $l = 1$: mesones *escalares* 0^{++}, *axiales-vectoriales* 1^{++} y 1^{+-}, y tensoriales 2^{++}.

Como ya hemos dicho, el modelo quark explota la simetría aproximada de *QCD* bajo el grupo vectorial —sólo rota significativamente por la masa del quark *strange*— y registra el espectro de mesones en forma de multipletes de $SU_V(3)$ degenerados en masa. Es claro que la diferencia de masa entre aquellos estados en los que haya extrañeza no nula respecto de otros en los que no esté presente el quark *strange* será grande[7].

Este estructuración en multipletes se cumple razonablemente bien para el caso de los multipletes $8 \oplus 1$ pseudoescalares (0^{-+}) y vectoriales (1^{--}), representados respectivamente la figura 1.1, y cuyas propiedades se detallan en el cuadro 1.2; pero no es tan útil en el caso de las primeras resonancias ligeras escalares 0^{++} (ver cuadro 1.3), donde la naturaleza $\bar{q}q'$ no es tan clara y sigue siendo objeto de intenso debate en la comunidad científica[8].

En la sección 2.3 de esta memoria tendremos ocasión de ver que la generación dinámica de la $f_0(500)$ a través de la Teoría Quiral Unitarizada juega un papel decisivo en la descripción del escenario de restauración de la simetría

[7] Existe una diferencia de entre 150-300 MeV por cada quark o anti-quark *strange* de valencia presente en la composición del mesón.

[8] Para una revisión de este tema ver la *Note on Scalar Mesons* en [14].

J^{PC}	$n^{2s+1}l_J$	$I=1$	$I=1/2$	$I=0$	$I=0$
		$\bar{u}d, u\bar{d}, \frac{1}{\sqrt{2}}(d\bar{d}-u\bar{u})$	$u\bar{s}, d\bar{s}, \bar{d}s, -\bar{u}s$	f	f'
0^{-+}	1^1S_0	$\pi(140)$	$K(496)$	$\eta(548)$	$\eta'(958)$
1^{--}	1^3S_1	$\rho(770)$	$K^*(892)$	$\phi(1020)$	$\omega(782)$
1^{+-}	1^1P_1	$b_1(1235)$	$K_{1B}^{\dagger}$	$h_1(1380)$	$h_1(1170)$
0^{++}	1^3P_0	$a_0(1450)$	$K_0^*(1430)$	$f_0(1710)$	$f_0(1370)$
1^{++}	1^3P_1	$a_1(1260)$	$K_{1A}^{\dagger}$	$f_1(1420)$	$f_1(1285)$
2^{++}	1^3P_2	$a_2(1320)$	$K_2^*(1430)$	$f_2'(1525)$	$f_2(1270)$

Cuadro 1.2: Asignaciones sugeridas en [14] para la clasificación de las primeras resonancias $l=0$ y $l=1$. El número n hace referencia al número cuántico radial, los valores entre paréntesis representan la masa en MeV, y la segunda fila indica la composición de las funciones de onda (*Ibíd.* para ver la definición de f y f'.). Nótese que no se incluyen los mesones $a_0(980)$, $f_0(980)$ y $f_0(500)$ por ser considerados resonacias mesón-mesón o estados tetraquark.

J^{PC}	$I=1$	$I=1/2$	$I=0$
0^{++}	$a_0(980)$	$K_0^*(800)$	$f_0(980), f_0(500)$

Cuadro 1.3: Resonancias 0^{++} por debajo de 1 GeV, no incluidas en la tabla 1.2. La jerarquía de masas en este caso puede explicarse asumiendo una naturaleza de *tetraquark*, aunque lo más probable es que resulten una mezcla de todos estos estados [21–23].

quiral propuesto a través de la degeneración de las susceptibilidades escalar y pseudoescalar.

La ruptura espontánea de la simetría quiral

Si la simetría bajo el grupo quiral se implementara bajo el modo de Weyl-Wigner —y no tuviéramos en cuenta el hecho de que la simetría bajo el grupo unitario axial es anómala— entonces el espectro hadrónico consistiría en multipletes de isoespín degenerados en masa con sus compañeros quirales, es decir, existirían —dejando a un lado los efectos procedentes de la anomalía axial— grupos de partículas degenerados en masa con los mismos números cuánticos que diferirían sólo en el comportamiento bajo paridad.

En el peor de los casos posibles uno esperaría encontrar al menos una simetría de isoespín aproximada, rota tanto más cuanto mayor sea la diferencia en masa de los quarks considerados en la composición de los hadrones.

Sin embargo, lejos de evidenciar esta naturaleza, la diferencia de masas de los multipletes 1^{--} y 1^{++} no puede explicarse a través de una ruptura explícita de la simetría quiral debida al carácter finito de las masas. En efecto, la resonancia $\rho(770)$ es alrededor de 490 MeV más pesada que su hipotético compañero quiral, la $a_1(1260)$; diferencia que es considerablemente mayor para el caso del pión $\pi(140)$ y la $a_0(1450)$ debido a la anomalía de la simetría $U_A(1)$, o para las componentes del campo $(\sigma, vec\pi)$ en modelos de tipo $O(4)$.

Una posible explicación teórica de este comportamiento es que —pese a la existencia de una simetría a nivel *lagrangiano* en el límite quiral— el vacío no es invariante bajo la parte axial del grupo quiral. En efecto, actualmente se asume que la simetría quiral se implementa en *QCD* mediante el llamado modo de Nambu-Goldstone [24–28], dando lugar a un patrón de ruptura espontánea en la forma

$$SU_R(N_f) \times SU_L(N_f) \to SU_V(N_f), \qquad N_f = 2, 3. \tag{1.17}$$

El triplete (octete) de mesones pseudoescalares 0^{-+} ha de ser identificado, entonces, con los bosones de Goldstone resultantes de la ruptura espontánea de la parte axial en la teoría de dos (tres) sabores, a razón de uno por cada generador de la simetría espontáneamente roto por el vacío, y con sus mismos números cuánticos. Por razones que ya he tratado anteriormente, estas aseveraciones son tanto más puras cuando más nos acercamos al supuesto de una simetría exacta, es decir, será una hipótesis más acertada respecto a la observación el considerar a los piones como bosones de Goldstone que hacer lo propio con las partículas presentes en el esquema de tres sabores, donde —una vez más— la gran masa del quark *strange* distorsiona el planteamiento teórico.

Sin embargo, incluso en el caso más favorable desde este punto de vista, los piones presentan una masa de aproximadamente 140 MeV que, si bien es considerablemente menor que la masa de las restantes partículas del espectro hadrónico, no puede considerarse nula. ¿Qué sucede? La respuesta es sencilla si se advierte que la hipótesis de partida, es decir, que los piones son bosones de Goldstone, presupone la existencia de una simetría exacta en la que los quarks ligeros tienen masa nula.

En una situación real —como ya he indicado anteriormente— esto no es cierto debido a que los quarks ligeros tienen masa, así que la simetría quiral es sólo aproximada: se encuentra rota explícitamente por el término de masas y las corrientes asociadas a la invariancia quiral ya no se conservan. El hecho de que los bosones de Goldstone de la teoría tengan masa (constituyendo en sentido estricto pseudobosones de Goldstone) se debe a la ruptura explícita inducida por las masas de los quarks ligeros *up* y *down*[9].

A pesar de ello, la masa de estos quarks es pequeña comparada con la escala Λ_χ —por debajo de la cual tiene sentido tomar un límite de baja energía en *QCD* y cuyo valor puede fijarse aproximadamente en 1 GeV—, por lo que puede considerarse nula en primera instancia (límite quiral), suponiendo exacta la simetría de isoespín así como la ruptura espontánea de la parte axial del grupo quiral. Este será el punto de partida que tomaremos para la construcción del *lagrangiano* efectivo.

El Teorema de Goldstone también permite ver que la ruptura espontánea de la simetría quiral implica que las cargas Noether axiales no aniquilan el vacío. A consecuencia de esto el elemento de matriz que conecta los estados de bosones de Goldstone con el vacío[10] tiene la forma

$$\left\langle 0|A^c_\mu(x)|\phi^d(p)\right\rangle = ip_\mu \delta^{cd} e^{-ip\cdot x} F_B, \tag{1.18}$$

donde F_B es la constante de desintegración de cada uno de los bosones de Goldstone procedentes de la ruptura espontánea, asociado a la combinación de isoespín dada por lo índices c, d. Para $N_f = 3$ y a muy baja energía se cumple $F_B = F(1 + \mathcal{O}(m)) \simeq 93$ MeV, siendo $\mathcal{O}(m)$ términos que van con la masa de los quarks, es decir, la constante de desintegración de todos y cada uno de los bosones es, al orden más bajo, igual a la constante de desintegración del pión en el límite quiral, F.

Tomando la divergencia de la ecuación (1.18) obtenemos

$$\left\langle 0|\partial^\mu A^c_\mu(x)|\phi^d(p)\right\rangle = \delta^{cd} e^{-ip\cdot x} M_B^2 F_B, \tag{1.19}$$

considerando que el mesón está en la capa de masas, *i.e.* $p^2 = M_B^2$, con M_B la masa del bosón.

[9] Y del quark *strange* en el caso de la teoría de tres sabores.

[10] Este elemento controla, por ejemplo, la desintegración debida a Interacción Débil del pión.

A pesar de que el elemento de matriz (1.18) es distinto de cero en el límite quiral, la ecuación (1.19) indica que la violación de la corriente asociada a la invariancia bajo el conjunto axial de transformaciones es tanto menor cuanto menor sea la masa asociaciada a los bosones de Goldstone generados durante la ruptura espontánea. Por esta razón se la conoce como *Conservación Parcial de la Corriente Axial (PCAC)*. Nuevamente, el escenario más favorable para este supuesto es aquél en el que la ruptura debida a masas de quarks sea mínima, es decir, en el caso de dos sabores.

La ruptura espontánea $SU_V(N_f) \times SU_A(N_f) \to SU_V(N_f)$ puede ser caracterizada por un parámetro de orden asociado a valores esperados en el vacío para operadores invariantes bajo el grupo $SU_V(N_f)$ pero que se transforman de forma no trivial bajo el grupo quiral completo. Si este valor esperado es no nulo, el vacío no puede ser invariante bajo el grupo quiral y se obtiene de esta manera un objeto que da cuenta de la ruptura de simetría, tanto explícita como espontánea.

El operador $\bar{q}q$ es invariante bajo las transformaciones de fase global $q \mapsto e^{-i\sum_a \theta_V^a \Gamma_a} q$, asociadas al grupo de isoespín $SU_V(N_f)$; pero no lo es bajo las correspondientes a la parte axial $q \mapsto e^{-i\sum_a \theta_A^a \Gamma_a \gamma_5} q$, por lo que es sensible a rotaciones quirales. En efecto, bajo $SU_V(N_f) \times SU_A(N_f) \to SU_V(N_f)$ se tiene, infinitesimalmente,

$$\bar{q}q \mapsto \bar{q}q - 2i \sum_a \Gamma_a \delta\theta_V^a \, \bar{q}\gamma_5 q. \tag{1.20}$$

El valor esperado en el vacío de este operador es el llamado condensado escalar de quarks, y su cálculo con ruptura de isoespín —así como de sus derivadas respecto de la masa quark (susceptibilidades quirales escalares)— en el escenario efectivo proporcionado por la Teoría Quiral de Perturbaciones tanto a temperatura cero como en un baño térmico— ha sido uno de los objetivos fundamentales de esta investigación.

La $\eta'(960)$ y la anomalia axial

Como ya se ha dicho anteriormente, el modelo quark acomoda los estados 0^{-+} de acuerdo a la suma directa $8 \oplus 1$ en que se descompone el producto de representaciones $3 \otimes 3$ en la teoría de tres sabores. Mediante la ruptura espontánea de simetría es posible explicar la diferencia en las naturalezas del (triplete) octete de mesones pseudoescalares y el resto de mesones ligeros.

No obstante, ¿qué tiene que decir la simetría acerca del estado singlete restante cuando se consideran tres sabores? Echando un vistazo al espectro hadrónico conocido, la partícula más ligera con los números cuánticos apropiados es la llamada $\eta'(960)$, demasiado masiva incluso habida cuenta de los efectos asociados a la extrañeza.

Sin entrar en demasiados detalles debido a que no es parte fundamental en el desarrollo teórico que debe acompañar a los resultados, la gran masa de esta partícula es debida a la presencia de la llamada *anomalía axial* [16–19]: la corriente (1.14) asociada a la invariancia global bajo el grupo $U_A(1)$, clásicamente conservada, deja de serlo durante el proceso de cuantización.

Si esta anomalía no estuviera presente, el patrón de ruptura del grupo sería similar al de la parte axial de la simetría quiral y daría lugar a una novena pseudopartícula de Goldstone[11], que habría de ser identificada[12] con la η'.

1.1.2 Teoría Quiral de Perturbaciones

La Teoría Quiral de Perturbaciones (*ChPT*) es la teoría efectiva más general compatible con las simetrías del *lagrangiano* de *QCD* a bajas energías [29–31]. En ella —a diferencia de lo que sucede en la Cromodinámica Cuántica— los grados de libertad son bosones de Goldstone, y permite un método sistemático para describir las consecuencias de las simetrías globales de sabor de *QCD* a bajas energías.

Su carácter perturbativo se sustenta en una doble expansión en momentos externos de los bosones y en masas de los quarks, respecto a una escala típica de energías $\Lambda_\chi \sim 4\pi F_\pi \sim 1$ GeV, que —como ya hemos visto— distingue de forma aproximada el régimen de baja energía. Se espera, entonces, que a baja energía sólo unos pocos términos de la serie sean relevantes.

Debido a que basa su efectividad en la reproducción de las propiedades de simetría del *lagrangiano* de *QCD* —más, por supuesto, la invariancia bajo simetrías C, P, T y Lorentz— funciona mejor en el caso en que se considere la teoría de dos sabores frente a la de tres debido, nuevamente, a que la introducción de la masa del quark *strange* empeora la convergencia.

De cualquier forma, esta expansión falla al llegar a momentos o energías del orden de la masa de las primeras resonancias ligeras (alrededor de $M_\rho = 770$ MeV), cuyos efectos en este régimen de energía aparecen en la teoría a través de las constantes de acoplo de los diferentes términos del *lagrangiano* (llamadas constantes de baja energía: en adelante *LECs*). Para poder hacer predicciones con la teoría efectiva estas constantes deben determinarse a partir de datos experimentales u otros argumentos teóricos como la saturación por resonancias (ver subsección 1.1.3 en este mismo capítulo), cálculos en el límite de gran N_C o resultados en el retículo, por poner algunos ejemplos.

[11] Recuérdese que la masa finita de los quarks también rompe explícitamente la simetría bajo $U_A(1)$.

[12] En rigor la ausencia de la anomalía introduciría una nueva partícula conocida como η_0, que vendría a mezclarse con la η_8 del octete dando lugar a la mezcla $\eta - \eta'$.

Es fácil darse cuenta de que las únicas posibles contribuciones al *lagrangiano* efectivo sin campos externos tienen un número par de derivadas de campos de bosones de Goldstone, de modo que el *lagrangiano* quiral efectivo más general adopta la forma

$$\mathcal{L}_{\text{eff}} = \sum_{n=1}^{\infty} \mathcal{L}_{(2n)} = \mathcal{L}_{(2)} + \mathcal{L}_{(4)} + \dots \tag{1.21}$$

donde el subíndice entre paréntesis hace referencia al número de derivadas o potencias de masa en cada término.

El *lagrangiano* contiene, entonces, infinitos términos que dan lugar a infinitos vértices de interacción entre los bosones de Goldstone. Sin embargo el punto fundamental en el que reside la utilidad práctica de *ChPT* es que se trata de una expansión en momentos y masas, es decir, esencialmente se trata de una serie perturbativa en escalas de energía. A consecuencia de esto no todos los diagramas contribuyen al mismo orden para un cierto proceso, por lo que en el contexto de una teoría efectiva de baja energía bastará — como ya se ha dicho— con considerar sólo los términos con un número reducido de derivadas.

El efecto de un vértice correspondiente a un término de n derivadas para un cierto diagrama es de orden p^n/Λ_χ^{n-4}, por lo que términos con un número mayor de derivadas tendrán un efecto muy pequeño sobre los cálculos a baja energía. Llamaremos en adelante contribuciones $\mathcal{O}(p^n)$ a aquellos términos que involucren n derivadas o potencias de la masa[13]. Las correcciones más importantes a estos serán de orden $\mathcal{O}(p^{n+2})$.

En órdenes superiores el *lagrangiano* incorpora muchas más constantes de acoplamiento para cada término compatible con las simetrías, por lo que la capacidad predictiva útil de la teoría queda restringida a órdenes bajos de la expansión.

Teoría Quiral de Perturbaciones a *leading order*

Comenzaremos por exponer el *lagrangiano* quiral efectivo a *leading order* en el límite quiral, es decir, sin incluir por el momento los términos de masa y electromagnético que implementan la ruptura explícita de la simetría quiral. Éstos se incluirán mediante el llamado Método de las Fuentes Externas, planteado de forma sistemática por Gasser y Leutwyler en [31] y para el caso electromagnético en [32] .

Al orden más bajo el *lagrangiano* efectivo en el límite quiral consiste sólo en el término cinético

$$\mathcal{L}_{\text{L.O.}} = \frac{F^2}{4} \left\langle \partial_\mu U \, \partial^\mu U^\dagger \right\rangle, \tag{1.22}$$

[13] Ha de considerarse siempre, pese a la notación usada, que la expansión se realiza en momentos o energías respecto a la escala típica de perturbaciones quirales Λ_χ.

donde F es una constante con dimensiones de energía que se identificará, como veremos, con la constante de desintegración del pión en el límite quiral, <> representa la traza en el espacio de sabor; y $U(x)$ es la matriz de campos en la llamada parametrización exponencial, definida por

$$U(x) = \exp\left(i\frac{\mathbf{\Phi}}{F}\right) \in SU(N_f), \tag{1.23}$$

donde $\mathbf{\Phi}$ es la matriz que reune los campos locales de bosones de Goldstone. En $SU(2)$, y en la base de carga, toma la forma

$$\mathbf{\Phi} = \begin{pmatrix} \pi^0 & \sqrt{2}\pi^+ \\ \sqrt{2}\pi^- & -\pi^0 \end{pmatrix}, \tag{1.24}$$

mientras que en $SU(3)$

$$\mathbf{\Phi} = \begin{pmatrix} \pi^0 + \frac{1}{\sqrt{3}}\eta & \sqrt{2}\pi^+ & \sqrt{2}K^+ \\ \sqrt{2}\pi^- & -\pi^0 + \frac{1}{\sqrt{3}}\eta & \sqrt{2}K^0 \\ \sqrt{2}K^- & \sqrt{2}\bar{K}^0 & -\frac{2}{\sqrt{3}}\eta \end{pmatrix}. \tag{1.25}$$

El prefactor del término cinético ha sido elegido convenientemente de tal modo que —al expandir la matriz de campos— se obtenga el término cinético habitual para un bosón.

La invariancia de este *lagrangiano* frente a las rotaciones quirales (1.5) determina las propiedades de transformación de la matriz de campos. En efecto, la matriz de campos $U(x)$ ha de transformarse bajo el grupo quiral como

$$U(x) \mapsto L U(x) R^\dagger, \tag{1.26}$$

donde $L, R \in SU_{L,R}(N_f)$. Nótese que esta transformación lineal en $U(x)$ induce un cambio no lineal en los campos de bosones de Goldstone $\mathbf{\Phi} \sim \sum_a \phi_b \Gamma^b$.

En este nuevo lenguaje las corrientes conservadas asociadas a la invariancia bajo el grupo quiral completo del *lagrangiano* (1.22) se escriben como

$$\begin{aligned} V_a^\mu &= -i\frac{F^2}{2}\left\langle \Gamma_a [U, \partial^\mu U^\dagger] \right\rangle, \\ A_a^\mu &= -i\frac{F^2}{2}\left\langle \Gamma_a \left\{U, \partial^\mu U^\dagger\right\} \right\rangle, \end{aligned} \tag{1.27}$$

y permiten calcular el elemento de matriz de la corriente axial entre un estado de un bosón de Goldstone y el vacío mediante la expansión de la matriz U en términos de los campos en $\mathbf{\Phi}$. Con todo, resulta

$$\left\langle 0 | A_a^\mu | \phi_b \right\rangle = i p^\mu F \delta_{ab}, \tag{1.28}$$

que es la traducción al lenguaje de la teoría efectiva de la relación de *PCAC* que ya escribimos en (1.18). Aquí —nuevamente— a, b son índices de isoespín y ϕ_b hace referencia a cada uno de los bosones de Goldstone $\sum_b \phi_b \Gamma^b \sim \mathbf{\Phi}$. Particularizando la ecuación (1.28) en el caso de dos sabores se entiende el porqué de la identificación de la constante F del *lagrangiano* (1.22) con la constante de desintegración del pión al orden más bajo.

El Método de las Fuentes Externas

El objetivo fundamental del Método de las Fuentes Externas es el de encontrar un método funcional sistemático para el cálculo de funciones de Green. La idea fundamental sobre la que se basa fue enunciada por Leutwyler en [33]: si la teoría está libre de anomalías, la construcción de un *lagrangiano* con acoplo a corrientes externas consistente con la invariancia bajo el grupo quiral es equivalente a exigir la invariancia de la acción asociada cuando se consideran rotaciones quirales locales, es decir, cuando se *afora* el grupo quiral haciéndolo depender del punto.

Las posibles corrientes a las que puede acoplarse el *lagrangiano* fermiónico original de *QCD*, $\mathcal{L}^0_{QCD}$, —que tomamos como punto de partida— son las cuatro (nueve) fuentes vectoriales: tres (ocho) corrientes externas vectoriales denotadas por $v^\mu(x)$, y una asociada al singlete, $v_s^\mu(x)$; tres (ocho) fuentes axiales-vectoriales, $a^\mu(x)$; y las fuentes escalares, $s(x)$; y pseudoescalares, $p(x)$.

Consideremos el *lagrangiano*

$$\begin{aligned}\mathcal{L}_{QCD}\,[\bar{q}, q, v, v_s, a, s, p] &= \mathcal{L}^0_{QCD} \; + \bar{q}\gamma^\mu(v_\mu + \frac{1}{3}v_{s,\mu} + \gamma_5 a_\mu)q - \bar{q}(s - i\gamma_5 p)q \\ &= \mathcal{L}^0_{QCD} \; + \bar{q}_L\gamma^\mu l_\mu q_L + \bar{q}_R\gamma^\mu r_\mu q_R + \frac{1}{3}\left(\bar{q}_L\gamma^\mu v_{s,\mu} q_L + \bar{q}_R\gamma^\mu v_{s,\mu} q_R\right) \\ &\qquad - \bar{q}_R(s + ip)q_L - \bar{q}_L(s - ip)q_R, \quad (1.29)\end{aligned}$$

donde

$$r_\mu = v_\mu + a_\mu, \qquad l_\mu = v_\mu - a_\mu,$$

son combinaciones lineales de las fuentes externas. De la misma manera en que surgían a la hora de calcular las corrientes conservadas asociadas a la invariancia bajo el grupo quiral, estas fuentes son matrices hermíticas de dimensión $N_f \times N_f$ en el espacio de sabor[14].

[14] Por supuesto han de ser también singletes de color. Por poner un ejemplo, en el caso de tres sabores las fuentes externas se escriben como

$$v^\mu = \sum_{a=1}^{8} \frac{\lambda^a}{2} v_a^\mu, \qquad a^\mu = \sum_{a=1}^{8} \frac{\lambda^a}{2} a_a^\mu, \quad s = \sum_{a=0}^{8} \lambda^a s_a, \qquad p = \sum_{a=0}^{8} \lambda^a p_a, \tag{1.30}$$

Para que el *lagrangiano* (1.29) sea invariante bajo rotaciones quirales locales se han de cumplir dos premisas. La primera es que a la par que se efectúan los cambios en los dobletes (tripletes) de sabor de quiralidad definida definidos por las asignaciones

$$\begin{aligned} q_L &\mapsto \exp\left(-i\frac{\Theta(x)}{3}\right)L(x)\,q_L, \\ q_R &\mapsto \exp\left(-i\frac{\Theta(x)}{3}\right)R(x)\,q_R, \end{aligned} \tag{1.31}$$

se cumplan las siguientes leyes de transformación para los campos externos

$$\begin{aligned} l_\mu &\mapsto L(x)\,l_\mu\,L^\dagger(x) + i\Big(\partial_\mu L(x)\Big)L^\dagger(x), \\ r_\mu &\mapsto R(x)\,r_\mu\,R^\dagger(x) + i\Big(\partial_\mu R(x)\Big)R^\dagger(x), \\ v_{s,\mu} &\mapsto v_{s,\mu} - \partial_\mu\Theta(x), \\ (s-ip) &\mapsto L(x)\,(s-ip)\,R^\dagger(x), \end{aligned} \tag{1.32}$$

donde

$$\{L(x) = e^{-i\theta_L^a(x)\Gamma_a},\, R(x) = e^{-i\theta_R^a(x)\Gamma_a}\} \in SU_L(N_f)\times SU_R(N_f),$$

son elementos del grupo quiral aforado.

La segunda es que las derivadas que aparecen actuando sobre los espinores sean derivadas covariantes que incorporen la conexión definida a través de

$$D_\mu q = \partial_\mu - i r_\mu\, q + i q\, l_\mu\ , \tag{1.33}$$

que se transforma de la misma manera que el campo bajo rotaciones quirales locales.

La similitud con la construcción de una teoría *gauge* es ahora claramente perceptible. Los acoplos de las fuentes externas vía la derivada covariante son el análogo a la introducción de los campos *gauge*, mientras que los términos con derivadas en las transformaciones (1.32) constituyen —tomando a la mano el ejemplo de *QED*— el equivalente al término de compensación que se introduce en la ley de transformación del campo del fotón al asumir la invariancia de los espinores bajo cambios de fase local. Esta analogía se ofrece fundamental a la hora de implementar los efectos de la ruptura electromagnética puesto que permite de manera natural el acoplo de campos *gauge* externos a la teoría efectiva.

---

donde $\{\lambda_a\}_{a=0}^8$ es el conjunto de matrices 3×3 de Gell-Mann.

Nótese que no se incluye aquí el singlete axial debido a que en *QCD* esta simetría es anómala, siendo la ausencia de éstas requisito fundamental para la aplicación del Método de las Fuentes Externas. Además, ha de tenerse en cuenta que el singlete vectorial entra en el acoplo de forma proporcional a $\lambda_0 = \sqrt{2/3}\mathrm{Id}_3$.

En este sentido, consideremos ahora el aditamento al *lagrangiano* (1.22) de nuevos términos que implementen las fuentes de ruptura de isoespín intrínseca y electromagnética. Es claro que debemos seguir exactamente el mismo proceso que hemos efectuado anteriormente. De este modo, al final habremos obtenido una forma elegante de obtener funciones de Green en las que intervengan las corrientes externas dentro del marco de la teoría efectiva a través de derivar la acción con fuentes, e igualándolas —después— a su valor físico. Está claro que un enfoque perturbativo de este tipo requiere tácitamente que las fuentes sean *pequeñas*, en un sentido práctico determinado por el acoplo y por la escala de energía típica de la expansión.

El esquema de trabajo en nuestra investigación será entonces el siguiente: acóplese a la teoría efectiva la matriz de masa y el campo del fotón a través de la consideración de las siguientes fuentes externas

$$s = \mathcal{M}, \qquad r_\mu = l_\mu = QA_\mu, \qquad p = 0, \qquad a_\mu = v_{s,\mu} = 0. \tag{1.34}$$

Después, constrúyase el *lagrangiano* efectivo más general mediante la consideración de todos los términos posibles invariantes bajo las simetrías C, P, T, Lorentz y bajo el grupo quiral, lo que implica la ley de transformación (1.26) para la matriz de campos y las transformaciones (1.32) para las fuentes externas.

Naturalmente, las fuentes $\mathcal{M}$ y QA_μ son matrices constantes en el espacio de sabor y no cambian cuando la matriz de campos $U(x)$ se transforma bajo $SU_L(N_f) \times SU_R(N_f)$. No obstante —de acuerdo al resultado anteriormente expuesto— a la hora de añadir nuevos términos al *lagrangiano* efectivo es necesario respetar la simetría bajo el grupo quiral aforado si se quieren introducir fuentes externas de una manera consistente.

¿Cómo solucionar este problema? La solución es sencilla: basta hacer que el campo local $\mathcal{M}(x)$, y los campos espúreos de quiralidad definida $Q_L(x)$ y $Q_R(x)$ se transformen bajo el grupo quiral aforado como

$$\begin{aligned} \mathcal{M}(x) &\mapsto L(x)\,\mathcal{M}(x)\,R^\dagger(x), \\ Q_L(x) &\mapsto L(x)\,Q_L(x)\,L^\dagger(x), \\ Q_R(x) &\mapsto R(x)\,Q_R(x)\,R^\dagger(x), \end{aligned} \tag{1.35}$$

que es precisamente el comportamiento que exigen las leyes de transformación (1.32) para la elección de campos externos (1.34) relevante para este trabajo[15].

Con esta prescripción en mano, deben añadirse al *lagrangiano* (1.22) todos los términos posibles para $U(x), Q_L, Q_R$ y $\mathcal{M}$; de modo que sean invariantes bajo las

[15] Nótese que no se incluyen en (1.35) los términos con derivadas de los campos espúreos $Q_{L,R}(x)$ tal y como exige (1.32). Esto es debido a que —al final del proceso de construcción del *lagrangiano* con fuentes externas— la matriz de carga debe ser una matriz constante, por lo que todos los nuevos términos a proporcionales a $\partial_\mu Q_{L,R}(x) \to \partial_\mu Q$ son idénticamente nulos.

transformaciones (1.35) y bajo aquélla correspondiente a la matriz de campos, *i.e.*

$$U(x) \mapsto L(x)U(x)R^{\dagger}(x), \tag{1.36}$$

sin olvidar que es necesario incorporar a las derivadas parciales las conexiones que acoplan los campos externos a la matriz de campos

$$\begin{aligned} D_{\mu}U &= \partial_{\mu}U - ir_{\mu}U + iUl_{\mu} \\ &= \partial_{\mu}U - iQ_{R}A_{\mu}U + iUQ_{L}A_{\mu}, \end{aligned} \tag{1.37}$$

satisfaciéndose $D_{\mu}U \mapsto L(x)\Big(D_{\mu}U\Big)R^{\dagger}(x)$ bajo transformaciones quirales dependientes del punto.

Al final del proceso, por supuesto, habrá que volver a escribir

$$Q_{L,R}(x) \to Q, \qquad s(x) \to \mathcal{M}, \tag{1.38}$$

de modo que los términos rompan explícitamente la simetría bajo el grupo quiral: tal y como ha ser.

Con todo, el *lagrangiano* quiral efectivo a *leading-order* convenientemente expandido a través de la implementación de efectos de ruptura intrínseca y electromagnética resulta

$$\mathcal{L}_{(2)} = \frac{F^2}{4}\left\{\left\langle D_{\mu}U\, D^{\mu}U^{\dagger}\right\rangle + \left\langle \chi(U+U^{\dagger})\right\rangle\right\} + C\left\langle QUQU^{\dagger}\right\rangle, \tag{1.39}$$

donde se han introducido sendas *constantes de baja energía* asociadas a los nuevos términos de ruptura: C para introducir el término electromagnético *leading-order*, y B_0 —que tiene dimensiones de energía— a través de la matriz $\chi = 2B_0(s+ip)\big|_{p=0}$, que refleja la dependencia lineal en la masa quark observada en el cuadrado de la masa de los bosones de Goldstone.

La constante C puede determinarse aproximadamente, por ejemplo, mediante la sustitución de los valores físicos para la masa de los piones cargados ($M^2_{\pi^0} = 135$ MeV y $M^2_{\pi^{\pm}} = 139{,}6$ MeV, [15]) en la expresión para la diferencia de masas electromagnética *a nivel árbol* en $SU(2)$–$ChPT$

$$M^2_{\pi^{\pm}} - M^2_{\pi^0} = 2\frac{Ce^2}{F^2} + \mathcal{O}(p^4), \tag{1.40}$$

de donde $C \simeq (104.13\ \text{MeV})^4$, si se tiene en cuenta que $F \simeq F_{\pi} = 92{,}4$ MeV a ese orden. Por su parte, B_0 puede relacionarse con el condensado escalar de quarks a *leading order* a través de

$$\left\langle \bar{q}q\right\rangle = F^2B_0\Big(1+\mathcal{O}(p^2)\Big). \tag{1.41}$$

Si más allá de la simple consideración de efectos de carga se requiere la presencia de fotones como grados de libertad adicionales —como de hecho será necesario al calcular las correcciones a la auto-energía de un gas de piones debido al intercambio de fotones en el capítulo 3— habrá que añadir a este *lagrangiano* los términos asociados a su dinámica y aquél de fijación del *gauge*; *i.e.*, para un *gauge* covariante: $-\frac{1}{4}F^{\mu\nu}F_{\mu\nu} - \frac{1}{2}\lambda(\partial_\mu A^\mu)^2$, donde $F^{\mu\nu}$ es el tensor campo electromagnético y λ, el parámetro de *gauge*. Obsérvese que estos términos no modifican el comportamiento bajo el grupo quiral por ser identidades en el espacio de sabor.

Una vez seguidos todos estos pasos ya se está en condiciones de calcular valores esperados asociados a estas corrientes: simplemente derívese la acción respecto de las fuentes externas auxiliares, y evalúense éstas al final del cálculo en su valor físico.

Como se ha comentado anteriormente, este procedimiento implica que las fuentes externas vienen introducidas por acoplos numéricos que admiten una expansión perturbativa controlable respecto a la escala típica de energía de la teoría. En el caso de la masa, esto es cierto para los quarks ligeros *up* y *down* frente a la escala $\Lambda_\chi \sim 1\,\mathrm{GeV}$, y algo menos confiable en el caso de que se incluya el sector de extrañeza no nula. Para la carga, la serie perturbativa se hace controlable debido a las potencias de la carga eléctrica del electrón e, a través de la carga de los quarks presentes en la matriz de carga.

Renormalización y contaje quiral

ChPT es una teoría no renormalizable en el contexto habitual en que se tratan las teorías cuánticas de campos, puesto que incorpora un número infinito de contratérminos a través de los infinitos términos de que consta el *lagrangiano* quiral efectivo. Sin embargo, admite una renormalización ligada a un concepto más amplio y que requiere la prescripción tanto del proceso como del orden al que se llevarán los cálculos: *la renormalización orden a orden* [30, 31].

Como es bien conocido, los diagramas con *loops* dan lugar a integrales divergentes. Sin embargo, fijado un cierto orden para un determinado proceso, es posible resolver el problema *absorbiendo* las contribuciones infinitas de los *loops* del orden principal con la ayuda de las constantes de acoplo de los términos del *lagrangiano next-to-leading order*. Mediante la regularización dimensional de las integrales divergentes es posible renormalizar las constantes de baja energía redefiniéndolas —para cálculos a un *loop*— como

$$S_i(\mu_\chi) = S_i^r(\mu_\chi) + \frac{\mathcal{D}_i}{32\pi^2}\lambda, \tag{1.42}$$

es decir, mediante su descomposición en una parte finita, $S_i^r(\mu_\chi)$, y una parte divergente, $\mathcal{D}_i$.

La parte finita tiene carácter fenomenológico, ya que codifica la física subyacente a la teoría completa[16], y depende—en general— de la escala de renormalización quiral, μ_χ. La parte divergente es —en el esquema de regularización dimensional— proporcional a

$$\lambda = \frac{\mu_\chi^{d-4}}{16\pi^2}\left(\frac{1}{d-4} - \frac{1}{2}\Big(\log 4\pi + \Gamma'(1) + 1\Big)\right), \tag{1.43}$$

donde d es el número de dimensiones del espacio en el que se calcula la integral asociada al diagrama y $\Gamma'(1)$ es la constante de Euler. Esta parte puede cancelar las divergencias procedentes de los *loops*, obteniéndose de esta manera resultados finitos para los observables.

Existe una dificultad importante de índole práctica para la ejecución de este esquema de trabajo: a medida que calculamos correcciones procedentes de órdenes mayores, aparecen muchísimas más constantes de energía procedentes de los contratérminos que hay que determinar de forma fenomenológica —lo que resulta altamente no trivial en muchas ocasiones— restando efectividad a la capacidad predictiva de *ChPT*.

Como ya se ha apuntado anteriormente, la clave en el manejo de la teoría efectiva de baja energía es el contaje de las potencias de momentos transferidos y masas de piones con las que contribuye cada diagrama a un cierto proceso. Si los momentos transferidos o las masas en el proceso son mucho menores que la escala Λ_χ, se espera que contribuciones de orden superior sean cada vez más pequeñas haciendo que el principal aporte al proceso provenga de los términos con pocas derivadas o potencias de masas.

Sea un diagrama genérico que contiene N_d vértices contribuyendo cada uno como $\mathcal{O}(p^d)$, con d el número de derivadas del término considerado en el *lagrangiano* efectivo. Sea, además, l el número de *loops* que posee el diagrama, e I el número de líneas internas.

Por análisis dimensional, el orden en momentos total para el diagrama es $D = 4l - 2I + \sum_{d=2}^{\infty} dN_d$, ya que cada *loop* introduce un p^4 a través de la integración $\int d^4p$, cada vértice introduce introduce un factor p^d y cada propagador interno va con un $1/p^2$. Además, el número de líneas internas está relacionado con el número de *loops* y el número de vértices de todo diagrama conectado a través de $l = 1 + I - \sum_d N_d$, es decir, $I = l - 1 + \sum_d N_d$.

A partir de estas consideraciones, el orden total de momentos asociado al

[16] No todas las *LECs* pueden fijarse directamente mediante métodos experimentales. Algunas necesitan de escenarios teóricos adicionales como el límite de N_C grande o la inclusión de resonancias vectoriales. Consultar, por ejemplo, [34–36].

diagrama —también llamado grado de divergencia superficial— resulta ser

$$D = 2l + 2 + \sum_{d=2}^{\infty} (d-2)N_d, \tag{1.44}$$

lo que constituye el Teorema de Contaje de Potencias de Weinberg [29], implementado a un *loop* en *ChPT* [33,37].

El incremento de los órdenes de los momentos a través de los *loops* está siempre compensado por las constantes con dimensión procedentes de los vértices: de ahí el carácter relativo respecto a la escala $\Lambda_\chi \simeq 4\pi F$. En efecto, los vértices procedentes de términos con dos derivadas aportan el factor F^2 al denominador para mantener las dimensiones del observable inalteradas. Además, cada *loop* introduce un factor $1/(4\pi)^2$, por lo que resulta justificada la elección de la escala de perturbaciones quiral como $4\pi F$, cuyo valor numérico es comparable al de la masa de las primeras resonancias ligeras.

Un último comentario es pertinente a la hora de establecer sistemáticamente un método de contaje quiral en presencia de un acoplo electromagnético externo: debido a la ecuación (1.37) la inclusión de ruptura electromagnética en el *lagrangiano* quiral efectivo puede considerarse de orden $\mathcal{O}(p)$ a efectos de contaje, es decir,

$$\mathcal{O}(e) \sim \mathcal{O}(p). \tag{1.45}$$

Órdenes superiores en el *lagrangiano* quiral efectivo

En la siguiente memoria sólo estaremos interesados en cálculos a un *loop* de bosones de Goldstone, por lo que sólo necesitamos los órdenes $\mathcal{L}_{(2)}$, y $\mathcal{L}_{(4)}$ a *nivel árbol*. Para $N_f = 2$, los términos del *lagrangiano next-to-leading-order* incluyendo ruptura intrínseca fueron publicados por primera vez en [30] y toman la forma

$$\begin{aligned}
\mathcal{L}_{(4)}^{N_f=2} = {} & \frac{l_1}{4}\left\langle (D_\mu U)(D^\mu U)^\dagger \right\rangle + \frac{l_2}{4}\left\langle (D_\mu U)(D_\nu U)^\dagger \right\rangle \left\langle (D^\mu U)(D^\nu U)^\dagger \right\rangle \\
& + \frac{l_3}{16}\left\langle \chi U^\dagger + U\chi^\dagger \right\rangle^2 + \frac{l_4}{4}\left\langle (D_\mu U)(D^\mu \chi)^\dagger + (D_\mu \chi)(D^\mu U)^\dagger \right\rangle \\
& + l_5\left(\left\langle f_{\mu\nu}^R U f_L^{\mu\nu} U \right\rangle - \frac{1}{2}\left\langle f_{\mu\nu}^L f_L^{\mu\nu} + f_{\mu\nu}^R f_R^{\mu\nu} \right\rangle \right) - 2h_2 \left\langle f_{\mu\nu}^L f_L^{\mu\nu} + f_{\mu\nu}^R f_R^{\mu\nu} \right\rangle \\
& + i\frac{l_6}{2}\left\langle f_{\mu\nu}^R (D^\mu U)(D^\nu U)^\dagger + f_{\mu\nu}^L (D^\mu U)^\dagger (D^\nu U) \right\rangle \\
& - \frac{l_7}{16}\left\langle \chi U^\dagger - U\chi^\dagger \right\rangle^2 + \frac{h_1 + h_3}{4}\left\langle \chi\chi^\dagger \right\rangle \\
& + \frac{h_1 - h_3}{16}\left(\left\langle \chi U^\dagger + U\chi^\dagger \right\rangle^2 + \left\langle \chi U^\dagger - U\chi^\dagger \right\rangle^2 - 2\left\langle \chi U^\dagger \chi U^\dagger + U\chi^\dagger U\chi^\dagger \right\rangle \right),
\end{aligned} \tag{1.46}$$

donde

$$f_L^{\mu\nu} = \partial^\mu l^\nu - \partial^\nu l^\mu - i[l^\mu, l^\nu],$$
$$f_R^{\mu\nu} = \partial^\mu r^\nu - \partial^\nu r^\mu - i[r^\mu, r^\nu], \tag{1.47}$$

son los tensores de intensidad asociados a los campos externos.

El *lagrangiano* (1.46) incluye las constantes de baja energía $\{l_i\}_{i=1}^7$, y los términos de contacto h_1, h_2 y h_3 que acompañan términos del *lagrangiano* en los que no está presente la matriz de campos y cuyo valor, por tanto, no puede ser determinado por el experimento. La renormalización de las constantes de baja energía que aparecen puede encontrarse también en [30].

Para $N_f = 3$, los términos del sector puramente fuerte pueden encontrarse en [31]

$$\begin{aligned}
\mathcal{L}_{(4)}^{N_f=3} &= L_1 \left\langle (D^\mu U^\dagger)(D_\mu U) \right\rangle^2 + L_2 \left\langle (D^\mu U^\dagger)(D^\nu U) \right\rangle \left\langle (D_\mu U^\dagger)(D_\nu U) \right\rangle \\
&+ L_3 \left\langle (D^\mu U^\dagger)(D_\mu U)(D^\nu U)^\dagger (D_\nu U) \right\rangle + L_4 \left\langle (D^\mu U^\dagger)(D_\mu U) \right\rangle \left\langle \chi^\dagger U + \chi U^\dagger \right\rangle \\
&+ L_5 \left\langle (D^\mu U^\dagger)(D_\mu U)(\chi^\dagger U + U^\dagger \chi) \right\rangle + L_6 \left\langle \chi^\dagger U + \chi U^\dagger \right\rangle^2 \\
&+ L_7 \left\langle \chi^\dagger U - \chi U^\dagger \right\rangle^2 + L_8 \left\langle \chi^\dagger U \chi^\dagger U + \chi U^\dagger \chi U^\dagger \right\rangle \\
&- i L_9 \left\langle \left(F_{\mu\nu}^R (D^\mu U)(D^\nu U^\dagger) + F_{\mu\nu}^L (D^\mu U)(D^\nu U^\dagger) \right) \right\rangle \\
&+ L_{10} \left\langle U^\dagger F_{\mu\nu}^R U F^{L,\mu\nu} \right\rangle + H_1 \left\langle F_{\mu\nu}^R F^{R,\mu\nu} + F_{\mu\nu}^L F^{L,\mu\nu} \right\rangle + H_2 \left\langle \chi^\dagger \chi \right\rangle,
\end{aligned} \tag{1.48}$$

siendo $F_{L,V}^{\mu\nu}$ el equivalente a $f_{L,R}^{\mu\nu}$ en tres sabores. El *lagrangiano* (1.48) incluye las *LECs* $\{L_i\}_{i=1}^{10}$ y los términos de contacto H_1 y H_2, y una vez más se remite al lector a [31] para su separación en partes divergente y finita.

Los acoplos electromagnéticos a estos *lagrangianos* fueron calculados en [38, 39] para $N_f = 2$, donde introducen las constantes de baja energía electromagnéticas (*EM LECs*) $\{k_i\}_{i=1}^{14}$. Por completitud los incluimos también a continuación

$$\begin{aligned}
\mathcal{L}_{(4,e^2)}^{N_f=2} = F^2 \Bigg(& k_1 \left\langle (D^\mu U)^\dagger (D_\mu U) \right\rangle \left\langle Q^2 \right\rangle + k_2 \left\langle (D^\mu U)^\dagger (D_\mu U) \right\rangle \left\langle Q U Q U^\dagger \right\rangle \\
& + k_3 \left(\left\langle (D^\mu U)^\dagger Q U \right\rangle \left\langle (D_\mu U)^\dagger Q U \right\rangle + \left\langle (D^\mu U) Q U^\dagger \right\rangle \left\langle (D_\mu U) Q U^\dagger \right\rangle \right) \\
& + k_4 \left\langle (D^\mu U)^\dagger Q U \right\rangle \left\langle (D_\mu U) Q U^\dagger \right\rangle + k_5 \left\langle \chi^\dagger U + U^\dagger \chi \right\rangle \left\langle Q^2 \right\rangle \\
& + k_6 \left\langle \chi^\dagger U + U^\dagger \chi \right\rangle \left\langle Q U Q U^\dagger \right\rangle \\
& + k_7 \left\langle (\chi U^\dagger + U \chi^\dagger) Q + (\chi^\dagger U + U^\dagger \chi) Q \right\rangle \langle Q \rangle \\
& + k_8 \left\langle (\chi U^\dagger - U \chi^\dagger) Q U Q U^\dagger + (\chi^\dagger U - U^\dagger \chi) Q U^\dagger Q U \right\rangle \\
& + k_9 \left\langle (D_\mu U)^\dagger [c_R^\mu Q, Q] U + (D_\mu U) [c_L^\mu Q, Q] U^\dagger \right\rangle
\end{aligned}$$

$$+k_{10}\left\langle (c_R^\mu Q)U(c_{L,\mu}Q)U^\dagger\right\rangle + k_{11}\left\langle (c_R Q)\cdot(c_R Q)\cdot(c_L Q)\cdot(c_L Q)\right\rangle\Big) + F^4\Big(k_{12}\left\langle Q^2\right\rangle^2 + k_{13}\left\langle QUQU^\dagger\right\rangle\left\langle Q^2\right\rangle + k_{14}\left\langle QUQU^\dagger\right\rangle^2\Big), \quad (1.49)$$

donde $c^{L,R}$ vienen definidos a través de su actuación sobre la matriz de carga

$$\begin{aligned} c_\mu^L Q &= \partial_\mu Q - i[l_\mu, Q], \\ c_\mu^R Q &= \partial_\mu Q - i[r_\mu, Q]. \end{aligned} \quad (1.50)$$

Para $N_f = 3$ el *lagrangiano* electromagnético fue publicado en [40, 41], y recoge las *EM LECs* $\{K_i\}_{i=1}^{14}$. Con todo

$$\begin{aligned} \mathcal{L}_{(4,e^2)}^{N_f=3} = F^2\Big(& K_1\left\langle (D^\mu U)^\dagger (D_\mu U)\right\rangle\left\langle Q^2\right\rangle + K_2\left\langle (D^\mu U)^\dagger (D_\mu U)\right\rangle\left\langle QUQU^\dagger\right\rangle \\ & + K_3\Big(\left\langle (D^\mu U)^\dagger QU\right\rangle\left\langle (D_\mu U)^\dagger QU\right\rangle + \left\langle (D^\mu U)QU^\dagger\right\rangle\left\langle (D_\mu U)QU^\dagger\right\rangle\Big) \\ & + K_4\left\langle (D^\mu U)^\dagger QU\right\rangle\left\langle (D_\mu U)QU^\dagger\right\rangle + K_5\Big\langle\Big((D^\mu U)^\dagger (D_\mu U) \\ & + (D^\mu U)(D_\mu U)^\dagger\Big)Q^2\Big\rangle + K_6\left\langle (D^\mu U)^\dagger (D_\mu U)QU^\dagger QU + \right. \\ & \left. (D^\mu U)(D_\mu U)^\dagger QUQU^\dagger\right\rangle + K_7\left\langle (\chi U^\dagger + U\chi^\dagger)\right\rangle\left\langle Q^2\right\rangle \\ & + K_8\left\langle \chi^\dagger U + U^\dagger\chi)Q\right\rangle\left\langle QUQU^\dagger\right\rangle \\ & + K_9\left\langle (\chi^\dagger U + U^\dagger\chi + \chi U^\dagger + U\chi^\dagger)Q^2\right\rangle \\ & + K_{10}\left\langle (\chi U + U^\dagger\chi)QU^\dagger QU + (\chi U^\dagger + U\chi^\dagger)QUQU^\dagger\right\rangle \\ & + K_{11}\left\langle (\chi U^\dagger - U\chi^\dagger)QUQU^\dagger + (\chi^\dagger U - U^\dagger\chi)QU^\dagger QU\right\rangle \\ & + K_{12}\left\langle (D^\mu U)^\dagger [c_\mu^R Q, Q]U + (D^\mu U)[c_\mu^L Q, Q]U^\dagger\right\rangle \\ & + K_{13}\left\langle c_R^\mu QU c_\mu^L QU^\dagger\right\rangle + K_{14}\left\langle c_R^\mu Q c_\mu^R Q + c_L^\mu Q c_\mu^L Q\right\rangle\Big) \\ & + F^4\Big(K_{15}\left\langle QUQU^\dagger\right\rangle^2 + \left\langle QUQU^\dagger\right\rangle\left\langle Q^2\right\rangle + K_{17}\left\langle Q^2\right\rangle^2\Big). \end{aligned} \quad (1.51)$$

Las condiciones de renormalización para las constantes de baja energía en $N_f = 2,3$ pueden encontrarse en la bibliografía citada anteriormente.

1.1.3 Resonancias

Método de la Amplitud Inversa y Teoría Quiral Unitarizada

Las resonancias mesónicas más ligeras, *vid.* la $f_0(500)/\sigma$ y la $\rho(770)$, juegan un rol crucial en la descripción a bajas energías de la Interacción Fuerte para procesos relacionados con temperatura o densidad finita, ambos escenarios que se dan en las Colisiones Relativistas de Iones Pesados.

ChPT es incapaz de tener en cuenta este tipo de estados más allá de la física encriptada en las constantes de baja energía de la teoría. Debido a que la Teoría Quiral constituye una expansión perturbativa en la energía, viola la cotas de unitariedad exacta, por lo que necesita de métodos adicionales para conseguir su unitarización. Estos métodos se han mostrado satisfactorios y confiables a temperatura cero describiendo las interacciones mesón-mesón o mesón-barión, generando dinámicamente las resonancias más ligeras [42–49] incluso a temperatura y densidad finitas [50–53].

A continuación presentaré el llamado Método de la Amplitud Inversa (*IAM*), usado para conseguir la unitarización de las amplitudes de dispersión en la Teoría Quiral de Perturbaciones. Como veremos, será de grande y amplia utilidad en la sección 2.3 en lo relativo a la presentación del escenario de restauración de la simetría quiral dado por la degeneración de las susceptibilidades escalar y pseudoescalar, ésta última caracterizada a través del condensado escalar de quarks.

Su nombre proviene del hecho de que la imposición de la condición de unitariedad implica que el inverso de cualquier onda parcial con isoespín I y momento angular total J bien definidos, t_{IJ}, en el proceso de dispersión $\pi\pi \to \pi\pi$, debe satisfacer

$$\operatorname{Im} t_{IJ} = \sigma_0(s)|t_{IJ}(s)|^2 \to \operatorname{Im} \frac{1}{t_{IJ}} = -\sigma_0(s), \tag{1.52}$$

donde $s > (2M_\pi)^2$ es la energía en el centro de masas y $\sigma_0(s)$ es el espacio de fases para el canal de dos partículas, $|\pi\pi>$, a la energía s, definido como

$$\sigma_0(s) = \sqrt{1 - \frac{4M_\pi^2}{s}}. \tag{1.53}$$

Consideremos ahora la expansión *next-to-leading-order* para la onda parcial de dispersión del proceso mencionado

$$t_{IJ}(s) = t_{IJ}^{(2)}(s) + t_{IJ}^{(4)}(s) + \mathcal{O}(p^6), \tag{1.54}$$

IJ	$16\pi F_\pi^2 A_{IJ}$	s_2^{IJ}/M_π^2
00	1	1/2
11	1/6	4
20	−1/2	-2

Cuadro 1.4: Valores numéricos que permiten calcular las ondas parciales de dispersión de dos piones a dos piones a *leading-order* en *ChPT* a través de $t_{IJ}^{(2)} = A_{IJ}(s - s_2^{IJ})$.

donde —como ya he dicho en secciones previas— p hace referencia a un momento externo, una temperatura o una masa en relación con la escala de energía que controla la expansión quiral, $\Lambda_\chi \sim 1\,\mathrm{GeV}$.

En la sección 2.3 estaremos interesados en la aplicación del *IAM* para dos piones idénticos, *i.e.* en el límite de isoespín, por lo que $I+J$ debe ser par debido al requerimiento de que la amplitud total de dispersión sea totalmente simétrica; además —para las energías y temperaturas de interés en cuanto a aplicabilidad de la Teoría Quiral— sólo las ondas parciales con $J \leq 1$ son relevantes.

De acuerdo al contaje quiral que ya hemos discutido en apartados previos, $t_{IJ}^{(2)}$ da cuenta de los diagramas a *nivel árbol* que involucran vértices procedentes de $\mathcal{L}_{(2)}$, de carácter independiente de la temperatura, y cuyos valores están recogidos en el cuadro 1.4. El mismo análisis puede aplicarse a $t_{IJ}^{(4)}$: en este caso contribuyen los diagramas a un *loop* que contienen vértices procedentes de $\mathcal{L}_{(2)}$ más los términos a *nivel árbol* procedentes de $\mathcal{L}_4$, necesarios para renormalizar las divergencias. Un análisis numérico de los valores de $t_{IJ}^{(4)}$ puede encontrarse, por ejemplo, en [49].

La expansión (1.54) satisface una versión *perturbativa* de la relación de unitariedad completa. En efecto se cumple

$$\mathrm{Im}\, t_{IJ}^{(4)} = \sigma_0(s)\, |t_{IJ}^{(2)}(s)|^2, \tag{1.55}$$

y de modo similar para órdenes superiores, *mutatis mutandi*; lo que implica que la expansión quiral no es completamente compatible con las condiciones impuestas por la condición de unitariedad global (1.52) debido a que crece ilimitadamente con la energía —comportamiento característico en las interacciones fuertes— y es, por tanto, incapaz de reproducir resonancias. Los métodos de unitarización permiten precisamente construir amplitudes de dispersión basadas en expansiones perturbativas de modo que sean *exactamente* unitarias.

En concreto, el IAM [42–44] se construye a partir de la demanda de unitariedad exacta y de la compatibilidad de los resultados a baja energía con las predicciones provistas por *ChPT*. De acuerdo a este método, las ondas parciales

a orden $\mathcal{O}(p^4)$ vienen dadas por

$$t_{IJ}^U(s) = \frac{[t_{IJ}^{(2)}]^2}{t_{IJ}^{(2)}(s) - t_{IJ}^{(4)}(s)}. \tag{1.56}$$

Los efectos derivados de la aparición de resonancias ligeras se advierten a través de la presencia de picos en la sección eficaz de dispersión. Además, éstas pueden ser identificadas como polos en la amplitud de dispersión una vez que han sido continuadas analíticamente a la segunda hoja de Riemann (la condición de causalidad impide su presencia en la primera hoja).

La amplitud (1.56) es analítica en todo el plano complejo salvo en el eje real y tiene un corte derecho de unitariedad que comienza en el umbral de producción de dos piones, $s = (2M_\pi)^2$; así como un corte izquierdo para $s < 0$ procedente de diagramas en el canal $t - u$ [49].

Estas propiedades analíticas permiten definir de modo completo la amplitud unitarizada en la segunda hoja de Riemann, mediante el empalme de su parte imaginaria en la primera hoja a través del corte derecho. Si denotamos mediante $t^{(I)}$ la amplitud de dispersión en la primera hoja de Riemann —fuera del eje real—, entonces la amplitud de dispersión en la segunda hoja viene dada a través de la condición de empalme

$$\operatorname{Im} t^{(II)}(s - i0^+) = \operatorname{Im} t^{(I)}(s + i0^+), \qquad s > (2M_\pi)^2. \tag{1.57}$$

De esta manera se concluye que

$$t^{(II)}(s) = \frac{t^{(I)}(s)}{1 - 2i\sigma_0(s)t^{(I)}(s)}. \tag{1.58}$$

La masa y la anchura de una resonancia parametrizada *à la Breit-Wigner* pueden relacionarse [54] con el polo, s_p, de la expresión (1.58) en el semiplano complejo inferior a través de

$$s_p =: \left(M_R - \frac{i}{2}\Gamma_R\right)^2, \tag{1.59}$$

expresión que en el límite de resonancias estrechas, $M_R >> \Gamma_R$, define la masa y la anchura (en reposo) de las resonancias que obtengamos a partir de la dispersión de piones. Ha de notarse que el uso de una parametrización de tipo Breit-Wigner no está exclusivamente reservado para partículas *estrechas*. Tendremos ocasión de comprobar esto al mostrar los resultados atinentes a la $f_0(500)/\sigma$ —una resonancia particularmente ancha— en la publicación 2.3.1.

Modelo de intercambio de resonancias

En el capítulo 3 discutiremos la *estabilidad* de los resultados de *ChPT* frente a la inclusión de resonancias ligeras a través de un modelo de intercambio basado en un *lagrangiano* [32, 55] que incluye los términos $\mathcal{O}(p^2)$ del *lagrangiano* quiral efectivo y le añade términos $\mathcal{O}(p^4)$ resultantes del acoplo de campos de tipo vectorial ($J^{PC}=1^{--}$) y de tipo vectorial-axial ($J^{PC}=1^{++}$) —además de incluir acoplo electromagnético explícito—.

Una vez fijadas las constantes de acoplo que introduce cada uno de los nuevos términos de interacción con los bosones de Goldstone y que deben determinarse a través de métodos auxiliares —ya sean de carácter experimental o asunciones teóricas adicionales—, la descripción que proporciona este modelo se estima como razonablemente precisa para energías bajas e intermedias, *i.e.* hasta aproximadamente 1 GeV.

El *lagrangiano* del modelo puede escribirse como sigue:

$$\begin{aligned}\mathcal{L} = -\frac{1}{4}F_{\mu\nu}F^{\mu\nu} + \frac{F^2}{4}\mathrm{Tr}\left(D_\mu U D^\mu U^\dagger + \chi U^\dagger + \chi^\dagger U\right) - \frac{1}{2}\mathrm{Tr}\left(\nabla^\lambda V_{\lambda\nu}\nabla_\mu V^{\nu\mu}\right.\\ \left. -\frac{1}{2}M_V^2 V^{\mu\nu}V_{\mu\nu}\right) + \frac{F_V}{2\sqrt{2}}\mathrm{Tr}\left(V_{\mu\nu}f_+^{\mu\nu}\right) + i\frac{G_V}{\sqrt{2}}\mathrm{Tr}\left(V_{\mu\nu}u^\mu u^\nu\right)\\ -\frac{1}{2}\mathrm{Tr}\left(\nabla^\lambda A_{\lambda\nu}\nabla_\mu A^{\nu\mu} - \frac{1}{2}M_A^2 A^{\mu\nu}A_{\mu\nu}\right) + \frac{F_A}{2\sqrt{2}}\mathrm{Tr}\left(A_{\mu\nu}f_-^{\mu\nu}\right), \quad (1.60)\end{aligned}$$

donde U y χ son las matrices de campos y de masa usuales de *ChPT*, M_V y M_A son las masas de las resonancias que saturan los canales vectorial y vectorial-axial, respectivamente; y F_V, F_A y G_V son las constantes que introducen los acoplos con las resonancias y cuyo valor numérico puede consultarse en, por ejemplo, [32].

En realidad sólo es necesario uno de los parámetros —F_V, por ejemplo— debido a que los restantes pueden obtenerse a partir de las llamadas reglas de suma de Weinberg [56], que en el límite quiral toman la forma

$$F_V^2 - F_A^2 = F_\pi^2, \quad (1.61)$$
$$F_V^2 M_V^2 - F_A^2 M_A^2 = 0, \quad (1.62)$$

y de hipótesis adicionales como *vector resonance dominance approximation* [57], que —aplicada al cálculo del factor de forma del pión— da lugar a la aproximación $F_V G_V \simeq F_\pi^2$; o la llamada relación *KSRF*, $F_V = \sqrt{2}F_\pi$ [58, 59]

Por último, la derivada covariante, D_μ, incorpora el acoplo vectorial al campo externo del fotón, $v_\mu = QA_\mu$, y viene dada por la expresión (1.33). Además —respecto a los acoplos con las resonancias y considerando fuentes externas de

tipo vectorial y axial— tenemos

$$\begin{aligned} u_\mu &= iu^\dagger(D_\mu U)u^\dagger = u_\mu^\dagger, \\ f_\pm^{\mu\nu} &= uF_L^{\mu\nu}u^\dagger \pm u^\dagger F_R^{\mu\nu}, \\ F_{R,L}^{\mu\nu} &= \partial^\mu(v^\mu \pm a^\nu) - \partial^\nu(v^\mu \pm a^\mu) - i\,[v^\mu \pm a^\mu, v^\nu \pm a^\nu], \end{aligned} \tag{1.63}$$

con $u^2 = U$, y siendo v_μ y a_μ los posibles acoplos externos de tipo vectorial y vectorial-axial, respectivamente. Nótese que si sólo se incluye —como será, de hecho, el caso que nos ocupe— el campo electromagnético, entonces ha de escribirse $a_\mu = 0$, $v_\mu = eQA_\mu$.

Las matrices que contienen los campos de las resonancias son:

$$V_{\mu\nu} = \begin{pmatrix} \frac{\rho^0}{\sqrt{2}} + \frac{\omega_8}{\sqrt{6}} & \rho^+ & K^{*+} \\ \rho^- & -\frac{\rho^0}{\sqrt{2}} + \frac{\omega_8}{\sqrt{6}} & K^{*0} \\ K^{*-} & \overline{K^{*0}} & -\frac{2}{\sqrt{6}}\omega_8 \end{pmatrix}_{\mu\nu}, \tag{1.64}$$

$$A_{\mu\nu} = \begin{pmatrix} \frac{a_1^0}{\sqrt{2}} + \frac{f_1}{\sqrt{6}} & a_1^+ & K_1^+ \\ a_1^- & -\frac{a_1^0}{\sqrt{2}} + \frac{f_1}{\sqrt{6}} & K_1^0 \\ K^{-1} & \overline{K_1^0} & -\frac{2}{\sqrt{6}}f_1 \end{pmatrix}_{\mu\nu}, \tag{1.65}$$

mientras que el operador ∇ viene definido a través de su acción sobre un campo tensorial completamente covariante como

$$\nabla_\lambda R_{\mu\nu} = \partial_\lambda R_{\mu\nu} + [\Gamma_\lambda, R_{\mu\nu}], \tag{1.66}$$

siendo $R_{\mu\nu} = V_{\mu\nu}$, $A_{\mu\nu}$, y

$$\Gamma_\lambda = \frac{1}{2}\left\{ u^\dagger[\partial_\lambda - i(v_\lambda + a_\lambda)]u + u[\partial_\lambda - i(v_\lambda - a_\lambda)]u^\dagger \right\}. \tag{1.67}$$

Con todo esto ya estamos en condiciones de calcular el propagador de Feynman de cualquier resonancia. En efecto, en el espacio de posiciones —y haciendo uso de la invariancia de los campos bajo traslaciones— puede escribirse

$$\begin{aligned} \left\langle 0\right| \mathcal{T}\left(R_{\mu\nu}(x)R_{\rho\sigma}(0)\right) \left|0\right\rangle = \frac{-i}{M^2}\int \frac{d^4k}{(2\pi)^4}\frac{e^{-ix\cdot k}}{M^2 - k^2 - i\epsilon}\Big\{ & g_{\mu\rho}g_{\nu\sigma}(M^2 - k^2) \\ & + g_{\mu\rho}k_\nu k_\sigma - g_{\mu\sigma}k_\nu k_\rho - (\mu \leftrightarrow \nu)\Big\}, \end{aligned} \tag{1.68}$$

donde $g_{\mu\nu}$ es el tensor asociado a la métrica de Minkowski y M es la masa de la resonancia definida a través del campo $R_{\mu\nu}$.

En el capítulo 3 estaremos interesados en el cálculo de las correcciones a la auto-energía de un pión a un *loop* en un contexto de dos sabores, por lo que los términos relevantes del *lagrangiano* (1.60) —una vez expandido— son

$$\begin{aligned}\mathcal{L}_\Sigma = & ieA^\mu(\pi^+\partial_\mu\pi^- - \pi^-\partial_\mu\pi^+) + e^2A^\mu A_\mu\pi^+\pi^- \\ & - \frac{e}{2}F_V F^{\mu\nu}\rho^0_{\mu\nu}\left(1 - \frac{1}{F_\pi^2}\pi^+\pi^-\right) + i\frac{G_V}{F_\pi^2}\rho^0_{\mu\nu}\left(\partial^\mu\pi^+\partial^\nu\pi^- - \partial^\mu\pi^-\partial^\nu\pi^+\right) \\ & - 2e\frac{G_V}{F_\pi^2}A^\mu\rho^0_{\mu\nu}\left(\pi^+\partial_\mu\pi^- + \pi^-\partial_\mu\pi^+\right) - ie\frac{F_A}{2F_\pi^2}F^{\mu\nu}\left(a^-_{1,\mu\nu}\pi^+ - a^+_{1,\mu\nu}\pi^-\right). \quad (1.69)\end{aligned}$$

Ha de tenerse en cuenta que el cálculo perturbativo dentro de este modelo debe realizarse con un cierto cuidado puesto que no disponemos de un esquema de contaje de potencias que permita una expansión controlada en las constantes de acoplo de las interacciones entre resonancias y piones. Tendremos ocasión de ver esto más detenidamente en la sección 3.1, al presentar la publicación 3.1.1.

Saturación por resonancias

Como ya se ha dicho con anterioridad, el *lagrangiano* quiral efectivo depende —a cualquier orden— de un número determinado de constantes de baja energía que un enfoque basado en simetrías no puede determinar. Estas *LECs* vienen determinadas por la dinámica de la teoría subyacente a través de la escala de renormalización y de efectos asociados a la masa de las partículas pesadas.

Sin embargo, no es posible calcularlas mediante procedimientos perturbativos en *QCD*, sino que —como también dijimos— deben ser obtenidos a partir de información experimental en el sector de baja energía de la Interacción Fuerte, o mediante métodos auxiliares como, por ejemplo, el límite de gran N_C.

Estas constantes reciben contribuciones de diversas fuentes, entre ellas los efectos debidos a resonancias ligeras, aunque también de otros estados hadrónicos. Aunque es posible mostrar [30] que los valores observados para las *LECs* pueden reproducirse razonablemente bien si se asume que su valor está completamente dominado, por ejemplo, por el intercambio de una partícula $\rho(770)$ —lo que se conoce como *vector meson dominance*— [57], también otras resonancias ligeras contribuyen.

En el capítulo 2 —al hablar de las constantes electromagnéticas de baja energía relevantes en el cálculo de los condensados— y en el capítulo 3 —en relación con las contribuciones de los mesones $a_1(1260)$ y $\rho(770)$ a la auto-energía de un gas de piones— haremos uso de la llamada *hipótesis de saturación por resonancias*, que establece que las *LECs* están saturadas por las primeras resonancias ligeras.

A lo largo de toda esta subsección estudiaremos cómo pueden éstas ser incluidas en el *lagrangiano* quiral y, así, estimar su contribución a las constantes de baja energía. Escribamos las *LECs* renormalizadas como

$$L_i^r(\mu_\chi) = \sum_{R\in\{V,A,S,P\}} L_i^R + \hat{L}_i(\mu_\chi), \tag{1.70}$$

siendo μ_χ la escala quiral de renormalización[17]; L_i^R, con $R \in \{V,A,S,P\}$, las contribuciones a las mismas asociadas a los canales vectorial, axial-vectorial, escalar y pseudoescalar, respectivamente; y $\hat{L}_i(\mu_\chi)$ la parte restante.

A partir del modelo (1.60) e introduciendo —además de las interacciones con los campos vectorial y vectorial-axial— los acoplos (lineales) *leading-order* con el octete y singlete escalar, S y S_1; y el octete y singlete pseudoescalar, P y P_1; a través de

$$\begin{aligned} \mathcal{L}_S : &= c_d \left\langle S u_\mu u^\mu \right\rangle + c_m \left\langle S\chi_+ \right\rangle + \hat{c}_d S_1 \left\langle u_\mu u^\mu \right\rangle + \hat{c}_m S_1 \left\langle \chi_+ \right\rangle, \\ \mathcal{L}_P : &= i d_m \left\langle P\chi_- \right\rangle + i\hat{d}_m \left\langle P_1\chi_- \right\rangle, \end{aligned} \tag{1.71}$$

con c_d, $\hat{c}_d$, c_m, $\hat{c}_m$, d_m y $\hat{d}_m$ ciertas constantes de acoplo, y

$$\chi_\pm := u^\dagger \chi u^\dagger \pm u\chi^\dagger u; \tag{1.72}$$

es posible determinar [32] las contribuciones resonantes a las constantes de baja energía comparando con el *lagrangiano* $\mathcal{L}_{(4)}$ de *SU(3)-ChPT*. Nótese que esto es así debido a que los acoplos son de orden $\mathcal{O}(p^2)$ y, por tanto, el intercambio de resonancias produce contribuciones de orden $\mathcal{O}(p^4)$. Además, debido a este contaje, las únicas contribuciones relevantes para el cálculo de las *LECs* son las que proceden de las partes sin derivadas de los propagadores de las resonancias.

Las contribuciones de las resonancias vectoriales a las *LECs* vienen dadas por [32, 60]

$$\begin{aligned} L_1^V &= \tfrac{G_V^2}{8M_V^2}, \quad L_2^V = 2L_1^V, \quad L_3^V = -6L_1^V \\ L_9^V &= \tfrac{G_V F_V}{2M_V^2}, \quad L_{10}^V = -\tfrac{F_V^2}{4M_V^2}, \quad H_1^V = -\tfrac{F_V^2}{8M_V^2}. \end{aligned}$$

La resonancia axial contribuye como

$$L_{10}^A = \frac{F_A^2}{4M_A^2}, \quad H_1^A = -\frac{F_A^2}{8M_A^2}. \tag{1.73}$$

[17] Es natural suponer que, si las resonancias ligeras dominan la cantidad $L_i^r(\mu_\chi)$, entonces la escala de renormalización quiral ha de estar en un entorno cercano a esta zona del espectro.

	$L_i^r(M_\rho)$	V	A	S	S_1	η_1	Total
L_1^r	0.7 ± 0.3	0.6	0	-0.2	0.2	0	0.6
L_2^r	1.3 ± 0.7	1.2	0	0	0	0	1.2
L_3^r	-4.4 ± 2.5	-3.6	0	0.6	0	0	-3.0
L_4^r	-0.3 ± 0.5	0.0	0	-0.5	0.5	0	0.0
L_5^r	1.4 ± 0.5	0.0	0	1.4	0	0	1.4
L_6^r	-0.2 ± 0.3	0.0	0	-0.3	0.3	0	0-0
L_7^r	-0.4 ± 0.2	0.0	0	0	0.5	0	-0.3
L_8^r	0.9 ± 0.3	0.0	0	0.9	0	0	0.9
L_9^r	6.9 ± 0.7	6.9	0	0	0	0	6.9
L_{10}^r	-5.2 ± 0.3	-10.0	4.0	0	0	0	-6.0

Cuadro 1.5: Contribuciones V, A, S, S_1 y η_1 a las *LECs* en unidades de 10^{-3}, y renormalizadas a la escala $M_\rho = 770$ MeV. Las entradas de la segunda columna pertenecen a [31]. Las entradas a partir de la sexta columna proceden de [32].

Las partes asociadas al octete y al singlete escalar son:

$$\begin{aligned} &L_1^S = -\tfrac{c_d^2}{6M_S^2}, \quad L_3^S = -3L_1^S, \quad L_4^S = -\tfrac{c_d c_m}{3M_S^2}, \quad L_5^S = -3L_4^S \\ &L_6^S = -\tfrac{c_m^2}{2M_S^2}, \quad L_8^S = -L_6^S, \quad H_2^S = 2L_8^S, \\ &L_1^{S_1} = -\tfrac{\tilde{c}_d^2}{2M_{S_1}^2}, \quad L_4^{S_1} = \tfrac{\tilde{c}_d \tilde{c}_m}{M_{S_1}^2}, \quad L_6^{S_1} = -\tfrac{\tilde{c}_m^2}{2M_{S_1}^2}. \end{aligned} \tag{1.74}$$

Finalmente las contribuciones del octete y el singlete pseudoescalar son

$$\begin{aligned} &L_7^P = \tfrac{d^2}{6M_P^2}, \qquad L_8^P = -3L_7^P, \quad H_2^P = -6L_7^P \\ &L_1^{P_1} = -\tfrac{\tilde{d}^2}{2M_{\eta_1}^2}. \end{aligned} \tag{1.75}$$

Donde quiera que aparezcan, las contribuciones asociadas a los canales vectorial y axial-vectorial dominan sobre todas las demás en el sector de baja energía, dejando muy poco protagonismo a contribuciones adicionales. Como H_2^r no puede ser determinada fenomenológicamente pero aparece en el cálculo de los condensados escalares —como veremos en el capítulo 2—, asumiremos dominancia escalar con el fin de utilizar la aproximación $H_2^r = 2L_8^r$. En el cuadro 1.5 mostramos las diferencias entre los resultados obtenidos en [32] y los valores experimentales en [31].

Puede aplicarse el mismo razonamiento para resonancias en distintos canales con objeto de obtener valores numéricos de las constantes de baja energía electromagnéticas, incluyendo la constante C que corrige la masa de los piones cargados a *nivel árbol* y que está prácticamente dominada por el intercambio de una $\rho(770)$ y una $a_1(1260)$ [61].

Por mor de la concisión, referimos aquí al lector a la literatura especializada para un tratamiento más extenso de estas cuestiones —así como para consultar la procedencia de la mayor parte de los resultados numéricos que utilizamos para verificar los resultados de la publicación 2.1.1—. De este modo puede consultarse la discusión acerca de los valores para las *EMLECs* de 2.1.1, o los trabajos [62–65].

1.1.4 Temperatura finita: fenomenología y formalismo

Con el fin de estudiar la evolución térmica de los observables que estudiemos en los capítulos 2.1 y 3, analizaremos brevemente las implicaciones que surgen al considerar la simetría quiral en un escenario térmico, así como las propiedades y resultados fundamentales a la hora de realizar la extensión de la Teoría Quiral de Perturbaciones a temperatura finita a través del llamado Formalismo de Tiempo Imaginario (*ITF*) [66, 67].

Al introducir la temperatura, se introduce una nueva escala de energía que influye en la expansión perturbativa que se hacía en *ChPT*. En efecto, además de la escala de masas o momentos externos que situábamos en $\Lambda_\chi \sim 4\pi F \sim 1\,\text{GeV}$ hay ahora una escala de expansión térmica, Λ_T, que se sitúa aproximadamente en unos $150-200$ MeV, valor del orden de la temperatura asociada al cambio de fase que se produce entre la fase hadrónica y la fase partónica del diagrama de fases de *QCD* a potencial químico nulo[18] [68, 69].

De esta manera, distinguiremos tres regímenes térmicos en relación con esta nueva escala térmica.

i) Régimen de bajas temperaturas, $T << \Lambda_T$. En este rango todos los efectos térmicos debidos a partículas pesadas (es decir, asociados a partículas que no son bosones de Goldstone y que serán, típicamente, resonancias) pueden ser despreciados debido a que están suprimidos exponencialmente a través de factores de Boltzmann de la forma $e^{-\frac{M_h}{T}}$, donde M_h es la masa del hadrón pesado considerado. El *lagrangiano* quiral efectivo permanece inalterado al considerar efectos térmicos, pero será necesario modificar los propagadores asociados a los bosones de Goldstone de modo que den cuenta de la evolución térmica [70].

ii) Régimen de temperaturas intermedias, $T \lesssim \Lambda_T$. Las partículas pesadas comienzan a ser importantes y sus efectos han de tenerse en cuenta. El rango térmico de este régimen acaba en la llamada transición quiral, proceso en el que la simetría quiral se restaura y deja de estar espontáneamente rota.

iii) Régimen de temperaturas altas, $T > \Lambda_T$. Se produce a temperaturas mayores que la temperatura asociada a la restauración de la simetría quiral y a la

[18] Puede también identificarse a Λ_T como la temperatura tal que el promedio térmico de la energía para un gas de bosones de Goldstone coincide con la escala de energía Λ_χ. En este caso, y a partir del uso del Teorema de Equipartición para un gas relativista, el valor obtenido es un poco mayor: $\Lambda_T \sim 300$ MeV, pero se convendrá en que —de cara a un tratamiento perturbativo de baja energía— los resultados serán más confiables eligiendo el valor más conservativo, *i.e.* el valor numérico más bajo. Además, parte de los resultados mostrados muestran comportamientos cualitativos compatibles con la restauración de la simetría quiral.

transición de desconfinamiento[19]. Los quarks y los gluones se convierten en los grados de libertad relevantes y se forma el denominado genéricamente *Plasma de Quarks y Gluones (QGP)* [72, 73].

Parece claro que la región de interés para la memoria de investigación que ocupa estas líneas es aquélla en la que la temperatura es lo suficientemente baja como para suponer que las partículas pesadas se hallan térmicamente desacopladas y que la convergencia de la serie perturbativa quiral en Λ_T sea razonable. Esto se consigue para temperaturas por debajo de los 100 MeV, de interés fenomenológico debido a que no están muy lejos de las temperaturas asociadas al *freeze-out* térmico en Colisiones Relativistas de Iones Pesados [74–76] (ver comentario en la subsección 1.1.4).

En cualquier caso, las predicciones de *ChPT* pueden ser extrapoladas cualitativamente por encima de este valor de $T \simeq 100$ MeV con el fin de colegir propiedades que puedan ayudar a explicar rasgos del comportamiento de la materia hadrónica en regiones cuya temperatura es ligeramente inferior a la transición de restauración de simetría quiral.

Naturalmente, el carácter crítico de la transición de fase no podrá ser reproducido utilizando un esquema de cálculo basado únicamente en *ChPT*, así que los resultados cuyas gráficas se continúen hasta regiones térmicas por encima de los valores estándar que garantizan la convergencia de la serie quiral térmica en la sección 2.2 y en el capítulo 3 deben tomarse como predicciones cualitativas *model-independent* a partir de una teoría efectiva de baja energía.

No obstante —tal y como veremos en la sección 2.3— la implementación en *ChPT* de los efectos causados por las resonancias más ligeras del espectro hadrónico a través del *IAM* permite cambiar el comportamiento cualitativo de observables como la susceptibilidad escalar o el condensado de quarks, acercándolos a la descripción que de ellos hacen cerca de la región crítica los estudios basados en simulación en el retículo a temperatura finita.

Motivación (i): Colisiones Relativistas de Iones Pesados

Como ya se ha visto, *QCD* provee un escenario teórico adecuado para el estudio de la Interacción Fuerte a través de un número reducido de parámetros que deben determinarse experimentalmente. Sin embargo, los grados de libertad a través de los cuales se estructura no permiten estudiar el comportamiento de la materia confinada más allá del límite en donde el acoplamiento es lo suficientemente débil como para poder utilizar métodos perturbativos.

[19] Las simulaciones en el retículo muestran que ambas transiciones ocurren a la misma temperatura o con unos pocos MeV de diferencia [71].

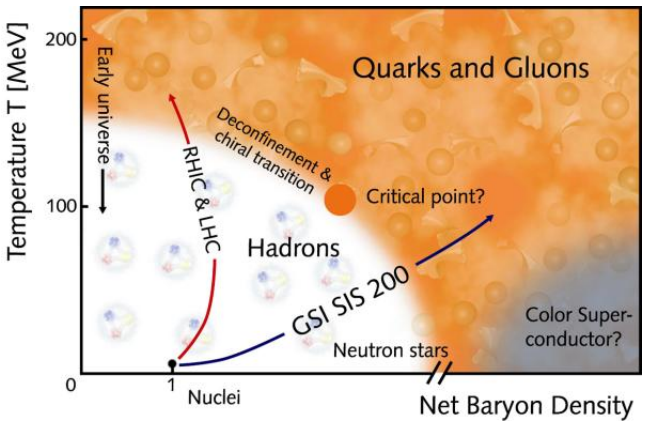

Figura 1.2: Mapa de fases de *QCD* en función del potencial químico y temperatura para valores físicos de las masas de los quarks.
Fuente: GSI.

Las colisiones entre iones pesados a energías relativistas y ultrarelativistas permiten producir materia en condiciones extremas de densidad y temperatura cuyo comportamiento puede predecirse con *QCD*. Este tipo de experimentos permite probar la teoría subyaciente mediante el estudio de las transiciones de desconfinamiento y de restauración quiral —propiedades de carácter fundamental en *QCD*— así como el comportamiento de la materia en las fases hadrónica y desconfinada (*QGP*). Además de esto, el estudio de colisiones entre iones pesados también permite caracterizar la dinámica de la materia nuclear en base a variables macroscópicas, tales como temperatura y densidad, y a partir de ellas estudiar la correspondiente ecuación de estado.

A energías en el centro de masas de entre unos pocos y unas decenas de GeV por nucleón ($\sqrt{s} << 100A\cdot$GeV), los iones que coliden se frenan mutuamente y se consiguen altas densidades bariónicas, mientras que para energías mucho más altas ($\sqrt{s} \gtrsim 100A\cdot$GeV), los dos iones se atraviesan el uno al otro y la región de colisión adquiere cotas bajas de densidad bariónica, pero alcanza temperaturas muy altas. Ambos escenarios pueden encontrarse en la figura (1.2): mientras que *RHIC*[20] y LHC[21] mantienen una línea destinada a experimentos de muy alta energía por nucléon en el centro de masa, GSI SIS 300 planea estudiar la región de alta densidad bariónica[22]. Esta figura distingue una zona de fase hadrónica para bajas temperaturas y bajo potencial químico, separada de las zonas en las que la materia se encuentra desconfinada en forma de *QGP*, y la

[20] BNL, Nueva York, Estados Unidos. Colisiones *Au-Au* con una energía en centro de masa de $\sqrt{s} = 200$ GeV por nucleón, $T_{max} \sim 230$ MeV.
[21] CERN, Ginebra, Suiza. Colisiones *Pb-Pb* con una energía en centro de masa de $\sqrt{s} = 5500$ GeV por nucleón, $T_{max} \sim 260$ MeV.
[22] Darmstadt, Alemania. Colisiones *Au-Au* con una energía en centro de masa de $\sqrt{s} = 40$ GeV por nucleón.

fase de superconductividad de color (*SCC*), caracterizada por bajas temperaturas y alto potencial químico [77, 78].

A partir de la figura (1.2), puede verse que para potencial químico nulo la transición de desconfinamiento se produce avanzando a través del eje de ordenadas en sentido creciente de temperatura, hasta una densidad bariónica crítica de $\rho_0 = 0{,}125$ GeV/fm^3, lo que se cree que podría suceder en los núcleos de ciertas estrellas de neutrones. Por otro lado, para potenciales químicos bajos, la transición podría conseguirse aumentando la temperatura hasta un valor crítico de $T_C = 150 - 200$ MeV$= (1{,}8 - 2{,}4) \times 10^{12}$ K, condiciones que pudieron darse a partir de los dos primeros microsegundos de existencia del universo tras el *Big Bang*.

La evolución espacio-temporal de una colisión ultrarrelativista de iones pesados puede catalogarse en tres etapas: el momento de la colisión, el proceso de termalización, y la hadronización (seguida de un desacoplo o *freeze-out*). Durante la colisión, un gran número de partones se producen determinando las condiciones inciales de toda la evolución posterior. Existen varios modelos[23] para explicar esta etapa inicial, aunque los mecanismos todavía no se comprenden perfectamente.

Inmediatamente después de la colisión el gas de partones está fuera del equilibrio, hasta que las colisiones secundarias entre ellos conducen a un estado de equilibrio y a la posibilidad de describir el sistema mediante un enfoque hidrodinámico. La temperatura del gas comienza a decrecer en el transcurso de su expansión hasta que la temperatura crítica de confinamiento se alcanza. En ese momento el sistema hadroniza y, después, atraviesa una etapa de desacoplo en el que el gas se halla diluido y las interacciones entre partículas cesan (*freeze-out*).

Este *freeze-out* se define en las *RHIC* como el tiempo propio a partir del cual el tiempo medio característico entre colisiones de las partículas del plasma es mayor que el del tiempo característico asociado a la expansión en el seno del plasma; y a partir del cual, también, el equilibrio térmico local se rompe. Existen dos tipos de *freeze-out*: por un lado se puede hablar de *freeze-out* químico, tras el que el número de especies en el plasma queda fijo; y el *freeze-out* térmico, a partir del cual el equilibrio cinético cesa [72].

Motivación (ii): resultados en el retículo

En esta sección presentaré los conceptos básicos que serán utilizados en la sección 2. Ello incluirá una breve introducción al carácter de la transición quiral

[23] *E.g.: Color Glass Condensate* [79], *color-string percolation* [80], ó modelos perturbativos basados en *QCD* [72]. Para una revisión de los distintos escenarios: ver [81].

en función de las masas de los quarks, una pequeña reseña del formalismo *staggered* para fermiones y, finalmente, la descripción de los observables relevantes para nuestro trabajo, en concreto los condensados y la susceptibilidad sustraídos, y las masas de *screening*.

Si consideramos *QCD* con dos sabores y en el límite quiral, la transición de restauración de la simetría quiral es un cambio de fase de segundo orden y pertenece a la clase de universalidad $O(4)$, característica de los modelos de espín en tres dimensiones [82]. Por debajo de la curva que separa las dos fases la simetría quiral está espontáneamente rota y existen tres piones sin masa.

Sin embargo —como ya se ha tenido oportunidad de mostrar al analizar el patrón de ruptura de la simetría quiral en *QCD*— en el mundo físico que nos alberga los quarks *up* y *down* tienen una masa distinta de cero. En ese caso el carácter de la transición pasa a ser un *crossover* analítico [68, 83]: se producen, en efecto, variaciones importantes en ciertos observables, pero —a diferencia de lo que sucede en una transición de segundo orden— no hay discontinuidades asociadas a su descripción.

La naturaleza de la transición quiral en función de los valores de las masas ligeras $m_u = m_d$ y la masa del quark *strange* para potencial químico nulo puede bosquejarse en la llamada *gráfica de Columbia* [84], ilustrada en la figura 1.3.

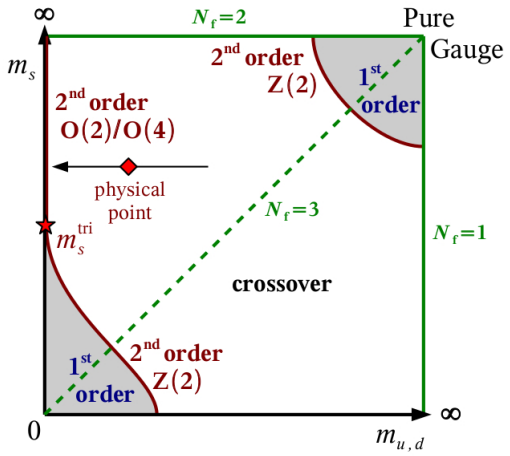

(a)

Figura 1.3: *Gráfica de Columbia*: Carácter de la transición de fase quiral en función de la masa de los quarks para potencial químico nulo. El punto físico está incluido en la región que indica un *crossover*. Las flechas rojas indican el desplazamiento esperado cuando nos acercamos al límite quiral.

En la sección 2 compararemos los resultados calculados mediante *ChPT* con aquéllos que pueden obtenerse mediante simulación en el retículo. El condensa-

do total de quarks a temperatura finita, $\langle\bar{q}q\rangle_T$, contiene una parte de temperatura cero que presenta divergencias ultravioletas, así como términos de contacto procedentes de la ambigüedad inherente a su definición [31]. Con el fin de obtener resultados finitos en el retículo se han propuesto diversos métodos de *renormalización*. El que más será usado en nuestros resultados consiste (ver —por ejemplo— [85, 86] y la discusión en la sección **III** de la publicación 2.2.1) en utilizar el condensado asociado al quark *strange* para calcular el condensado sustraído, $\Delta_{l,s}$, definido a través de

$$\langle\bar{q}q\rangle \to \Delta_{l,s} := \frac{\langle\bar{q}q\rangle_T - \frac{2m_l}{m_s}\langle\bar{s}s\rangle_T}{\langle\bar{q}q\rangle_0 - \frac{2m_l}{m_s}\langle\bar{s}s\rangle_0}, \tag{1.76}$$

donde m_l es la masa asociada a un sabor ligero genérico (o a cada uno de los condensados ligeros por separado) y m_s es la masa del quark *strange*.

De un modo parecido se procede para *renormalizar* las susceptibilidades. Por ejemplo, en [86] —y para la susceptibilidad escalar total— se procede a la sustracción de la parte de temperatura cero dando lugar a la susceptibilidad sustraída, $\Delta\chi$, definida como

$$\Delta\chi(T) = \chi(T) - \chi(0). \tag{1.77}$$

El hecho de que esta cantidad sea directamente medible en el retículo permite tanto la comprobación de la regla de suma que será mostrada en la sección 2 y que representa uno de los resultados de la publicación 2.2.1, como de varios de los resultados de 2.3.1.

Debido a que, como ya hemos dicho, para valores físicos de las masas de los quarks la transición quiral es un *crossover* analítico, el análisis de distintos parámetros de orden da lugar a distintos valores de la *temperatura crítica*[24].

Al presentar algunos de los resultados en la sección 2.1 hablaremos de formalismo de fermiones *staggered* o de *Kogut-Susskind* [87]. Este formalismo pretende arreglar el problema del doble conteo de fermiones (*fermion doubling*) que viene asociado a la discretización de la acción para fermiones libres. Puede probarse [88] que es imposible poner en el retículo fermiones quirales sin producir este problema de doble conteo. El formalismo de *Kogut-Susskind* es uno de los varios métodos[25] que se han propuesto para intentar reducir el número de fermiones espúreos por cada grado de libertad real.

Este procedimiento, entonces, introduce copias espúreas para cada sabor denominadas *tastes* [92] que presenta ciertas similitudes con las violaciones a la simetría de isoespín que se analizan en esta memoria. Las nuevas copias hacen que la acción en el retículo sea invariante bajo un grupo quiral aumentado

[24] Nótese que en rigor debiéramos hablar de *pseudotemperatura crítica* debido a la inexistencia de una transición de fase en sentido riguroso.

[25] *E.g.* fermiones de Wilson [89], fermiones de *Ginsparg-Wilson* [90], *domain wall fermions* [91].

$SU(4) \times SU(4)$ cuya ruptura da lugar a quince pseudo-bosones de Goldstone (más un estado de tipo η') por cada sabor quark. Todos estos nuevos mesones se degeneran en el límite del continuo (al que se llega cuando el espaciado de la red tiende a cero).

En la sección 2.1, a la hora de hablar de los resultados de la publicación 2.2.1, tendremos ocasión de ver la relación entre los resultados que hemos calculado usando *ChPT* y las contribuciones espúreas a las componentes conexa y disconexa de la susceptibilidad quiral escalar que se producen para retículos de espaciado no nulo.

Formalismo de Tiempo Imaginario

De entre los varios métodos enfocados a extender a temperatura finita una teoría cuántica de campos[26], el formalismo de tiempo imaginario (*ITF*) es el más antiguo. Permite calcular fuciones de Green a temperatura finita explotando la analogía entre el operador de Boltzmann y el operador de evolución temporal para tiempos imaginarios [66].

Como no se ha considerado potencial químico distinto de cero, todos los resultados que aparezcan a continuación habrán de entenderse en el contexto de una colectividad canónica. En ella —como es bien sabido— la descripción de un sistema en equilibrio térmico a temperatura T se realiza a través de la llamada función de partición

$$Z(\beta) = \mathrm{Tr}\left(e^{-\beta H}\right), \tag{1.78}$$

donde $\beta = 1/T$ y H es el hamiltoniano del sistema cuántico de muchas partículas, independiente del tiempo[27], y la traza se toma sobre una base completa de autoestados.

Naturalmente, en la colectividad sólo son importantes los promedios térmicos definidos, para un operador genérico $A(t, \vec{x})$ en imagen de Heisenberg, a través de

$$\langle A \rangle_\beta = \mathrm{Tr}\left(\frac{1}{Z(\beta)} e^{-\beta H} A\right). \tag{1.79}$$

Debido a la ciclicidad de la traza involucrada en la anterior ecuación es posible escribir, además,

$$\langle A(t_1)A(t_2)\rangle_\beta = \left\langle A(t_1 + i\beta)A(t_2)\right\rangle, \tag{1.80}$$

que expresa la periocidad en el tiempo imaginario de cualquier observable térmico y conocida como *relación de Kubo-Martin-Schwinger (KMS)* [95, 96]. Nótese que

[26] Véase, por ejemplo, [93, 94].

[27] Dar cabida a un intercambio adicional de partículas desde un reservorio involucraría el reemplazo de H por $H - \mu N$, donde N es el operador número de partículas y μ es el potencial químico.

se ha se ha utilizado formalmente lo que ya se mencionaba anteriormente: la semejanza del operador de Boltzmann $e^{\beta H}$, con el propagador temporal e^{-iHt}, en $t = -i\tau\big|_{\tau=\beta}$, idea fundamental sobre la que recae el formalismo *ITF*.

En efecto

$$e^{-\beta H} A(t - i\beta, \vec{x}) e^{\beta H} = A(t, \vec{x}). \tag{1.81}$$

A través de la ecuación (1.79) es posible calcular el propagador de Feynman térmico asociado al campo escalar a través de

$$\begin{aligned} G(t - t', \vec{x} - \vec{x}') :&= \left\langle \mathcal{T}\left(\phi(t, \vec{x})\phi(t', \vec{x}')\right)\right\rangle_\beta \\ &= \theta(t - t')G^>(t - t', \vec{x} - \vec{x}') + \theta(t' - t)G^<(t - t', \vec{x} - \vec{x}'), \end{aligned} \tag{1.82}$$

siendo $\mathcal{T}$ el producto cronológico usual y

$$\begin{aligned} G^>(t, \vec{x}) &:= \left\langle \phi(t, \vec{x})\, \phi(0, \vec{0})\right\rangle_\beta, \\ G^<(t, \vec{x}) &:= \left\langle \phi(0, \vec{0})\, \phi(t, \vec{x})\right\rangle_\beta = G^>(-t, -\vec{x}), \end{aligned} \tag{1.83}$$

que, debido a la relación *KMS* satisfacen, además,

$$G^>(t, \vec{x}) = G^<(t + i\beta, \vec{x}). \tag{1.84}$$

Las transformadas de Fourier asociadas a los operadores $G^>$ y $G^<$ en la variable temporal son

$$G^{(<,>)}(k_0, \vec{x}) = \int_{-\infty}^{\infty} dt\, e^{ik_0 t} G^{(<,>)}(t, \vec{x}), \tag{1.85}$$

objetos que, debido a la ecuación (1.84), cumplen

$$G^<(k_0, \vec{x}) = e^{-\beta k_0} G^>(k_0, \vec{x}). \tag{1.86}$$

El propagador de Feynman $G(t, \vec{x})$ y los propagadores $G^>(t, \vec{x})$, $G^<(t, \vec{x})$, pueden escribirse en términos de una sola función: la llamada función espectral térmica $\rho(k_0)$, definida a través de

$$\rho(k_0) = G^>(k_0) - G^<(k_0) = \int_{-\infty}^{\infty} dt\, e^{ik_0 t} \left\langle [\phi(t, \vec{x}), \phi(0, \vec{x})]\right\rangle_\beta. \tag{1.87}$$

Puede demostrarse [94] que se trata de una función real, impar en k_0 y que verifica la llamada condición de positividad: $\mathrm{Sgn}(k_0)\rho(k_0) > 0$. Además, en términos de la función espectral, puede escribirse

$$\begin{aligned} G^>(k_0) &= (1 + n_B(k_0))\rho(k_0), \\ G^<(k_0) &= n_b(k_0)\rho(k_0), \end{aligned} \tag{1.88}$$

donde n_B es la función de Bose-Einstein definida a través de

$$n_B(\omega_k) := \frac{1}{\exp \beta\omega_k - 1}. \tag{1.89}$$

Es posible [97] construir la teoría cuántica del campo escalar ϕ mediante la descripción de la función de partición a través de una integral euclídea de caminos en tiempo imaginario $\tau = it$, con $\tau \in \mathbb{R}$,

$$Z[\beta, j] = \int_p [d\phi] \exp\left(S_E(\beta) + \int_0^\beta j(\tau)\phi(\tau) d\tau \right), \tag{1.90}$$

donde $S_E(\beta)$ es la acción euclídea del *lagrangiano* integrada sobre $[0 < \tau < \beta, -\infty < x_i < \infty]$, y el subíndice p en la integral hace referencia a que ha de integrarse sobre caminos que satisfagan la condición de periocidad

$$\phi(\beta, \vec{x}) = \phi(0, \vec{x}), \tag{1.91}$$

traducción al lenguaje de integral de caminos de la relación (1.80), que indica que los observables son periódicos en tiempo imaginario con periodo β.

El segundo término de la exponencial da cuenta de posibles fuentes externas con las que calcular, previa diferenciación, funciones de Green libres a través de

$$\left\langle \mathcal{T}_\tau \left(\phi(\tau_1) \dots \phi(\tau_n) \right) \right\rangle_\beta = (-i)^n \frac{1}{Z[\beta, 0]} \frac{\delta^{(n)} Z[\beta, j]}{\delta j(\tau_1) \dots \delta j(\tau_n)}, \tag{1.92}$$

siendo $\mathcal{T}_\tau$ el operador de ordenación de los campos en la variable τ, definido —por ejemplo y por simplicidad— a través de la función de dos puntos

$$\mathcal{T}_\tau \left(\phi(\tau_1, \vec{x}) \phi(\tau_2, \vec{y}) \right) = \begin{cases} \phi(\tau_1, \vec{x})\, \phi(\tau_2, \vec{y}), & si \quad \tau_1 > \tau_2 \\ \\ \phi(\tau_2, \vec{y})\, \phi(\tau_1, \vec{x}), & si \quad \tau_2 > \tau_1. \end{cases} \tag{1.93}$$

A continuación, caractericemos el *propagador en tiempo imaginario* o *propagador de Matusbara* del campo escalar ϕ como el objeto

$$\Delta(\tau, \vec{x}) := \left\langle \mathcal{T}_\tau \left(\phi(\tau, \vec{x})\, \phi(0, \vec{0}) \right) \right\rangle_\beta, \tag{1.94}$$

definido en el intervalo $\tau \in [-\beta, \beta]$. Debido a su periocidad en el intervalo $[0, \beta]$ su transformada de Fourier resulta

$$\Delta(i\omega_n, \vec{k}) := \int_0^\beta d\tau \exp\left(i\omega_n \tau\right) \Delta(\tau, \vec{k}), \tag{1.95}$$

que lleva asociada la transformación inversa

$$\Delta(\tau,\vec{k}) = \beta^{-1}\sum_n \exp\left(-i\omega_n\tau\right)\Delta(i\omega_n), \tag{1.96}$$

donde las frecuencias ω_n son las llamadas *frecuencias de Matsubara*

$$\omega_n = \frac{2\pi n}{\beta}, \quad n\in\mathbb{Z}. \tag{1.97}$$

En términos de la llamada función espectral el propagador de Matsubara puede escribirse como

$$\Delta(i\omega_n,\vec{k}) = \int_{-\infty}^{\infty}\frac{dk_0}{2\pi}\frac{\rho(k_0)}{k_0 - i\omega_n}, \tag{1.98}$$

cuya expresión para un campo escalar libre de masa m es

$$\Delta_0(i\omega_n) = \frac{1}{\omega_n^2 + \vec{k}^2 + m^2}. \tag{1.99}$$

Con ayuda de esta función espectral térmica podemos calcular también los propagadores *avanzado* , Δ_A, y *retardado*, Δ_R, a través de

$$\begin{aligned}\Delta_R(k_0) &= i\int_{-\infty}^{\infty}\frac{ds}{2\pi}\frac{\rho(s)}{k_0 - s + i0^+},\\ \Delta_A(k_0) &= -i\int_{-\infty}^{\infty}\frac{ds}{2\pi}\frac{\rho(s)}{k_0 - s - i0^+},\end{aligned} \tag{1.100}$$

lo que conduce a la identificación

$$\Delta_R(k_0) = -i\Delta(k_0 + i0^+), \qquad \Delta_A(k_0) = i\Delta(k_0 - i0^+). \tag{1.101}$$

Con objeto de hacer una interpretación física del propagador de Feynman a temperatura finita calculémoslo escribiendo los campos a través de su expansión en modos de Fourier y usando la ecuación (1.79). En este caso resulta

$$\begin{aligned} iG(x-y) &= \frac{1}{Z(\beta)}\sum_n \left\langle \mathcal{T}\left(\phi(x)\phi(y)\right)\right\rangle_\beta e^{-\beta E_n}\\ &= \int\frac{d^3k}{(2\pi)^3}\frac{1}{2\omega_k}\Big((1+n_B(\omega_k))e^{-iK(x-y)} + n_B(\omega_k))e^{iK(x-y)}\Big), \end{aligned} \tag{1.102}$$

donde $\mathcal{T}$ es el operador de ordenación cronológica en las variables x_0 e y_0, $K = (k_0,\vec{k})$ es el cuadrimomento del escalar, y $\omega_k := k_0$.

La ecuación (1.102) tiene una interpretación física en términos de propagación de partículas. En efecto, los tres sumandos representan, respectivamente, la

emisión espontánea a temperatura cero de una partícula en y y su absorción en x (para $x_0 > y_0$), la emisión inducida de partículas en y, y la absorción en x; estos dos últimos proporcionales a funciones de Bose y concomitantes a la presencia de un baño térmico.

Además, a la vista de esta ecuación puede verse que la única modificación a la hora de considerar la evolución térmica de los valores esperados es la del añadir dos contribuciones térmicas en el propagador, libres de divergencias, y que se anulan a temperatura cero. Es precisamente por esto que no es necesario modificar el esquema de renormalización.

Para escribir reglas de Feynman con las que acometer el cálculo diagramático a temperatura finita, será necesario continuar el tiempo analíticamente hacia valores puramente complejos que satisfagan —a consecuencia de la relación (1.80)— la desigualdad $0 \leq \tau := it < \beta$, y cambiar las integrales en la energía por sumas sobre frecuencias discretas (de Matsubara), $k_0 = i\omega_n := 2\pi i n \beta^{-1}$, con la medida apropiada, *i.e.*

$$\int \frac{dk_0}{2\pi} \to i\beta^{-1} \sum_{n=-\infty}^{\infty} . \tag{1.103}$$

Además, las condiciones de conservación de la energía escritas a través de deltas de Dirac para los momentos en cada vértice han de reemplazarse por funciones delta de Kronecker para las frecuencias de Matsubara.

Con estos cambios el propagador térmico puede escribirse como

$$iG(x) = i\beta^{-1} \sum_n \int \frac{d^3k}{(2\pi)^3} \frac{i}{K^2 - m^2} e^{-iK\cdot x} \tag{1.104}$$

donde ha de entenderse $K_0 = i\omega_n$, $x = (\tau, \vec{x})$; con lo que en el espacio de momentos viene dado por

$$iG(K) = \frac{i}{K^2 - m^2} = \frac{i}{k_0^2 - \vec{k}^2 - m^2}, \tag{1.105}$$

con $k_0 = i\omega_n = 2\pi i n T$, $n \in \mathbb{Z}$.

Nótese que los vértices y los factores de simetría de cada diagrama permanecen inalterados: sólo se modifica, como ya se ha dicho, la expresión para las funciones de Green. Además, el formalismo de Matsubara sólo es aplicable a problemas en equilibrio, puesto que la variable temporal ha sido eliminada del juego y sólo es posible describir propiedades estáticas.

Debido a la inclusión del sumatorio en la expresión (1.104), será necesario evaluar sumas sobre frecuencias de Matsubara. En este sentido será particularmente útil usar el Teorema de Cauchy aplicado a un recinto de integración apropiado[28].

[28] Ver [94], por ejemplo.

Sea $f(z)$ una función compleja sin ningún corte, que va a cero suficientemente rápido cuando $|z| \to 0$, entonces

$$\beta^{-1} \sum_n f(i\omega_n) = -\sum_{i_{\text{ceros}}} \frac{\text{Res}(f; z = z_i)}{e^{\beta k_0} - 1}. \tag{1.106}$$

En nuestra memoria de investigación aparecerán tres tipos distintos de funciones térmicas. Por un lado, para el cálculo del condensado será necesario evaluar *loops* o *tadpoles* térmicos de bosones de Goldstone, apareciendo la expresión

$$\begin{aligned} \int \frac{d^3k}{(2\pi)^3} \Delta(\tau, \vec{k}) &= \int \frac{d^3k}{(2\pi)^3} T \sum_n \frac{1}{\omega_n^2 + m^2 + \vec{k}^2} \\ &= \int \frac{d^3k}{(2\pi)^3} \frac{1}{2E_k} + \int \frac{d^3k}{(2\pi)^3} \frac{n_B(E_k)}{E_k} \\ &= G(x=0)^{T=0} + g_1(m,T), \end{aligned} \tag{1.107}$$

donde $E_k^2 = m^2 + \vec{k}^2$ y la función térmica $g_1(m,T)$ está definida por

$$g_1(m,T) = \frac{1}{2\pi^2} \int_0^\infty dk \frac{k^2}{E_k} n_B(E_k). \tag{1.108}$$

El segundo objeto aparece en las susceptibilidades quirales escalares y, por tanto, es precisamente la derivada de la función $g_1(m,T)$ respecto de la masa m del escalar. Se tiene entonces

$$g_2(m,T) = -\frac{\partial g_1(m,T)}{\partial m^2} = \frac{1}{4\pi^2} \int_0^\infty dk \, \frac{n_B(E_k)}{E_k}. \tag{1.109}$$

El tercer objeto es la llamada función J, que aparece de forma natural en la dispersión de dos partículas en dos partículas o en el análisis de la auto-energía que se discutirá al hablar de los resultados en 3.1.1. Puede definirse, a temperatura finita y para masas arbitrarias m_1 y m_2, como

$$J_T(m_1, m_2, |\vec{p}|, i\omega_n) = T \sum_{n \in \mathbb{Z}} \int \frac{d^3q}{(2\pi)^3} \frac{1}{(i\omega_n)^2 - E_1^2} \frac{1}{(i\omega_n - p_0)^2 - E_2^2}, \tag{1.110}$$

con $E_1^2 := m_1^2 + \vec{q}^2$ y $E_2^2 = (\vec{q} - \vec{p})^2 + m_2^2$. Un análisis pormenorizado de las propiedades analíticas y asintóticas de esta función puede encontrarse en el apéndice **B** de 3.1.1.

IAM a temperatura finita

La introducción de interacciones unitarizadas para los piones mejora las predicciones de *ChPT* a través de una descripción más precisa de algunos de

los fenómenos de interés en el estudio de las Colisiones de Iones Pesados como, por ejemplo, el análisis térmico de resonancias o coeficientes de transporte [50, 98–101]. Además, el uso de la llamada Expansión del Virial dentro del contexto de la Teoría Quiral —incluyendo correcciones debidas a unitarización— permite parametrizar de modo consistente las desviaciones respecto al comportamiento mostrado por las contribuciones de tipo gas libre incluidas en la descripción a través del llamado *Hadron Resonance Gas* [102–104].

El *IAM* puede extenderse a temperatura finita incluyendo las correcciones térmicas correspondientes al proceso de dispersión de piones, calculadas en [105] a un *loop* en *ChPT*. La única dependencia térmica está contenida en $t^{(4)}(s,T)$ debido a que —como ya he comentado con anterioridad— la amplitud $t^{(2)}(s)$ no contiene diagramas con *loops* y, por tanto, no contiene funciones de Green térmicas. Las relaciones de unitariedad perturbativas análogas a la relación (1.55) siguen siendo válidas una vez se haya modificado el espacio de fases por el correspondiente espacio de fases térmico definido por

$$\sigma_T(s) := \sigma_0(s)\left\{1 + 2n_B\left(\frac{\sqrt{s}}{2}\right)\right\}, \tag{1.111}$$

y que resulta amplificado respecto al espacio de fases a temperatura cero a través de un factor que tiene en cuenta la diferencia entre la contribución por emisión inducida por el incremento de estados de dos piones salientes, $(1+n_B(E_1))(1+n_B(E_2))$, y la absorción que se produce toda vez que los piones coliden con partículas procedentes del baño térmico, $n_B(E_1)n_B(E_2)$; con E_1 y E_2 las energías de los dos piones externos que colisionan[29].

La moraleja que debemos extraer de todo esto es que podemos seguir utilizando el *IAM* a temperatura finita siempre que reemplacemos el espacio de fases $\sigma_0(s)$ por el espacio de fases térmico $\sigma_T(s)$, y las ondas parciales por sus correspondientes a temperatura finita a través de la consideración de funciones de Green térmicas para los diagramas asociados. Debido a que las colisiones de orden superior están muy suprimidas en el baño térmico, se admite que en este último paso sólo es necesario considerar estados intermedios de dos piones, lo que da lugar a la llamada descripción de *medio diluido*.

Con todo, la expresión general para la amplitud térmica unitarizada a $\mathcal{O}(p^4)$ es, prescindiendo en beneficio de la simplicidad de los índices de isoespín y momento angular,

$$t^{\mathrm{IAM}}_{\mathrm{NLO}} = \frac{\left(t^{(2)}(s)\right)^2}{t^{(2)}(s) - t^{(4)}(s,T)}. \tag{1.112}$$

[29] Nótese que las ondas parciales siempre están definidas en el centro de masa, razón por la que $E_1 = E_2 = \frac{\sqrt{s}}{2}$ y el espacio de fases térmico resulta ser precisamente el definido por la ecuación (1.111).

Por último, para un breve resumen acerca de las propiedades más relevantes de las resonancias $\rho(770)$ y $f_0(500)/\sigma$ generadas a través de la aplicación del *IAM* en *ChPT* puede encontrarse en la sección **IV.A** de la publicación 2.3.1.

Introducción a los resultados

A lo largo de los capítulos 2 y 3 presentaré los principales resultados de la investigación que ha dado lugar a la presente memoria. Todos ellos conciernen al estudio de las propiedades térmicas de gases de bosones de Goldstone a través de un enfoque efectivo que tiene a la Teoría Quiral de Perturbaciones como principal herramienta de estudio.

Las modificaciones sufridas por un observable debidas a la ruptura de isoespín —tanto intrínseca como electromagnética— pueden considerarse en la mayor parte de los casos como pequeñas correcciones numéricas. Sin embargo en determinadas parcelas de conocimiento se han mostrado como un factor relevante —e incluso fundamental— a la hora de explicar la fenomenología de ciertos procesos. Tal es el caso del estudio de las correcciones electromagnéticas a las masas de los mesones ligeros y las correcciones al llamado Teorema de Dashen [40,106–110], las amplitudes de scattering pion-pion [38,39] o pión-kaón [111–113], así como a posibles escenarios para violación de la simetría CP [114], *mixing* de las partículas f_0 y a_0 [115] y decaimiento de kaones [116–118], o el análisis de observables asociados precisamente a la ruptura como la regla de suma [31] que permite conectar los cocientes de los condensados asociados a los quark *down* y *strange* frente al más ligero quark *up*. Una lista más pormenorizada y actualizada de procesos hadrónicos en los que la ruptura de isoespín juega un rol importante puede consultarse en la referencia [119].

El capítulo 2 consta de tres secciones. En las dos primeras, *vid.* 2.1 y 2.2, se estudiarán los efectos de la ruptura de isoespín de la simetría quiral sobre los parámetros de orden (condensado de quarks y susceptibilidades quirales escalares) de un gas de mesones ligeros (piones, kaones y etas) tanto a temperatura cero como a temperatura finita. Para ello se implementarán los efectos de carga electromagnética y de ruptura intrínseca a través de la inclusión de fuentes externas en los canales vectorial y escalar, respectivamente. La sección 2.3 estudiará la relación entre la susceptibilidad pseudoescalar y el condensado escalar de quarks, así como el escenario de restauración de simetría quiral basado en la degeneración de las susceptibilidades escalar y pseudoescalar en el marco de *ChPT* y de *ChPT* unitarizada.

En el capítulo 3 analizaré las correcciones a la auto-energía de un gas de piones inmerso en un baño térmico permitiendo el intercambio de fotones virtuales. Esto conducirá —previa definición— a la posibilidad de establecer una masa térmica para los piones de la colectividad, así como al estudio de las propiedades exhibidas por observables asociados a la parte imaginaria de la auto-energía, como por ejemplo la anchura térmica o el recorrido libre medio.

Parte del interés fenomenológico de este estudio reside en que, debido al acoplo con la interacción electromagnética, la parte real de la auto-energía de piones cargados y neutros —así como la anchura de desintegración térmica asociada a procesos de dispersión con partículas del medio— exhibe diferencias. Aunque creemos que estas diferencias son numéricamente pequeñas podrían, en principio, ser detectadas en los experimentos de Colisiones de Iones Relativistas y, por tanto, su consideración puede ayudar a arrojar algo más de luz acerca de las fases hadrónica y de termalización en este tipo de procesos.

En este mismo capítulo revisaré qué modificaciones a los resultados que he obtenido previamente en *ChPT* y qué nueva información se obtiene cuando se incluye la física de resonancias ligeras. Esta extensión se efectuará a través de la inclusión explícita de las primeras partículas pesadas del espectro hadrónico mediante la saturación de los canales vectorial y axial por las partículas ρ y a_1 en forma de estados asintóticos vía un modelo de resonancias.

Es precisamente este contexto *más allá de la física de piones* el que permite establecer una relación entre los capítulos 2 y 3 por medio del análisis de dos escenarios de restauración de simetría quiral relacionados con la degeneración en masa de las corrientes asociadas a los canales escalar-pseudoescalar y axial-vectorial, respectivamente.

2

Ruptura de isoespín sobre parámetros de orden asociados a la restauración de la simetría quiral

Este capítulo está formado por las secciones 2.1, 2.2 y 2.3, que contienen las publicaciones 2.1.1, 2.2.1 y 2.3.1, respectivamente.

Los principales objetivos de esta investigación en relación con los procesos de baja energía que se producen durante la fase hadrónica de la Colisión de Iones Relativistas han sido el estudio sistemático a través de *ChPT* —y de su extensión unitarizada en el caso de la sección 2.3— de los parámetros de orden asociados a la ruptura espontánea y a la restauración de la simetría quiral, así como la comparación de estos resultados con los que aparecen en la literatura publicada sobre el tema hasta la fecha usando tanto teorías efectivas [120–124] como estudios en el retículo [125–127].

Parámetros de orden a temperatura cero

La publicación 2.1.1 analiza el comportamiento del condensado de quarks a temperatura cero en *SU(2)-ChPT*, así como para los mesones ligeros procedentes de la ruptura espontánea de la simetría $SU_L(3) \times SU_R(3)$, *vid.*: piones, kaones y etas.

Las correcciones debidas a la ruptura de la simetría de isoespín a través de la Teoría Quiral de Perturbaciones en el cálculo de condensados de quarks han sido realizadas mediante un análisis sistemático a partir del *lagrangiano* quiral efectivo para el caso de dos sabores en [39], y a través de la introducción de correcciones electromagnéticas a la masa de kaones y piones en [121]. En este último caso sólo las constantes de baja energía electromagnéticas que intervienen en en el cálculo de las masas son tomadas en cuenta.

El interés inicial de esta investigación fue el de complementar estos resultados y confirmar que la ruptura de isoespín sobre estos observables representa una pequeña corrección. En efecto, el análisis sistemático en la teoría de dos y tres sabores que presento aborda el estudio completo y sistemático de la sensibilidad de los condensados con efectos de ruptura de isoespín intrínseca y electromagnética al cambio en las constantes de baja energía, y permite analizar la compatibilidad de nuestros resultados con anteriores trabajos. Además, de esta manera, puede evaluarse la importancia de considerar o no este tipo de correcciones en relación con los errores que actualmente presentan las técnicas de simulación en el retículo.

Asimismo, los resultados que defiendo plantean el uso de una hipótesis acerca del comportamiento del vacío de *QCD* respecto de la inclusión de efectos de ruptura electromagnética. Debido a que el condensado de quarks, $<\bar{q}q>$, es un parámetro de orden de la simetría quiral; exhibe un valor no nulo como consecuencia de la ruptura explícita y espontánea de esta simetría. Por este motivo resulta natural esperar que cualquier nuevo término que venga a romper explícitamente la simetría quiral —por ejemplo los términos de ruptura de isoespín— contribuyan a hacer que su valor absoluto aumente, en analogía con el comportamiento de la magnetización espontánea en un material ferromagnético bajo la influencia de un campo magnético externo.

No es posible esgrimir un argumento que asegure, *a priori*, el comportamiento ferromagnético del vacío de *QCD*. Sin embargo, existen varios indicadores que evidencian un comportamiento similar como respuesta ante estímulos análogos. Sirvan a modo de ejemplo la modificación del condensado debida exclusivamente

a ruptura intrínseca a órdenes $O(p^4)$ y $O(p^6)$ en *ChPT* [120], el cambio de la temperatura crítica de restauración quiral al aumentar la masa de los piones [70,128] o el hecho de que los resultados del retículo[1] para el condensado sean sistemáticamente mayores [125] que los obtenidos por estimación directa [123]. Todos ellos indican que existen indicios de una respuesta ferromagnética del vacío de *QCD* bajo cambios en la masa.

Es claro, no obstante, que existen diferencias importantes entre ambas fuentes de ruptura que hacen que el problema deba tratarse con cuidado. En el capítulo 1 ya he hablado acerca del problema de la incorporación de fuentes externas al *lagrangiano* de *ChPT*, y del hecho de que la ruptura electromagnética tiene una naturaleza distinta a la ruptura intrínseca en tanto que se acopla al canal vectorial en lugar de ser una fuente de tipo escalar. Al estudiar el patrón de ruptura explícita debida a la presencia de carga mostré cómo —incluso en el hipotético caso de que los valores de las cargas de los quarks ligeros sean iguales— la simetría quiral se rompe en presencia de una fuente externa escalar (necesaria para calcular los condensados), así que es, también, un factor que contribuye a aumentar el valor absoluto del condensado de quarks.

A través de la asunción de esta hipótesis hemos obtenido más información acerca de los valores numéricos que toman estas mismas combinaciones de constantes electromagnéticas de baja energía que aparecen en el cálculo de los condensados. El conocimiento general de estas constantes en la literatura es —hasta donde he podido consultar— bastante limitado, siendo considerablemente más abundante en la teoría de tres sabores, donde han sido calculados a partir de saturación de resonancias [130], y en modelos de gran N_C y de *Nambu-Jona-Lasinio* [131] complementados a partir de información obtenida mediante métodos de *QCD* perturbativa [132] y el uso de reglas de suma [133,134] a partir de resonancias ligeras.

Esto no deja, sin embargo, en una posición de marcada inferioridad a la teoría de dos sabores puesto que —a este orden y mediante un proceso de desacoplo del quark *strange*— es posible relacionar las combinaciones de constantes de baja energía en las dos teorías a costa de introducir una dependencia explícita a través de masas de mesones. Este desacoplo ha sido ya realizado parcialmente para ciertas combinaciones de *LECs* que aparecen en el cálculo de la masa del pión neutro [135], en dispersión de piones [31,135,136] y en el análisis de la vida media del pionio [135,137]; y de modo exhaustivo a partir de un análisis del *lagrangiano* utilizando métodos funcionales en el límite quiral [138]. En este sentido los resultados que presento constituyen un análisis complementario a los

[1] Aunque a fecha de hoy la técnica de estas simulaciones ha conseguido trabajar de modo controlado con masas de piones similares a las físicas [129], en el trabajo citado las masas para el pión permanecen por encima del valor físico.

ya existentes para las relaciones de desacoplo del quark *strange* en el marco de la Teoría Quiral de Perturbaciones.

De cualquier modo, la separación de las contribuciones electromagnéticas e intrínsecas en cualquier observable es siempre ambigüa [108, 131, 133, 139] y depende de la prescripción que se utilice. Esto es debido a que observables que pertenecen de modo genuino a *QCD* (como por ejemplo las masas de los quarks) dependen implícitamente de correcciones electromagnéticas a través de las ecuaciones de evolución del Grupo de Renormalización en la teoría completa (*QCD+EM*).

No existe una prescripción única y general que permita separar los efectos electromagnéticos de los de ruptura intrínseca y, por tanto, la identificación de *EM LECs* de forma independiente a las *LECs* de naturaleza no electromagnética no está asegurada en general para todo orden.

Pese a esto, debido a que las *LECs* que aparecen en el *lagrangiano* quiral $\mathcal{O}(p^4)$ son, por definición, independientes de la carga y de las masas de los quarks, es posible extraer la correspondencia entre las *EM LECs* *a nivel árbol* haciendo $m_u = m_d$ en la condición general. Una vez hecha esta identificación, hemos realizado también la correspondencia entre las *LEC* no electromagnéticas *a nivel árbol*, obteniendo a este orden la separación completa de efectos de carga (perfectamente coincidente con los resultados de [138]). Hay que notar, no obstante, que este método de aproximación no es necesariamente válido para órdenes superiores debido a la existencia de términos en el *lagrangiano* que mezclan las dos fuentes de ruptura de isoespín.

A pesar de esta separación, los resultados presentes en la literatura calculan las constantes de baja energía electromagnética a partir de análisis experimentales, por lo que estas *LECs experimentales* distan de tener una naturaleza independiente de la carga y de la masa. La voluntad de comparar nuestros resultados con estas últimas hace necesario tener en cuenta esta posible fuente de errores a la hora de estimar la conveniencia del uso de las relaciones de correspondencia entre constantes de baja energía *a nivel árbol*.

En este punto entra en juego un nuevo argumento para la discusión de los resultados: si bien es posible llegar a separar las *LECs* a través una nueva aproximación basada en el hecho de que las correcciones electromagnéticas son pequeñas en el caso del condensado ligero total, en general habrá que utilizar la relación completa que incluye la mezcla entre los distintos tipos de constantes de baja energía.

En efecto, esta aproximación no es confiable en el caso del parámetro de orden de la ruptura de isoespín, *vid.* $<\bar{u}u - \bar{d}d>$, donde los efectos de ruptura

intrínseca y electromagnética son los únicos que contribuyen, siendo formal y numéricamente comparables.

Resulta entonces que las condiciones de correspondencia sobre los grupos de constantes de baja energía que aparecen en este último han de tomarse *cum grano salis* a la hora de comparar con las *EM LECs* de la literatura debido a que la separación directa de la parte electromagnética haciendo $m_u = m_d$ no es numéricamente confiable.

La existencia de esta ambigüedad sumada, por supuesto, a la distinta precisión numérica de cada trabajo, hace que los datos obtenidos para las *EM LECs* en la literatura no sean completamente compatibles entre sí: los resultados dependen forzosamente de la prescripción usada para la separación, y ésta afecta de modo necesario a la dependencia con la escala de renormalización de *QCD* y con el *gauge*.

A pesar de esta dificultad existe un rango de de estabilidad en el que la variación con esta escala de renormalización es suave y compatible con los errores teóricos [131, 132]. Además, el hecho de que los resultados para *SU(3)-ChPT* se escriban en términos de los grupos de constantes K_7^r, $K_8^r(\mu)$ y $K_9^r(\mu) + K_{10}^r(\mu)$, todos ellos independientes del *gauge* [132, 133], refuerza su carácter predictivo, toda vez que ya fueron comprobadas —al igual que todos y cada uno de los observables que presento en este trabajo— como independientes de la escala de renormalización de la Teoría Quiral.

Desde un punto de vista pragmático, muchos de los trabajos de investigación consultados asumen la llamada *hipótesis de valores naturales*, según la cual cualquier constante de baja energía yace en el intervalo $[-1/16\pi^2, 1/16\pi^2]$ cuando se evalúa la escala de renormalización quiral en la masa de la primera resonancia ligera, *i.e.* $\mu_\chi = M_\rho$ [39, 40]. La publicación 2.1.1 muestra que —mediante el uso de la hipótesis ferromagnética— se obtienen ligaduras (independientes del *gauge* y de la escala quiral) que constriñen el intervalo en el que yace el valor numérico de las combinaciones de constantes de baja energía que aparecen en los resultados que expongo.

Estas cotas mejoran la aproximación de valores naturales, si bien es cierto que al incluir el sector de extrañeza no nula (*SU(3)-ChPT*) la hipótesis pierde efectividad —incluso al considerar sólo el condensado ligero $<\bar{u}u + \bar{d}d>$— debido a que la masa del quark *strange* es considerablemente más grande que cualquiera de las masas ligeras m_u, m_d y distorsiona la serie perturbativa quiral. En cualquier caso, y debido a que los valores calculados para estas constantes en la literatura son aproximadamente del mismo orden, he asumido valores naturales siempre que sea necesario extraer información numérica de los resultados.

Aunque la descripción de baja energía de los parámetros de orden que se

efectúa en el presente trabajo puede escribirse en términos de cantidades físicas como masas y constantes de desintegración de grados de libertad confinados evitando —al menos inicialmente— su relación con parámetros típicos de *QCD*, estos comentarios son útiles debido a que una parte de los objetivos tiene como finalidad la comparación entre las estimaciones de *EM LECs* procedentes de la Teoría Quiral a través de cotas basadas en la de respuesta ferromagnética del vacío y *EM LECs* obtenidas mediante rastreo bibliográfico, obtenidas a partir de diversos métodos. Es de vital importancia, entonces, ser consistente con la prescripción de separación de efectos de carga e intrínsecos que se usen en esos trabajos.

La equivalencia formal entre los grupos de constantes de baja energía también permite analizar las diferencias entre los condensados totales en la teoría de dos y tres sabores de una forma auto-contenida y homogénea, permitiendo mostrar que los resultados obtenidos —al menos en el contexto de Teoría Quiral de Perturbaciones estándar[2]— indica que los condensados de quarks ligeros, u y d, toman prácticamente el mismo valor numérico cerca del límite quiral.

Existe una dificultad añadida en la evaluación de los condensados a partir de este análisis efectivo: es bien sabido [31] que la definición del condensado de quarks, $<\bar{q}q>$, adolece de una ambigüedad que se refleja en la Teoría Quiral de Perturbaciones a través de su dependencia en los llamados términos de contacto: constantes que, al igual que las *LECs*, son necesarias para absorber las divergencias procedentes de los diagramas de *loops* pero que, sin embargo, —y a diferencia de lo que sucede con las constantes de baja energía— no tienen contenido físico en tanto que no es posible su determinación a partir de experimentos.

Resulta, por tanto, altamente deseable encontrar resultados que no dependan de este tipo de término, y eso es precisamente lo que se consigue a través de la regla de suma que relaciona las cantidades $<\bar{d}d>/<\bar{u}u>$ y $<\bar{s}s>/<\bar{u}u>$ con parámetros físicos de la teoría directamente vinculados a la ruptura de isoespín.

Con todo, los principales resultados de la publicación 2.1.1 pueden resumirse como sigue:

- El cálculo de los condensados de quark a un *loop* incorporando las modificaciones debidas a la ruptura, tanto intrínseca como electromagnética, en la Teoría Quiral de Perturbaciones para dos y tres sabores proporciona resultados finitos, *model-independent* e independientes, también, de la escala de renormalización de la Teoría Quiral.

  Los resultados numéricos se han calculado exclusivamente en *SU(3)-ChPT* debido a la falta de información inicial sobre las *EM LECs* en *SU(2)-ChPT*.

[2] Ver referencias [140–142] para encontrar diversos análisis en diferentes escenarios de ruptura de simetría quiral.

Las correcciones son pequeñas ($\sim 1\,\%$) respecto a la asunción de la simetría de isoespín desde el principio, y compatibles con los errores actuales que presentan los cálculos en el retículo [125].

Asumiendo, a efectos numéricos, la aproximación de valores naturales encontramos que las diferencias en los condensados $<\bar{u}u>$, $<\bar{d}d>$ y $<\bar{s}s>$ —convenientemente normalizados a su valor *leading order*— respecto de los que aparecen en [121], varían entre un $2\,\%$ para los condensados ligeros, y el $4\,\%$ para el *strange*. Aunque estos valores representan pequeñas correcciones, son numéricamente relevantes debido a la precisión con que se calculan estas cantidades en la citada publicación.

En cuanto a la asimetría de vacío, $<\bar{d}d>/<\bar{u}u>-1$, cuyo valor es nulo en el límite de isoespín (y por tanto debiera reflejar mayor sensibilidad): las diferencias entre considerar apropiadamente las contribuciones de todas las *EMLECs* e incluirlas a través de correcciones procedentes de términos que violan el Teorema de Dashen se sitúan entre un $15\,\%$ y un $24\,\%$, según se escojan las cotas inferior o superior de la aproximación de valores naturales. Esto indica que el tratamiento completo a nivel *lagrangiano* de los efectos de carga es importante para el estudio de observables que son idénticante nulos en el límite de isoespín.

- La asunción de la hipótesis de respuesta ferromagnética para el vacío —junto con una prescripción adecuada para la separación de la parte electromagnética de la no electromagnética en el cálculo de los condensados— da lugar a distintas cotas inferiores para el valor numérico de las combinaciones de constantes electromagnéticas de baja energía que aparecen en el cálculo del parámetro de orden asociado a la restauración de simetría quiral, $<\bar{q}q>$, tanto en dos como en tres sabores.

  La restricción es mayor en el caso de condensados ligeros en *SU(3)-ChPT*, pero asimismo menos confiables debido a la distorsión que introduce la masa del quark *strange* en la serie perturbativa quiral.

  Estas cotas inferiores son independientes de la escala de renormalización de la Teoría Quiral y, por tanto, representan verdaderas predicciones *model independent* en el sector de baja energía de la Interacción Fuerte. A la hora de comparar estos resultados con el resto de valores presentes en la literatura especializada —basados en cálculos de *QCD*— es necesario indicar qué tipo de prescripción de separación entre efectos electromagnéticos y no electromagnéticos se usa. Esta misma prescripción introduce indefectiblemente una dependencia en la escala de renormalización de *QCD* y en el *gauge*.

  Con estos resultados en mano —y utilizando la misma prescripción[3] que en los trabajos consultados— se ha comprobado que las constantes de baja

[3] Consistente en la separación directa de la parte $e = 0$.

energía que toman parte en el cálculo de las ligaduras presentadas en este trabajo son independientes del *gauge*. También se ha probado que todos y cada uno de los valores de las constantes de baja energía electromagnéticas que se han consultado en la literatura cumplen estas ligaduras, lo que constituye una comprobación de consistencia a los resultados que defiendo.

❧ Las correcciones a la regla de suma que conecta los cocientes $<\bar{d}d>/<\bar{u}u>$ y $<\bar{s}s>/<\bar{u}u>$ debidas a ruptura electromagnética son del mismo orden numérico que las debidas a ruptura intrínseca (las únicas consideradas en el artículo original [31]), y han de ser incluidas, por tanto, en un análisis consistente de la violación de isoespín. Esta regla de suma permite calcular la asimetría de vacío, arrojando un resultado compatible con los que he encontrado en la literatura.

El resultado final es independiente de la escala de renormalización de la Teoría Quiral y de términos de contacto, por lo que constituye un genuino observable en el sector de baja energía de la Interacción Fuerte.

❧ De modo complementario a los resultados en el límite de isoespín que aparecen en [138], se ha efectuado una correspondencia entre el condensado ligero calculado en *SU(2)-ChPT* y en *SU(3)-ChPT* a partir del desacoplo en masa del quark *strange*. Esta correspondencia se extiende a las constantes de baja energía de ambas teorías, donde las de naturaleza electromagnética se mezclan —en pie de igualdad— con aquéllas de carácter no electromagnético. Esto indica que al considerar los valores físicos para la masa y carga de los quarks es necesario acometer nuevas aproximaciones si se pretende separar ambos grupos de constantes y hacer explícita la correspondencia entre *EM LECs* de las teorías de dos y tres sabores.

Considerando formalmente las constantes de baja energía electromagnéticas que aparecen en el *lagrangiano* como independientes de la masa y la carga sí es posible separar ambos efectos y escribir relaciones de correspondencia entre grupos de constantes homólogas de *SU(2)-ChPT* y *SU(3)-ChPT* a partir de expandir en $1/m_s$ las expresiones para el condensado ligero total y el parámetro de orden de la ruptura de isoespín. Sin embargo estas relaciones pueden no ser numéricamente confiables a la hora de compararlos con los resultados para las constantes de baja energía que aparecen en la literatura debido a que los métodos que se usan para su determinación distan mucho de considerar unas *LECs a nivel árbol*.

Una cierta solución intermedia para la separación de estas *LECs* consiste en asumir, en la relación de correspondencia completa, la hipótesis adicional de que las correcciones electromagnéticas dan lugar sólo a una pequeña modificación. Aunque está hipótesis es verdaderamente razonable en el caso

del condensado total, dista bastante de ser numéricamente confiable en el caso de la diferencia de condensados ligeros.

2.1.1 Publicación:

A. Gómez Nicola, R. Torres Andrés,
Isospin-breaking quark condensates in Chiral Perturbation Theory,
J. Phys. G **39** (2012), 015004

J. Phys. G: Nucl. Part. Phys. **39** (2012) 015004 (21pp) doi:10.1088/0954-3899/39/1/015004

Isospin-breaking quark condensates in chiral perturbation theory

A Gómez Nicola and R Torres Andrés

Departamento de Física Teórica II, Univ. Complutense. 28040 Madrid, Spain

E-mail: gomez@fis.ucm.es and rtandres@fis.ucm.es

Received 30 July 2011
Published 1 December 2011
Online at stacks.iop.org/JPhysG/39/015004

Abstract

We analyze the isospin-breaking corrections to quark condensates within one-loop $SU(2)$ and $SU(3)$ chiral perturbation theory including $m_u \neq m_d$ as well as electromagnetic (EM) contributions. The explicit expressions are given and several phenomenological aspects are studied. We analyze the sensitivity of recent condensate determinations to the EM low-energy constants (LEC). If the explicit chiral symmetry breaking induced by EM terms generates a ferromagnetic-like response of the vacuum, as in the case of quark masses, the increasing of the order parameter implies constraints for the EM LEC, which we check with different estimates in the literature. In addition, we extend the sum rule relating quark condensate ratios in $SU(3)$ to include EM corrections, which are of the same order as the $m_u \neq m_d$ ones, and we use that sum rule to estimate the vacuum asymmetry within ChPT. We also discuss the matching conditions between the $SU(2)$ and $SU(3)$ LEC involved in the condensates, when both isospin-breaking sources are taken into account.

(Some figures may appear in colour only in the online journal)

1. Introduction

The low-energy sector of QCD has been successfully described over recent years within the chiral Lagrangian framework. Chiral perturbation theory (ChPT) is based on the spontaneous breaking of the chiral symmetry $SU_L(N_f) \times SU_R(N_f) \to SU_V(N_f)$ with $N_f = 2, 3$ light flavours and provides a consistent and systematic model-independent scheme to calculate low-energy observables [1–3]. The effective ChPT Lagrangian is constructed as the more general expansion $\mathcal{L} = \mathcal{L}_{p^2} + \mathcal{L}_{p^4} + \cdots$ compatible with the QCD underlying symmetries, where p denotes derivatives or meson mass and external momentum below the chiral scale $\Lambda_\chi \sim 1$ GeV.

The $SU_V(N_f)$ group of vector transformations corresponds to the isospin symmetry for $N_f = 2$. In the $N_f = 3$ case, the vector group symmetry is broken by the strange-light quark mass difference $m_s - m_{u,d}$, although m_s can still be considered as a perturbation compared to Λ_χ, leading to $SU(3)$ ChPT [3]. In the $N_f = 2$ case, the isospin symmetric limit is a very good

approximation in nature. However, there are several known examples where isospin breaking is phenomenologically relevant at low energies, such as sum rules for quark condensates [3], meson masses and corrections to Dashen's theorem [4], pion–pion [5, 6] and pion–kaon [7, 8] scattering in connection with mesonic atoms [9, 10], CP violation [11], $a_0 - f_0$ mixing [12], kaon decays [13, 14] and other hadronic observables (see [15] for a recent review).

The two possible sources of isospin breaking are the $m_d - m_u$ light quark mass difference and electromagnetic (EM) interactions. Both can be accommodated within the ChPT framework. The former is accounted for by modifying the quark mass matrix and generates a $\pi^0\eta$ mixing term in the $SU(3)$ Lagrangian [3]. The expected corrections from this source are of order $(m_d - m_u)/m_s$. On the other hand, EM interactions, which in particular induce mass differences between charged and neutral light mesons, can be included in ChPT via the external source method and give rise to new terms in the effective Lagrangian [4–6, 16–18] of order $\mathcal{L}_{e^2}$, $\mathcal{L}_{e^2p^2}$ and so on, with e the electric charge. These terms fit into the ChPT power counting scheme by considering formally $e^2 = \mathcal{O}(p^2/F^2)$, with F the pion decay constant in the chiral limit.

The purpose of this paper is to study the isospin-breaking corrections to quark condensates, whose main importance is their relation to the symmetry properties of the QCD vacuum. The singlet contributions $\langle\bar{u}u + \bar{d}d\rangle$ for $SU(2)$ and $\langle\bar{u}u + \bar{d}d + \bar{s}s\rangle$ for $SU(3)$ are order parameters for chiral symmetry, while the isovector one $\langle\bar{u}u - \bar{d}d\rangle$ behaves as an order parameter for isospin breaking, which is not spontaneously broken [19]. We will calculate the condensates within one-loop ChPT, which ensures the model independence of our results, and will address several phenomenological consequences. The two sources of isospin breaking will be treated consistently on the same footing, which will allow us to test the sensibility of previous phenomenological analysis to the EM low-energy constants (LEC). Moreover, the EM corrections induce an explicit breaking of chiral symmetry which will lead to lower bounds for certain combinations of the LEC involved, provided the vacuum response is ferromagnetic, as in the case of quark masses. In addition, in $SU(3)$ one can derive a sum rule relating the different condensate ratios for $m_u \neq m_d$ [3] which, as we will show here, receives an EM correction not considered before and of the same order as that proportional to $m_u - m_d$. The latter is useful to estimate the vacuum asymmetry $\langle\bar{d}d\rangle/\langle\bar{u}u\rangle$ reliably within ChPT. An additional aspect that we will discuss is the matching of the $SU(2)$ and $SU(3)$ LEC combinations appearing in the condensates when both isospin-breaking sources are present, comparing with previous results in the literature. The analysis carried out in this work will serve also to establish a firm phenomenological basis for its extension to finite temperature, in order to study different aspects related to chiral symmetry restoration [20].

With the above motivations in mind, the paper is organized as follows: in section 2 we briefly review the effective Lagrangian formalism needed for our present work, paying special attention to several theoretical issues and to the numerical values of the parameters and LEC needed here. Quark condensates for $SU(2)$ are calculated and analyzed in section 3, where we discuss the general aspects of the bounds for the EM LEC based on chiral symmetry breaking. In that section we also comment on the analogy with lattice analysis. The $SU(3)$ case is separately studied in section 4. In that section, we first perform a numerical analysis of the isospin-breaking corrections, paying special attention to the effect of the EM LEC in connection with previous results in the literature. In addition, we obtain the EM corrections to the sum rule for condensate ratios, which we use to estimate the vacuum asymmetry within ChPT. We also provide the LEC bounds for this case, checking them with previous LEC estimates and, finally, we discuss the matching conditions for the LEC involved. In the appendix we collect the Lagrangians of fourth order and the renormalization of the LEC used in the main text.

2. Formalism: effective Lagrangians for isospin breaking

The effective chiral Lagrangian up to fourth order is given schematically by

$$\mathcal{L}_{\text{eff}} = \mathcal{L}_{p^2+e^2} + \mathcal{L}_{p^4+e^2p^2+e^4}. \tag{1}$$

The second-order Lagrangian is the familiar nonlinear sigma model, including now the gauge coupling of mesons to the EM field through the covariant derivative, plus an extra term:

$$\mathcal{L}_{p^2+e^2} = \frac{F^2}{4}\,\text{tr}\,[D_\mu U^\dagger D^\mu U + 2B_0\mathcal{M}(U+U^\dagger) + C\text{tr}[QUQU^\dagger]. \tag{2}$$

Here, F is the pion decay constant in the chiral limit and $U(x) \in SU(N_f)$ is the Goldstone boson (GB) field in the exponential representation $U = \exp[\mathrm{i}\Phi/F]$ with

$$SU(2): \Phi = \begin{pmatrix} \pi^0 & \sqrt{2}\pi^+ \\ \sqrt{2}\pi^- & -\pi^0 \end{pmatrix},$$
$$SU(3): \Phi = \begin{pmatrix} \pi^0 + \frac{1}{\sqrt{3}}\eta & \sqrt{2}\pi^+ & \sqrt{2}K^+ \\ \sqrt{2}\pi^- & -\pi^0 + \frac{1}{\sqrt{3}}\eta & \sqrt{2}K^0 \\ \sqrt{2}K^- & \sqrt{2}\bar{K}^0 & \frac{-2}{\sqrt{3}}\eta \end{pmatrix}, \tag{3}$$

with η the octet member with $I_3 = S = 0$. The covariant derivative is $D_\mu = \partial_\mu + \mathrm{i}A_\mu[Q,\cdot]$ with A the EM field. $\mathcal{M}$ and Q are the quark mass and charge matrices, respectively, i.e. in $SU(3)$ $\mathcal{M} = \text{diag}(m_u, m_d, m_s)$ and $Q = \text{diag}(e_u, e_d, e_s)$ with $e_u = 2e/3$, $e_d = e_s = -e/3$ for physical quarks. The additional term in (2), the one proportional to C, can be understood as follows: the QCD Lagrangian for $m_u = m_d$ coupled to the EM field is not invariant under an isospin transformation $q \to gq$ with $g \in SU(N_f)$ and q the quark field. However, it would be isospin invariant if the quark matrix Q is treated as an external field transforming as $Q \to g^\dagger Qg$. Therefore, the low-energy effective Lagrangian has to include all possible terms compatible with this new symmetry, in addition to the standard QCD symmetries. The lowest order $\mathcal{O}(e^2)$ is the C-term in (2), since U transforms as $U \to g^\dagger Ug$. Actually, one allows for independent 'spurion' fields $Q_L(x)$ and $Q_R(x)$ transforming under $SU_L(N_f) \times SU_R(N_f)$ so that one can build up the new possible terms to any order in the chiral Lagrangian expansion, taking in the end $Q_L = Q_R = Q$ [4].

In the previous expressions, $F, B_0 m_{u,d,s}, C$ are the low-energy parameters to this order. Working out the kinetic terms, they can be directly related to the leading-order (LO) tree-level values for the decay constants and masses of the GB. In $SU(2)$, the tree-level masses to LO are

$$M^2_{\pi^+} = M^2_{\pi^-} = 2\hat{m}B_0 + 2C\frac{e^2}{F^2},$$
$$M^2_{\pi^0} = 2\hat{m}B_0, \tag{4}$$

with $\hat{m} = (m_u + m_d)/2$ the average light quark mass. Note that both terms contributing to the charged pion mass are of the same order in the chiral power counting, although numerically $\left(M^2_{\pi^\pm} - M^2_{\pi^0}\right)/M^2_{\pi^0} \simeq 0.1$, which we will use in practice as a further perturbative parameter to simplify some of the results.

In the $SU(3)$ case, the mass term in (2) induces a mixing contribution between the π^0 and the η meson fields given by $\mathcal{L}_{\text{mix}} = (B_0/\sqrt{3})(m_d - m_u)\pi^0\eta$. Therefore, the kinetic term has to be brought to the canonical form before identifying the GB masses, which is performed by the field rotation [3]:

$$\pi^0 = \bar{\pi}^0\cos\varepsilon - \bar{\eta}\sin\varepsilon,$$
$$\eta = \bar{\pi}^0\sin\varepsilon + \bar{\eta}\cos\varepsilon, \tag{5}$$

where the mixing angle is given by

$$\tan 2\varepsilon = \frac{\sqrt{3}}{2}\frac{m_d - m_u}{m_s - \hat{m}}. \tag{6}$$

Once the above $\pi^0\eta$ rotation is carried out, the $SU(3)$ tree-level meson masses to LO read

$$\begin{aligned}
M^2_{\pi^+} &= M^2_{\pi^-} = 2\hat{m}B_0 + 2C\frac{e^2}{F^2},\\
M^2_{\pi^0} &= 2B_0\left[\hat{m} - \frac{2}{3}(m_s - \hat{m})\frac{\sin^2\varepsilon}{\cos 2\varepsilon}\right],\\
M^2_{K^+} &= M^2_{K^-} = (m_s + m_u)B_0 + 2C\frac{e^2}{F^2},\\
M^2_{K^0} &= (m_s + m_d)B_0,\\
M^2_{\eta} &= 2B_0\left[\frac{1}{3}(\hat{m} + 2m_s) + \frac{2}{3}(m_s - \hat{m})\frac{\sin^2\varepsilon}{\cos 2\varepsilon}\right].
\end{aligned} \tag{7}$$

The above five equations are the extension of the Gell-Mann–Oakes–Renner (GOR) relations [21] to the isospin asymmetric case and allow us to relate the four constants $B_0 m_{u,d,s}$ and C (ε is given in terms of quark masses in (6)) with the five meson masses or their combinations. The additional equation provides the following relation between the tree-level LO masses:

$$\left(M^2_{K^\pm} - M^2_{\pi^\pm}\right)^2 - 3\left(M^2_{\eta} - M^2_{K^0}\right)\left(M^2_{K^0} - M^2_{\pi^0}\right) = 0. \tag{8}$$

The above equation is compatible with the one obtained in [22] neglecting $\mathcal{O}(m_u - m_d)^2$ terms. Actually, note that although all terms in (7) are formally of the same chiral order, numerically (see below) we expect $\varepsilon \sim (\sqrt{3}/4)(m_d - m_u)/m_s \ll 1$ and hence the mixing-angle corrections to the squared masses to be $\mathcal{O}(M^2_\pi \varepsilon)$ and $\mathcal{O}(M^2_\eta \varepsilon^2)$ for the neutral pion and eta, respectively. On the other hand, in the isospin-symmetric limit ($m_u = m_d$ and $e = 0$), (8) is nothing but the Gell-Mann–Okubo formula $4M^2_K - 3M^2_\eta - M^2_\pi = 0$ [23]. Neglecting only the $m_d - m_u$ mass difference in (7) leads to Dashen's theorem $M^2_{K^\pm} - M^2_{K^0} = M^2_{\pi^\pm} - M^2_{\pi^0}$ [24] and then equation (8) reduces to $4M^2_{K^0} - 3M^2_\eta - M^2_{\pi^0} = 0$, i.e. the Gell-Mann–Okubo formula for neutral states. However, the violation of Dashen's theorem at tree level due to those quark mass differences is significant numerically for kaons. In our present treatment we consider those differences on the same footing as the EM corrections to the masses. For pions, the main effect in the $\pi^0 - \pi^+$ mass difference comes from the EM contribution [25].

All the previous expressions hold for tree-level LO masses M^2_a with $a = \pi^\pm, \pi^0, K^\pm, \eta$, in terms of which we will write all of our results. They coincide with the physical masses to LO in ChPT, i.e. $M^2_{a,\mathrm{phys}} = M^2_a(1 + \mathcal{O}(M^2))$. Calculating the ChPT corrections to a given order then allows us to determine the numerical values of the tree-level masses, knowing their physical values and to that order of approximation. The same holds for F, which coincides with the meson decay constants in the chiral limit $F^2_{a,\mathrm{phys}} = F^2(1 + \mathcal{O}(M^2))$. Next to leading order (NLO) $\mathcal{O}(M^2)$ corrections to meson masses and decay constants were given in [2, 3] for $e^2 = 0$. EM corrections to the masses can be found in [4] for $SU(3)$ and in [6, 18] for $SU(2)$ including both $e^2 \neq 0$ and $m_u \neq m_d$ isospin-breaking terms.

The fourth-order Lagrangian in (1) consists of all possible terms compatible with the QCD symmetries to that order, including the EM ones. The $\mathcal{L}_{p^4}$ Lagrangian is given in [2] for the $SU(2)$ case, $h_{1,2,3}$ (contact terms) and $l_{1\ldots7}$ denoting the dimensionless LEC multiplying each independent term, and in [3] for $SU(3)$ the LEC named $H_{1,2}$ and $L_{1\ldots10}$. The EM $\mathcal{L}_{e^2p^2}$ and $\mathcal{L}_{e^4}$ for $SU(2)$ are given in [5, 6], $k_{1,\ldots13}$ denoting the corresponding EM LEC, and in [4]

for $SU(3)$ with the $K_{1\ldots17}$ EM LEC. For completeness, in the appendix we give the relevant terms needed in this work. The LEC are renormalized in such a way that they absorb all the one-loop ultraviolet divergences coming from $\mathcal{L}_{p^2}$ and $\mathcal{L}_{e^2}$, according to the ChPT counting, and depend on the $\overline{MS}$ low-energy renormalization scale μ in such a way that the physical quantities are finite and scale independent. The renormalization conditions for all the LEC can be found in [2, 4, 6, 17] and in the appendix we collect only those needed in this work.

As customary, we denote the scale-dependent and renormalized LEC by a superscript 'r'. The renormalized LEC are independent of the quark masses by definition, although their finite parts are unknown, i.e. they are not provided within the low-energy theory. The numerical values of the LEC at a given scale can be estimated by fitting meson experimental data, theoretically by matching the underlying theory under some approximations, or from the lattice. These procedures allow us to obtain estimates for the 'real-world' LEC at the expense of introducing residual dependences of those LEC on the parameters of the approximation procedure, which typically involves a truncation of some kind. Examples of these are the m_s dependence on the $SU(2)$ LEC when matching the $SU(3)$ ones, the correlations between LEC, masses and decay constants through the fitting procedure, the QCD renormalization scale and gauge dependence of some of the EM LEC or the dependence with lattice artifacts such as finite size or spurious meson masses. We will give more details below, specially regarding the EM LEC which will play an important role in our present work. An exception to the LEC estimates are the contact LEC h_i and H_i, which are needed for renormalization but cannot be directly measured. The physical quantities depending on them are therefore ambiguous, which comes from the definition of the condensates in QCD perturbation theory, requiring subtractions to converge [2]. It is therefore phenomenologically convenient to define suitable combinations which are independent of the h_i, H_i. We will bear this in mind throughout this work, providing such combinations when isospin breaking is included.

We will analyze in one-loop ChPT (NLO) the quark condensates, which for a given flavour q_i can be written at that order as

$$\langle \bar{q}_i q_i \rangle = -\left\langle \frac{\partial \mathcal{L}_{\text{eff}}}{\partial m_i} \right\rangle. \tag{9}$$

The above equation is nothing but the functional derivative with respect to the ith component of the scalar current, particularized to the values of the physical quark masses, according to the external source method [2, 3]. Therefore, we will be interested only in the terms of the fourth-order Lagrangian containing at least one power of the quark masses. These are the operators given in equations (A.1) and (A.2) for $SU(2)$ and $SU(3)$, respectively. Thus, the LEC that enter our calculation are $l_3, h_1, h_3, k_5, k_6, k_7$ in $SU(2)$, and L_6, L_8, H_2, K_7, K_8, K_9, K_{10} in $SU(3)$. Besides, up to NLO, only tree-level diagrams from the fourth-order Lagrangian can contribute to the condensates, so that in practice it is enough to set $U = \mathbb{1}$ in (A.1)–(A.2) for getting those tree-level contributions from (9).

2.1. Masses and LECs

For most of the numerical values of the different LECs and parameters in the $SU(3)$ case, we will follow [26], where fits to K_{l4} experimental data are performed in terms of $\mathcal{O}(p^6)$ ChPT expressions, including the isospin mass difference $m_u/m_d \neq 1$ and EM corrections to the meson masses, extending a previous work [27] where isospin breaking was not considered. Those fits have been improved in a recent work [28], which takes into account new phenomenological and lattice results. We will however stick to the values of [26], since our main interest is to compare the isospin-breaking condensates with the two sources included and to estimate the

effect of the EM LEC. In the new fits [28] isospin breaking is included only to correct for the charged kaon mass and the condensate values are not provided. For a review of different estimates of the quark masses and condensates see also [29] and [30]. In addition, in [31] a recent update of lattice results for low-energy parameters can be found, including LEC and the quark condensate. We will use the central values of the main fit in [26]. The value of $m_s/\hat{m} = 24$ [29, 30] is used as an input in [26], as well as $L_6^r = 0$, as follows e.g. from OZI rule or large-N_c arguments [3]. The more recent fits [28] consider an updated value of $m_s/\hat{m} = 27.8$ in accordance with recent determinations [31] and a nonzero value of L_6^r is obtained as an output. The suppression of L_6^r has been questioned in connection with a reduction of the light quark condensate when the number of flavours is increased [32], within the framework of generalized ChPT. In that context, the chiral power counting is modified due to the smallness of the condensate. Here, we will adhere to the standard ChPT picture, where the condensate and the GOR-like relations are dominated by the LO [33], sustained by the recent lattice LEC estimates [31]. The values of $F = 87.1$ MeV, $2B_0\hat{m} = 0.0136$ GeV^2, $m_u/m_d = 0.46$ and $L_8(\mu = 770\,\text{MeV}) = 0.62 \times 10^{-3}$ are outputs from the main fit in [26]. With those values we obtain from (6) $\varepsilon = 0.014$ and from (7) the tree-level masses of π^0, K^0, η.

To calculate the tree-level charged meson masses, we also need the value of the C constant, which can be inferred also from the results in [26] since the EM correction is numerically very small in the charged kaon mass with respect to the pure QCD contribution. This allows us to extract the tree-level charged kaon mass directly from the expressions for $M_{K^\pm}/M_{K^\pm,\text{QCD}}$ in [26], approximating $M_{K^\pm,\text{QCD}}$ by the full physical mass. From there we extract the value of C by subtracting the tree-level QCD part in (7) calculated with the above given quark masses. In this way we obtain $C = 5.84 \times 10^7$ MeV^4, which is very close to the values obtained simply from the charged–neutral pion mass difference in (7) setting the masses and F to their physical values [6] or from resonance saturation arguments [4]. From that C value we obtain the tree-level charged pion mass, using again (7). Nevertheless, to the order we are calculating we could have used the physical meson masses and decay constants instead of the tree level ones as well, since formally the difference is hidden in higher orders. The main reason why we choose the values in [26] is to compare directly with their numerical quark condensates and estimate the importance of the K_i^r corrections (see section 4.1 for details). The constant H_2 will also appear explicitly in quark condensates. Since it cannot be fixed with meson experimental data, when needed we will estimate it from scalar resonance saturation arguments as $H_2^r = 2L_8^r$ [16, 26], although we will comment below more about the H_2^r dependence of the results and provide physical quantities which are independent of the contact terms.

Regarding the EM LEC, the $SU(3)$ K_i^r have been estimated in the literature under different theoretical schemes. Resonance saturation was used in [35], large-N_c and NJL models in [34], complemented with QCD perturbative information in [36] and a sum-rule approach combined with low-lying resonance saturation has been followed in [37, 38]. The works [34, 36–38] have in common the use of perturbative QCD methods for the short-distance part of the LEC and different model approaches for the long-distance part. This procedure implies that the LEC estimated in that way depend (roughly logarithmically) in general on the QCD renormalization scale, which we call μ_0 to distinguish it from the low-energy scale μ, as well as on the gauge parameter. A closely related problem is that the separation of the strong ($e = 0$) and EM contributions for a given physical quantity is in principle ambiguous [34, 37, 39, 40]. The origin of this ambiguity [40] is that QCD scaling quantities such as quark masses also contain EM contributions through the renormalization group evolution in the full QCD+EM theory. Thus, a particular prescription for disentangling those contributions must be provided. In addition, when matching such quantities between the low-energy sector and the underlying theory, the choice of a given prescription will necessarily affect the scale and gauge

dependence of the EM LEC. These theoretical uncertainties, as well numerical ones, make those theoretical EM LEC estimates not fully compatible. For these reasons, in many works analyzing EM corrections, the LEC are simply assumed to lie within 'natural' values $|K_i^r|, |k_i^r| \lesssim \frac{1}{16\pi^2} \simeq 6.3 \times 10^{-3}$ at the scale $\mu \sim M_\rho$ [4, 6]. The above theoretical issues will be addressed in more detail in sections 3 and 4.4. The LEC dependences on the QCD scale and on the gauge parameter do no affect our results directly, being only relevant when comparing them with approaches where those LEC are obtained by matching the underlying theory. In that context we will see that the LEC combinations that we will deal with are gauge independent and lie within the stability range where the dependence on μ_0 is smooth and the matching makes sense [34, 36]. The theoretical errors quoted, e.g., in [34] account for the uncertainty related to the μ_0 dependence.

As for the $SU(2)$ k_i^r, no direct estimate is available to our knowledge, although one can relate them to the K_i^r by performing formally a $1/m_s$ expansion in a given physical quantity calculated in $SU(3)$ and comparing to the corresponding $SU(2)$ expression, similarly as the $l_i \leftrightarrow L_i$ conversion given in [3]. This has been done partially for some combinations of the LEC, namely those appearing in the neutral pion mass [41], in pion scattering [9, 41] and in the pionium lifetime [41, 42]. More recently, a full matching of the EM $SU(2)$ and $SU(3)$ LEC at the Lagrangian level has been performed in [43] using functional integral methods in the chiral limit. In this work, we will provide a complementary analysis. Namely, in section 4 we will obtain the matching relations between the LEC involved in the quark condensates, including both $m_u - m_d$ and EM contributions. Those relations will be consistent with the results in [43] and phenomenologically useful when dealing with approximate LEC determinations where isospin and mass corrections may be entangled.

3. Two-flavour quark condensates and bounds for the EM LEC

We start by giving the explicit one-loop ChPT expressions for the quark condensates in $SU(2)$ with all the isospin-breaking corrections included, which we derive from (9):

$$\langle \bar{q}q \rangle \equiv \langle \bar{u}u + \bar{d}d \rangle$$
$$= -2F^2 B_0 \left[1 - \mu_{\pi^0} - 2\mu_{\pi^\pm} + 2\frac{M_{\pi^0}^2}{F^2} \left(l_3^r(\mu) + h_1^r(\mu) \right) + e^2 \mathcal{K}_2^r(\mu) + \mathcal{O}(p^4) \right], \tag{10}$$

$$\langle \bar{u}u - \bar{d}d \rangle = 4B_0^2 (m_d - m_u) h_3 - \tfrac{8}{3} F^2 B_0 e^2 k_7 + \mathcal{O}\left(p^2\right), \tag{11}$$

where

$$\mathcal{K}_2^r(\mu) = \frac{4}{9}[5(k_5^r(\mu) + k_6^r(\mu)) + k_7], \tag{12}$$

and throughout this work we will follow the same notation as in [2, 3]:

$$\mu_i = \frac{M_i^2}{32\pi^2 F^2} \log \frac{M_i^2}{\mu^2}; \qquad \nu_i = \frac{1}{32\pi^2} \left[1 + \log \frac{M_i^2}{\mu^2} \right]. \tag{13}$$

The μ_i arise from the finite part of the one-loop tadpole-like contribution $G_i(x = 0)$, with G the free meson propagator [2]. The renormalization conditions for the LEC involved in (10)–(11) can be found in [2] and [6] and we give them in the appendix. With that LEC renormalization, one can check that the condensates in (10)–(11) are finite and scale independent, which is a nontrivial consistency check. Recall that h_3 and k_7 do not need to be renormalized. The condensates still depend on the h_1 and h_3 contact LEC, which, as explained above, yield an ambiguity in the determination of the condensates. The result (10) for $e \neq 0$

and $m_u \neq m_d$ reduces for $e = 0$ to the expressions given in [2]. The condensate difference (11) is given in [2] for $e = 0$, which we agree with, and in [6] for $e \neq 0$, which we also agree with, except for the relative sign between the two terms, which should be a minus in their equation (3.12) [44].

Let us now argue on how the EM corrections to the condensates may lead to constraints for the EM LEC. Those corrections come directly from the coupling of the EM field to the quarks in the QCD action, which break chiral symmetry. Actually, to understand better the origin of the different sources involved in chiral symmetry and isospin breaking, it is useful to keep the charges of the u and d flavours arbitrary and to separate the isoscalar and isovector contributions of the charge matrix in $SU(2)$:

$$Q = \frac{e_u + e_d}{2}\,\mathbb{1} + \frac{e_u - e_d}{2}\tau_3, \tag{14}$$

with $\tau_3 = \mathrm{diag}(1, -1)$ corresponding to the third isospin component. The EM part of the QCD Lagrangian $\bar{q}\gamma^\mu A_\mu Q q$ breaks the explicitly chiral symmetry $SU_L(2) \times SU_R(2)$ if $e_u \neq e_d$, through the isovector part in (14). The isovector also breaks the isospin symmetry $SU_V(2)$ ($L = R$) except for transformations in the third direction, which corresponds to electric charge conservation. On the other hand, the mass term $\bar{q}\mathcal{M}q$ breaks chiral symmetry for any nonzero value of the quark masses, preserving isospin symmetry if $m_u = m_d$. Altogether, the conclusion is that the QCD Lagrangian is chiral invariant only if $e_u = e_d$ *and* $m_u = m_d = 0$. Thus, chiral symmetry is explicitly broken even if $e_u = e_d$, as long as any of the quark masses $m_q \neq 0$, or equivalently, in the presence of an external scalar source, as needed to derive the condensates. If $e_u = e_d$ and $m_u = m_d \neq 0$, chiral symmetry is broken but isospin symmetry is conserved.

Now, let us recall how this charge and mass symmetry-breaking pattern translates into the low-energy sector. The LO $\mathcal{L}_{p^2+e^2}$ in (2) contains separate combinations of the charge and mass terms, both sharing the QCD pattern. Thus, the charge contribution proportional to C in (2) can be decomposed according to (14), giving a constant term proportional to $(e_u+e_d)^2$ independent of masses and fields, plus the term $C\left[(e_u - e_d)^2/4\right]\mathrm{tr}\left[\tau_3 U \tau_3 U^\dagger\right]$, which contributes directly to the pion EM mass difference in (4). Therefore, in the second-order Lagrangian all the EM chiral symmetry-breaking terms are proportional to $(e_u - e_d)^2$. This is no longer true for the fourth-order Lagrangian in (A.1), for which the symmetries of the theory allow for crossed mass-charge terms, like those proportional to k_5, k_6 and k_7. Those crossed terms break chiral symmetry even for $e_u = e_d$ for any nonzero quark mass, the strength of chiral breaking being proportional both to the quark charge e and to the quark mass $\hat{m}$. Consequently, they contribute to $\langle\bar{q}q\rangle = -2\langle\partial\mathcal{L}/\partial(m_u + m_d)\rangle$, the expectation value of the $SU_V(2)$ singlet behaving as an order parameter for chiral symmetry breaking. Setting $U = \mathbb{1}$ in the Lagrangian gives a piece proportional to $k_5 + k_6$ yielding $(e_u + e_d)^2$ and $(e_u - e_d)^2$ contributions to $\langle\bar{q}q\rangle$ and another one proportional to k_7 contributing both to $\langle\bar{q}q\rangle$ and to $\langle\bar{u}u - \bar{d}d\rangle = -2\langle\partial\mathcal{L}/\partial(m_u - m_d)\rangle$, the isotriplet order parameter of isospin breaking:

$$\begin{aligned}\mathcal{L}^{\langle\bar{q}q\rangle}_{e^2p^2} = 2F^2B_0\{&(k_5 + k_6)[(e_u + e_d)^2 + (e_u - e_d)^2](m_u + m_d) + 2k_7[(e_u + e_d)^2(m_u + m_d)\\ &+ (e_u - e_d)(e_u + e_d)(m_u - m_d)]\} + \cdots,\end{aligned}$$

where the dots indicate terms not contributing to the condensates at this order.

Thus, we see how the two sources of isospin breaking show up in the order parameter (11), which does not receive pion loop contributions in $SU(2)$. The latter is the explicit confirmation that isospin symmetry is not spontaneously broken in QCD [19], since all the contributions to this order parameter vanish for $m_u = m_d$ and $e = 0$.

On the other hand, the quark condensate $\langle\bar{q}q\rangle$ behaves as an order parameter for chiral symmetry and therefore measures the different sources of symmetry breaking: spontaneous and

explicit. Thus, it is naturally expected that its absolute value increases when a new symmetry-breaking source, such as the EM contribution, is switched on. This increasing behavior is what we denote as ferromagnetic, in analogy with the behavior of the magnetization in a ferromagnetic material under an external magnetic field.

There is no *a priori* formal argument to ensure the ferromagnetic-like nature of the QCD low-energy vacuum. We can nevertheless learn from the response of the system to the light quark mass $\hat{m}$, which is the actual counterpart of the magnetic field in a ferromagnet, since it breaks the chiral symmetry explicitly by coupling to the order parameter. For the mass, this ferromagnetic behavior is actually followed by the $e = 0$ condensates in the standard ChPT framework, both to $\mathcal{O}(p^4)$ and to $\mathcal{O}(p^6)$ with the LEC in [27], although assuming L_6 suppression and the dependence on contact terms still introducing a source of ambiguity. With the recent fit giving nonzero L_6^r and a new value also for L_8^r [28] we also get that $\langle \bar{u}u + \bar{d}d \rangle$ increases with light quark masses, from our $\mathcal{O}(p^4)$ expressions. The same ferromagnetic effect implies the increasing of the critical temperature of chiral restoration when increasing the pion mass, confirmed by ChPT calculations [45] and lattice simulations [46]. Finally, lattice results for the condensate [31] reveal a systematic increase of its absolute value with respect to direct estimates [29], reflecting again the same behavior, since the pion masses used in the lattice remain above the physical values. The EM symmetry breaking is of different nature from the mass, the former coming from vector-like interactions while the latter is of scalar type. However, as we have discussed in the previous paragraphs, their symmetry-breaking effects on certain observables are similar. Thus, the isovector part in (14) increases the masses of the charged mesons, according to (4) and (7), while the isovector and isoscalar both mix with the mass and contribute to $\langle \bar{q}q \rangle$. There are other arguments pointing in the same direction when EM interactions are switched on. At finite temperature, the EM pure thermal corrections to the condensate also increase its absolute value for any temperature [20]. On the other hand, the condensate increases under the influence of an external magnetic field eH, which can be also understood as the reduction of the free energy $\epsilon \sim m_q \langle \bar{q}q \rangle < 0$ (to LO) needed to compensate for the EM energy increasing $\Delta\epsilon_{EM} \sim (eH)^2/2 > 0$ [47].

Our purpose here will be to explore the consequences of that EM ferromagnetic behavior to LO. If the vacuum response is ferromagnetic, certain bounds for the EM LEC involved should be satisfied. We will derive those bounds and show that they are independent of the low-energy scale and thus can be checked in terms of physical quantities. Next we will check that the bounds are satisfied for the different estimates available for the EM LEC, with more detail for the $SU(3)$ case in section 4.4, where we also discuss the gauge independence of our results. This will provide a consistency check for the ferromagnetic behavior.

An important comment is that we will discuss the ferromagnetic-like condition on the EM correction to $\langle \bar{q}q \rangle$ and, as explained above, the splitting of the $e = 0$ and $e \neq 0$ parts in QCD+EM is ambiguous [39, 40]. This does not affect the low-energy representation of the condensates, which can be written in terms of physical quantities such as meson masses and decay constants. However, we will test our bounds with the EM LEC estimates obtained by matching low-energy results with the underlying theory [34–37]. Therefore, we have to be consistent with the prescription for charge splitting followed in those works. This amounts to the direct separation of the $e = 0$ part, which still may contain residual charge and μ_0 QCD scale dependence through running parameters. The consequence is that the EM LEC thus defined are in general μ_0-dependent, as discussed in [40]. Therefore, those estimates are reliable only if there is a stability range where the dependence on μ_0 is smooth and lies within the theoretical errors [34]. Actually, such stability range criteria are met for the LEC involved in our analysis (see section 4.4). Within that range, our identification of the e^2-dependent part

in $\langle\bar{q}q\rangle$ is consistent with the splitting scheme followed in those works. Actually, in that scheme F_0 is μ_0-independent and the e^2-dependent part of the μ_0 running of $B_0 m_{u,d}$ is the same as that of $m_{u,d}$ in perturbative QCD+EM [40]. Hence, it is consistent to assume that the ChPT LO of $\langle\bar{q}q\rangle = -2B_0F_0^2 + \cdots$ does not introduce any residual e^2 dependence when performing the charge splitting in the low-energy expression. Using a different splitting prescription would lead in general to different bounds and a different definition of the EM LEC. For instance, an alternative splitting procedure is introduced in [40] by matching running parameters of the e^2 theory with those of the $e^2 = 0$ one at a given matching scale μ_1. In that way, the EM part can be chosen as μ_0-independent but it depends on the matching scale μ_1. We will not consider that splitting here, since there are no available theoretical estimates for the LEC defined with that scheme. The scale dependence for the LEC in either scheme is roughly expected to be logarithmic.

Having the above considerations in mind, and going back to the case of physical quark charges, we separate the EM corrections to the condensate through the ratio

$$\frac{\langle\bar{q}q\rangle^{e\neq 0}}{\langle\bar{q}q\rangle^{e=0}} = 1 + 2\left[\mu_{\pi^0} - \mu_{\pi^\pm}\right] + e^2\mathcal{K}_2^r(\mu) + \mathcal{O}(p^4)$$
$$= 1 + e^2\mathcal{K}_2^r(\mu) - \frac{4Ce^2}{F^4}\nu_{\pi^0} + \mathcal{O}(\delta_\pi^2) + \mathcal{O}(p^4), \tag{15}$$

with ν_i defined in (13) and where we have expanded in $\delta_\pi \equiv \left(M_{\pi^\pm}^2 - M_{\pi^0}^2\right)/M_{\pi^0}^2 \simeq 0.1$, as $\mu_{\pi^\pm} - \mu_{\pi^0} = \delta_\pi M_{\pi^0}^2(\nu_{\pi^0}/F^2) + \mathcal{O}(\delta_\pi^2)$, which is numerically reliable and can be performed in addition to the chiral expansion, in order to simplify the previous expression.

We note that in $SU(2)$ and to this order, the ratio (15) is not only finite and scale independent but it is also independent of the not-EM LEC, including the contact h_1, h_3, and therefore free of ambiguities related to the condensate definition. In fact, this ratio is also independent of B_0, unlike the individual quark condensates, which only have physical meaning and give rise to observables when multiplied by the appropriate quark masses, since $m_i B_0 \sim M_i^2$. In $SU(2)$, the above ratio does not depend on the mass difference $m_d - m_u$ either, i.e. it depends only on the sum $\hat{m}$ and its deviations from unity are therefore purely of EM origin. All these properties make the ratio (15) a suitable quantity to isolate the EM effects on the condensate. Thus, the ferromagnetic-like nature of the chiral order parameter $\langle\bar{q}q\rangle$, within its low-energy representation, would require that this ratio is greater than 1, or equivalently to this order, $\partial\langle\bar{q}q\rangle/\partial e^2 \geqslant 1$. That condition leads to the following lower bound for the combination of EM LEC involved to this order, neglecting the $\mathcal{O}(\delta_\pi^2)$ in (15) which changes very little the numerical results:

$$5\left[k_5^r(\mu) + k_6^r(\mu)\right] + k_7^r \geqslant \frac{9C}{F^4}\nu_{\pi^0}. \tag{16}$$

We remark that the bound (16) is independent of the low-energy scale μ at which the LEC on the left-hand side are evaluated as long as the same scale is used on the right-hand side. Thus, it provides a well-defined low-energy prediction, expressed in terms of meson masses. The LEC on the left-hand side could be estimated by fitting low-energy processes or theoretically from the underlying theory, with all the related subtleties commented above.

Condition (16) and the corresponding ones for $SU(3)$ that will be derived in section 4.4 are obtained as a necessary condition that the LEC should satisfy if the QCD physical vacuum is ferromagnetic. This positivity condition on the quark condensate probes the vacuum by taking the mass derivatives (9) through the external source method so that the quark masses have to be kept different from zero and in that way the explicit symmetry-breaking corrections are revealed in the condensate. If one is interested in the chiral limit, it must be taken only

after differentiation, i.e. directly in equation (15). In that case, it is not justified to perform the additional δ_π expansion in the charge because the $e = 0$ masses vanish and one would be left only with the $\mu_{\pi^\pm}$ contribution in the rhs of (15), now with $M^2_{\pi^\pm} = 2Ce^2/F^2$. That would actually give a larger negative value for the lower bound, coming from the smallness of the charged part of the pion mass (see details below) so that the bound in the chiral limit is less predictive. The fact that our bounds depend on quark masses is similar to other bounds on LEC obtained from QCD inequalities [48].

Nevertheless, the main physical interest is to test this bound for physical masses, using different estimates of the LEC in the literature. Thus, as a rough estimate, setting $\mu = M_\rho \simeq 770$ MeV and with the physical pion masses $M_{\pi^\pm} \simeq 139.57$ MeV, $M_{\pi^0} \simeq 134.97$ MeV, the bound (16) gives $5\left[k^r_5(M_\rho) + k^r_6(M_\rho)\right] + k^r_7 \geqslant -6.32(5.62) \times 10^{-2}$ taking $F = 87.1(92.4)$ MeV. This is a bit more restrictive than the 'natural' lower bound -6.93×10^{-2} for the above LEC combination, obtained by setting all of them to $-1/(16\pi^2)$. The chiral limit gives -0.17 (with the value of C discussed in section 2.1 and $F = 87.1$ MeV), i.e. much less restrictive, as commented above. More detailed numerical analysis will be done for $SU(3)$ in section 4.4.

On the other hand, the maximum value for the ratio (15) for the k^r_i within 'natural' values is obtained by setting the three of them to $k^r_i(\mu = M_\rho) = 1/(16\pi^2)$, giving $\frac{\langle\bar{q}q\rangle^{e\neq 0}}{\langle\bar{q}q\rangle^{e=0}} = 1.0054$, which gives an idea of the size of this correction. We remark that the term proportional to ν_π on the ratio (15) comes directly from the dependence of the pion masses on e^2, so that it parametrizes the corrections in the condensate coming from any source of pion mass increasing, not only the EM one. Therefore, the same result can be used in order to provide a rough estimate of lattice errors in the condensate due to including heavier pion masses as lattice artifacts. In some lattice algorithms like the staggered fermion one, the situation is very similar to the mass differences induced by the charge terms. In that formalism, the finite lattice spacing induces terms [49] that break explicitly the so-called taste symmetry (four different quark species or 'tastes' are introduced for every quark flavour) leaving a residual $U(1)$ symmetry, pretty much in the same way as the charge term in (2). As a rough estimate, we can then replace $2Ce^2/F^4$ by the corresponding δ_π from the lattice, obtained as the difference between the mass of the lightest lattice meson and the true pion mass. For a lattice pion mass of about 300 MeV, the ν_π term in (15) gives a correction of about 6%, which for a condensate value of $(250\ \text{MeV})^3$ represents about $(5\ \text{MeV})^3$, which is within the order of magnitude quoted in [31]. Nevertheless, it should be taken into account that the staggered ChPT [49] has a much richer structure than the EM terms considered here and in particular there will be other operators contributing to the condensates at tree level, multiplied by the pertinent LEC. If those constants are of natural size, we expect the size of the corrections to the condensate to remain within the range quoted above.

4. Three flavour quark condensates

4.1. Results for light and strange condensates

In the $SU(3)$ case, we derive to one loop in ChPT the light condensate $\langle\bar{q}q\rangle_l = \langle\bar{u}u + \bar{d}d\rangle$ and the strange one $\langle\bar{s}s\rangle$, taking into account both $m_u - m_d$ and $e \neq 0$ corrections. Apart from the kaon and eta loops, an important distinctive feature in this case is the appearance of the $\pi^0\eta$ mixing term with the tree-level mixing angle ε defined in (6) which is one of the sources of isospin-breaking corrections. The results we obtain for the condensates with all the corrections

included are the following:

$$\langle\bar{q}q\rangle_l^{SU(3)} \equiv \langle\bar{u}u+\bar{d}d\rangle^{SU(3)} = -2F^2B_0\left\{1+\frac{8B_0}{F^2}\left[\hat{m}\left(2L_8^r(\mu)+H_2^r(\mu)\right)\right.\right.$$
$$\left.+4(2\hat{m}+m_s)L_6^r(\mu)\right]+e^2\mathcal{K}_{3+}^r(\mu)-\frac{1}{3}\left(3-\sin^2\varepsilon\right)\mu_{\pi^0}-2\mu_{\pi^\pm}-\mu_{K^0}$$
$$\left.-\mu_{K^\pm}-\frac{1}{3}(1+\sin^2\varepsilon)\mu_\eta+\mathcal{O}(p^4)\right\} \tag{17}$$

$$\langle\bar{u}u-\bar{d}d\rangle^{SU(3)} = 2F^2B_0\left\{\frac{4B_0}{F^2}(m_d-m_u)\left(2L_8^r(\mu)+H_2^r(\mu)\right)-e^2\mathcal{K}_{3-}^r(\mu)\right.$$
$$\left.+\frac{\sin 2\varepsilon}{\sqrt{3}}\left[\mu_{\pi^0}-\mu_\eta\right]+\mu_{K^\pm}-\mu_{K^0}\right\}+\mathcal{O}\left(p^2\right) \tag{18}$$

$$\langle\bar{s}s\rangle = -F^2B_0\left\{1+\frac{8B_0}{F^2}\left[m_s\left(2L_8^r(\mu)+H_2^r(\mu)\right)+4(2\hat{m}+m_s)L_6^r(\mu)\right]+e^2\mathcal{K}_s^r(\mu)\right.$$
$$\left.-\frac{4}{3}\left[\mu_{\pi^0}\sin^2\varepsilon+\mu_\eta\cos^2\varepsilon\right]-2\left[\mu_{K^\pm}+\mu_{K^0}\right]+\mathcal{O}\left(p^4\right)\right\}, \tag{19}$$

where we use the notation (13) and

$$\begin{aligned}\mathcal{K}_{3+}^r(\mu) &= \tfrac{4}{9}\left[6\left(K_7+K_8^r(\mu)\right)+5\left(K_9^r(\mu)+K_{10}^r(\mu)\right)\right],\\ \mathcal{K}_{3-}^r(\mu) &= \tfrac{4}{3}\left[K_9^r(\mu)+K_{10}^r(\mu)\right],\\ \mathcal{K}_s^r(\mu) &= \tfrac{8}{9}\left[3\left(K_7+K_8^r(\mu)\right)+K_9^r(\mu)+K_{10}^r(\mu)\right].\end{aligned} \tag{20}$$

Note that in some of the above terms we have preferred, for simplicity, to leave the results in terms of quark instead of meson masses. An important difference between the $SU(2)$ and $SU(3)$ cases is that now there are loop corrections in $\langle\bar{u}u-\bar{d}d\rangle$, where eta and pion loops enter through the mixing angle and kaon ones through the charged–neutral kaon mass difference. We have checked that the results are finite and scale independent with the renormalization of the LEC given in the appendix and that they agree with [3] for $e=0$. Some unpublished results related to the $SU(2)$ and $SU(3)$ isospin-breaking condensates can also be found in [50].

Numerical results for the condensates to this order can be found in [26]. As explained in section 2.1, the effect of the K_i^r constants (20) in the condensates is not fully considered in that work, where the EM contributions are included through the corrections of Dashen's theorem [34], so that only the K_i^r combinations entering mass renormalization appear. Then, we will use our results with all corrections included to estimate the range of sensitivity to the K_i^r of the condensates, analyzing the possible relevance for the fit in [26]. Our results are displayed in table 1. As discussed in section 2.1, we take the same input values $L_6^r=0$, $m_s/\hat{m}=24$ as in [26] as well as the assumption $H_2^r=2L_8^r$, and the output values of $B_0m_{u,d,s}$, m_u/m_d, F, L_8^r from their main fit. In the second and third columns of table 1, we give the results with all the EM K_i^r fixed to their minimum and maximum 'natural' values. Since the K_i^r appear all with positive sign in (20), the absolute values of the condensates obtained in this way are, respectively, lower and upper bounds within the natural range. We compare with the results quoted in [26] to the same $\mathcal{O}(p^4)$ order (fourth column) for their main fit and we also show for comparison the results in the isospin limit $e=0$, $m_u=m_d$ (fifth column). Our results agree reasonably with [26], although we note that the values in that work lie

Table 1. Results for quark condensates. We compare with the values of [26] to $\mathcal{O}(p^4)$ using the same set of low-energy parameters as in the main fit of that work, except the K_i^r, which we consider at their lower (second column) and upper (third column) 'natural' values. We also quote the values in the isospin limit to the same chiral order.

	$K^r_{7-10} = -\frac{1}{16\pi^2}$	$K^r_{7-10} = \frac{1}{16\pi^2}$	[26] value $\mathcal{O}(p^4)$	Isospin limit
$-\langle\bar{u}u\rangle_0/(B_0F^2)$	1.278	1.292	1.271	1.290
$-\langle\bar{d}d\rangle_0/(B_0F^2)$	1.297	1.305	1.284	1.290
$-\langle\bar{s}s\rangle_0/(B_0F^2)$	1.899	1.907	1.964	1.904
$\frac{\langle\bar{d}d\rangle}{\langle\bar{u}u\rangle} - 1$	0.015	0.010	0.013	0

outside the natural range for the individual condensates. The largest relative corrections are about 2% for the light condensates and about 4% for the strange one. These isospin-breaking corrections are significant given the precision of the condensates quoted in [26]. On the other hand, the corrections lie within the error range quoted by lattice analysis [31]. In turn, note the bad ChPT convergence properties of the strange condensate, somehow expected since $\langle\bar{s}s\rangle$ is much more sensitive to the strange quark mass m_s than the light condensate [27] and therefore the large strange explicit chiral symmetry breaking m_s is responsible in this case for the spoiling of the ChPT series, based on perturbative mass corrections. For the vacuum asymmetry $\frac{\langle\bar{d}d\rangle}{\langle\bar{u}u\rangle} - 1$, the natural value band covers the result in [26], although the numerical discrepancies in that case are relatively larger, between 15% and 24% for the lower and upper limits of the K_i^r, respectively. Recall that this quantity vanishes to LO in ChPT, according to (18), so that we expect it to be more sensitive to the K_i^r correction, which in this case comes mostly from the combination $K_9^r + K_{10}^r$. Nevertheless, it is worth noting that the results [26] imply $\langle\bar{d}d\rangle/\langle\bar{u}u\rangle > 1$ and $\langle\bar{s}s\rangle/\langle\bar{u}u\rangle > 1$, both in disagreement with many sum rule estimates of the condensate ratios [29]. Not surprisingly, we have the same discrepancy, since we use the same ChPT approach and the same numerical constants, except for the K_i^r corrections. The discrepancy in the relatively large value of $\langle\bar{s}s\rangle/\langle\bar{u}u\rangle$ comes possibly from the bad convergence of the ChPT series for the strange condensate, which in addition is very sensitive to the choice of H_2^r [26]. The light condensates converge much better and although the sign of $\langle\bar{d}d\rangle/\langle\bar{u}u\rangle - 1$ is under debate, its magnitude is very small. In the latter case, our present calculation may become useful since the $K_9^r + K_{10}^r$ contribution may change the sign of the vacuum asymmetry, although its precise value to fit a given prediction for $\langle\bar{d}d\rangle/\langle\bar{u}u\rangle - 1$ would still be subject to the H_2^r value. For this reason, it is important to make predictions for quantities which are independent of this ambiguity, as we have done in section 3 and as we will do in section 4.2, where the sum rule for condensate ratios will allow us to make a more reliable estimate of the vacuum asymmetry including both sources of isospin breaking. Finally, we comment on the numerical differences by considering the more recent low-energy fits in [28]. Still keeping $H_2^r = 2L_8^r$, these new values for the low-energy parameters increase considerably the total and strange condensates, which to $\mathcal{O}(p^4)$ give $\langle\bar{q}q\rangle/(2B_0F^2) \simeq -2.15$ and $\langle\bar{s}s\rangle/(B_0F^2) = -2.79$. These higher values are mostly due to the much smaller $F = 65$ MeV, obtained in the main fit of [28] to accommodate a rather high L_4^r also with a large error $L_4^r = (0.75 \pm 0.75) \times 10^{-3}$ (an output result in [28]). With the previous value $F = 87.1$ MeV but keeping the rest of LEC and masses as in [28] we obtain $\langle\bar{q}q\rangle/(2B_0F^2) \simeq -1.63$ and $\langle\bar{s}s\rangle/(B_0F^2) = -1.99$. The EM corrections remain of the same size and therefore their relative effect is somewhat smaller. As commented before, $m_u \neq m_d$ isospin breaking is not implemented in those new fits and EM corrections are included only in kaon masses.

4.2. Sum rule corrections

As noted in [3], for $m_u \neq m_d$ one can combine the isospin-breaking condensates into a sum rule relating the isospin asymmetry $\langle \bar{d}d\rangle/\langle \bar{u}u\rangle$ with the strange one $\langle \bar{s}s\rangle/\langle \bar{u}u\rangle$. Such relation is phenomenologically interesting because it does not include contact terms and hence is suitable for numerical estimates on the size of the isospin-breaking corrections. Our purpose in this section is to discuss the EM $e \neq 0$ contribution to that sum rule. To LO in $m_u - m_d$ and e^2 we find

$$\begin{aligned}\Delta_{SR} &\equiv \frac{\langle \bar{d}d\rangle}{\langle \bar{u}u\rangle} - 1 + \frac{m_d - m_u}{m_s - \hat{m}}\left[1 - \frac{\langle \bar{s}s\rangle}{\langle \bar{u}u\rangle}\right] \\ &= \frac{m_u - m_d}{m_s - \hat{m}}\frac{1}{16\pi^2 F^2}\left[M_K^2 - M_\pi^2 + M_\pi^2 \log\frac{M_\pi^2}{M_K^2}\right] \\ &\quad + e^2\left[\frac{C}{8\pi^2 F^4}\left(1 + \log\frac{M_K^2}{\mu^2}\right) - \frac{8}{3}\left(K_9^r(\mu) + K_{10}^r(\mu)\right)\right]. \end{aligned} \tag{21}$$

The last term proportional to e^2 is scale independent and is the charge correction to the result in [3]. With the numerical set we have been using, the $m_d - m_u$ term on the right-hand side gives -3.3×10^{-3}, whereas the e^2 term gives -3.37×10^{-3} with $K_9^r(M_\rho) + K_{10}^r(M_\rho) = 1/(8\pi^2)$ and -9.4×10^{-4} with $K_9^r(M_\rho) + K_{10}^r(M_\rho) = 2.7\times 10^{-3}$, the central value given in [34]. Therefore, the charge term above is of the same order as the pure QCD isospin correction and must be included when estimating the relative size of condensates through this sum rule. In fact, using the values quoted in [29] $m_u/m_d = 0.55$, $m_s/m_d = 18.9$ and $\langle \bar{s}s\rangle/\langle \bar{u}u\rangle = 0.66$, we obtain from (21) with physical pion and kaon masses

$$-0.015 < \frac{\langle \bar{d}d\rangle}{\langle \bar{u}u\rangle} - 1 < -0.009,$$

where the lower (upper) bound corresponds to the natural value $K_9^r + K_{10}^r = +(-)1/(8\pi^2)$, while the value without considering the charge correction is -0.012 and the value quoted in [29] collecting various estimates in the literature is -0.009. The inclusion of the charge corrections may then help to reconcile this sum rule with the different condensate estimates available. In fact, through this sum rule we see that ChPT is also compatible with the asymmetries $\langle \bar{d}d\rangle/\langle \bar{u}u\rangle$ and $\langle \bar{s}s\rangle/\langle \bar{u}u\rangle$ both being smaller than 1 (see our comments in section 4.1). Note that the ferromagnetic-like arguments used in sections 3 and 4.4 cannot be applied to $\langle \bar{u}u - \bar{d}d\rangle$, which does not behave as an order parameter under chiral transformations, since it is not invariant under $SU_V(2)$. Finally, we recall that estimates based on the sum rule (21) are more precise than the ones we have made directly from the condensates in section 4.1, since this sum rule is free of the H_2^r ambiguity.

4.3. Matching of LEC

Our aim in this section is to explore the consequences of including the two sources of isospin breaking for the matching of the LEC involved in the condensates. For that purpose, we perform a $1/m_s$ expansion in the $SU(3)$ sum and difference condensates given in (17)–(18). Matching the $\mathcal{O}(1)$ and $\mathcal{O}(\log m_s)$ terms with the corresponding $SU(2)$ expressions in (10)–(11) yields the following relations between the LEC, for the sum and difference of condensates respectively:

$$\begin{aligned}2M_{\pi^0}^2\left[l_3^r(\mu) + h_1^r(\mu)\right] + e^2F^2\mathcal{K}_2^r(\mu) &= 2M_{\pi^0}^2\left[16L_6^r(\mu) + 4L_8^r(\mu) + 2H_2^r(\mu) - \frac{\nu_\eta}{18} - \frac{\nu_{K^0}}{2}\right] \\ &\quad + e^2F^2\left[\mathcal{K}_{3+}^r(\mu) - \frac{2C}{F^4}\nu_{K^0}\right], \end{aligned} \tag{22}$$

$$B_0(m_d-m_u)h_3-\frac{2e^2F^2}{3}k_7=B_0(m_d-m_u)\left[4L_8^r(\mu)+2H_2^r(\mu)-\frac{\nu_\eta}{3}-\frac{\nu_{K^0}}{2}+\frac{1}{96\pi^2}\right]$$
$$-\frac{2e^2F^2}{3}\left[K_9^r(\mu)+K_{10}^r(\mu)-\frac{3C}{2F^4}\nu_{K^0}\right]. \tag{23}$$

In the above expressions, we have displayed the $SU(2)$ contribution on the left-hand side and the $SU(3)$ ones on the right-hand side, with $\mathcal{K}_2^r(\mu)$ and $\mathcal{K}_{3+}^r(\mu)$ given in (12) and (20). Note that the $1/m_s$ expansion has been implemented also in the tree-level relations (7), so that $M_{\pi^0}^2=(m_u+m_d)B_0+\mathcal{O}(1/m_s)$, $M_{K^0}^2=B_0m_s+\mathcal{O}(1)$ and $M_\eta^2=4B_0m_s/3+\mathcal{O}(1)$. It is important to point out that the pion mass charge difference is not negligible in the $1/m_s$ expansion, and for that reason we keep M_{π^0} in (22). For kaons, it is justified to consider the charge contribution negligible against the dominant m_s term, so that at this order $M_{K^\pm}$ and M_{K^0} are not distinguishable.

In the sum matching relation (22), the isospin corrections are not very significant. The mass difference m_u-m_d does not appear in the neutral and kaon masses to LO in $1/m_s$ and the charge correction, although of the same chiral order as the $M_{\pi^0}^2$ term, numerically $e^2F^2/M_{\pi^0}^2\simeq Ce^2/(F^2M_{\pi^0}^2)\simeq 0.05$. However, in the difference matching (23), the m_u-m_d corrections contribute on the same footing as the EM ones and are numerically comparable.

The above matching relations can be used directly for the approximated LEC (estimated theoretically or fitted to data) and for physical masses, since the difference from the tree-level masses and LEC is hidden in higher orders. On the other hand, for the tree-level LEC, i.e. the ChPT $O(p^4)$ Lagrangian parameters, since they are formally independent of the light quark masses, we can just take the chiral limit $m_u=m_d=0$ in the above expressions (22)–(23) and read off the corresponding matching of the e^2 contributions. Using the latter again in (22)–(23) then gives independent relations between the tree-level LEC involved at $e^2=0$ and the EM ones. Doing so, the EM and not-EM LEC combinations decouple and the results are compatible with those obtained in [3] for $e=0$ and in [43] for $e\neq 0$ (setting $m_u=m_d=0$ from the very beginning):

$$\begin{aligned}
&l_3^r(\mu)+h_1^r(\mu)=16L_6^r(\mu)+4L_8^r(\mu)+2H_2^r(\mu)-\frac{\nu_\eta}{18}-\frac{\nu_{K^0}}{2},\\
&h_3=4L_8^r(\mu)+2H_2^r(\mu)-\frac{\nu_\eta}{3}-\frac{\nu_{K^0}}{2}+\frac{1}{96\pi^2},\\
&5(k_5^r(\mu)+k_6^r(\mu))=6(K_7+K_8^r(\mu))+4(K_9^r(\mu)+K_{10}^r(\mu))-\frac{3C}{F^4}\nu_{K^0},\\
&k_7=K_9^r(\mu)+K_{10}^r(\mu)-\frac{3C}{2F^4}\nu_{K^0},
\end{aligned} \tag{24}$$

where the ν functions are evaluated exactly in the chiral limit, i.e. for $M_{K^0}^2=B_0m_s$ and $M_\eta^2=4B_0m_s/3$, the first and third equations coming from (22) and the second and fourth from (23).

Then, our first conclusion is that to this order of approximation, the formal matching of the condensates is consistent with the matching relations previously obtained. In other words, mass and charge terms can be separately matched. This would be no longer true at higher orders where for instance $e^2(m_u-m_d)$ contributions may appear.

Although relations (22) and (23) reduce to (24) in the chiral limit for the tree-level LEC, it is better justified to use the original expressions (22)–(23) when dealing with physical meson masses and when the LEC are obtained either from phenomenological or theoretical analysis. The LEC obtained in that way are approximations to the Lagrangian values and consequently they depend on mass scales characteristic of the approximation method used. For instance, the

LEC obtained by phenomenological fits are sensitive to variations both in $\hat{m}$ and in $m_u - m_d$ [26], in resonance saturation approaches they depend on vector meson masses [37, 38] which themselves depend on quark masses and in the NJL model some LEC such as K_{10}^r depend on the scale where the quark masses are renormalized [34]. We do not expect large differences between using the general matching relation (22) or the first and third equations in (24), since the latter can also be understood as the $e = 0$ limit of the former and we have seen that this is numerically a good approximation. However, that is not so clear for (22) where the two isospin-breaking contributions are of the same order, both in the chiral expansion and numerically.

Finally, we can use the previous matching relations to estimate numerically the $SU(2)$ condensates in (10)–(11) without having to appeal to the values of the $SU(2)$ LEC. Doing so we obtain $-\langle \bar{u}u + \bar{d}d\rangle^{SU(2)}/B_0F^2 \simeq (2.16, 2.18)$ and $\langle \bar{u}u - \bar{d}d\rangle^{SU(2)}/B_0F^2 \simeq (0.014, 0.02)$ where we indicate in brackets the natural range of the EM LEC, to be compared to $-\langle \bar{u}u + \bar{d}d\rangle^{SU(3)}/B_0F^2 \simeq (2.58, 2.6)$ and $\langle \bar{u}u - \bar{d}d\rangle^{SU(3)}/B_0F^2 \simeq (0.013, 0.018)$ from table 1. The larger difference in $\langle \bar{u}u + \bar{d}d\rangle$ comes from the $\mathcal{O}(m_s)$ and $\mathcal{O}(m_s \log m_s)$ terms in the $1/m_s$ expansion, which were separated when doing the matching and which are absent in the condensate difference. In fact, the numerical contribution of those terms to $-\langle \bar{u}u + \bar{d}d\rangle^{SU(3)}/B_0F^2$ is about 0.41, which explains perfectly the numerical differences and confirms the idea that in standard ChPT the light condensates calculated either in the $SU(2)$ or in the $SU(3)$ cases give almost the same answer near the chiral limit. This may be not the case in other scenarios of chiral symmetry breaking [32].

4.4. EM corrections and SU(3) LEC bounds

We have seen in the $SU(2)$ case that the EM ratio given in (15) is a relevant physical quantity allowing us to establish a constraint for the EM LEC based on explicit chiral symmetry breaking. The same argument applied to the $SU(3)$ case also leads to a constraint on the EM LEC obtained from the full condensate $\langle \bar{q}q\rangle = \langle \bar{u}u + \bar{d}d + \bar{s}s\rangle$, which behaves as an order parameter, being an isosinglet under $SU_V(3)$. In addition, we can still consider the light condensate $\langle \bar{q}q\rangle_l$ as the order parameter of chiral transformations of the $SU(2)$ subgroup, which in principle will lead to a different constraint. In fact, the latter is nothing but the constraint obtained in the $SU(2)$ case (16), once the equivalence between the LEC obtained in section 4.3 is used. As for the full condensate, it should be kept in mind that the large violations of chiral symmetry due to the strange quark mass may spoil our simple description of small explicit breaking. As commented above, this reflects to the strange condensate in the large NLO contributions, which in the standard ChPT framework depends strongly on m_s, unlike the light condensate. Therefore, the bounds of the LEC obtained for the full condensate are less trustable, since neglecting higher orders, say of $\mathcal{O}(e^2 m_s)$, is not so well justified for $\langle \bar{s}s\rangle$. Proceeding then as in section 3, where the same prescription of charge splitting when comparing with QCD approaches is understood, we calculate the ratios

$$\left[\frac{\langle \bar{q}q\rangle_l^{e\neq 0}}{\langle \bar{q}q\rangle_l^{e=0}}\right]^{SU(3)} = 1 + \frac{4e^2}{9}\left[6\left(K_7 + K_8^r(\mu)\right) + 5\left(K_9^r(\mu) + K_{10}^r(\mu)\right)\right] - \frac{2Ce^2}{F^4}\left[2\nu_{\pi^\pm} + \nu_{K^\pm}\right] + \mathcal{O}(\delta_\pi^2, \delta_K^2) + \mathcal{O}(p^4) \tag{25}$$

$$\left[\frac{\langle \bar{q}q\rangle^{e\neq 0}}{\langle \bar{q}q\rangle^{e=0}}\right]^{SU(3)} = 1 + \frac{8}{9}e^2\left[2(K_9^r(\mu) + K_{10}^r(\mu)) + 3(K_7 + K_8^r(\mu))\right] - \frac{8Ce^2}{3F^4}\left[\nu_{\pi^\pm} + \nu_{K^\pm}\right] + \mathcal{O}(\delta_\pi^2, \delta_K^2) + \mathcal{O}(p^4), \tag{26}$$

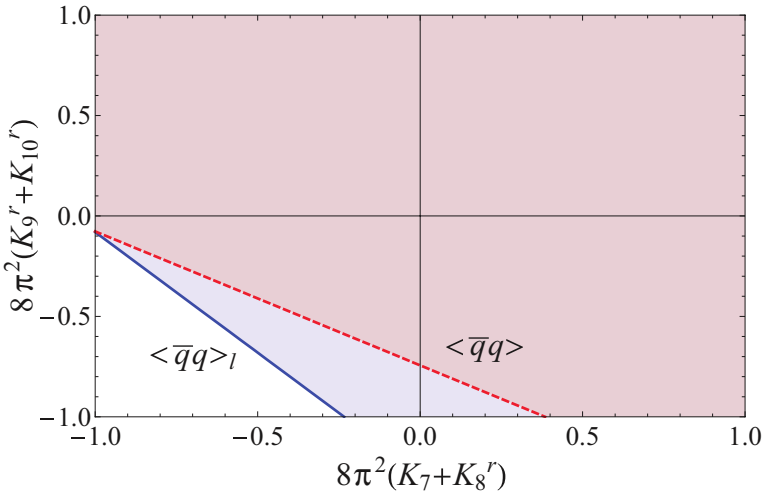

Figure 1. Regions in the LEC space constrained by the bounds on the light condensate (27), above the full blue line, and the full one (28), above the dashed red line. The LEC are renormalized at $\mu = M_\rho$ and are plotted within the natural range.

where, as in the $SU(2)$ case, we have expanded in δ_π and also in $\delta_K = (M^2_{K^\pm} - M^2_{K^\pm,e=0})/M^2_{K^\pm} \simeq 0.008$, which allows us to express the results in terms of the full $\pi^\pm$ and $K^\pm$ masses. Otherwise we should take into account that now $M_{\pi^\pm}(e=0) \neq M_{\pi^0}$, unlike the $SU(2)$ case, and $M_{K^\pm}(e=0) \neq M_{K^0}$, by terms of order $m_d - m_u$. This is important when using this result for numerical estimates, since, as discussed before, the separation of the $e=0$ correction to the masses is formally not unique. As in $SU(2)$, the ratios (25)–(26) are finite and independent of the scale μ, of B_0 and of the not-EM LEC, so they are free of contact ambiguities.

As in section 3, we want to explore the consequences of the ferromagnetic nature of the physical QCD vacuum under explicit chiral symmetry breaking for the EM LEC. Here, also the charge-mass crossed terms in the fourth-order Lagrangian (A.2) give explicit breaking contributions to the quark condensate coming now from the isoscalar, isovector and strangeness part of the charge matrix. For physical quark charges, demanding that the ratios (25)–(26) are greater than 1 we obtain the following EM bounds, to LO in the chiral expansion and in δ_π, δ_K:

$$\langle\bar{q}q\rangle_l \to 6\left(K_7 + K_8^r(\mu)\right) + 5\left(K_9^r(\mu) + K_{10}^r(\mu)\right) \geqslant \frac{9C}{2F^4}\left(2\nu_{\pi^\pm} + \nu_{K^\pm}\right) \qquad (27)$$

$$\langle\bar{q}q\rangle \to 2\left(K_7 + K_8^r(\mu)\right) + 3\left(K_9^r(\mu) + K_{10}^r(\mu)\right) \geqslant \frac{3C}{F^4}\left(\nu_{\pi^\pm} + \nu_{K^\pm}\right). \qquad (28)$$

We remark that these constraints are independent of the low-energy scale μ. It is also clear that the light bound (27) is nothing but the one obtained in the $SU(2)$ case (16) once the equivalence between the LEC given in the third equation of (24) is used. In figure 1, we have plotted these two constraints in the $(K_7 + K_8^r) - (K_9^r + K_{10}^r)$ plane at $\mu = M_\rho$ and within the natural region. We have used the same numerical values for the tree-level LO masses C and F as in previous sections. We observe that the bound on the full condensate is more restrictive than the light one in that range. However, as we have commented above, it is also less trustable, due to the large distortion of the chiral invariant vacuum due to the strange mass. Both bounds also give a more restrictive condition than just the natural size.

Let us now check these bounds against some estimates of the K_i^r in the literature. We start with the sum rule approach for $K^r_{7\ldots10}$ in [37]. In that work, $K_7 = K_8^r(M_\rho) = 0$, but what

is more relevant for us is that the combination $K_9^r + K_{10}^r$ at any scale is gauge independent despite being both K_9^r, K_{10}^r dependent on the gauge parameter ξ, as one can readily check from the explicit expressions given in [37] (cf their equations (94) and (95)). This is an interesting consistency check of our present bounds (27) and (28), which are gauge independent in addition to their μ low-energy scale independence commented previously, supporting their validity and predictive character. Numerically, the constant K_9^r could not be estimated in [37] due to the slow convergence of the integrals involved, but they provide a numerical estimate for $K_{10}^r(M_\rho) = 5.2 \times 10^{-3}$ at $\mu_0 = 0.7$ GeV and $\xi = 1$, for which we obtain $K_9^r(M_\rho) \geqslant -0.021$ from (27) and $K_9^r(M_\rho) \geqslant -0.015$ from (28). See our comments about the μ_0 scale dependence in section 3.

In [35] resonance saturation gives $K_{7\ldots10}^r(M_\rho) = 0$, which is compatible with our present bound. This is apparently incompatible with a previous value for $K_8^r(M_\rho) = (-4 \pm 1.7) \times 10^{-3}$ obtained in [4]. The possible reasons to explain this difference were discussed in [35]. That value for K_8^r is compatible with our bounds as long as $6K_7 + 5(K_9^r + K_{10}^r) \geqslant -0.05$ from (27) and $2K_7 + 3(K_9^r + K_{10}^r) \geqslant -0.02$ from (28).

In [34], based on large N_c and the NJL model, the LEC estimates give $K_7 = 0$, $K_8(M_\rho) = (-0.8 \pm 2.0) \times 10^{-3}$ (K_7 and K_8 are $\mathcal{O}(1/N_c)$ suppressed) and $K_9^r(M_\rho) + K_{10}^r(M_\rho) = (2.7 \pm 1.0) \times 10^{-3}$, all of them at $\mu_0 = 0.7$ GeV. These values are also compatible with both bounds (27) and (28). We note that in [36], where the short-distance contributions are evaluated as in [34], the explicit expressions given for the LEC again show that K_7, K_8^r and $K_9^r + K_{10}^r$ are gauge independent. Furthermore, K_9^r and K_{10}^r, dominant for large N_c in that approach, show a rather large stability range in the μ_0 scale around $\mu_0 = 0.7$ GeV [34, 36]. Since $K_9^r + K_{10}^r$ is the only combination surviving for large N_c in our bounds, the comparison with those works is robust concerning the gauge and QCD scale dependence.

5. Conclusions

In this work, we have carried out an analysis of strong and electromagnetic isospin-breaking corrections to the quark condensates in standard one-loop ChPT, providing their explicit expressions and studying some of their main phenomenological consequences for two and three light flavours.

Our results have allowed us to analyze the sensitivity of recent isospin-breaking numerical analysis of the condensates to considering all the EM LEC involved. The effect of those LEC is smaller for individual condensates than for the vacuum asymmetry, where they show up already in the LO. These corrections lie within the error range quoted in lattice analysis. Our analysis can also be used to estimate corrections to the quark condensate coming from lattice artificially large meson masses.

We have shown that if EM explicit chiral symmetry breaking induces a ferromagnetic-like response of the physical QCD vacuum, as in the case of quark masses, one obtains useful constraints as lower bounds for certain combinations of the EM LEC, both in the two and three flavour sectors. We have explored the consequences of this behaviour for the ratios of $e \neq 0$ to $e = 0$ light and total quark condensates, which are free of contact-term ambiguities, and for a given convention of charge separation. The large ChPT corrections to the strange condensate make the constraints on the full condensate less reliable. In this context, we have discussed the different sources for EM explicit chiral symmetry-breaking and isospin-breaking terms, by considering formally arbitrary quark charges. Thus, there are chiral symmetry-breaking terms proportional to the sum of charges squared, coming from crossed charge-mass contributions in the effective action, which show up in the vacuum expectation value. In accordance with the external source method, we keep the quark masses different from zero to account correctly

for all the explicit symmetry-breaking sources. The chiral limit can be taken at the end of the calculation. The bounds obtained are explicitly independent of the low-energy scale μ, then providing a complete and model-independent prediction at low energies. However, when this low-energy representation is compared with theoretical estimates based on QCD, one has to take into account that due to the convention used in the charge separation, the estimated LEC depend on the QCD renormalization scale μ_0, as well as being gauge dependent. Our bounds are numerically compatible with those estimates, based on sum rules, resonance saturation and QCD-like models, within the stability range of μ_0 where those approaches are reliable. Furthermore, the LEC combinations appearing in our bounds are gauge independent. We believe that our results can be useful in view of the few estimates of the EM LEC in the literature.

We have found that the EM correction to the sum rule relating condensate ratios is of the same order as the previously calculated $e = 0$ one, and therefore must be taken into account when using this sum rule to estimate the relative size of quark condensates. We have actually showed that using the complete sum rule, which is also free of contact terms, yields a ChPT model-independent prediction for the vacuum asymmetry compatible with the results quoted in the literature.

Finally, we have performed a matching between the $SU(2)$ and $SU(3)$ condensates, including all isospin-breaking terms. Matching the sum and difference of light condensates gives rise to matching relations between the LEC involved, where EM and not-EM LEC enter on the same footing in the chiral expansion. These matching relations may be useful when working with physical masses and LEC estimated by different approximation methods. In the case of the sum, the charge contribution is numerically small with respect to the pion mass one, but in the difference the two sources of isospin breaking are comparable. Taking the chiral limit, EM and not-EM constants decouple and the matching conditions are compatible with previous works for the LEC in the Lagrangian, which are defined in this limit.

Acknowledgments

We are grateful to J R Peláez and E Ruiz Arriola for useful comments. RTA would like to thank Buenaventura Andrés López for invaluable advice. This work was partially supported by the Spanish research contracts FPA2008-00592, FIS2008-01323, UCM-Santander 910309 GR58/08, GR35/10-A and the FPI programme (BES-2009-013672).

Appendix. Fourth-order Lagrangians and renormalization of the LEC

Here, we collect some results available in the literature and needed in the main text. To calculate the quark condensates to NLO one needs the $\mathcal{L}_{p^4+p^2e^2+e^4}$ Lagrangians to absorb the divergences coming from loops with vertices from $\mathcal{L}_{p^2+e^2}$. We denote by a superscript $\bar{q}q$ the relevant terms in the Lagrangian, which are those containing the quark mass matrix. For $SU(2)$ they are [5, 6]

$$\begin{aligned}\mathcal{L}^{\bar{q}q}_{p^4} &= \frac{l_3}{16}\mathrm{tr}[\chi(U+U^\dagger)]^2 + \frac{1}{4}(h_1+h_3)\mathrm{tr}[\chi^2] + \frac{1}{2}(h_1-h_3)\det(\chi),\\ \mathcal{L}^{\bar{q}q}_{p^2e^2} &= F^2(k_5\mathrm{tr}[\chi(U+U^\dagger)]\mathrm{tr}[Q^2] + k_6\mathrm{tr}[\chi(U+U^\dagger)]\mathrm{tr}[QUQU^\dagger] + k_7\mathrm{tr}[(\chi U^\dagger + U\chi)Q\\ &\qquad + (\chi U + U^\dagger\chi)Q]\mathrm{tr}[Q]),\end{aligned} \tag{A.1}$$

where $\chi = 2B_0\mathcal{M}$, whereas for $SU(3)$ [4]

$$\begin{aligned}\mathcal{L}^{\bar{q}q}_{p^4} &= L_6\mathrm{tr}[\chi(U+U^\dagger)]^2 + L_8\mathrm{tr}[\chi U\chi U + \chi U^\dagger\chi U^\dagger] + H_2\mathrm{tr}[\chi^2],\\ \mathcal{L}^{\bar{q}q}_{p^2e^2} &= F^2(K_7\mathrm{tr}[\chi(U+U^\dagger)]\mathrm{tr}[Q^2] + K_8\mathrm{tr}[\chi(U+U^\dagger)]\mathrm{tr}[QUQU^\dagger]\\ &\quad + K_9\mathrm{tr}[(\chi U + U^\dagger\chi + \chi U^\dagger + U\chi)Q^2] + K_{10}\mathrm{tr}[(\chi U + U^\dagger\chi)QU^\dagger QU\\ &\quad + (\chi U^\dagger + U\chi)QUQU^\dagger]),\end{aligned} \tag{A.2}$$

and $\mathcal{L}^{\bar{q}q}_{e^4} = 0$ for both cases.

In order to renormalize the meson loops it is necessary to separate the LECs appearing in the NNLO Lagrangian into finite and divergent parts. The renormalization of the LEC involved in the calculation of the $SU(2)$ condensates is given by [2, 5, 6]

$$\begin{aligned} l_i &= l_i^r(\mu) + \gamma_i\lambda,\\ h_i &= h_i^r(\mu) + \delta_i\lambda,\\ k_i &= k_i^r(\mu) + \sigma_i\lambda,\end{aligned}$$

with $\gamma_3 = -\frac{1}{2}, \delta_1 = 2, \delta_3 = 0$, and $\sigma_5 = -\frac{1}{4} - \frac{1}{5}Z, \sigma_6 = \frac{1}{4} + 2Z$ and $\sigma_7 = 0$, for physical quark charges $e_u = 2e/3$, $e_d = -e/3$, being $Z := \frac{C}{F^4}$. The part that diverges in $d = 4$ dimensions is isolated from the loop integrals and is expressed as

$$\lambda = \frac{\mu^{d-4}}{16\pi^2}\left(\frac{1}{d-4} - \frac{1}{2}[\log 4\pi + \Gamma'(1) + 1]\right),$$

where $-\Gamma'(1)$ is the Euler constant. As for the $SU(3)$ ones, we have [3, 4]

$$\begin{aligned} L_i &= L_i^r(\mu) + \Gamma_i\lambda,\\ H_i &= H_i^r(\mu) + \Delta_i\lambda,\\ K_i &= K_i^r(\mu) + \Sigma_i\lambda,\end{aligned}$$

with $\Gamma_6 = \frac{11}{144}, \Gamma_8 = \frac{5}{48}, \Delta_2 = \frac{5}{24}$, and $\Sigma_7 = 0, \Sigma_8 = Z, \Sigma_9 = -\frac{1}{4}, \Sigma_{10} = \frac{1}{4} + \frac{3}{2}Z$.

References

[1] Weinberg S 1979 *Physica* A **96** 327
[2] Gasser J and Leutwyler H 1984 *Ann. Phys.* **158** 142
[3] Gasser J and Leutwyler H 1985 *Nucl. Phys.* B **250** 465
[4] Urech R 1995 *Nucl. Phys.* B **433** 234
[5] Meissner U G, Muller G and Steininger S 1997 *Phys. Lett.* B **406** 154
Meissner U G, Muller G and Steininger S 1997 *Phys. Lett.* B **407** 454 (erratum)
[6] Knecht M and Urech R 1998 *Nucl. Phys.* B **519** 329
[7] Nehme A and Talavera P 2002 *Phys. Rev.* D **65** 054023
[8] Kubis B and Meissner U G 2002 *Nucl. Phys.* A **699** 709
Kubis B and Meissner U G 2002 *Phys. Lett.* B **529** 69
[9] Knecht M and Nehme A 2002 *Phys. Lett.* B **532** 55
[10] Schweizer J 2004 *Eur. Phys. J.* C **36** 483
[11] Ecker G, Muller G, Neufeld H and Pich A 2000 *Phys. Lett.* B **477** 88
[12] Hanhart C, Kubis B and Pelaez J R 2007 *Phys. Rev.* D **76** 074028
[13] Nehme A 2004 *Phys. Rev.* D **69** 094012
Nehme A 2004 *Phys. Rev.* D **70** 094025
[14] Colangelo G, Gasser J and Rusetsky A 2009 *Eur. Phys. J.* C **59** 777
[15] Rusetsky A 2009 *PoS* C D **09** 071 (arXiv:0910.5151 [hep-ph])
[16] Ecker G, Gasser J, Pich A and de Rafael E 1989 *Nucl. Phys.* B **321** 311
[17] Neufeld H and Rupertsberger H 1996 *Z. Phys.* C **71** 131
[18] Schweizer J 2003 *J. High Energy Phys.* JHEP02(2003)007

[19] Vafa C and Witten E 1984 *Nucl. Phys.* B **234** 173
[20] Gómez Nicola A and Torres Andrés R 2011 *Phys. Rev.* D **83** 076005
[21] Gell-Mann M, Oakes R J and Renner B 1968 *Phys. Rev.* **175** 2195
[22] Ditsche C, Kubis B and Meissner U G 2009 *Eur. Phys. J.* C **60** 83
[23] Gell-Mann M 1961 *Caltech Report CTSL-20*
Okubo S 1962 *Prog. Theor. Phys.* **27** 949
[24] Dashen R F 1969 *Phys. Rev.* **183** 1245
[25] Das T, Guralnik G S, Mathur V S, Low F E and Young J E 1967 *Phys. Rev. Lett.* **18** 759
[26] Amoros G, Bijnens J and Talavera P 2001 *Nucl. Phys.* B **602** 87
[27] Amoros G, Bijnens J and Talavera P 2000 *Nucl. Phys.* B **585** 293
Amoros G, Bijnens J and Talavera P 2001 *Nucl. Phys.* B **598** 665 (erratum)
[28] Bijnens J and Jemos I 2011 arXiv:1103.5945 [hep-ph]
[29] Narison S 2004 *QCD as a Theory of Hadrons: From Partons to Confinement* (Cambridge: Cambridge University Press) (arXiv:hep-ph/0202200)
[30] Ioffe B L 2006 *Prog. Part. Nucl. Phys.* **56** 232
[31] Colangelo G *et al* 2010 arXiv:1011.4408 [hep-lat]
[32] Descotes-Genon S and Stern J 2000 *Phys. Lett.* B **488** 274
Moussallam B 2000 *Eur. Phys. J.* C **14** 111
Moussallam B 2000 *J. High Energy Phys.* JHEP08(2000)005
[33] Colangelo G, Gasser J and Leutwyler H 2001 *Phys. Rev. Lett.* **86** 5008
[34] Bijnens J and Prades J 1997 *Nucl. Phys.* B **490** 239
[35] Baur R and Urech R 1997 *Nucl. Phys.* B **499** 319
[36] Pinzke A 2004 arXiv:hep-ph/0406107
[37] Moussallam B 1997 *Nucl. Phys.* B **504** 381
[38] Ananthanarayan B and Moussallam B 2004 *J. High Energy Phys.* JHEP06(2004)047
[39] Bijnens J 1993 *Phys. Lett.* B **306** 343
[40] Gasser J, Rusetsky A and Scimemi I 2003 *Eur. Phys. J.* C **32** 97
[41] Gasser J, Lyubovitskij V E, Rusetsky A and Gall A 2001 *Phys. Rev.* D **64** 016008
[42] Jallouli H and Sazdjian H 1998 *Phys. Rev.* D **58** 014011
Jallouli H and Sazdjian H 1998 *Phys. Rev.* D **58** 099901 (erratum)
[43] Haefeli C, Ivanov M A and Schmid M 2008 *Eur. Phys. J.* C **53** 549
[44] Knecht M private communication
[45] Gerber P and Leutwyler H 1989 *Nucl. Phys.* B **321** 387
[46] Cheng M *et al* 2010 *Phys. Rev.* D **81** 054504
[47] Shushpanov I A and Smilga A V 1997 *Phys. Lett.* B **402** 351
Agasian N O 2000 *Phys. Lett.* B **488** 39
Cohen T D, McGady D A and Werbos E S 2007 *Phys. Rev.* C **76** 055201
[48] Comellas J, Latorre J I and Taron J 1995 *Phys. Lett.* B **360** 109
[49] Aubin C and Bernard C 2003 *Phys. Rev.* D **68** 034014
[50] Nehme A 2002 La Brisure d'Isospin dans les Interactions Meson–Meson à Basse Energie *PhD Thesis* CPT Marseille

Parámetros de orden a temperatura finita

El estudio a temperatura cero realizado en la sección anterior sirve de base para el tratamiento térmico del problema, objeto de estudio de la publicación 2.2.1. En él presento un estudio termodinámico de los parámetros de orden de la ruptura de simetría de isoespín y la restauración de la simetría quiral a través del análisis de condensados de quarks asociados a diferentes combinaciones de sabores y de sus correspondientes susceptibilidades quirales escalares.

Como ya se ha comentado al hablar de la publicación 2.1.1, el condensado total es el parámetro de orden de la restauración quiral. Sin embargo —tal y como se entiende actualmente [83]— la transición quiral es un *crossover* suave para el caso físico $N_f = 2+1$, así que resulta que es posible obtener diferentes temperaturas críticas dependiendo de qué observable se examine. Es por esto que el estudio *model-independent* de las susceptibilidades dentro del contexto de *ChPT* también aporta una información valiosa acerca de la transición y de su naturaleza. Las predicciones de la Teoría Quiral demuestran ser compatibles con las predicciones originales acerca de la restauración de la simetría quiral [143] y con recientes cálculos en el retículo [86, 128, 144].

La principal motivación a este respecto en el trabajo que presento se centra en la posibilidad de establecer un análisis en el continuo de carácter *model-independent* para las susceptibilidades quirales escalares conexa, disconexa y total; así como su comparación con los resultados obtenidos mediante el formalismo *staggered* en el retículo. Como mostraré, la consideración de un escenario que incluya la ruptura de isoespín consistentemente es fundamental para la obtención de las contribuciones dominantes de cada una de las partes de la susceptibilidad y, por consiguiente, de su *scaling* con los parámetros de masa quark y temperatura. Esto resulta de todo punto esencial incluso cuando el interés final sea un estudio en el límite de isoespín.

De acuerdo al esquema seguido para la anterior publicación, analizaré punto por punto los principales resultados de la publicación 2.2.1:

- El condensado total de quarks en $SU(2)$ sólo recibe correcciones térmicas debidas a ruptura electromagnética, mientras que en $SU(3)$ tanto la parte de ruptura intrínseca, asociada en este caso a la dependencia cuadrática en el ángulo de mezcla $\epsilon \sim \frac{m_d - m}{m_s}$, como la ruptura electromagnética contribuyen.

  En ambos casos, estas correcciones se traducen en una modificación de la temperatura crítica respecto al límite de isoespín de menos de un 1 %. Un punto importante en este aspecto es la dirección en la que esta modifica-

ción se produce cuando se consideran o no los efectos de ruptura electromagnética. En efecto al comparar la temperatura de restauración obtenida formalmente al anularse el condensado $e \neq 0$ con aquélla obtenida para el caso $e = 0$ encontramos que se produce un aumento, hecho que refuerza la hipótesis de respuesta ferromagnética del vacío que se presentó al analizar la publicación 2.1.1.

El parámetro de orden de ruptura de isoespín no recibe correcciones térmicas en *SU(2)* (las contribuciones procedentes de los *loops* de piones los condensados $<\bar{u}u>$ y $<\bar{d}d>$ son iguales y se cancelan en la diferencia) por lo que ambos condensados se anulan a la misma temperatura. Sin embargo, cuando se incluyen efectos asociados a kaones y etas, este observable se amplifica suavemente a través de una dependencia cuadrática en la temperatura: $(m_u - m_d)\frac{T^2}{M_\eta^2}$. Aunque las desviaciones respecto al valor a temperatura cero son apreciables para temperaturas altas, están controladas por una escala de energía mucho mayor que la dependencia en $1/F_\pi^2$ característica del parámetro de orden de la restauración quiral.

Esta amplificación térmica de los efectos de ruptura de isoespín no se muestra en los condensados asociados a los quark *up* y *down* debido a que en esos casos hay una supresión en ϵ que hace que las temperaturas críticas de ambos sean prácticamente iguales. Además se comprueba, como en el caso a temperatura cero, que el parámetro de orden asociado a la ruptura de isoespín, i. e $<\bar{u}u - \bar{d}d>$, es cero en el caso de que la masas de los quarks ligeros y sus cargas sean iguales entre sí. Este resultado constituye una comprobación del Teorema de Vafa-Witten [20], en virtud del cual la simetría bajo el subgrupo quiral de isoespín no puede estar rota espontáneamente.

❧ Diversos grupos fenomenológicos especializados en simulaciones en el retículo a temperatura finita han estudiado el modo de evitar la ambigüedad introducida en el cálculo de los condensados a través de, por ejemplo, la sustracción de la parte de temperatura cero [86], o de una combinación adecuada dependiente de las masas de los quarks y del condensado *strange* [128].

En este contexto, en la presente publicación muestro que la regla de suma de [31] —que ya analicé a temperatura cero incluyendo consistentemente ambas fuentes de ruptura de isoespín— puede extenderse sin problemas a temperatura finita puesto que las funciones térmicas que corrigen los condensados entran de igual modo que los logaritmos quirales, lo que hace que se siga manteniendo la independencia respecto de términos de contacto.

Debido a que las correcciones atinentes a la ruptura de isoespín en el cociente $<\bar{u}u> / <\bar{d}d>$ son grandes para temperaturas moderadas, las modificaciones térmicas a esta regla de suma son importantes dentro del rango de temperaturas en las que *ChPT* arroja predicciones razonables, llegando a

ser formalmente comparables al valor de temperatura cero cerca de la región crítica[4].

Hasta aquí he presentado los principales puntos en relación al tratamiento térmico de los condensados. A partir de ahora trataré los resultados concernientes al estudio de las susceptibilidades quirales escalares.

La inclusión de diferentes masas para los quarks ligeros lleva directamente a la definición de tres susceptibilidades escalares distintas e independientes: χ_{uu}, χ_{dd} y $\chi_{ud} = \chi_{du}$, obtenidas a partir de la derivación de cualquiera de los condensados respecto de la masa asociada a cada uno de los quarks ligeros.

Estas tres pueden ser relacionadas entre sí para dar lugar a las llamadas susceptibilidades conexa y disconexa —según el carácter de los diagramas de líneas quark asociados a cada una—. Junto a la susceptibilidad escalar total, todas ellas son observables de uso frecuente en las simulaciones en el retículo debido a que incluyen información acerca de los polos de mesones en distintos canales.

El escenario basado en el análisis de la ruptura de isoespín para definir de una forma natural las susceptibilidades disconexa y conexa ha sido analizado inicialmente para el límite quiral en [145] y, más adelante, en [146] al estudiar la polarización del vacío. El trabajo [145] muestra —de una forma *model-independent*— que es posible identificar las susceptibilidades conexa y disconexa con combinaciones de las derivadas de los condensados asociados a diferentes sabores respecto de la masa de los quarks ligeros; de modo que, al final, —al tomar el límite de isoespín $m_u \to m_d$— las expresiones conduzcan a los resultados conocidos para la susceptibilidad total[5].

La susceptibilidad disconexa representa una medida de las fluctuaciones del parámetro de orden de la restauración de la simetría quiral, mientras que la conexa lo es del parámetro de orden de la ruptura de isoespín. Un análisis de órdenes en el ángulo de mezcla (que es esencialmente tanto como hacer un análisis en $m_u - m_d$) indica que el condensado total de quarks es cuadrático en ϵ mientras que la componente del iso-triplete $<\bar{u}u - \bar{d}d>$ depende linealmente.

Este comportamiento provoca que las correcciones debidas a ruptura explícita para la susceptibilidad disconexa sean proporcionales a $m_u - m_d$, mientras que para la conexa los efectos sean $O(1)$, de modo que no se anulan en el límite de isoespín, contrariamente a lo que pudiera parecer haciendo $m_u = m_d$ desde el

[4] A este respecto considero importante recalcar una vez más lo dicho en la sección 1.1.4: como sea que *ChPT* no permite un tratamiento cuantitativo de los resultados por encima del régimen de baja temperatura, toda extrapolación o mención a esta región ha de entenderse de manera cualitativa.

[5] El criterio de similitud con el resultado en el límite quiral permite que esta identificación no sea única: existe una cierta libertad residual uniparamétrica para elegir la separación conexa-disconexa.

principio. Es, por tanto, fundamental considerar $m_u \neq m_d$ desde el comienzo aun cuando el interés principal se halle en el cálculo de cantidades definidas en el límite de isoespín.

Con todo, la publicación 2.2.1 llega a las siguientes conclusiones:

❧ Las correcciones electromagnéticas al condensado total de quarks en la teoría de dos sabores pueden relacionarse directamente con la diferencia $\chi(T)^{SU(2)} - \chi(0)^{SU(2)}$ para la susceptibilidad escalar total a través de una regla de suma, finita e independiente de la escala de renormalización quiral y de términos de contacto. De hecho este observable ha sido directamente calculado en el retículo por distintos grupos (e.g. [86, 147]).

Extrapolando las predicciones de *ChPT* hacia el régimen de altas temperaturas puede colegirse que —con el crecimiento de las fluctuaciones que se espera para este observable cerca del punto crítico y aunque las correcciones debidas a la ruptura de isoespín no son numéricamente importantes— podrían esperarse efectos de amplificación apreciables cerca de la región crítica.

Para el caso de tres sabores la situación es algo más complicada debido a que las masas de kaones y etas también dependen de las masas de los quarks *up* y *strange*. En esta situación la regla de suma contiene una parte directamente relacionada con $\chi(T)^{SU(3)} - \chi(0)^{SU(3)}$, y otra parte con derivadas del condensado *strange* respecto de la masa de quarks ligeros. Con todo —debido a la supresión a través de funciones de Boltzmann de los grados de libertad pesados— el condensado asociado al quark *strange* varía más suavemente con la temperatura que los ligeros, por lo que también en la teoría de tres sabores los resultados para la regla de suma están dominados por la susceptibilidad escalar total.

Un punto importante en el análisis de esta regla de suma en relación con las simulaciones en el retículo —y, en concreto, con el formalismo *staggered*— reside en que en este esquema de cálculo existen correcciones de espaciado finito debido a la presencia de copias espúreas (*tastes*) asociadas a cada sabor [86, 89, 148]. Debido a que la masa de las copias se corrige con el espaciado de la red de forma similar a como entran las correcciones electromagnéticas a *nivel árbol* en la masa de los bosones de Goldstone, la regla de suma permite comparar las diferencias entre los resultados para los condensados en el límite del continuo y los obtenidos mediante simulación en el retículo usando acciones de tipo *staggered*.

Basándome en los parámetros usados en [86], las publicaciones que defiendo arrojan un resultado para el condensado en el continuo que difiere un 20 % respecto a un retículo con extensión temporal $N_t = 12$ [86], y un 12 % para el caso de un retículo con $N_t = 16$ [147]. A partir de este argumento

de extrapolación se colige, también, que las correcciones debidas a efectos de *taste-breaking* son susceptibles de verse amplificadas en un entorno de la temperatura crítica de restauración.

En el contexto de una teoría de $N_f = 2+1$ sabores con masas ligeras no nulas no es fácil asociar estas variaciones en los condensados con el consiguiente cambio asociado a la temperatura crítica a través de expresiones analíticas cerradas. Esto se debe a la presencia de funciones térmicas, $g_1(M,T)$ y $g_2(M,T)$, que establecen dependencias no triviales con la temperatura.

A modo de análisis aproximado, la publicación 2.2.1 indica que, a través del uso de las expresiones para los condensados en el límite quiral, el cambio respecto al valor en el continuo de la temperatura crítica —tomando los datos que aparecen en la publicación [86]— se situaría más o menos en los 10 MeV.

Aunque a fecha de hoy se están realizando importantes esfuerzos para reducir esta fuente de incertidumbres a través del uso de retículos más finos y de la mejora de las acciones utilizadas, creo que la estimación y el control de estos errores mediante comparación con los resultados en el límite del continuo es esencial debido a que sigue constituyéndose como uno de los principales factores que explican las discrepancias en la estimación de la temperatura crítica de restauración quiral en los diferentes grupos de investigación.

❧ La publicación que presento analiza de modo sistemático las correcciones a un *loop* para las susceptibilidades conexa y disconexa en la Teoría Quiral de Perturbaciones para tres sabores con ruptura de isoespín, tanto a temperatura cero como a temperatura finita. Las susceptibilidades calculadas son finitas e independientes de la escala de renormalización de la Teoría Quiral. Además, como los términos asociados a las *EM LECs* no llevan asociadas masas de quarks, también son independientes de éstas.

El análisis del comportamiento en el régimen infrarrojo ($\hat{m} << m_s, M_\pi << T << M_{K,\eta}$) es una herramienta útil para el estudio formal de los *scalings* de las susceptibilidades con la masa de los quarks ligeros y la temperatura. La susceptibilidad disconexa a temperatura cero diverge logarítmicamente ($\sim \log M_\pi$) en el infrarrojo como producto de su dependencia en las funciones $g_2(M_\pi,T)$ y $\nu_\pi \sim \log M_\pi^2$, y diverge también como T/M_π cuando se considera su equivalente sustraído $\chi_{\rm dis}(T) - \chi_{\rm dis}(0)$ en las mismas condiciones, predicciones ambas que ya fueron presentadas en [145] usando este mismo esquema efectivo.

En este sentido los resultados de nuestra publicación constituyen una prueba de consistencia de aquéllos, extendiéndolos fuera del límite quiral y permitiendo —a través de un análisis consistente y sistemático a partir

de la Teoría Quiral— corroborar la idea de que la susceptibilidad disconexa está dominada en este régimen por *loops* de bosones de Goldstone, como cabría esperar debido a que este observable mide las fluctuaciones del parámetro de orden asociado a la restauración de simetría quiral.

El carácter lineal de la dependencia respecto del ángulo de mezcla en el iso-triplete $<\bar{u}u - \bar{d}d>$ da lugar a correcciones de $\mathcal{O}(1)$ en ε para la susceptibilidad conexa que no desaparecen tomando el límite de isoespín. La parte de temperatura cero depende del término de contacto H_2^r por lo que sólo tiene sentido físico[6] considerar sustracciones del tipo $\chi_{\rm con}(T) - \chi_{\rm con}(0)$.

El estudio de la susceptibilidad conexa a temperatura cero en el límite infrarrojo indica que —de modo análogo a como sucedía con los resultados obtenidos en *ChPT* para tres sabores con ruptura de isoespín— ésta no tiene parte divergente cuando se considera el caso de dos sabores ligeros idénticos, *p.ej.* $N_f = 2+1$, en consonancia también con el estudio de [145]. Además, nuestro análisis permite afirmar que —como herencia del comportamiento del condensado iso-triplete que ya hemos analizado— la susceptibilidad conexa tiene una dependencia cuadrática en la temperatura sobre la masa M_η^2 cuando se considera la cantidad $\chi_{\rm con}(T) - \chi_{\rm con}(0)$.

Aunque en el caso de tres sabores con ruptura de isoespín la parte conexa contiene términos subdominantes en ε con divergencias infrarrojas proporcionales a $\varepsilon^2 g_2(M_\pi, T)$ y $\varepsilon^2 \nu_\pi(M_\pi)$, estos están controlados perturbativamente por la escala de ruptura intrínseca; de tal modo que en el límite $N_f = 2+1$ su comportamiento infrarrojo es perfectamente regular.

Este análisis en ε indica también que los efectos de ruptura de isoespín son mayores para la parte disconexa que para la conexa, y se amplifican con la temperatura. En efecto, aunque los términos subdominantes en el ángulo de mezcla son en ambas partes de orden $\mathcal{O}(\varepsilon^2)$, en la parte disconexa hay contribuciones de tipo $\varepsilon^2 \partial g_2(M_\pi, T)/\partial M_\pi^2$, y $\varepsilon^2 \partial \nu(M_\pi)/\partial M_\pi^2$, más divergentes.

Como acabamos de ver, en el límite quiral la parte divergente infrarroja de este observable es proporcional a $n_f^2 - 4$, con n_f el número de sabores ligeros idénticos en el gas [145]; y por tanto se anula en el caso $n_f = 2$ dando lugar a un comportamiento perfectamente regular. Obtener este tipo de *scalings* con m_q y T en el límite del continuo a partir de esquemas de trabajo *model-independent* es especialmente importante para detectar y explicar ciertos comportamientos anómalos que aparecen al usar el formalismo *staggered*. Uno de ellos tiene que ver con el hecho de que esta técnica introduce dependencias espúreas para retículos de volumen finito que provocan

[6] Las estimaciones numéricas a temperatura cero que aparecen en la publicación se han efectuado considerando el valor numérico para H_2^r que aparece en [32,121] a partir de argumentos basados en saturación de resonancias.

la aparición de contribuciones artificiales en el infrarrojo susceptibles de alterar sus resultados [149, 150].

Por otro lado, los términos dominantes $\mathcal{O}(1)$ en ϵ para $\chi_{\text{con}}(T)$ son proporcionales a $1/m_s$ y por tanto explican por qué esta parte de la susceptibilidad incrementa en los cálculos en el retículo [149] al disminuir m_s frente a las masas de los quarks ligeros. Este comportamiento no se aprecia en sus resultados para los condensados debido a que en ellos este efecto se encuentra suprimido por potencias de ϵ.

Como acabamos de ver, el cálculo en el continuo que aparece en la publicación 2.2.1 revela que la parte finita de $\chi_{\text{con}}(T)$ no es nula en el límite de isoespín y permite relacionar las propiedades de *scaling* térmico de la susceptibilidad conexa cerca del límite quiral como directamente vinculadas con la mezcla π^0–η. Al igual que sucedía con la componente $\bar{q}\tau^3 q$ del isotriplete, la dependencia cuadrática en la temperatura está controlada por un parámetro genuinamente asociado a la ruptura intrínseca de isoespín, *vid.* la masa M_η, que es mucho mayor que el parámetro quiral típico, F_π, asociado a las variaciones térmicas de la susceptibilidad disconexa.

Por este motivo el comportamiento de la susceptibilidad conexa está numéricamente dominada por su valor a temperatura cero, lo que explica también por qué las simulaciones en el retículo presentan un *scaling* en $1/m_s$ mucho más parecido a los de modelos $O(N)$ —tomados como referencia para el ajuste de sus datos— cuando se sustrae la parte de temperatura cero, con respecto al caso sin sustraer.

Además de todo esto, el hecho de que los efectos de *taste-breaking* se analicen de una manera mucho más cómoda utilizando un sólo sabor abre la puerta a la posibilidad de que se haga una interpretación demasiado simplista de la situación, es decir, asumir simplemente que la susceptibilidad total es cuatro veces la susceptibilidad asociada a un sólo sabor genérico tomando el límite de isoespín desde el principio. Como ya hemos comentado, este esquema de trabajo es incorrecto puesto que no permite calcular las contribuciones dominantes para la susceptibilidad conexa.

Pese a que las correcciones debidas a ruptura de isoespín son numéricamente pequeñas en la susceptibilidad total, esta visión demasiado simplista exhibe también diferencias numéricas importantes con respecto a la consideración de la situación de asimetría de isoespín desde el principio: las desviaciones de $4\chi_{uu} - \chi$ respecto de cero son numéricamente computables en un 30 % a temperatura cero, y de hasta un 10 % cuando se analiza la variación térmica de sus respectivos valores sustraídos, i.e.

$$\frac{\chi_{uu}(T) - \chi_{uu}(0)}{\chi(T) - \chi(0)}.$$

❧ El escenario propuesto por *ChPT* reproduce el comportamiento creciente para las susceptibilidades a temperaturas bajas e intermedias de una forma *model-independent*, aunque es evidente que por sí sola es incapaz de dar cuenta de efectos críticos como la presencia de un máximo en las susceptibilidades escalares conexa y disconexa cerca de la región térmica crítica. En la sección 2.3 —concretamente en la publicación 2.3.1— se verá cómo la extensión unitarizada de *ChPT* permite la reproducción de ciertos comportamientos críticos para el condensado y las susceptiblidades.

Los resultados en el régimen infrarrojo permiten afirmar que el comportamiento crítico que se espera en el caso de la susceptibilidad disconexa sea mucho más pronunciado que el de la conexa. Resulta natural asociar este comportamiento —una vez más— a la naturaleza misma de cada observable: la susceptibilidad conexa está directamente relacionada con efectos de ruptura intrínseca a través de las fluctuaciones del parámetro de orden de la ruptura de isoespín, mientras que la parte disconexa mide las fluctuaciones del condensado total de quarks. Diversos cálculos en el retículo [149, 150] reflejan estas predicciones.

En cualquier caso, debido al orden de las correcciones que se desprecian —y a pesar de constituir una interesante herramienta a la hora de aproximarnos al estudio de las propiedades críticas— nuestros resultados sugieren que los términos dominantes en el régimen infrarrojo no son una buena aproximación numérica en el caso de que se trate con piones de masa igual al valor físico, lo que indica que un estudio fuera del límite quiral como el que hemos realizado aporta valiosa información al campo.

2.2.1 Publicación:
A. Gómez Nicola, R. Torres Andrés,
Isospin breaking and chiral symmetry restoration,
Phys. Rev. D **83** (2011), 076005

PHYSICAL REVIEW D **83,** 076005 (2011)

Isospin breaking and chiral symmetry restoration

A. Gómez Nicola* and R. Torres Andrés†

Departamento de Física Teórica II, Universidad Complutense, 28040 Madrid, Spain

(Received 14 February 2011; published 12 April 2011)

We analyze quark condensates and chiral (scalar) susceptibilities including isospin-breaking effects at finite temperature T. These include $m_u \neq m_d$ contributions as well as electromagnetic ($e \neq 0$) corrections, both treated in a consistent chiral Lagrangian framework to leading order in $SU(2)$ and $SU(3)$ chiral perturbation theory, so that our predictions are model-independent. The chiral restoration temperature extracted from $\langle \bar{q}q \rangle = \langle \bar{u}u + \bar{d}d \rangle$ is almost unaffected, while the isospin-breaking order parameter $\langle \bar{u}u - \bar{d}d \rangle$ grows with T for the three-flavor case $SU(3)$. We derive a sum rule relating the condensate ratio $\langle \bar{q}q \rangle(e \neq 0)/\langle \bar{q}q \rangle(e = 0)$ with the scalar susceptibility difference $\chi(T) - \chi(0)$, directly measurable on the lattice. This sum rule is useful also for estimating condensate errors in staggered lattice analysis. Keeping $m_u \neq m_d$ allows one to obtain the connected and disconnected contributions to the susceptibility, even in the isospin limit, whose temperature, mass, and isospin-breaking dependence we analyze in detail. The disconnected part grows linearly, diverging in the chiral (infrared) limit as T/M_π, while the connected part shows a quadratic behavior, infrared regular as T^2/M_η^2, and coming from $\pi^0\eta$ mixing terms. This smooth connected behavior suggests that isospin-breaking correlations are weaker than critical chiral ones near the transition temperature. We explore some consequences in connection with lattice data and their scaling properties, for which our present analysis for physical masses, i.e. beyond the chiral limit, provides a useful model-independent description for low and moderate temperatures.

DOI: 10.1103/PhysRevD.83.076005 PACS numbers: 11.10.Wx, 11.30.Rd, 12.39.Fe

I. INTRODUCTION

The low-energy sector of QCD has been successfully described over recent years within the chiral Lagrangian framework. Chiral perturbation theory (ChPT) is based on the spontaneous breaking of chiral symmetry $SU_L(N_f) \times SU_R(N_f) \to SU_V(N_f)$ with $N_f = 2, 3$ light flavors and provides a consistent, systematic, and model-independent scheme to calculate low-energy observables [1–3]. The effective ChPT Lagrangian is constructed as an expansion of the form $\mathcal{L} = \mathcal{L}_{p^2} + \mathcal{L}_{p^4} + \cdots$, where p denotes a meson energy scale compared to the chiral scale $\Lambda_\chi \sim 1$ GeV. For the $N_f = 3$ case, the vector group symmetry is broken by the strange-light quark mass difference $m_s - m_{u,d}$, although m_s can still be considered as a perturbation compared to Λ_χ, leading to $SU(3)$ ChPT, which reduces formally to $SU(2)$ in the $m_s \to \infty$ limit [3]. The formalism can also be extended to finite temperature T, in order to describe meson gases and their evolution toward chiral symmetry restoration for T below the critical temperature T_c [4,5], where $T_c \simeq 180$–200 MeV from lattice simulations [6–9]. The use of ChPT in this context is important in order to provide model-independent results for the evolution of the different observables with T, supporting the original predictions for chiral restoration [10]. The latter are confirmed by lattice simulations, which are consistent with a crossover-like transition for $N_f = 3$ ($2 + 1$ flavors in the physical case), which becomes of second order for $N_f = 2$, in the $O(4)$ universality class, and first order in the degenerate case of three equal flavors.

The $SU_V(2)$ vector group is the isospin symmetry, which is a very good approximation to nature. However, there are several examples where isospin-breaking corrections are phenomenologically relevant, such as sum rules for quark condensates [3], meson masses [11], or pion scattering [12,13]. For a recent review see [14]. The two possible sources of isospin breaking are the QCD $m_d - m_u$ light quark mass difference and electromagnetic interactions. Both can be accommodated within the ChPT framework. The expected corrections from the first source are of order $(m_d - m_u)/m_s$ and are encoded in the quark mass matrix, generating also a $\pi^0\eta$ mixing term in the $SU(3)$ Lagrangian [3]. The electromagnetic interactions are included in the ChPT effective Lagrangian via the external source method and give rise to new terms [11–13,15] of order $\mathcal{L}_{e^2}$, $\mathcal{L}_{e^2p^2}$ and so on, with e the electric charge. These terms are easily incorporated into the ChPT power counting scheme by considering formally $e^2 = \mathcal{O}(p^2/F^2)$, with F the pion decay constant in the chiral limit.

The purpose of this paper is to study within ChPT isospin-breaking effects related to the thermodynamics of the meson gas. We will be particularly interested in the physical quantities directly related to spontaneous chiral symmetry breaking and its restoration, namely, the quark condensates and their corresponding susceptibilities at finite temperature. The quark condensate is the order parameter of chiral restoration, but since the transition is

*gomez@fis.ucm.es
†rtandres@fis.ucm.es

a smooth crossover for the physical case, different observables can yield different transition temperatures. Thus, the susceptibilities, defined as derivatives of the condensates with respect to the quark masses, provide also direct information about the transition and its nature, since they tend to peak around the transition point reflecting the growth of correlations.

Let us mention some of the motivations we have in mind for the present analysis. For the physical values of quark and meson masses, we are interested in the effect of the isospin-breaking terms in the light quark condensate $\langle \bar{u}u + \bar{d}d \rangle$ and therefore on the ChPT estimates of the critical temperature. In addition, in the isospin asymmetric case, one has $\langle \bar{u}u \rangle \neq \langle \bar{d}d \rangle$ and in fact $\langle \bar{u}u - \bar{d}d \rangle$ can be considered an order parameter for isospin breaking. Actually, isospin is not spontaneously broken in QCD [16], which means that this order parameter should vanish for $m_u = m_d$ and $e = 0$. This is an important difference with the scalar condensate $\langle \bar{u}u + \bar{d}d \rangle$, which is nonzero in the chiral limit. It is relevant to estimate the thermal evolution of $\langle \bar{u}u - \bar{d}d \rangle$, since in principle the two condensates melt at different critical temperatures. A further motivation is the analysis of the three independent susceptibilities, directly related to the isosinglet, connected (isotriplet), and disconnected susceptibilities [17] often discussed in lattice analysis [18–21]. Including properly the $m_u - m_d$ dependence of condensates is then essential to analyze the temperature and mass evolution of the connected and disconnected pieces measured in the lattice. In particular, the linear $m_d - m_u$ corrections to condensates survive the $m_u = m_d$ limit in the susceptibilities. The contributions coming from $\pi^0\eta$ mixing in the $SU(3)$ case belong to this type and are particularly important regarding the temperature dependence. This is not only interesting for physical masses but also to explore the scaling near the chiral limit, which in lattice studies has been used to investigate the nature of the transition [20]. In the lattice works, this scaling may be contaminated by lattice artifacts such as taste breaking in the staggered fermion formalism, which can generate contributions to susceptibilities masking the true scaling behavior [20,21]. Our study provides then a model-independent setup for disentangling these effects and establishes the expected results in the continuum limit.

We will work in ChPT to one loop, considering on the same footing the two sources of isospin breaking. In a previous work [22] we have studied the quark condensates at $T = 0$ and several related phenomenological aspects of the isospin asymmetric case. We will refer to that work for more details about the formalism, the numerical values of the low-energy constants, and other related issues.

The paper is organized as follows. In Sec. II we will review the main aspects of the isospin-breaking ChPT formalism related to the present work. Our results for the quark condensates at finite T both in the $SU(2)$ and $SU(3)$ cases are given and analyzed in Sec. III. In that section we explore the temperature dependence of isospin breaking, as well as that of the sum rule relating condensate ratios. Section IV is devoted to the analysis of the different isospin-breaking scalar susceptibilities and their relation to the connected and disconnected ones. In Sec. IV A we provide an interesting sum rule relating the electromagnetic differences in the condensates with the total susceptibility. We explore the possibility of using that sum rule to estimate the errors in the staggered fermion lattice analysis of the condensates, in connection with the taste-breaking effect. In Sec. IV B we make a thorough study of the connected and disconnected contributions to the susceptibility and their dependence with temperature, the quark mass, and the isospin ratio m_u/m_d. We pay special attention to the connection of our results with different lattice analysis in the literature.

II. FORMALISM

The effective chiral Lagrangian up to fourth order in p (a meson mass, momentum, temperature, or derivative) including electromagnetic interactions proportional to e^2 is given schematically by $\mathcal{L}_{\text{eff}} = \mathcal{L}_{p^2+e^2} + \mathcal{L}_{p^4+e^2p^2+e^4}$. The most general second-order Lagrangian is the familiar nonlinear sigma model, including the gauge coupling of mesons to the electromagnetic field through the covariant derivative, plus an additional term proportional to a low-energy constant C compatible with the $e \neq 0$ symmetries of the QCD Lagrangian [11,15],

$$\mathcal{L}_{p^2+e^2} = \frac{F^2}{4}\,\text{tr}[D_\mu U^\dagger D^\mu U + 2B_0\mathcal{M}(U + U^\dagger)] + C\,\text{tr}[QUQU^\dagger]. \tag{1}$$

Here, $U(x) = \exp[i\Phi/F] \in SU(N_f)$, with Φ the Goldstone boson (GB) matrix field for pions ($N_f = 2$) plus kaons and η ($N_f = 3$), the latter being the octet member with $I_3 = S = 0$. The covariant derivative is $D_\mu = \partial_\mu + iA_\mu[Q, \cdot]$ with A_μ the electromagnetic (EM) field. $\mathcal{M}$ and Q are the quark mass and charge matrices, i.e., in $SU(3)$ $\mathcal{M} = \text{diag}(m_u, m_d, m_s)$ and $Q = (e/3)\text{diag}(2, -1, -1)$. Both the mass term and the charge one proportional to C in (1) break explicitly the chiral symmetry $SU_L(N_f) \times SU_R(N_f)$ under which $U \to LUR^\dagger$ with $L, R \in SU(N_f)$. The vector symmetry $L = R$ is also broken for unequal quark masses and charges. Thus, in the light sector (u, d) the part of the mass term proportional to $\hat{m} = (m_u + m_d)/2$, the average light quark mass, is also proportional to the identity flavor matrix and therefore invariant under $SU_V(2)$, while the part proportional to the mass difference $m_\delta = (m_u - m_d)/2$ and T_3, the third isospin generator, is the one carrying out the QCD isospin breaking. The only remaining symmetry of the Lagrangian (1) is the $U(1)$ $L = R = \exp(i\lambda Q)$ corresponding to charge conservation.

Working out the kinetic terms in (1) allows one to relate the low-energy parameters F, $B_0 m_{u,d,s}$, C to the leading-order tree-level values for the decay constants and masses of the pseudo-Goldstone bosons. For $SU(2)$ the masses read

$$M^2_{\pi^+} = M^2_{\pi^-} = 2\hat{m}B_0 + 2C\frac{e^2}{F^2}, \qquad M^2_{\pi^0} = 2\hat{m}B_0. \quad (2)$$

In the $SU(3)$ case, the mass term in (1) induces a mixing between the π^0 and the η fields given by $\mathcal{L}_{\rm mix} = (B_0/\sqrt{3})(m_d - m_u)\pi^0\eta$. This mixing between the two states with $I_3 = S = 0$ will play an important role in what follows. The kinetic term has then to be brought to the canonical form before identifying the GB masses, which can be easily done by the field rotation [3]

$$\pi^0 = \bar{\pi}^0\cos\varepsilon - \bar{\eta}\sin\varepsilon, \qquad \eta = \bar{\pi}^0\sin\varepsilon + \bar{\eta}\cos\varepsilon, \quad (3)$$

where the mixing angle is given by

$$\tan 2\varepsilon = \frac{\sqrt{3}}{2}\frac{m_d - m_u}{m_s - \hat{m}}. \quad (4)$$

Once the above $\pi^0\eta$ rotation is performed, the $SU(3)$ tree-level meson masses to leading order read

$$\begin{aligned} M^2_{\pi^+} &= M^2_{\pi^-} = 2\hat{m}B_0 + 2C\frac{e^2}{F^2}, \\ M^2_{\pi^0} &= 2B_0\left[\hat{m} - \frac{2}{3}(m_s - \hat{m})\frac{\sin^2\varepsilon}{\cos 2\varepsilon}\right], \\ M^2_{K^+} &= M^2_{K^-} = (m_s + m_u)B_0 + 2C\frac{e^2}{F^2}, \\ M^2_{K^0} &= (m_s + m_d)B_0, \\ M^2_{\eta} &= 2B_0\left[\frac{1}{3}(\hat{m} + 2m_s) + \frac{2}{3}(m_s - \hat{m})\frac{\sin^2\varepsilon}{\cos 2\varepsilon}\right]. \end{aligned} \quad (5)$$

For pions, the main effect in the $\pi^0 - \pi^+$ mass difference comes from the EM contribution [23], while in the kaon and eta cases the violations of Dashen's theorem $M^2_{K^\pm} - M^2_{K^0} = M^2_{\pi^\pm} - M^2_{\pi^0}$ [24] ($m_u = m_d$ limit) indicate that $m_u - m_d$ corrections are relevant and must be kept on the same footing as the EM ones [11,25]. We emphasize that all the previous expressions hold for tree-level leading-order masses M^2_a with $a = \pi^\pm$, π^0, $K^\pm$, η, in terms of which we will express all our results. They coincide with the physical masses to leading order in ChPT, i.e., $M^2_{a,\rm phys} = M^2_a(1 + \mathcal{O}(M^2))$ and so on for the meson decay constants $F^2_a = F^2(1 + \mathcal{O}(M^2))$.

The fourth-order Lagrangian consists of all possible terms compatible with the QCD symmetries to that order, including the EM ones. The $\mathcal{L}_{p^4}$ Lagrangian is given in [2] for the $SU(2)$ case, $h_{1,2,3}$ (contact terms) and $l_{1\ldots7}$ denoting the dimensionless low-energy constants (LEC) multiplying each independent term, and in [3] for $SU(3)$, the LEC named $H_{1,2}$ and $L_{1\ldots10}$. The electromagnetic $\mathcal{L}_{e^2p^2}$ and $\mathcal{L}_{e^4}$ for $SU(2)$ are given in [12,13], $k_{1,\ldots13}$ denoting the corresponding LEC, and in [11] for $SU(3)$ with the $K_{1\ldots17}$ LEC. The relevant terms needed for this work are given in [22].

The LEC are renormalized in such a way that they absorb all the one-loop ultraviolet divergences coming from $\mathcal{L}_{p^2}$ and $\mathcal{L}_{e^2}$, according to the ChPT counting, rendering the observables finite and scale-independent. The numerical values of the LEC at a given scale can be fitted to meson experimental data, except the contact h_i and H_i. The latter are needed for renormalization but cannot be directly measured, reflecting an ambiguity in the observables depending on them. The origin of this ambiguity is in the very same definition of the condensates in perturbation theory [2]. It is therefore convenient to define suitable combinations which are independent of those constants and therefore can be determined numerically. We will bear this in mind throughout this work and we will try to provide such combinations when isospin breaking is included. The numerical values we will use for masses and low-energy constants in the $SU(3)$ case are the same as in [22] unless otherwise stated. In $SU(3)$ they come from the fits performed in [26].

III. QUARK CONDENSATES AT FINITE TEMPERATURE

The quark condensates for a given flavor q_i at finite temperature T are given by

$$\langle\bar{q}_i q_i\rangle_T = -\frac{1}{\beta V}\frac{\partial}{\partial m_i}\log Z = \left\langle\frac{\partial\mathcal{L}_{\rm eff}}{\partial m_i}\right\rangle_T, \quad (6)$$

where $\beta = 1/T$, V is the system volume, Z the partition function, and $\langle\cdot\rangle_T$ denotes a thermal average. We will denote by $\langle\bar{q}q\rangle_T = \langle\bar{u}u + \bar{d}d\rangle_T = -\frac{1}{\beta V}\frac{\partial}{\partial\hat{m}}\log Z$ the order parameter of chiral symmetry, while $\langle\bar{u}u - \bar{d}d\rangle_T = -\frac{1}{\beta V}\frac{\partial}{\partial m_\delta}\log Z$ behaves as an order parameter of isospin breaking, since it is the expectation value of the part of the mass term in the QCD Lagrangian proportional to $m_u - m_d$ and $e(q_u - q_d)$, respectively. It is still invariant under transformations in the third direction of isospin, which reflects electric charge conservation.

In ChPT to one loop we obtain then the $SU(2)$ finite temperature extension of the $T = 0$ results in [22], which we give also for consistency,

$$\begin{aligned} \langle\bar{q}q\rangle_T &\equiv \langle\bar{u}u + \bar{d}d\rangle_T \\ &= \langle\bar{q}q\rangle_0 + B_0[g_1(M_{\pi^0}, T) + 2g_1(M_{\pi^\pm}, T)] + \mathcal{O}(p^2), \\ \langle\bar{q}q\rangle_0 &= -2F^2B_0\Big[1 - \mu_{\pi^0} - 2\mu_{\pi^\pm} + 2\frac{M^2_{\pi^0}}{F^2}(l^r_3(\mu) \\ &\quad + h^r_1(\mu)) + e^2\mathcal{K}^r_2(\mu) + \mathcal{O}(p^4)\Big], \end{aligned} \quad (7)$$

$$\begin{aligned} \langle\bar{u}u - \bar{d}d\rangle_T &= \langle\bar{u}u - \bar{d}d\rangle_0 \\ &= 4B_0^2(m_d - m_u)h_3 - \frac{8}{3}F^2B_0e^2k_7 + \mathcal{O}(p^2), \end{aligned} \quad (8)$$

where

$$\mathcal{K}^r_2(\mu) = \frac{4}{9}[5(k^r_5(\mu) + k^r_6(\mu)) + k_7], \tag{9}$$

and

$$\mu_i = \frac{M_i^2}{32\pi^2 F^2}\log\frac{M_i^2}{\mu^2},$$
$$g_1(M,T) = \frac{1}{2\pi^2}\int_0^\infty dp\,\frac{p^2}{E_p}\,\frac{1}{e^{\beta E_p}-1}, \tag{10}$$

with $E_p^2 = p^2 + M^2$.

The expression (7) contains the leading-order tree-level term from $\mathcal{L}_2$ given by $\langle\bar{q}q\rangle_0 = -2F^2B_0$, the one-loop tadpolelike contribution $G_i(x=0)$, with G the free meson thermal propagator, whose finite part yields the combinations $\mu_i + g_1(M_i,t)/(2F^2)$ (we follow the same finite-T notation as in [5]) and the tree level from the fourth-order Lagrangian. The latter shows up only at $T=0$, which contains the LEC renormalized at the scale μ of dimensional regularization in the $\overline{\text{MS}}$ scheme [2,13] so that the full expressions for the condensates are finite and scale-independent. Note that $\langle\bar{q}q\rangle_0$ includes the contact term h_1^r. The isospin breaking in $\langle\bar{q}q\rangle_T$ for $SU(2)$ is purely electromagnetic, showing up explicitly in the e^2 terms and implicitly through the pion mass differences. The temperature dependence is encoded in the functions $g_1(M,T)$ which increase with T and behave near the chiral limit ($T \gg M$) as $g_1(M,T) = \frac{T^2}{12}[1 + \mathcal{O}(M/T)]$.

Note that the effect of the electromagnetic corrections is to decrease the thermal part of $\langle\bar{q}q\rangle_T$, since $M_{\pi^\pm} > M_{\pi^0}$. On the other hand, $\langle\bar{q}q\rangle_0$ increases for the available estimates of the EM LEC, reflecting its ferromagnetic nature [22]. Our first conclusion is then that the critical temperature, estimated as that for which the condensate vanishes, increases with respect to the $e=0$ case, which is also a ferromagnetic-like behavior induced by the explicit chiral symmetry breaking of the EM quark coupling in the QCD action. A simple estimate of the size of this effect can be obtained by taking the chiral limit $m_u = m_d = 0$ so that $M_{\pi^0} = \mu_{\pi^0} = 0$, $M^2_{\pi^\pm} = 2Ce^2/F^2$, and $T_c = \sqrt{8F}\sqrt{1 + e^2\mathcal{K}^r_2 - 2\mu_{\pi^\pm}}$, which gives $T_c^{e\neq0}/T_c^{e=0} \simeq 1.003$ with the parameters used in [22] and setting the involved k_i to their maximum expected "natural" values $k_i = 1/(16\pi^2)$. Thus, in principle we expect rather small corrections to chiral restoration from the electromagnetic breaking. Nevertheless, in Sec. IV A we will go back to this point in connection with a sum rule relating the charge breaking with the susceptibility, suggesting larger corrections either for higher order transitions or for finite lattice spacing.

The two sources of explicit isospin breaking in the Lagrangian show up in the condensate difference (8), which depends linearly on $m_u - m_d$ with the contact h_3 and vanishes for $m_u = m_d$ and $e=0$ in accordance with the absence of spontaneous isospin breaking [16] mentioned in the introduction. Recall that h_3 and k_7 do not need to be renormalized and are therefore finite and scale independent. An important point is that $\langle\bar{u}u - \bar{d}d\rangle$ does not receive pion loop corrections in the two-flavor case and it is therefore temperature-independent to the one-loop order. In other words, isospin breaking in $SU(2)$ does not change with T and the two condensates melt at the same temperature. This picture will change for $N_f = 3$ due to kaon loops and $\pi^0\eta$ mixing.

In the $SU(3)$ case, we calculate to one loop at finite temperature the light and strange condensates, taking into account both $m_u - m_d$ and $e \neq 0$ corrections. The condensates read now

$$\begin{aligned}
\langle\bar{q}q\rangle_T^{SU(3)} &\equiv \langle\bar{u}u + \bar{d}d\rangle_T^{SU(3)} \\
&= \langle\bar{q}q\rangle_0^{SU(3)} + B_0\Big[\frac{1}{3}(3-\sin^2\varepsilon)g_1(M_{\pi^0},T) + 2g_1(M_{\pi^\pm},T) + g_1(M_{K^0},T) \\
&\quad + g_1(M_{K^\pm},T) + \frac{1}{3}(1+\sin^2\varepsilon)g_1(M_\eta,T)\Big] + \mathcal{O}(p^2), \\
\langle\bar{q}q\rangle_0^{SU(3)} &= -2F^2B_0\Big\{1 + \frac{8B_0}{F^2}[\hat{m}(2L_8^r(\mu) + H_2^r(\mu)) + 4(2\hat{m}+m_s)L_6^r(\mu)] + e^2\mathcal{K}^r_{3+}(\mu) \\
&\quad - \frac{1}{3}(3-\sin^2\varepsilon)\mu_{\pi^0} - 2\mu_{\pi^\pm} - \mu_{K^0} - \mu_{K^\pm} - \frac{1}{3}(1+\sin^2\varepsilon)\mu_\eta + \mathcal{O}(p^4)\Big\},
\end{aligned} \tag{11}$$

$$\begin{aligned}
\langle\bar{u}u - \bar{d}d\rangle_T^{SU(3)} &= \langle\bar{u}u - \bar{d}d\rangle_0^{SU(3)} + B_0\Big\{\frac{\sin2\varepsilon}{\sqrt{3}}[g_1(M_{\pi^0},T) - g_1(M_\eta,T)] + g_1(M_{K^\pm},T) - g_1(M_{K^0},T)\Big\} + \mathcal{O}(p^2), \\
\langle\bar{u}u - \bar{d}d\rangle_0^{SU(3)} &= 2F^2B_0\Big\{\frac{4B_0}{F^2}(m_d - m_u)(2L_8^r(\mu) + H_2^r(\mu)) - e^2\mathcal{K}^r_{3-}(\mu) + \frac{\sin2\varepsilon}{\sqrt{3}}[\mu_{\pi^0} - \mu_\eta] + \mu_{K^\pm} - \mu_{K^0}\Big\} + \mathcal{O}(p^2),
\end{aligned} \tag{12}$$

$$\langle\bar{s}s\rangle_T = \langle\bar{s}s\rangle_0 + B_0\left\{\frac{2}{3}[g_1(M_{\pi^0},T)\sin^2\varepsilon + g_1(M_\eta,T)\cos^2\varepsilon] + g_1(M_{K^\pm},T) + g_1(M_{K^0},T)\right\} + \mathcal{O}(p^2),$$

$$\langle\bar{s}s\rangle_0 = -F^2B_0\left\{1 + \frac{8B_0}{F^2}[m_s(2L_8^r(\mu) + H_2^r(\mu)) + 4(2\hat{m} + m_s)L_6^r(\mu)] + e^2\mathcal{K}_s^r(\mu)\right.$$
$$\left. - \frac{4}{3}[\mu_{\pi^0}\sin^2\varepsilon + \mu_\eta\cos^2\varepsilon] - 2[\mu_{K^\pm} + \mu_{K^0}] + \mathcal{O}(p^4)\right\}, \quad (13)$$

where

$$\mathcal{K}_{3+}^r(\mu) = \frac{4}{9}[6(K_7 + K_8^r(\mu)) + 5(K_9^r(\mu) + K_{10}^r(\mu))],$$
$$\mathcal{K}_{3-}^r(\mu) = \frac{4}{3}[K_9^r(\mu) + K_{10}^r(\mu)],$$
$$\mathcal{K}_s^r(\mu) = \frac{8}{9}[3(K_7 + K_8^r(\mu)) + K_9^r(\mu) + K_{10}^r(\mu)]. \quad (14)$$

In some of the above terms we have preferred to leave the results in terms of quark instead of meson masses. As in the $SU(2)$ case, the results are finite and scale-independent, which concerns only the $T = 0$ part [22].

There are some important differences with respect to the $N_f = 2$ case which deserve to be mentioned. First, the presence of the $\pi^0\eta$ mixing angle ε (4) and the more complicated dependence of meson masses with quark masses (5), imply that now $m_u - m_d$ corrections show up in $\langle\bar{q}q\rangle$, apart from the EM ones. Note also that these corrections in $\langle\bar{q}q\rangle$ and $\langle\bar{s}s\rangle$ are at least $\mathcal{O}(\varepsilon^2)$ in the mixing angle, or equivalently in $m_u - m_d$, except for an $\mathcal{O}(e^2\varepsilon)$ term in the kaon contribution. This is so because, apart from the explicit ε dependence, one has to expand also the meson masses in (5) around $\varepsilon = 0$. All the masses depend quadratically on ε except $M_{K^\pm}^2 \sim -a\varepsilon$, $M_{K^0}^2 \sim a\varepsilon$ with $a = (2B_0/\sqrt{3})(m_s - \hat{m})$. Since, in addition, $M_{K^\pm}^2 = M_{K^0}^2 + 2Ce^2/F^2$ for $\varepsilon = 0$, we end up with the above-mentioned term.

Another important difference between the two cases is that for $SU(3)$ there are loop contributions to $\langle\bar{u}u - \bar{d}d\rangle_T$ in (12). Kaon loops arise from the charged-neutral kaon mass difference, while neutral pion and eta ones from $\pi^0\eta$ mixing. When expanding in ε now, the leading order is $\mathcal{O}(\varepsilon)$ even for $e = 0$. These linear terms will be crucial for our analysis of susceptibilities in Sec. IV. Those loop corrections introduce now a T dependence in $\langle\bar{u}u - \bar{d}d\rangle_T$, unlike the $SU(2)$ case. As it happened in the $SU(2)$ case, we see that $\langle\bar{u}u - \bar{d}d\rangle_T$ in (12) vanishes for e^2 and $m_u = m_d$, in agreement with [16], which still holds including thermal corrections.

At low and moderate temperatures $g_1(M_{\pi^0},T)$ dominates over the kaon and eta contributions in (12), but it should be remembered that ε in (4) brings up a $1/m_s$ dependence which reduces the size of the pion term. In order to make a crude estimate, let us consider again the chiral limit, but keeping now the leading order in $m_u - m_d$, which we take then very small but nonzero while taking $\hat{m} \to 0^+$. In this limit the kaon masses are roughly kept to their physical values, which are well above the critical temperature. Thus, we consider the regime $M_\pi \ll T \ll M_K$, in which the pion term behaves as $B_0(m_d - m_u)T^2/(24m_s) = B_0^2(m_d - m_u)T^2/(18M_\eta^2)$. The kaon and eta contributions go like $B_0T^2[(m_d - m_u)/m_s] \times \sqrt{M_{K,\eta}/T}e^{-M_{K,\eta}/T}$ [5], where we have taken also $e = 0$ for simplicity. The pion term is still dominant due to the exponential suppression of K,η. However, when compared to the $T = 0$ part in that regime, which goes like $(m_d - m_u)B_0^2$, we see that the quadratic growth with temperature is controlled by the scale M_η^2 instead of, say, the chiral restoring behavior of $\langle\bar{q}q\rangle_T$ which is controlled by F^2 in the chiral limit. Therefore, the order parameter for isospin breaking $\langle\bar{u}u - \bar{d}d\rangle_T$ grows with T, although it does so rather softly. Therefore, we do not expect big differences in the melting temperatures of the u and d condensates. This is also consistent with the expectation that in the limit where m_s is arbitrarily large, say compared to $\hat{m}$, the $SU(2)$ result should be recovered, for which there is no temperature dependence for the condensate difference.

The evolution with temperature of the condensate difference is shown in Fig. 1 for the full case of finite pion mass and both $e \neq 0$ and $m_u \neq m_d$. We have used the same set of low-energy constants and parameters as in [22], in particular $m_u/m_d = 0.46$ and $m_s/\hat{m} = 24$. For the EM LEC K_i involved, we have displayed in the figure the two curves corresponding to their maximum and minimum expected natural values. We also show for comparison the result for $m_u = m_d$, which shows that the charge contribution is actually of the same order as the one proportional to $m_u - m_d$. We see that the T-dependent amplification of the isospin difference is rather large. In fact, this order parameter reaches values comparable to its $T = 0$ value near the critical temperature, which is about $T_c \simeq 265$ MeV in $SU(3)$ ChPT. Nevertheless, due to the additional ε suppressing factor discussed above, this enhancement is not enough to produce a sizable difference in the melting temperature of the u, d condensates, as it is clearly seen in Fig. 1 (right), where we plot the two thermal condensates separately. The two plots shown in Fig. 1 correspond then, respectively, to the two order parameters involved here: isospin breaking and chiral restoration. In turn, note that the curves on the right plot are independent of the choice of LEC since to this order $\langle\bar{q}_iq_i\rangle_T/\langle\bar{q}_iq_i\rangle_0 = 1 - (\langle\bar{q}_iq_i\rangle_T - \langle\bar{q}_iq_i\rangle_0)/(B_0F^2) + \mathcal{O}(p^4)$ for $i = u, d$.

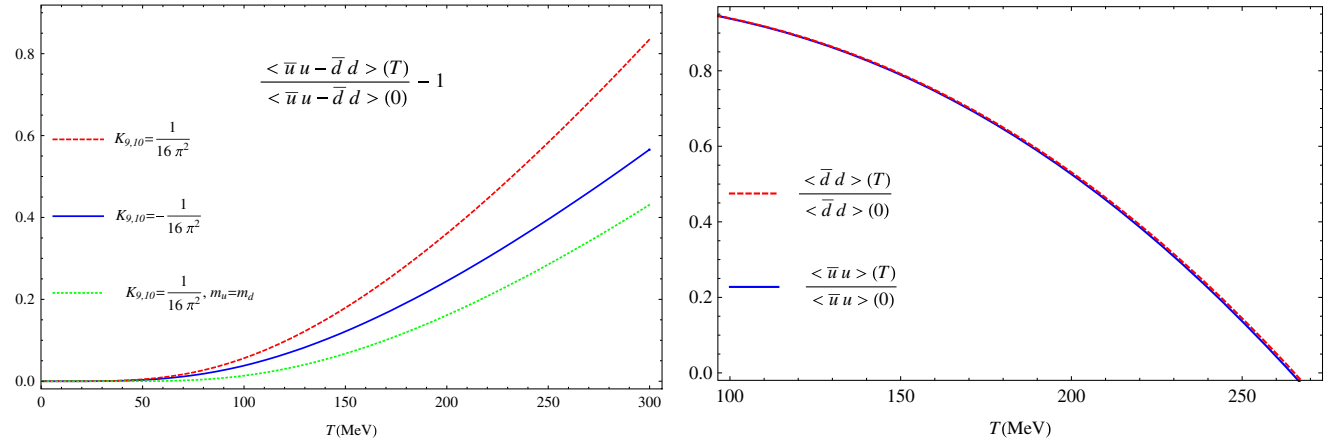

FIG. 1 (color online). Left: the $u-d$ condensate difference (isospin-breaking order parameter) at finite temperature in $SU(3)$, relative to its $T=0$ value. Right: the two condensates separately.

The individual condensates in (11)–(13) contain the contact terms H_2. These terms reflect an ambiguity in the quark condensates, inherent to their renormalization in QCD. It is therefore very important to deal with combinations of condensates which are free of this ambiguity. This very same source of ambiguity is also present in lattice simulations at finite T. A simple way to get rid of it is to subtract the $T=0$ contribution. This is the approach followed by the authors of Ref. [8] both for condensates and for susceptibilities. A different possibility is to consider the combination $\langle\bar{q}q\rangle-(\hat{m})/m_s\langle\bar{s}s\rangle$ [9], or for individual condensates in the isospin-breaking case, $\langle\bar{q}_iq_i\rangle-(m_i/m_s)\times\langle\bar{s}s\rangle$ with $i=u,d$. Another sum rule free of contact ambiguities often used in $T=0$ phenomenology to relate condensate ratios [3] is the following combination:

$$\begin{aligned}\Delta_{\mathrm{SR}}(T)&\equiv\frac{\langle\bar{d}d\rangle_T}{\langle\bar{u}u\rangle_T}-1+\frac{m_d-m_u}{m_s-\hat{m}}\left[1-\frac{\langle\bar{s}s\rangle_T}{\langle\bar{u}u\rangle_T}\right]\\&=\Delta_{\mathrm{SR}}(0)+\frac{m_d-m_u}{m_s-\hat{m}}\frac{1}{F^2}[g_1(M_K,T)-g_1(M_\pi,T)\\&\quad+(M_K^2-M_\pi^2)g_2(M_K,T)]-\frac{2Ce^2}{F^4}g_2(M_K,T),\end{aligned}\tag{15}$$

where $\mathcal{O}(m_u-m_d)^2$, $\mathcal{O}(e^4)$ $\mathcal{O}(e^2(m_u-m_d)^2)$ have been neglected and $\Delta_{\mathrm{SR}}(0)$ is given in [22] with both sources of isospin breaking contributing at the same order, not only in the chiral counting but also numerically.

We have seen in Sec. III that the $\langle\bar{d}d\rangle_T/\langle\bar{u}u\rangle_T$ ratio receives significant corrections at finite temperature. On the other hand, we expect the strange condensate to vary slowly with T, from chiral symmetry breaking due to the strange quark mass. Therefore, we expect that the thermal corrections to this sum rule are also sizable. These corrections are plotted in Fig. 2 for $K_9^r+K_{10}^r=1/(8\pi^2)$. They become comparable to the $T=0$ sum rule near the critical temperature.

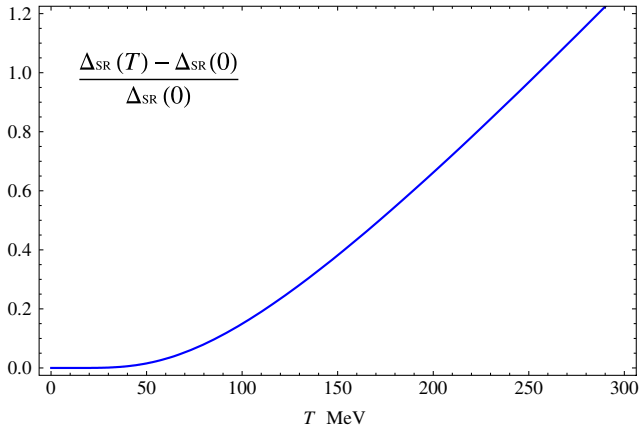

FIG. 2 (color online). Thermal corrections to the sum rule relating condensate ratios.

IV. SCALAR SUSCEPTIBILITIES AND ISOSPIN BREAKING

In the isospin-breaking case, the scalar susceptibilities are defined as

$$\begin{aligned}\chi_{ij}&=-\frac{\partial}{\partial m_i}\langle\bar{q}_jq_j\rangle_T=\frac{1}{\beta V}\frac{\partial^2}{\partial m_i\partial m_j}\log Z\\&=\int_0^\beta d\tau\int d^3\vec{x}\langle(\bar{q}_iq_i)(\vec{x},\tau)(\bar{q}_jq_j)(0,0)\rangle_T\\&\quad-\beta V\langle\bar{q}_iq_i\rangle_T\langle\bar{q}_jq_j\rangle_T,\\&i,j=u,d,s,\end{aligned}\tag{16}$$

so that in the light sector, the relevant one concerning chiral restoration, we have three independent scalar susceptibilities χ_{uu}, χ_{dd}, and $\chi_{ud}=\chi_{du}$.

At this point, it is instructive to recall the definition of the connected and disconnected parts of the susceptibility. Consider the isospin limit with two light identical flavors

of mass $\hat{m} = m_u = m_d$ and $e = 0$. There is only one light susceptibility in this case, which can be written as

$$\chi = -\frac{\partial}{\partial \hat{m}}\langle \bar{q}q\rangle_T = \frac{1}{\beta V}\frac{\partial^2}{\partial \hat{m}^2}\log Z = 4\chi_{\rm dis} + 2\chi_{\rm con}, \quad (17)$$

with

$$\chi_{\rm dis} = \langle (\mathrm{Tr} D_l^{-1})^2\rangle_A - \langle \mathrm{Tr} D_l^{-1}\rangle_A^2, \quad (18)$$

$$\chi_{\rm con} = -\langle \mathrm{Tr} D_l^{-2}\rangle_A, \quad (19)$$

where $D_l = i\partial\!\!\!/ - \hat{m}$ is the Dirac operator for every light flavor in the QCD Lagrangian and $\langle\cdot\rangle_A$ denotes integration over the gluon fields, so that formally $Z = \langle \exp\sum_j \mathrm{Tr}\log D_j\rangle_A$, where j runs over flavor and Tr runs over the space-time, Dirac, and color indices. This separation is important for lattice analysis, as we will discuss below, and reflects the contributions with connected and disconnected quark lines, since D_l^{-1} is the quark propagator. However, when considering the low-energy representation for the partition function and the susceptibilities in terms of GB fields, it is not so simple to separate the connected and disconnected parts if we take the isospin limit from the very beginning. A possible approach to perform such separation is to work within the partially quenched ChPT framework, as discussed in [27] for the vacuum polarization. We will however work within the isospin-breaking scenario we are considering here, which is very useful for this purpose, as noted first in [17] for the susceptibilities and used also in [28] for the vacuum polarization. The main point is that for $m_u \neq m_d$

$$\chi_{ud} = \langle (\mathrm{Tr} D_u^{-1})(\mathrm{Tr} D_d^{-1})\rangle_A - \langle \mathrm{Tr} D_u^{-1}\rangle_A \langle \mathrm{Tr} D_d^{-1}\rangle_A, \quad (20)$$

so that one has $\chi_{\rm dis} = \lim_{m_u\to m_d}\chi_{ud}$ and since $\partial_{\hat{m}} = \partial_{m_u} + \partial_{m_d}$, from (17) we have also $\chi_{\rm con} = \lim_{m_u\to m_d}[(\chi_{uu} + \chi_{dd})/2 - \chi_{ud}]$.

Therefore, with this observation in mind, we define in the isospin-breaking regime the following basis of total, connected, and disconnected susceptibilities in terms of the ij basis in (16):

$$\chi = \chi_{uu} + \chi_{dd} + 2\chi_{ud}, \quad (21)$$

$$\chi_{\rm con} = \frac{1}{2}(\chi_{uu} + \chi_{dd}) - \chi_{ud}, \quad (22)$$

$$\chi_{\rm dis} = \chi_{ud}, \quad (23)$$

which we can therefore obtain directly from our expressions for the isospin-breaking condensates obtained in the previous section. Observe that none of the K_i-dependent terms in the condensates depends on the quark masses and therefore the susceptibilities are independent of the EM LEC.

Note that according to (16), χ in (21) corresponds to the correlator of the isosinglet condensate $\langle \bar{q}q\rangle$, the order parameter of chiral restoration, while the connected contribution $\chi_{\rm con}$ is the correlator of the isotriplet $\bar{u}u - \bar{d}d$, the order parameter for isospin symmetry. A divergence or sudden growth of these susceptibilities would indicate then a phase transition for the corresponding order parameter.

We also remark that the definitions of the connected and disconnected parts in terms of uu, dd, ud ones are not unique. We could as well have defined $\chi_{\rm dis}$ as $\alpha(\chi_{uu} - \chi_{dd}) + \chi_{ud}$ for arbitrary α, which also reduces to the combination (18) in the isospin limit. We are following the same convention as [17]. These formulas can be easily extended to N_f identical flavors, for which $\chi = N_f\chi_{\rm con} + N_f^2\chi_{\rm dis}$.

In the following we will analyze several aspects related to the above defined susceptibilities in different limits.

A. Sum rule for EM-like corrections to condensates

Before studying in detail the different susceptibilities, in this subsection we will relate the EM corrections (and actually any chargelike correction to pion masses) to the condensates, found in Sec. III, with the total scalar susceptibility. Consider first the condensate calculated in $SU(2)$ in (7) and let us define the ratio

$$r(T) \equiv \frac{\langle \bar{q}q\rangle_T^{e\neq 0}}{\langle \bar{q}q\rangle_T^{e=0}}. \quad (24)$$

Now note that to one loop, the explicit dependence of the condensate in e^2 is only in the $T = 0$ part, since the charge dependence in $\mathcal{L}_2$ is contained implicitly in the pion mass differences. Therefore, $r(T) - r(0)$ depends on the charge only through the parameter $\delta_\pi \equiv (M_{\pi^\pm}^2 - M_{\pi^0}^2)/M_{\pi^0}^2$, in which we can further expand (for the EM pion mass difference $\delta_\pi \simeq 0.1$). Taking also into account that the condensate is just the sum of the tadpole contributions for the three pions, we can write

$$r(T) - r(0) = -\frac{M_\pi^2}{2B_0F^2}\delta_\pi \frac{\partial}{\partial M_{\pi^\pm}^2}[\langle \bar{q}q\rangle_T - \langle \bar{q}q\rangle_0] + \mathcal{O}(\delta_\pi^2) + \mathcal{O}(p^4) \quad (25)$$

$$= -\frac{M_\pi^2}{6B_0^2F^2}\delta_\pi \frac{\partial}{\partial \hat{m}}[\langle \bar{q}q\rangle_T - \langle \bar{q}q\rangle_0] + \mathcal{O}(\delta_\pi^2) + \mathcal{O}(p^4), \quad (26)$$

which, from the susceptibility definition in (21) can be written, to this order, as

$$r(T) - r(0) = \frac{2}{3}\frac{\hat{m}^2}{M_\pi^2F^2}\delta_\pi[\chi(T) - \chi(0)]. \quad (27)$$

This sum rule relates then pion mass deviations in the condensate with the total scalar susceptibility. Note that the above result is written only in terms of the quark mass, the pion mass and decay constant, and the charged-neutral mass difference, without specifying if the latter is of electromagnetic origin. It states that, even though the mass

deviation δ_π may be small, the corrections to the condensate may be amplified near the phase transition, where the susceptibility is maximum, if such transition is sufficiently strong. Actually, the quantity proportional to δ_π on the right-hand side of (27) is directly measurable on the lattice [8].

For the case of the electromagnetic mass difference in $SU(2)$ discussed in Sec. II, we have $\delta_\pi M^2_{\pi^0} = 2Ce^2/F^2$ and

$$r(T) - r(0) = \frac{2Ce^2}{F^4} g_2(M_{\pi^0}, T) + \mathcal{O}(e^4), \tag{28}$$

with

$$r(0) = 1 + e^2 \mathcal{K}^r_2(\mu) - \frac{4Ce^2}{F^4} \nu_{\pi^0}, \tag{29}$$

and

$$\nu_i = F^2 \frac{d}{dM_i^2} \mu_i = \frac{1}{32\pi^2}\left[1 + \log\frac{M_i^2}{\mu^2}\right],$$
$$g_2(M,T) = -\frac{dg_1(M,T)}{dM^2} = \frac{1}{4\pi^2}\int_0^\infty dp \frac{1}{E_p}\frac{1}{e^{\beta E_p} - 1}. \tag{30}$$

Note that $r(T)$ is finite, scale-independent, and also independent of the $e = 0$ LEC l_3, h_1, h_3. In particular, it is free of the contact-term ambiguity, which makes it a quantity suitable for physical predictions. It is also independent of B_0, unlike the individual quark condensates, which have only physical meaning when multiplied by the appropriate quark masses, since the $m_i B_0$ products give meson masses. In addition, the dependence with the EM LEC disappears in the difference $r(T) - r(0)$, which is the quantity directly related to the susceptibility through (27).

The above relation can also be explored for $SU(3)$. However, the connection with the susceptibility is not direct in that case. The e^2 dependence of $\langle \bar{q}q\rangle_T - \langle \bar{q}q\rangle_0$ enters now through $M_{\pi^\pm}$ and $M_{K^\pm}$. However, the condensates (11)–(13) depend on the light quark mass through all the meson masses M_π, M_K, M_η. The result is that $r(T) - r(0)$ can be expressed as the susceptibility term in (27) plus a linear combination of $\partial(\langle \bar{s}s\rangle_T - \langle \bar{s}s\rangle_0)/\partial m$ and $\partial(\langle \bar{s}s\rangle_T - \langle \bar{s}s\rangle_0)/\partial m_s$, to this chiral order and neglecting $\mathcal{O}(e^4)$ and $\mathcal{O}(m_u - m_d)$ isospin-breaking corrections in the right-hand side. Since the strange quark condensate has a much weaker dependence on temperature than the light one (or equivalently, we can approximately neglect the thermal functions evaluated on kaon and eta masses) we expect the T behavior of $r(T) - r(0)$ to be dominated by the light scalar susceptibility also in the $SU(3)$ case and therefore the sum rule (27) should hold approximately. In this case we have to one loop

$$r(T)^{SU(3)} - r(0)^{SU(3)}$$
$$= 1 + \frac{Ce^2}{F^4}[2g_2(M_{\pi^\pm}, T) + g_2(M_{K^\pm}, T)] + \mathcal{O}(e^4),$$
$$r(0)^{SU(3)} = 1 + e^2 \mathcal{K}^r_{3+}(\mu) - \frac{2Ce^2}{F^4}[2\nu_{\pi^\pm} + \nu_{K^\pm}] + \mathcal{O}(e^4),$$

where the expansion in e^2 to leading order allows one to express the result in terms of the $\pi^\pm$ and $K^\pm$ masses. As in $SU(2)$, $r(T)$ is finite, scale-independent, and independent of the $e = 0$ LEC, so that it is free of contact ambiguities.

We compare the above expression with the susceptibility in the $SU(3)$ case. As will become clear in Sec. IV B, the corrections to the total susceptibility χ from both sources of isospin breaking are small. Actually, we will see that the next-to-leading order correction in the QCD breaking is $\mathcal{O}(m_u - m_d)^2$. The one-loop result is

$$\frac{\chi(T) - \chi(0)}{B_0^2} = \frac{4\hat{m}^2}{M_\pi^4}[\chi(T) - \chi(0)]$$
$$= 2\left[3g_2(M_\pi, T) + g_2(M_K, T) + \frac{1}{9}g_2(M_\eta, T)\right]$$
$$+ \mathcal{O}(p^2) + \mathcal{O}(e^2) + \mathcal{O}\left(\frac{m_d - m_u}{m_s}\right)^2, \tag{31}$$

$$\frac{\chi(0)}{B_0^2} = \frac{4\hat{m}^2}{M_\pi^4}\chi(0)$$
$$= 16[8L_6^r(\mu) + 2L_8^r(\mu) + H_2^r(\mu)]$$
$$- 4\left[3\nu_\pi + \nu_K + \frac{1}{9}\nu_\eta\right] + \mathcal{O}(p^2) + \mathcal{O}(e^2)$$
$$+ \mathcal{O}\left(\frac{m_d - m_u}{m_s}\right)^2. \tag{32}$$

The two quantities are compared in Fig. 3. The deviations between them are negligible for the range of relevant temperatures. Therefore, although for physical masses the electromagnetic corrections are relatively small, they grow with the susceptibility, which is a model-independent prediction. For comparison, taking the value of $(\hat{m}^2)/(M_\pi^4)[\chi(T_c) - \chi(0)]$ from the lattice simulations in [8] for $2 + 1$ flavors with the lattice T_c value gives $r(T_c) - r(0) \simeq 0.013$, not far from the higher temperature values in Fig. 3, although the ChPT curve cannot reproduce the susceptibility peak, only the low and moderate T behavior. These small EM corrections for the condensate are in accordance with our simple estimates made in Sec. III and translate into a few MeV difference in the determination of the critical temperature from the order parameter.

The sum rule (27) has another interesting consequence, regarding lattice simulations. In the staggered fermion lattice formalism, the need to introduce four different copies (tastes) for every quark flavor leads to the so-called taste violation [8,19,29]. This is a lattice artifact which in some aspects is similar to the isospin or flavor violations

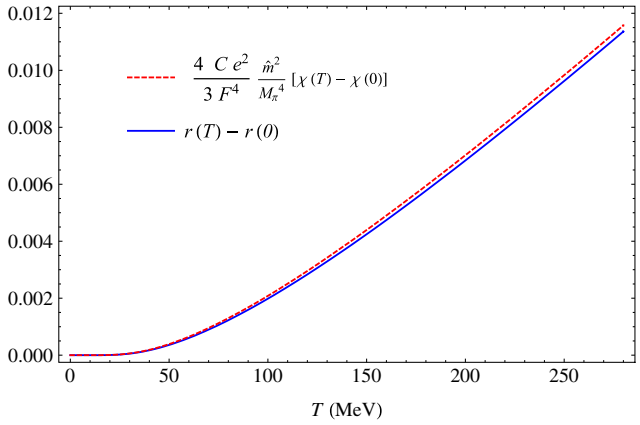

FIG. 3 (color online). The $r(T)$ function in $SU(3)$ encoding the EM corrections of the quark condensate. We compare it with the normalized light susceptibility for physical quark and meson masses. For these values, $r(0) \simeq 1.01$.

we are analyzing here. The new tastes enlarge the chiral symmetry group to $SU(4N_f) \times SU(4N_f)$, producing then 15 pseudo-Goldstone bosons plus one massive state (η'-like) for every quark flavor. All these new meson states become degenerate in the continuum limit, where taking the fourth root of the Dirac fermion determinant is enough to remove all the spurious copies. However, for finite lattice spacing a, the tree-level masses of those states receive $\mathcal{O}(a^2)$ contributions, which break explicitly the chiral group in the Lagrangian, only one Goldstone boson remaining massless in the chiral limit, leaving then a residual $O(2)$ or $U(1)$ symmetry. The mechanism is similar to the electric charge one we are analyzing here, by which the charged states receive $\mathcal{O}(e^2)$ corrections and the $U(1)$ EM symmetry remains. In fact, for the staggered case one can construct a generalized chiral Lagrangian including all possible terms compatible with the new symmetry. This is called staggered chiral perturbation theory [29,30]. Among the new terms one recognizes contributions of the form $\mathrm{Tr}[\xi U \xi U^\dagger]$ with ξ a given combination of $SU(4)$ generators, i.e., like the charge term in (1) in $SU(3)$. Obviously, the staggered case includes additional operators and the spectrum of states is more complicated. However, we can use the sum rule (27) to estimate roughly the expected differences between the lattice staggered condensate and the continuum one, considering the lightest states. For fine-enough lattices, one has $\delta_\pi^a = (M_{\pi,a}^2 - M_\pi^2)/M_\pi^2 \simeq ca^2$ for the lightest tastes of squared mass $M_{\pi,a}^2$ [8], where from the two smallest lattices in [8] we get $c \simeq 140\ \mathrm{fm}^{-2}$. With this δ_π^a we can then use (27) to estimate $r^a(T) - r^0(0)$. Consequently, we expect the larger errors coming from this taste violation effect to appear near T_c. That is indeed the case when we compare lattices of decreasing temporal extent $N_t = a/T$ for the condensate data given in [8]. More quantitatively, taking also the susceptibility values of [8], we get $r^a(T_c) - r^a(0) \simeq 0.07ca^2$. Estimating the $T = 0$ part using (29) with $e^2 \to \delta_\pi^a M_\pi^2 F^2/(2C)$, we get a relative correction for the condensates near T_c with respect to the continuum of about 20% for the $N_t = 12$ data in [8] and about 12% for the $N_t = 16$ ones in [31]. Following the same idea, we get a relative difference between the $N_t = 10$ and $N_t = 12$ lattices of around 8% near T_c, which is actually in good agreement with lattice data [8]. A direct translation into an error for the critical temperature is not easy to obtain. If we simply extrapolate the one-loop chiral limit expression $\langle \bar{q}q \rangle_T = \langle \bar{q}q \rangle_0 (1 - T^2/T_c^2)$, writing the left-hand side of (27) in the one-loop equivalent form (25), we get a very rough estimate $\Delta T_c \simeq 10$ MeV for $N_t = 12$ with respect to the continuum, although the chiral limit is not always numerically accurate, as we will actually see in the next section.

Estimating taste-violation effects is important, since they are one of the main sources of the discrepancies between different lattice groups for the determination of the critical temperature. An important effort has been made over recent years to minimize these effects, not only by considering finer lattices, but also by introducing lattice actions where taste symmetry is reduced [31].

B. Temperature and mass dependence of connected and disconnected susceptibilities. Relation with chiral restoration and lattice analysis

The behavior of condensates and susceptibilities with temperature and quark masses is crucial in order to understand the nature of the chiral phase transition when approaching the chiral region $(m_q, T) \to (0^+, T_c)$. Lattice simulations have addressed the question of how those quantities scale with m_q and T until very recently [20]. An essential part of this program concerns the scaling of the connected and disconnected parts of the scalar susceptibility. The disconnected piece is given in terms of closed quark lines and is therefore directly related to $\langle \bar{q}q \rangle$ and expected to be sensitive to chiral restoration. Actually, near the chiral limit, i.e., the infrared (IR) behavior, it is known to scale as $\chi_{\mathrm{dis}}^{\mathrm{IR}} \sim \log M_\pi^2$ for $T = 0$ and $\chi_{\mathrm{dis}}^{\mathrm{IR}} \sim T/M_\pi$ at finite temperature [17]. The infrared contribution is then controlled by the GB loop contributions. The situation is not so clear for the connected part, since its infrared divergent piece is proportional to $n_f^2 - 4$, with n_f the number of identical light flavors [17], and therefore it vanishes for $n_f = 2$. However, its IR finite part contributes in the physical case of massive pions and is actually an important difference between QCD and $O(N)$ models, on which the lattice scaling fits are based [20]. Besides, the connected contribution receives important "false" GB-like corrections coming from taste violation [20,21]. It is therefore important for lattice studies to provide the continuum result for the disconnected and connected susceptibilities in the physical case of $2 + 1$ flavors and massive pions.

Our present ChPT one-loop analysis allows us to obtain a model-independent prediction for the low-temperature and small-mass behavior of the susceptibilities. The inclusion of isospin-breaking effects is crucial. In fact, it will be useful for the following discussion to note that

$$\chi_{\rm con} = \frac{1}{2}(\chi_{uu} - \chi_{ud}) + \frac{1}{2}(\chi_{dd} - \chi_{ud}) = -\frac{1}{2}\partial_{m_\delta}\langle \bar{u}u - \bar{d}d\rangle, \tag{33}$$

$$\chi_{\rm dis} = -\frac{1}{4}[\partial_{\hat{m}}\langle \bar{u}u + \bar{d}d\rangle - 2\partial_{m_\delta}\langle \bar{u}u - \bar{d}d\rangle],$$

with $m_\delta = (m_u - m_d)/2$, so that $\chi_{\rm con}$ comes only from the condensate difference in (12) and its leading order is obtained from the linear terms in $m_u - m_d$.

Now, from our considerations in Sec. III, if we neglect for the moment the charge corrections and we take the quark mass derivatives in (11) we have, to leading order in m_δ, $\chi_{uu} \simeq \chi_{dd}$, $\chi_{uu} + \chi_{ud} \simeq \chi/2$, and $\chi_{uu} - \chi_{ud} \simeq \chi_{\rm con}$, where the leading terms χ, $\chi_{\rm con}$, and $\chi_{\rm dis} = \chi/4 - \chi_{\rm con}/2$ are $\mathcal{O}(1)$ in the m_δ counting and are given in $SU(3)$ by (31) and (32) and

$$\frac{\chi_{\rm dis}(T) - \chi_{\rm dis}(0)}{B_0^2} = \frac{1}{18}[27g_2(M_\pi, T) + g_2(M_\eta, T)] - \frac{g_1(M_\pi, T) - g_1(M_\eta, T)}{3(M_\eta^2 - M_\pi^2)} + \mathcal{O}(p^2) + \mathcal{O}\left(\frac{m_d - m_u}{m_s}\right)^2 + \mathcal{O}(e^2), \tag{34}$$

$$\frac{\chi_{\rm dis}(0)}{B_0^2} = \frac{1}{9}(288L_6^r(\mu) - \nu_\eta - 27\nu_\pi) - \frac{2F^2(\mu_\pi - \mu_\eta)}{3(M_\eta^2 - M_\pi^2)} + \mathcal{O}(p^2) + \mathcal{O}\left(\frac{m_d - m_u}{m_s}\right)^2 + \mathcal{O}(e^2), \tag{35}$$

$$\frac{\chi_{\rm con}(T) - \chi_{\rm con}(0)}{B_0^2} = g_2(M_K, T) + \frac{2[g_1(M_\pi, T) - g_1(M_\eta, T)]}{3(M_\eta^2 - M_\pi^2)} + \mathcal{O}(p^2) + \mathcal{O}\left(\frac{m_d - m_u}{m_s}\right)^2 + \mathcal{O}(e^2), \tag{36}$$

$$\frac{\chi_{\rm con}(0)}{B_0^2} = 2(4H_2^r(\mu) + 8L_8^r(\mu) - \nu_K) + \frac{4F^2(\mu_\pi - \mu_\eta)}{3(M_\eta^2 - M_\pi^2)} + \mathcal{O}(p^2) + \mathcal{O}\left(\frac{m_d - m_u}{m_s}\right)^2 + \mathcal{O}(e^2). \tag{37}$$

Several remarks are in order about the previous expressions. First, we emphasize that all of them are finite and scale-independent, which can be explicitly checked from the scale dependence of the LEC [22]. We also note that, unlike the disconnected part, the connected susceptibility does not receive contributions from the mass derivative of pion tadpoles, i.e., ν_π or $g_2(M_\pi, T)$. These turn out to be the dominant ones in the chiral limit (see below) and this is what we expected from our previous discussion on the infrared behavior. Thus, we identify the difference $\mu_\pi - \mu_\eta$ in (37) and the corresponding g_1 one in (36) as the contribution of $\pi^0\eta$ mixing, while the ν_K, $g_2(M_K)$ terms come from the expansion of the kaon contribution in the right-hand side of (12) around the isospin limit. From (33), the disconnected part receives in addition a contribution from the sum (11) and hence it incorporates the ν_π, $g_2(M_\pi)$ terms. Note also that the $T = 0$ part of $\chi_{\rm con}$ depends on the contact term H_2, while that dependence cancels in $\chi_{\rm dis}$. This means that only quantities such as $\chi_{\rm con}(T) - \chi_{\rm con}(0)$ can be unambiguously determined, similar to the quark condensate case (see our discussion at the end of Sec. III). This is a relevant comment for lattice evaluations of this quantity. In fact, as a consequence of the vanishing pion terms, we see that $\chi_{\rm con}(T) - \chi_{\rm con}(0)$ vanishes formally in the $m_s \to \infty$ limit, recovering the pure $SU(2)$ result that we would get from (8), which holds also for the other susceptibilities taking into account the conversion between the $SU(2)$ and $SU(3)$ LEC [22] (see below).

Regarding the expansion in $(m_u - m_d)$, as can be seen from (33), from the condensate expressions (11) and (12) and from the meson masses and mixing angle dependence on $\hat{m}$ and m_δ, that the linear order in m_δ cancels both in the connected and the disconnected parts and so we have written in the previous expressions and in the total susceptibility (31) and (32). It is important to remark that the $\mathcal{O}(m_\delta/m_s)^2 \sim \mathcal{O}(\varepsilon)^2$ corrections contain ''tadpole mass derivative'' terms ν_π, $g_2(M_\pi)$ in both $\chi_{\rm con}$ and $\chi_{\rm dis}$. However, an important difference between them is that those IR-dominant terms do not appear to leading order in the connected contribution. In fact, since $\nu_{\pi^0} = \nu_\pi + (\partial\nu_\pi/\partial M_\pi^2)\mathcal{O}(m_\delta/m_s)^2$, where the subscript π indicates just the $m_u = m_d$ and $e^2 = 0$ pion, the disconnected part receives an $\mathcal{O}(m_\delta/m_s)^2$ proportional to the second derivative of the pion tadpole and hence is more IR divergent, and so on for the thermal part $g_2(M_{\pi^0}, T)$. This contribution is not present in the connected part to that order. Thus, we expect the isospin-breaking corrections to be larger in the disconnected than in the connected susceptibility.

Another pertinent comment is that we have been able to obtain the leading order for $\chi_{\rm con}$ and $\chi_{\rm dis}$ only after considering properly all the $m_u \neq m_d$ contributions and then taking the $m_u = m_d$ limit. However, one can be led to misleading results by setting $m_u = m_d$ from the very beginning. For instance, for two equal masses one could think naively that $\chi_{uu} = \chi_{ud} = \chi_{dd} = \chi/4$, from the definition (21). However, from our previous analysis we see that in the isospin limit what we get actually is $\chi_{ud} = \chi/4 - \chi_{\rm con}/2$ and $\chi_{uu} = \chi_{dd} = \chi/4 + \chi_{\rm con}/2$ with $\chi_{\rm con}$

given in (36) and (37), i.e., not vanishing for $m_u = m_d$ and physical m_s, although formally suppressed in the $m_s \to \infty$ limit. Thus, in the isospin limit taking just one flavor susceptibility and multiplying by four does not give the total scalar susceptibility, which should be obtained instead by considering the derivative of the full sum of u and d condensates as given by (21). Note that this correction does not affect condensates, for which the $\langle \bar{u}u \rangle$ and $\langle \bar{d}d \rangle$ difference vanishes for $m_u = m_d$ and $e^2 = 0$ and therefore $\langle \bar{q}q \rangle = 2\langle \bar{u}u \rangle = 2\langle \bar{d}d \rangle$ in the isospin limit. This comment may be relevant for certain lattice analysis, where working within the one-flavor equivalent framework is often done, since in that way it is easy to discuss for instance the taste-breaking effect. This observation could then help to explain the worse $O(N)$ scaling properties of the susceptibility with respect to those of the condensate [20]. In that work, the lattice data for the susceptibility scaling function in the $2 + 1$ case suffer from a sizable increase as the strange quark mass is decreased relative to the light one. That increase is not seen in the quark condensate data and could be due partly to the definition used as we have just explained, since the positive term proportional to $\chi_{\rm con}$ increases with $1/m_s$, from (36) and (37). This is not the only effect that may cause this ''wrong'' scaling because, as pointed out in [20,21], taste breaking induces an artificial infrared pion contribution in $\chi_{\rm con}$ which is not present in the continuum, as our above expressions show. What we are pointing out here is that the one-flavor χ_{uu} and χ_{dd} are sensitive to isospin-breaking terms even for $m_u = m_d$ and in the continuum, unlike considering for instance the total susceptibility $\chi \sim \chi_{uu} + \chi_{ud}$ in (21) for which the $\chi_{\rm con}$ term cancels. In addition, as we will see below, $\chi_{\rm con}$ is dominated numerically by its $T = 0$ part, which would explain why the anomalous scaling is reduced for the subtracted susceptibility.

The charge corrections to susceptibilities in our previous expressions (32) and (37) arise only through the mass of the charged mesons $\pi^\pm$ and $K^\pm$. Thus, including the charge amounts to replace $3\nu_\pi \to \nu_{\pi^0} + 2\nu_{\pi^\pm}$ in (32) and (35) and $2\nu_K \to \nu_K + \nu_{K^\pm}$ in (32) and (37), and so on for the thermal parts $3g_2(M_\pi, T) \to g_2(M_{\pi^0}, T) + 2g_2(M_{\pi^\pm}, T)$ and $2g_2(M_K, T) \to g_2(M_K, T) + g_2(M_{K^\pm}, T)$. Although for physical values of the electric charge and masses these represent small perturbative corrections, the fact that near the chiral limit the coefficient of the IR-dominant ν_π and $g_2(M_\pi, T)$ reduces in $1/3$ for $e^2 \neq 0$ is the reflection in the scalar susceptibility of the behavior of the condensate in terms of δ_π corrections to the masses analyzed in Sec. IV A. Thus, when the mass corrections δ_π become sizable, as in the staggered lattice formalism, the susceptibility is reduced by that factor, which eventually would imply that the transition peak or maximum is displaced to a higher temperature, consistent with our analysis in the previous section about the increasing of T_c in the condensates. Recall that one cannot just expand the pion terms in e^2 and then take the chiral limit, since that expansion assumes that the charge part of $M_{\pi^\pm}$ is small compared to the quark mass one.

Before continuing, we also remark that our above results are compatible with the recent observation [21] that the connected and disconnected susceptibilities can be inferred from the zero momentum limit of the a_0 and f_0 correlators calculated previously in staggered ChPT [32]. The motivation of those works is precisely to estimate the contribution of heavy pion-like tastes to the IR part of $\chi_{\rm con}$, which could mask the scaling behavior. The continuum limit of the results in [21] reveals the same π, K, η loop contributions as in our expressions (34)–(37). We provide the full ChPT result, including the LEC contribution necessary to guarantee the finiteness and scale independence of the results, as well as the analysis of the higher order corrections in isospin breaking.

As discussed above, the behavior of the susceptibilities near the chiral limit (IR regime) is very illuminating regarding their approach to chiral restoration within the $O(4)$ or $SU(2)$ pattern in the continuum, i.e., without taste-breaking effects. Let us consider this regime first for $T = 0$ and only for the leading-order terms in the isospin expansion in (35) and (36), i.e., we set $m_u = m_d = \hat{m}$ and $e^2 = 0$ in the $T = 0$ susceptibilities and consider $\hat{m} \ll m_s$. We denote by a superscript IR the nonvanishing terms in that limit,

$$\frac{\chi^{\rm IR}_{\rm dis}(T=0)}{B_0^2} = -\frac{3}{32\pi^2}\log\frac{M_\pi^2}{\mu^2} + 32L_6^r(\mu) + \frac{1}{288\pi^2}\left(-28 + 5\log\frac{M_\eta^2}{\mu^2}\right), \quad (38)$$

$$\frac{\chi^{\rm IR}_{\rm con}(T=0)}{B_0^2} = 8[H_2^r(\mu) + 2L_8^r(\mu)] - \frac{1}{16\pi^2}\left(1 + \log\frac{M_K^2}{\mu^2} + \frac{2}{3}\log\frac{M_\eta^2}{\mu^2}\right). \quad (39)$$

The IR divergent $\log M_\pi^2$ term in (38) coincides with the one obtained in [17], where a cutoff regularization was used. Multiplied by 4, this is also the IR-dominant part in the total susceptibility χ. In addition to that term, we obtain here the regular part, not IR divergent but not vanishing in the chiral limit, which provides the dependence with the LEC and together with the logarithm gives the consistent scale-independent ChPT prediction. As for the connected part, again only the IR-divergent contribution is given in [17], which as commented above turns out to vanish exactly for two light fermions. Here we also give the regular contribution, also scale independent, which unlike the disconnected part depends on the contact term H_2^r. As an interesting consistency check, we can recover the $SU(2)$ limit from the above expressions, using the conversion between the LEC of $SU(2)$ and $SU(3)$ [3] $l_3^r + h_1^r - h_3 = 16L_6^r + 5\nu_\eta/18 - 1/(96\pi^2)$ and

$h_3^r = 4L_8^r + 2H_2^r - \nu_K/2 - \nu_\eta/3 + 1/(96\pi^2)$, so that $\chi_{\rm dis}^{SU(2)} = -3\nu_\pi + 2(l_3^r + h_1^r - h_3)$ and $\chi_{\rm con}^{SU(2)} = 4h_3^r$, which is the same result that we would have starting directly from the $SU(2)$ expressions in (7) and (8).

Let us consider now the dominant IR thermal contribution in the $2+1$ flavor case, i.e., apart from $\hat{m} \ll m_s$ we also consider temperatures $M_\pi \ll T \ll M_K$, so that we neglect all the Boltzmann exponentials $\exp(-M_{K,\eta}/T)$ and expand $g_1(M_\pi, T) = \frac{T^2}{12}[1 - 3M_\pi/(\pi T) + \mathcal{O}(M_\pi^2 \log M_\pi^2)]$ and $g_2(M_\pi, T) = T/(8\pi M_\pi) + \mathcal{O}(\log M_\pi^2)$ [5]. Thus, we get

$$\frac{[\chi_{\rm dis}(T) - \chi_{\rm dis}(0)]^{\rm IR}}{B_0^2} = \frac{3T}{16\pi M_\pi}, \tag{40}$$

$$\frac{[\chi_{\rm con}(T) - \chi_{\rm con}(0)]^{\rm IR}}{B_0^2} = \frac{T^2}{18M_\eta^2}. \tag{41}$$

The disconnected part (40) is again the one obtained in [17] in the IR limit. It diverges more strongly than the $T = 0$ contribution in (38) in this limit, revealing its critical behavior. The growth with T is linear over the GB mass scale. Recall that, apart from the thermally suppressed exponentials, we are neglecting also $\log M_\pi$ terms in the disconnected part (40). The situation is completely different for the connected contribution, which is regular, albeit not vanishing, in the chiral limit. The quadratically growing term in (41) survives for $M_\pi \to 0$ against neglected $\mathcal{O}(M_\pi)$ and is dominant over $\exp(-M_{K,\eta}/T)$. It vanishes formally as $m_s \to \infty$, recovering the $SU(2)$ limit. For physical masses though, a specific and model-independent difference between the $N_f = 2$ and $N_f = 2+1$ cases is the (soft) temperature dependence of the connected susceptibility, the scale that controls its growth being M_η^2 instead of the M_π^2 of the connected part. This is a consequence of $\chi_{\rm dis}$ measuring the fluctuations of the chiral restoration order parameter, while $\chi_{\rm con}$ is related to those of the isospin-breaking one, i.e., $\langle \bar{u}u - \bar{d}d \rangle$, which as we have seen in Sec. III increases moderately. Note that near the chiral limit we could as well have written the T^2 term divided by M_K^2 just by changing the multiplying factor. Keeping M_η^2 recalls its $\pi^0\eta$ origin, as is clearly seen in the original expressions in (36) and (37).

In Fig. 4 we plot our numerical ChPT results for the susceptibilities, including all the isospin-breaking corrections. The plots in that figure show the difference with respect to the $T = 0$ results, which are collected in Table I. At $T = 0$ we use the same LEC values as in [22], which are quoted in the table. Remember that the susceptibilities are independent of the EM LEC and that the disconnected one is independent of contact terms. The contact LEC H_2^r appearing in the connected contribution is estimated from resonance saturation arguments [15,26]. The normalization used $B_0^2 = M_\pi^4/(4\hat{m}^2)$ is the same one used in some lattice works [8].

We see in the plots that the general features explored in our previous analytical discussion are well reproduced. First, the $\mathcal{O}(e^2)$ and $\mathcal{O}(m_d - m_u)^2$ terms neglected in (31), (32), and (34)–(37) are numerically small for the relevant temperature range, for physical values of quark and meson masses. In fact, as anticipated in our previous discussion, we see that those isospin corrections are larger for the disconnected than for the connected part and are also larger with temperature, all due to the appearance of IR terms proportional to the second derivative of the tadpole in $\chi_{\rm dis}$. Remember that the leading order in the isospin limit comes actually from the $\mathcal{O}(m_d - m_u)$ terms in the condensates. Second, we appreciate qualitatively the linear and quadratic growth with temperature of the disconnected and connected parts, respectively, as expected from the infrared analysis. In fact, we see that although the connected term grows faster, its absolute value is much smaller due to the M_η^2 scale compared to the M_π^2 of the disconnected part. However, it is important to note that the IR limit expressions (40) and (41) are numerically rather far from the exact ones for the physical pion mass. The difference is larger for the disconnected contribution since, as stated above, in (40) we are neglecting $\mathcal{O}(\log M_\pi)$ terms, while in (41) the neglected terms are $\mathcal{O}(M_\pi)$. In fact, this justifies further our present analysis, since we provide the full expressions beyond the chiral limit. Also as discussed above, the infrared limit expressions for $T = 0$ given in (38) and (39) survive not only the chiral limit but also the $m_s \to \infty$ one, $\chi_{\rm dis}$ still diverging but only logarithmically, which for physical masses makes the two susceptibilities numerically comparable. This is clearly seen in the values given in the first two rows of Table I. Actually, for this very same reason, and following our previous discussion, the deviations of χ_{uu} from the naive isospin-limit expectation $\chi/4$ is much more pronounced at $T = 0$ than for finite T. This can be seen by comparing the last two columns in Table I which give about a 30% relative difference, while the last plot in Fig. 4, where we compare their thermal differences, gives only corrections below 10%. In fact, this is consistent with our previous discussion about the influence of the connected part in the scaling properties observed in the lattice. If we consider the subtracted susceptibilities as defined in [20] from the subtracted condensate $\langle \bar{u}u \rangle - (m_u/m_s)\langle \bar{s}s \rangle$, we see that the dependence on the LEC disappears in the $\hat{m}/m_s \to 0$ limit. Remember that in this limit all the $T = 0$ contribution of the connected part is absorbed in h_3^r (see our previous comments) and therefore considering the subtracted susceptibility is equivalent to switching off the dominant $T = 0$ part of the connected susceptibility. This is indeed observed in the lattice [20] since the subtracted susceptibility fits better the expected $O(N)$ scaling behavior than the unsubtracted one.

The variation with the quark mass is displayed for $T \neq 0$ in Fig. 5 and for $T = 0$ in Table I. It is important to remark that we have chosen to keep fixed the ratio $m_u/m_d \simeq 0.46$

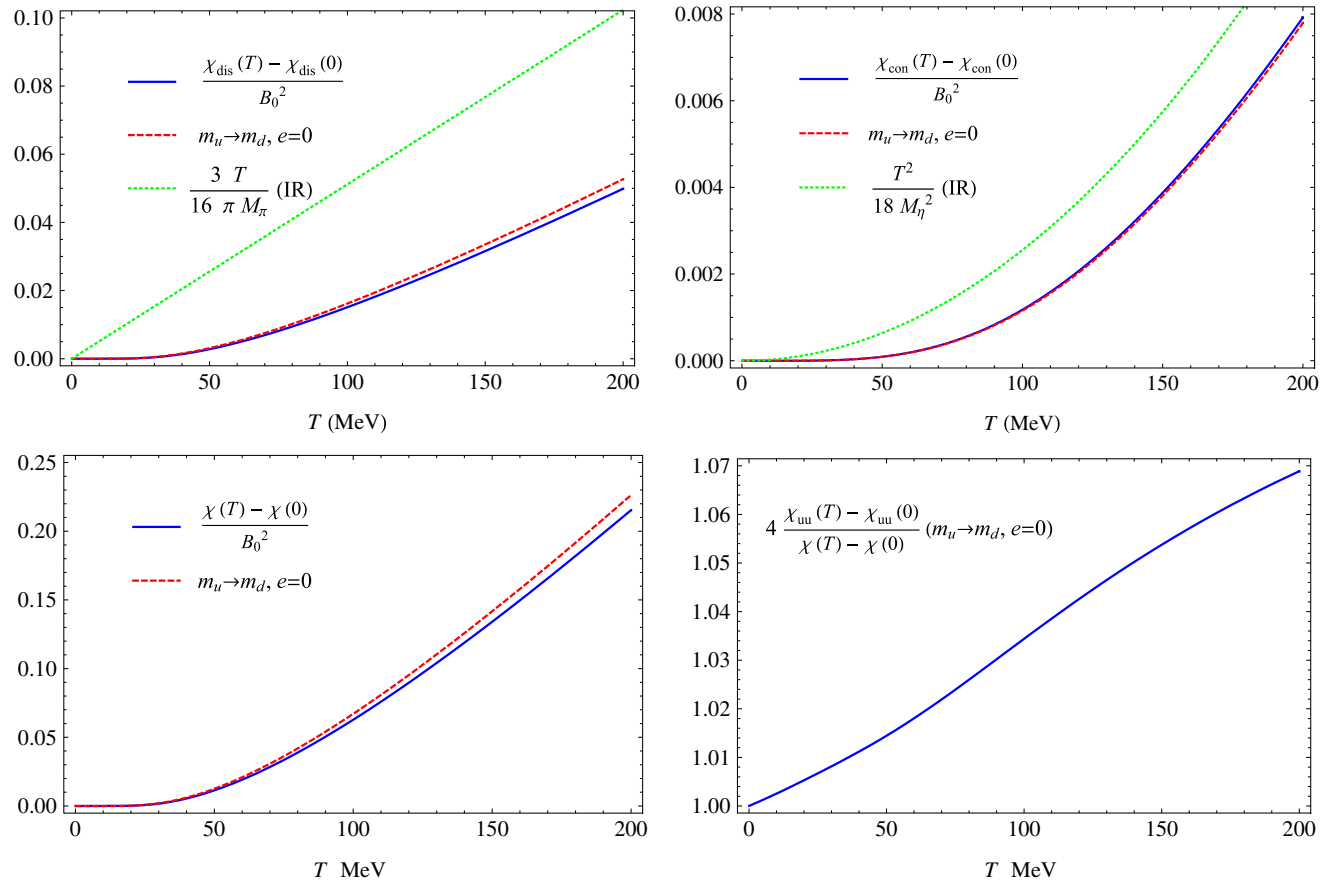

FIG. 4 (color online). Temperature dependence of disconnected, connected, and total susceptibilities in three-flavor ChPT, for physical quark and meson masses. The solid blue curves show the results with all the isospin-breaking corrections of higher order included, while in the dashed red ones we display the leading order in the isospin limit. We also show the IR expressions for the connected and disconnected parts, as well as the deviations of $4\chi_{uu}$ from $\chi_{\rm tot}$ in the isospin limit (last plot). The $T = 0$ results are given in Table I.

(same value used in our previous analysis [22]) and m_s, while we vary $\hat{m}/m_s$ above and below the physical quark mass ratio. In other words, when $\hat{m} \to 0^+$, $M_\pi \to 0^+$ while $M_{K,\eta}$ remain fixed. This is meant to be the relevant limit when approaching chiral restoration. In addition, since we can write $(m_d - m_u)/m_s = 2(\hat{m}/m_s)(1 - m_u/m_d) \times (1 + m_u/m_d)^{-1}$, ε scales in this limit as $\mathcal{O}(\hat{m})$. Recall that, although the values of the L_i^r are fitted to low-energy data with physical masses [26], those LEC are formally independent of the quark masses [3]. The same applies to the tree-level value of F we are using.

TABLE I. $T = 0$ values for the different susceptibilities in ChPT. The isospin limit (IL) values correspond to $m_u \to m_d$ and $e = 0$. For the third to sixth rows we fix m_s/m_d and m_s and vary the light to heavy quark mass ratio. The first and second rows correspond to the physical values. The LEC values used are $H_2^r = 2L_8^r = 1.24 \times 10^{-3}$, $L_6^r = 0$ at the scale $\mu = 770$ MeV.

	$\chi_{\rm dis}/B_0^2$	$\chi_{\rm con}/B_0^2$	χ/B_0^2	$4\chi_{uu}/B_0^2$
$m_s/\hat{m} = 24$	0.024	0.025	0.146	0.196
$m_s/\hat{m} = 24$, IL	0.025	0.025	0.148	0.197
$m_s/\hat{m} = 10$	0.016	0.024	0.113	0.163
$m_s/\hat{m} = 10$, IL	0.017	0.023	0.114	0.161
$m_s/\hat{m} = 100$	0.036	0.026	0.194	0.245
$m_s/\hat{m} = 100$, IL	0.038	0.025	0.203	0.254

As we expected from our previous IR analysis in Eqs. (40) and (41), the light quark mass dependence of the thermal disconnected susceptibility is much stronger than the connected one, as seen clearly in Fig. 5 and as long as we take the limit in the order specified above. In terms of chiral restoration, this anticipates a much stronger growth or peak near T_c for the disconnected part. From the same arguments, the behavior of the connected part is expected to be softer near the transition, although growing with T^2 for low and moderate temperatures. We also show in the figure the comparison with the infrared limit for the smaller $\hat{m}/m_s$ case, where it can be seen that the curves are now closer than for the physical pion mass case in Fig. 4.

In addition, the isospin corrections are also more important for the disconnected part, where they actually

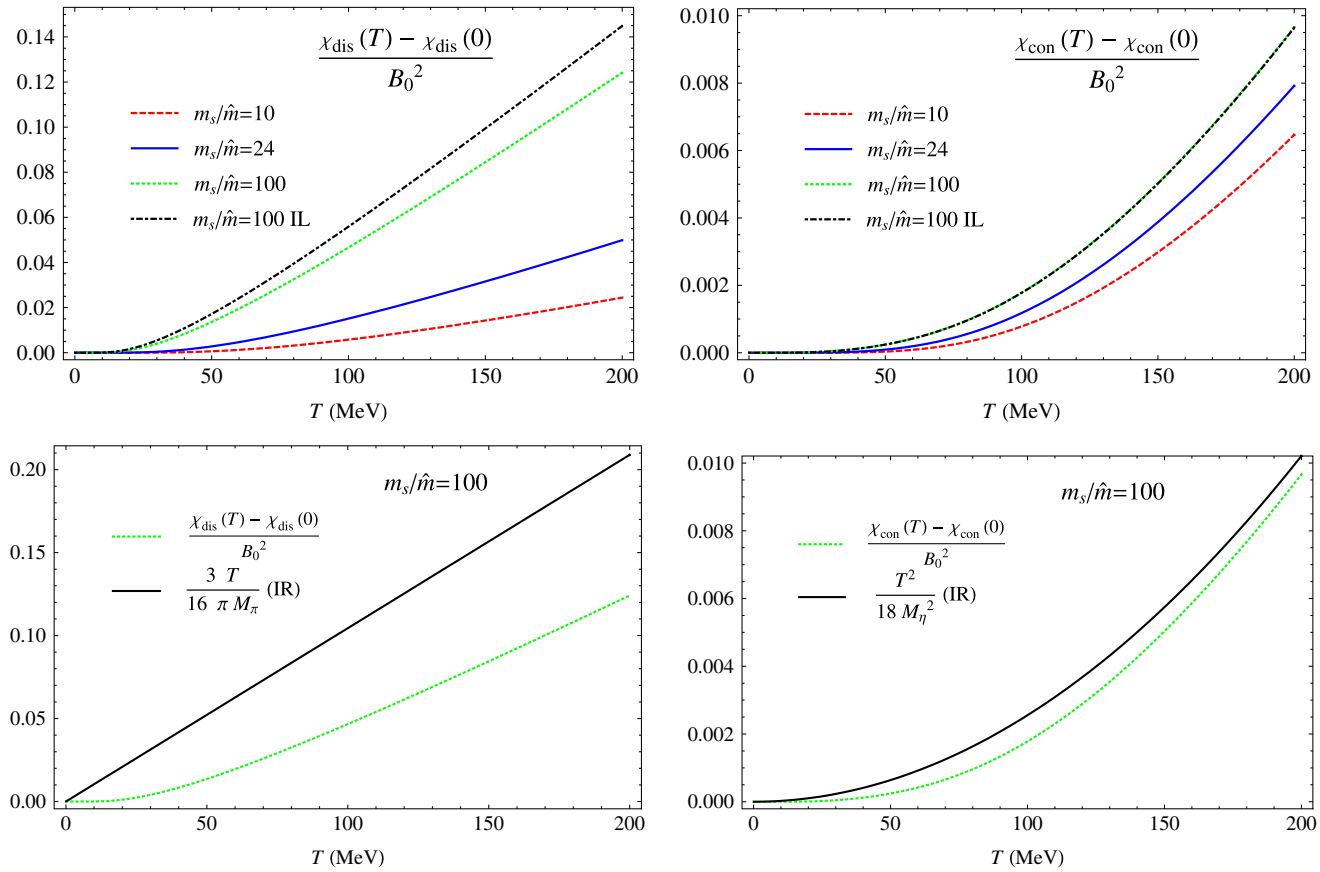

FIG. 5 (color online). Quark mass dependence of the thermal disconnected, connected, and total susceptibilities in three-flavor ChPT, for fixed m_s and fixed m_u/m_d. We also show the isospin limit (IL) $m_u \to m_d$ and $e^2 = 0$ in the smaller light mass case. The $T = 0$ results are given in Table I. For comparison, we also display the infrared limit in the $m_s/\hat{m} = 100$ case.

increase as $\hat{m}$ is decreased, than for the connected one, where the isospin limit and complete curves are almost indistinguishable in the figure. The same holds for the $T = 0$ contributions in Table I. According to our previous discussion, this behavior of the isospin corrections arises from the dominant IR terms $\chi_{\rm dis} \sim B_0^2(TM_\eta^2/M_\pi^3)\varepsilon^2 = \mathcal{O}(\sqrt{\hat{m}})$ as compared to $\chi_{\rm con} \sim B_0^2(T/M_\pi)\varepsilon^2 = \mathcal{O}(\hat{m}^{3/2})$. This effect is weaker for the $T = 0$ contributions since the IR leading corrections $\nu_\pi\varepsilon^2$ (in $\chi_{\rm con}$) and $(\partial\nu_\pi/\partial M_\pi^2)\varepsilon^2$ (in $\chi_{\rm dis}$) diverge softly, namely, as $\hat{m}^2 \log\hat{m}$ and $\hat{m}$ respectively. Thus, although the isospin corrections are amplified in the disconnected susceptibility for large temperatures and small masses, they are still perturbatively under control in the chiral limit.

The limit where $\hat{m}/m_s$ vanishes not by taking $\hat{m} \to 0^+$ but keeping $\hat{m}$ fixed and taking $m_s \to \infty$, is where we recover the pure $SU(2)$ results, as discussed before. In that case, it is the connected part which is more sensitive to the quark mass variation, vanishing for large M_η^2, while the disconnected one remains invariant. Although this is formally interesting for connecting the $SU(2)$ and $SU(3)$ cases, it is not so relevant for studying the critical behavior.

V. CONCLUSIONS

In this work we have analyzed the relevant observables regarding chiral symmetry restoration, namely, quark condensates and scalar susceptibilities, in the presence of isospin breaking. We have considered on the same footing the QCD (m_u/m_d mass difference) and electromagnetic corrections, to one loop in chiral perturbation theory, both in the $SU(2)$ and $SU(3)$ sectors. Our analysis provides useful and model-independent results regarding several relevant aspects of isospin breaking and chiral restoration, which may be particularly interesting for lattice studies.

The sum $\langle\bar{u}u + \bar{d}d\rangle_T$, the order parameter for chiral restoration, receives small isospin-breaking corrections for the physical values of masses and electric charge. These corrections affect only slightly (less than 1%) the value of the critical temperature, which they increase as a ferromagnetic response. The difference $\langle\bar{u}u - \bar{d}d\rangle_T$ is the order parameter of isospin breaking. It is temperature-independent in the $SU(2)$ limit, but when kaons and the eta are included, it shows an increasing behavior, which in the chiral limit is given by $(m_u - m_d)T^2/M_\eta^2$. The deviations with respect to its $T = 0$ value become sizable as the

temperature is increased, but they are controlled by a larger energy scale M_η^2 than the typical F_π^2 of $\langle \bar{u}u + \bar{d}d \rangle_T$. This large growth of isospin breaking does not reflect in the chiral restoration temperatures of $\langle \bar{u}u \rangle_T$ and $\langle \bar{d}d \rangle_T$, which remain close to each other, consistently with the idea that chiral restoration is little affected. We have also evaluated the temperature corrections to the sum rule relating the $\langle \bar{s}s \rangle_T / \langle \bar{u}u \rangle_T$ and $\langle \bar{u}u \rangle_T / \langle \bar{d}d \rangle_T$ ratios, which is useful because it does not involve undetermined contact low-energy constants. The corrections in this case come directly from the $\langle \bar{d}d \rangle_T / \langle \bar{u}u \rangle_T$ ratio and are therefore rather large for the temperatures of interest.

A very important part of the present work has been the analysis of scalar susceptibilities in the isospin asymmetric scenario. We have related the different flavor susceptibilities with the total, quark connected and quark disconnected susceptibilities often used in lattice analysis. Electromagnetic corrections to the quark condensate turn out to be directly related by a sum rule to the total susceptibility and then to the growth of fluctuations, which is meant to be maximum near the critical point. This sum rule is valid for any small deviation of the pion masses, as for instance the one arising in the staggered lattice formalism due to taste-breaking effects. Actually, we have made rough estimates of the corrections to condensates expected from this source, comparing lattices of different sizes among them and with the continuum limit. These estimates are in good agreement with the errors quoted in the lattice works.

The isospin asymmetric calculation allows for a direct extraction of the connected and disconnected susceptibilities, even in the isospin symmetric limit. The terms in $\langle \bar{u}u - \bar{d}d \rangle_T$ linearly proportional to $m_u - m_d$ give contributions to the connected part not vanishing in the isospin limit and which affect for instance the naive extrapolation of a given flavor susceptibility to the total one. Our analysis provides model-independent predictions for the mass, temperature, and isospin dependence of those quantities, which should be recovered in lattice analysis as they approach the continuum limit. In accordance with the behavior of the corresponding order parameters, the disconnected susceptibility shows a linear growth at low and moderate temperatures, infrared divergent near the chiral limit as T/M_π, whereas the connected one is infrared regular but survives the chiral limit as a growing T^2/M_η^2 behavior. The chiral or infrared limit gives qualitatively the behavior as the temperature approaches chiral restoration but numerically is not a good approximation for physical pion masses. The higher order isospin-breaking corrections are quadratic in $m_u - m_d$ and are enhanced in the chiral limit for the disconnected susceptibility, as long as m_s and m_u/m_d remain fixed. The ChPT susceptibilities reproduce the growing T-dependence at low and moderate temperatures in a model-independent way. Although they do not show the peaks expected near the transition, our small mass analysis allows one to infer that the disconnected part should have a more pronounced peak than the connected one, the latter expected to present a rather soft behavior. This difference can be interpreted from the different order parameters that fluctuate in each case: the chiral quark condensate for the disconnected piece and the isospin-breaking one in the connected case. In the formal $SU(2)$ limit $m_s \to \infty$ the connected contribution becomes temperature-independent, like $\langle \bar{u}u - \bar{d}d \rangle_T$. Our analysis for the susceptibilities is consistent with previous related work in the literature.

ACKNOWLEDGMENTS

We are grateful to W. Unger for useful comments. Work partially supported by Spanish research Contracts No. FPA2008-00592, FIS2008-01323, UCM-BSCH GR58/08 910309, and the FPI program (BES-2009-013672).

[1] S. Weinberg, Physica (Amsterdam) **96A**, 327 (1979).
[2] J. Gasser and H. Leutwyler, Ann. Phys. (N.Y.) **158**, 142 (1984).
[3] J. Gasser and H. Leutwyler, Nucl. Phys. **B250**, 465 (1985).
[4] J. Gasser and H. Leutwyler, Phys. Lett. B **184**, 83 (1987).
[5] P. Gerber and H. Leutwyler, Nucl. Phys. **B321**, 387 (1989).
[6] C. Bernard *et al.* (MILC Collaboration), Phys. Rev. D **71**, 034504 (2005).
[7] Y. Aoki, G. Endrodi, Z. Fodor, S. D. Katz, and K. K. Szabo, Nature (London) **443**, 675 (2006).
[8] Y. Aoki, S. Borsanyi, S. Durr, Z. Fodor, S. D. Katz, S. Krieg, and K. K. Szabo, J. High Energy Phys. 06 (2009) 088.
[9] M. Cheng *et al.*, Phys. Rev. D **81**, 054504 (2010).
[10] R. D. Pisarski and F. Wilczek, Phys. Rev. D **29**, 338 (1984).
[11] R. Urech, Nucl. Phys. **B433**, 234 (1995).
[12] U. G. Meissner, G. Muller, and S. Steininger, Phys. Lett. B **406**, 154 (1997); **407**, 454(E) (1997).
[13] M. Knecht and R. Urech, Nucl. Phys. **B519**, 329 (1998).
[14] A. Rusetsky, Proc. Sci., CD09 (2009) 071.
[15] G. Ecker, J. Gasser, A. Pich, and E. de Rafael, Nucl. Phys. **B321**, 311 (1989).
[16] C. Vafa and E. Witten, Nucl. Phys. **B234**, 173 (1984).
[17] A. V. Smilga and J. J. M. Verbaarschot, Phys. Rev. D **54**, 1087 (1996).

[18] C. E. Detar and R. Gupta (HotQCD Collaboration), Proc. Sci., LAT2007 (2007) 179.
[19] C. DeTar and U. M. Heller, Eur. Phys. J. A **41**, 405 (2009).
[20] S. Ejiri *et al.*, Phys. Rev. D **80**, 094505 (2009).
[21] W. Unger (RBC-Bielefeld Collaboration), Proc. Sci., LAT2009 (2009) 180.
[22] A. G. Nicola and R. T. Andres, arXiv:1009.2170.
[23] T. Das, G. S. Guralnik, V. S. Mathur, F. E. Low, and J. E. Young, Phys. Rev. Lett. **18**, 759 (1967).
[24] R. F. Dashen, Phys. Rev. **183**, 1245 (1969).
[25] J. Bijnens and J. Prades, Nucl. Phys. **B490**, 239 (1997).
[26] G. Amoros, J. Bijnens, and P. Talavera, Nucl. Phys. **B602**, 87 (2001).
[27] M. Della Morte and A. Juttner, J. High Energy Phys. 11 (2010) 154.
[28] A. Juttner and M. Della Morte, Proc. Sci., LAT2009 (2009) 143.
[29] W. J. Lee and S. R. Sharpe, Phys. Rev. D **60**, 114503 (1999).
[30] C. Aubin and C. Bernard, Phys. Rev. D **68**, 034014 (2003).
[31] S. Borsanyi, Z. Fodor, C. Hoelbling, S. D. Katz, S. Krieg, C. Ratti, and K. K. Szabo (Wuppertal-Budapest Collaboration), J. High Energy Phys. 09 (2010) 073.
[32] C. Bernard, C. E. DeTar, Z. Fu, and S. Prelovsek, Phys. Rev. D **76**, 094504 (2007).

Compañeros escalares-pseudoescalares en *QCD* y restauración de la simetría quiral

La siguiente sección ahondará en el estudio de las susceptibilidades quirales, proponiendo un escenario de restauración de simetría quiral basado en la degeneración de las susceptibilidades pseudoescalar y escalar.

Los resultados procedentes de simulaciones en el retículo [68, 86] apoyan el hecho de que la transición de deconfinamiento y la restauración de simetría quiral tienen lugar, si no a la misma temperatura, sí en un punto muy próximo que sitúan en torno a los $145-165$ MeV para $N_f = 2+1$ y potencial químico bariónico nulo. Estos resultados son bastante consistentes con el *crossover* suave que predice el patrón de ruptura $O(4) \to O(3)$ si se considera el caso de dos sabores en el límite quiral [83, 149]. Por otro lado, es natural suponer que —en el régimen de baja energía— los correladores en términos de los cuales se definen las susceptibilidades quirales escalar y pseudoescalar están saturados por las partículas asociadas a sus números cuánticos, *i.e.* la $f_0(500)/\sigma$ en el caso de la susceptibilidad quiral escalar, y el pión para la susceptibilidad pseudoescalar.

Uniendo estas dos últimas ideas es lícito conjeturar un escenario en el que la restauración de la simetría quiral dé lugar a la degeneración en masa de los compañeros quirales $f_0(500)$ y π que se manifiesta —por ejemplo— a través de la anulación tanto del valor esperado en el vacío como de la masa del campo (σ, π^a) del *Modelo Sigma Lineal* en el límite quiral para una cierta temperatura [151].

Sin embargo, como ya hemos visto en el capítulo 1, la $f_0(500)$ es una resonancia cuya interpretación en término de un estado asintótico es, siendo optimistas, compleja. Los resultados que defiendo muestran que no sólo no es necesaria esta descripción, sino que este escenario de degeneración escalar-pseudoescalar en el sector de baja energía de la Interacción Fuerte puede explicarse satisfactoriamente a través del análisis de las funciones de correlación en los canales apropiados mediante un enfoque efectivo dado por *ChPT* y su extensión unitarizada a través del *IAM*.

En efecto, el uso del *lagrangiano* quiral efectivo para dos sabores ligeros nos ha permitido probar que la susceptibilidad pseudoescalar —esencialmente un correlador de cuatro campos con los números cuánticos del pión— es proporcional al condensado escalar de quarks hasta *next-to-leading-order* en *ChPT* considerando temperatura finita. Resulta entonces que la susceptibilidad pseudoescalar varía como el parámetro de orden de la restauración de la simetría quiral y, por tanto,

exhibe un comportamiento *crítico*[7] mucho más acusado que $1/M_\pi^2(T)$, resultado que uno esperaría al saturar el correlador pseudoescalar por un estado de tipo pión.

En la literatura especializada existen interesantes resultados a este respecto construidos sobre la base de asunciones menos robustas. Por ejemplo cálculos basados en el álgebra de corrientes a temperatura cero en medios nucleares [152]; o fundamentados en identidades de Ward para *QCD* en el límite quiral, en conexión con el condensado escalar de quarks definido para fermiones de Wilson en el retículo [153–155]. Estos resultados nos han proporcionado una fuente importante de motivación para el estudio del tema, a la par que constituyen por sí mismos una prueba del interés que supone la consideración del problema desde un punto de vista *model-independent* en el marco de *ChPT*.

La aplicación del *IAM* [42–44] permite la generación dinámica de las resonancias más ligeras de los canales vectorial, $\rho(770)$; y escalar, $f_0(500)/\sigma$, como polos de la amplitud unitarizada en la segunda hoja de Riemann y puede extenderse también a temperatura finita [50, 105, 156].

Como puede verse en estas ultimas referencias —y también en la publicación 2.3.1, a modo de resumen—, el comportamiento de los canales vectorial-isovectorial y escalar en *UChPT* es radicalmente distinto. La posición del polo de la amplitud, $s_p := (M_p - i/2\Gamma_p)^2$, es tal que la $\rho(770)$ puede interpretarse satisfactoriamente como una resonancia estrecha parametrizada *à la Breit-Wigner* en la que $M_p^\rho(T) \gg \Gamma_p^\rho(T)$, variando $M_p^\rho(T)$ con la temperatura de modo muy suave en el rango térmico de aplicación de la teoría y siendo $\Gamma_p^\rho(T)/\Gamma_p^\rho(0)$ proporcional a σ_T/σ_0, *i.e.* a la variación térmica del espacio de fases (1.111) respecto al valor a temperatura cero (1.53).

De modo completamente opuesto, la $f_0(500)$ está lejos de poder ser interpretada como una resonancia estrecha puesto que los valores numéricos de $M_p^\sigma(T)$ y $\Gamma_p^\sigma(T)$ son del mismo orden, es decir, el polo de la amplitud unitarizada no se encuentra cercano al eje real. Es interesante y, como veremos, fundamental el hecho de que en este canal la parte real del polo —interpretada como la parte real de la auto-energía de la resonancia intercambiada en la dispersión— decrece rápidamente con la temperatura y tiene un mínimo.

¿Cómo utilizar este formalismo para estudiar el escenario de degeneración de las susceptibilidades escalar y pseudoescalar? Lo primero es asumir que el propagador escalar está completamente saturado por la $f_0(500)$ y que la masa de la partícula intercambiada en la dispersión de piones a momento nulo —tal y como exige la definición de la susceptibilidad en términos del propagador— no

[7] Obsérvese que el término crítico ha de entenderse aquí en la línea de lo que ya hemos comentado anteriormente acerca de la extrapolación de resultados de *ChPT* al estudio cualitativo de los fenómenos relacionados con la restauración quiral.

varía significativamente respecto de la parte real de la auto-energía, M_S, evaluada en el polo térmico del canal escalar calculado a partir del *IAM*.

Bajo estos supuestos es posible obtener la corrección debida a unitarización para la susceptibilidad quiral escalar. En efecto, como $\chi_S(T) \sim 1/M_S(T)^2$, entonces resulta que

$$\chi_S^U(T) = \frac{M_S^2(0)}{M_S^2(T)} \chi_S^{ChPT}(0), \tag{2.1}$$

donde hemos tomado de *ChPT* el resultado para la susceptibilidad quiral escalar a temperatura cero. El uso de esta hipótesis convierte el mínimo de la parte real del polo térmico de la amplitud en el canal $(I = 0, J = 0)$ en un máximo para la susceptibilidad escalar, lo que puede considerarse como una mejora de los resultados de *ChPT*, habida cuenta del comportamiento crítico que experimenta este observable cerca de la región crítica en simulaciones en el retículo.

Puesto que hemos comprobado que la susceptibilidad pseudoescalar es proporcional al condensado escalar de quarks, ya sólo nos queda obtener este último para emprender el análisis de nuestro escenario. Lamentablemente, debido a que desconocemos el modo de obtener el condensado de quarks en el límite quiral sin perder información acerca de su comportamiento crítico, éste no puede calcularse directamente a partir de integrar la expresión (2.1) respecto de la masa quark. Será necesario, por tanto, obtener una descripción aproximada.

En la publicación 2.3.1 hemos asumido la hipótesis de que la variación térmica respecto al valor de temperatura cero para el condensado y para la susceptibilidad escalar admite una parametrización en términos de funciones térmicas que sólo dependen de T/M —lo que es cierto, de hecho, hasta *next-to-leading-order* en *ChPT*—. De este modo sí podemos estar seguros de conocer el valor inicial necesario para la integración, puesto que viene dado por el condensado escalar de quarks en el régimen de muy baja temperatura, *i.e.* el proporcionado por *ChPT*.

Con todo, las conclusiones fundamentales de la publicación 2.3.1 pueden agruparse en tres grupos: resultados procedentes de *ChPT* pura, y una serie de resultados que se obtienen a través de la comparación con datos procedentes de la simulación en el retículo así como con predicciones calculadas mediante la extensión unitarizada de *ChPT* (que a su vez se comparan también con el retículo).

En cuanto a los resultados obtenidos a partir de la Teoría Quiral de Perturbaciones:

- *ChPT* arroja un comportamiento creciente para la susceptibilidad quiral escalar, intersectando a la susceptibilidad pseudoescalar a una temperatura de $0{,}9T_{C,\chi}$, donde $T_{C,\chi}$ es la temperatura para la que se anula el condensado de quarks en la Teoría Quiral. Este resultado ha de ser tomado, nuevamente,

con cuidado y bajo la advertencia de que se trata de una extrapolación de los resultados *model-independent* más allá de su régimen térmico de aplicabilidad.

Desde este punto de vista *ChPT* muestra un escenario posible de restauración de simetría quiral a través del análisis del patrón de degeneración de las susceptibilidades escalar y pseudoescalar.

El comportamiento de estos dos correladores está directamente asociado a los canales de la $f_0(500)/\sigma$ y al del pión, respectivamente; por lo que aceptando la hipótesis de que se hallan saturados a través de esos estados —algo razonable si se trabaja en el sector de baja energía— su degeneración implica la degeneración en masa del pión y de la σ.

En el marco de *ChPT* a *next-to-leading-order* hemos demostrado de forma *model-independent* que la susceptilidad pseudoescalar a temperatura finita es proporcional al condensado de quarks y al inverso de la masa de los quarks ligeros. Esto implica que la susceptibilidad pseudoescalar presenta una naturaleza similar a la del condensado escalar, es decir, tiende a reproducir de modo mucho más parecido el comportamiento *crítico* predicho por las simulaciones en el retículo que el que se obtendría si se asume la saturación del correlador pseudoescalar por un estado de un pión ($\chi_P \sim 1/M_\pi^2$), perfectamente válido —por otro lado— para temperaturas suficientemente bajas. Además, es posible escribir esta relación de modo que no dependa de la masa de los quarks ligeros ni de términos de contacto, sino sólo de parámetros de mesones a través de $\chi_P(T)/\chi_P(0) = <\bar{q}q>_T/<\bar{q}q>_0$.

Ha de notarse que, a diferencia de otros acercamientos al problema [152], este resultado no se basa en la validez del álgebra de corrientes, sino que está calculado en el contexto de una teoría efectiva teniendo en cuenta correcciones *next-to-leading-order* a las constantes $F_\pi(T)$, $M_\pi(T)$ y al condensado de quarks.

Con el fin de comprobar la validez de la relación entre la susceptibilidad pseudoescalar y el condensado de quarks ligeros que he mostrado en el punto anterior, ésta se ha evaluado a partir de datos extraídos de simulaciones en el retículo procedentes de los trabajos [126,127].

A pesar de que los datos están disponibles, los resultados que presento a continuación no han sido publicados con anterioridad, hasta donde hemos podido consultar.

❧ Hemos podido explicar —a través de la relación entre la susceptibilidad pseudoescalar con el condensado escalar de quarks— el rápido crecimiento observado [126] para el cociente $M_P^{sc}(T)/M_P^{sc}(0)$ de las *masas de apantallamiento* asociadas al canal pseudoescalar —definidas en el retículo a través del comportamiento del correlador pseudoescalar a largas distancias—.

En efecto: la identificación de las *masas de apantallamiento* con la masa asociada al polo del correlador en el canal pseudoescalar —suposición lícita siempre que la temperatura esté por debajo de la temperatura crítica observada en estos trabajos— conduce a

$$\frac{M_P^{sc}(T)}{M_P^{sc}(0)} = \left(\frac{\chi_P(0)}{\chi_P(T)}\right)^{\frac{1}{2}} = \left(\frac{<\bar{q}q>_0}{<\bar{q}q>_T}\right)^{\frac{1}{2}}, \tag{2.2}$$

lo que permite evaluar la utilidad de la relación que hemos deducido utilizando exclusivamente datos en el retículo obtenidos del mismo trabajo bajo las mismas condiciones[8].

El resultado final puede verse en la gráfica de la izquierda en la Figura 1 de la publicación 2.3.1, que corresponde al uso de los datos de [126] para las masas, y de [127] para los condensados, ambos calculados a partir de la misma acción y para la misma resolución.

❧ Comparando los datos de la publicación [86] para el condensado sustraído, —*i.e.* $\Delta_{l,s} \sim \chi_P(T)/\chi_P(0)$— y la susceptibilidad escalar normalizada a través del valor de la susceptibilidad pseudoescalar a temperatura cero obtenida mediante el uso de *ChPT*, podemos reproducir en el retículo el escenario de degeneración que ya observábamos en el contexto de la Teoría Quiral.

En un modelo $O(4)$ ideal, la degeneración habría de producirse cerca del máximo para la susceptibilidad quiral escalar, lo que se ve perfectamente en la gráfica derecha de la Figura 1 de la publicación 2.3.1. La temperatura crítica obtenida a partir de la susceptibilidad escalar en [86] es de $T_C \simeq 155$ MeV, y —como puede verse en la figura— la degeneración se ha hecho completamente efectiva a una temperatura unos 20 MeV por encima de este valor, manteniéndose incluso para temperaturas mayores.

El uso de *UChPT* para el cálculo del condensado escalar de quarks y la susceptibilidad quiral escalar a través de la incorporación de efectos asociados a las resonancias más ligeras muestra que la descripción de los resultados mejora aquéllos obtenidos usando sólo *ChPT*, en el sentido de que su comportamiento crítico se hace más parecido al previsto por las simulaciones en el retículo. Pese a esto, ha de tenerse en cuenta que —debido al conjunto de hipótesis de partida que hemos asumido, así como al propio carácter efectivo de la Teoría Unitarizada— el acercamiento a la región crítica puede estar fuera del alcance del rango térmico de aplicabilidad, por lo que hay que ser cautos a la hora de extrapolar los resultados en esta zona.

[8] Es necesario hacer notar aquí que el condensado escalar que se calcula en el retículo siempre se presenta sustraído. Sin embargo, el efecto de esta sustracción puede estimarse entre un 6 % a temperatura cero y un 15 % cerca de T_C (ver publicación 2.3.1 para más detalles al respecto).

Con todo, los resultados más importantes de la publicación que presento obtenidos mediante el uso de *UChPT* son los siguientes:

- La susceptibilidad escalar unitarizada coincide —a bajas energías– con la descripción que aporta *ChPT*, y complementa y mejora su comportamiento en un entorno de temperaturas cercano a la temperatura prevista para la transición de restauración de la simetría quiral.

  Como puede verse en la Figura 4 de la publicación 2.3.1, $\chi_S^U(T)$ presenta un máximo ubicado en una temperatura de $T_{C,U} := 157$ MeV, compatible con los resultados [86] obtenidos mediante simulación en el retículo. Tanto el rápido crecimiento como el máximo en la susceptibilidad escalar unitarizada son herencia directa del mínimo que desarrolla la parte real del polo térmico en el canal escalar al aplicar el *IAM* a la amplitud de dispersión de piones a un *loop*.

- La susceptibilidad escalar unitarizada respeta también las predicciones de [68,145,149] respecto al comportamiento cerca del límite quiral, *vid.* fuerte incremento en el ritmo de crecimiento y reducción de la temperatura crítica; como hemos podido constatar mediante el uso de una masa para el pión de $M_\pi = 10$ MeV, que da lugar a un valor nulo para la parte real del polo térmico en el canal escalar a una temperatura de 118 MeV y —por tanto y a través de la ecuación (2.1)— provoca una susceptibilidad escalar divergente para esa temperatura.

- El condensado de quarks unitarizado —calculado como anticipábamos al inicio de esta sección— coincide con las predicciones de *ChPT* a bajas temperaturas y mejora la predicción de *ChPT* cerca de la región crítica de temperaturas, en el sentido de que se acerca a los resultados obtenidos en [86].

- A través de la asunción de la validez —también en el contexto dado por la Teoría Quiral Unitarizada— de la relación que liga la susceptibilidad pseudoescalar con el condensado de quarks ligeros, podemos estudiar el patrón de degeneración de las susceptibilidades escalar y pseudoescalar.

  Como puede verse también en la Figura 4 de 2.3.1, la intersección entre ambas se produce unos 20 MeV por encima de la temperatura asociada al máximo de la susceptibilidad escalar unitarizada y —a diferencia de lo que sucedía utilizando los datos obtenidos en el retículo— no permanecen iguales para valores térmicos por encima de la temperatura crítica, donde nuestras extrapolaciones son ya demasiado forzadas.

  Aunque la justificación de todas las hipótesis efectuadas en los cálculos se hace de manera *ad hoc*, los resultados que defiendo muestran que la

introducción del estado térmico de la $f_0(500)/\sigma$ es esencial para una correcta descripción de la susceptibilidad escalar y, por tanto, del escenario de degeneración que se plantea en este trabajo. Además revelan que no es necesaria una descripción en términos de estados asintóticos para la σ, sino que el análisis de las funciones de correlación asociadas al canal escalar a través de la Teoría Quiral Unitarizada es adecuado en el régimen de trabajo considerado.

2.3.1 Publicación:

A. Gómez, J. Ruiz, R. Torres,
Chiral symmetry restoration
and scalar-pseudoscalar partners in QCD,
Phys. Rev. **D 88** (2013) 076007

PHYSICAL REVIEW D **88,** 076007 (2013)

Chiral symmetry restoration and scalar-pseudoscalar partners in QCD

A. Gómez Nicola,[1,*] J. Ruiz de Elvira,[1,2,†] and R. Torres Andrés[1,‡]

[1]*Departamento de Física Teórica II, Universidad Complutense, 28040 Madrid, Spain*
[2]*Helmholtz-Institut für Strahlen- und Kernphysik, Universität Bonn, D-53115 Bonn, Germany*

(Received 18 April 2013; published 11 October 2013)

We describe scalar-pseudoscalar partner degeneration at the QCD chiral transition in terms of the dominant low-energy physical states for the light quark sector. First, we obtain within model-independent one-loop chiral perturbation theory that the QCD pseudoscalar susceptibility is proportional to the quark condensate at low T. Next, we show that this chiral-restoring behavior for χ_P is compatible with recent lattice results for screening masses and gives rise to degeneration between the scalar and pseudoscalar susceptibilities (χ_S, χ_P) around the transition point, consistently with an $O(4)$-like current restoration pattern. This scenario is clearly confirmed by lattice data when we compare $\chi_S(T)$ with the quark condensate, expected to scale as $\chi_P(T)$. Finally, we show that saturating χ_S with the $\sigma/f_0(500)$ broad resonance observed in pion scattering and including its finite temperature dependence, allows us to describe the peak structure of $\chi_S(T)$ in lattice data and the associated critical temperature. This is carried out within a unitarized chiral perturbation theory scheme which generates the resonant state dynamically and is also consistent with partner degeneration.

DOI: 10.1103/PhysRevD.88.076007 PACS numbers: 11.10.Wx, 11.30.Rd, 12.38.Gc, 12.39.Fe

I. INTRODUCTION AND MOTIVATION

Chiral symmetry breaking $SU_V(N_f) \times SU_A(N_f) \to SU_V(N_f)$ and its restoration, with N_f light quark flavors, has been a milestone in our present understanding of the quantum chromodynamics (QCD) phase diagram and hadronic physics under extreme conditions of temperature T and baryon density, as those produced in heavy-ion and nuclear matter experimental facilities such as RHIC, CERN (ALICE), and FAIR. Lattice simulations support that deconfinement and chiral restoration take place very close to one another in the phase diagram. In the physical case $N_f = 2 + 1$ $(0 \neq m_u = m_d \equiv m_q \ll m_s)$ and for vanishing baryon chemical potential, they point towards a smooth crossover transition at pseudocritical temperature $T_c \sim 145$–165 MeV [1,2], the results being fairly consistent with the $O(4)$ universality class [3], which would hold for two light flavors in the chiral limit $m_q = 0$. The crossover nature of the transition means, in particular, that there is no unique way to identify the transition point, the most efficient one in lattice being the scalar susceptibility peak position, rather than the vanishing point for the quark condensate $\langle \bar{q}q \rangle_T$, the order parameter, which decreases asymptotically with T for $m_q \neq 0$.

The equivalence with the $O(4) \to O(3)$ breaking pattern for $N_f = 2$ led to early proposals of $\pi - \sigma$ meson degeneration ("chiral partners") at chiral restoration [4] which, in its simplest linear realization, takes place through the σ component of the $O(4)$ field (σ, π^a) acquiring a thermal vacuum expectation value and mass both vanishing at the transition in the chiral limit. Degeneration in the vector-axial vector sector (ρ and a_1 states) as a signature of chiral restoration has also been thoroughly studied [5]. Nowadays, we know that the σ state is well established as a $\pi\pi$ scattering broad resonance for isospin and angular momentum $I = J = 0$, known as $f_0(500)$ [6], which is then difficult to accommodate as an asymptotically free state, like in the linear model. Precisely, one of our main conclusions here will be that this asymptotic description is not needed. In fact, in order to study chiral partner degeneration in the scalar-pseudoscalar sector, it is more appropriate to analyze the corresponding current correlation functions [7] which can be derived from a chiral effective Lagrangian without introducing explicitly a particlelike σ degree of freedom. The scalar and pseudoscalar susceptibilities in terms of the corresponding QCD $SU(2)$ currents are given by

$$\begin{aligned}\chi_S(T) &= -\frac{\partial}{\partial m}\langle \bar{q}q \rangle_T \\ &= \int_E d^4x [\langle \mathcal{T}(\bar{q}q)(x)(\bar{q}q)(0)\rangle_T - \langle \bar{q}q \rangle_T^2] \\ &= \int_E d^4x \left[\frac{\delta}{\delta s(x)}\frac{\delta}{\delta s(0)} Z[s,p]|_{s=m_q, p^a=0}\right], \quad (1)\end{aligned}$$

$$\begin{aligned}\chi_P(T)\delta^{ab} &= \int_E d^4x \langle \mathcal{T} P^a(x) P^b(0)\rangle_T \equiv \delta^{ab}\int_E d^4x K_P(x) \\ &= \int_E d^4x \left[\frac{\delta}{\delta p^a(x)}\frac{\delta}{\delta p^b(0)} Z[s,p]|_{s=m_q, p^a=0}\right], \quad (2)\end{aligned}$$

where $q = (u, d)$ is the quark field, $P^a(x) = \bar{q}\gamma_5\tau^a q(x)$ and $K_P(x)$ are, respectively, the pseudoscalar current and its correlator, the Euclidean measure $\int_E d^4x = \int_0^\beta d\tau \int d^3\vec{x}$ with $\beta = 1/T$, and $\langle\cdot\rangle_T$ denotes a thermal

*gomez@fis.ucm.es
†elvira@hiskp.uni-bonn.de
‡rtandres@fis.ucm.es

average. For χ_P, parity invariance of the QCD vacuum ($\langle P^a \rangle_T = 0$) and isospin symmetry have been used. In the above equation, $Z[s, p]$ is the QCD generating functional with scalar and pseudoscalar sources (s, p^a) coupled to the massless Lagrangian in the light sector as $-s(x) \times (\bar{q}q)(x) + ip_a(x)P^a(x)$, so that $Z[m_q, 0]$ is the QCD partition function.

Thus, should the scalar and pseudoscalar currents become degenerate at chiral restoration, $\chi_P(T)$ and $\chi_S(T)$ would meet at that point. Since χ_S is expected to increase, as a measure of the fluctuations of the order parameter, at least up to the transition point, it seems plausible that they meet near the transition. In an ideal $O(4)$ pattern, the matching should take place near the maximum of χ_S.

Since P^a has the quantum numbers of the pion field π^a, its correlators, like $K_P(x)$, are saturated by the pion state at low energies. Let us first review the prediction arising from the low-energy theorems of current algebra, equivalent to the leading order (LO) in the low-energy expansion of chiral Lagrangians. At that order, one has $P^a \sim 2B_0 F \pi^a$ (from partial conservation of axial current (PCAC) theorem) with $B_0 = M^2/2m_q$ and where F and M are the pion decay constant and mass, respectively, so that $\chi_P \sim 4B_0^2 F^2 G_\pi(p = 0) + \cdots$ from Eq. (2), being $G_\pi(p)$ the pion propagator in momentum space $p \equiv (i\omega_n, \vec{p})$ and $\omega_n = 2\pi n T$ the Matsubara frequency with integer n. Thus, the pseudoscalar correlator, saturated with the dominant pion state, is just proportional to the pion propagator at this order. In addition, to LO the Euclidean propagator is just the free one $G_\pi^{\mathrm{LO}}(p) = 1/(-p^2 + M^2)$ (interactions are suppressed at low energies) with $p^2 = (i\omega_n)^2 - |\vec{p}|^2$, so that using also the Gell-Mann-Oakes-Renner (GOR) relation $M^2F^2 = -m_q\langle \bar{q}q \rangle$, valid at this order, we would get $\chi_P \sim -\langle \bar{q}q \rangle / m_q$, as a first indication of the relation between the pseudoscalar susceptibility and the quark condensate at the LO given by current algebra.

The latter result can actually be obtained formally as a Ward identity (WI) from the QCD Lagrangian [8], in connection with the definition of the quark condensate for lattice Wilson fermions [9]. However, both sides of the identity suffer from QCD renormalization ambiguities, so that this WI is formally well defined only for exact chiral symmetry [9,10]. It is therefore interesting to study, and so we will do in the next section, how this identity is realized within chiral perturbation theory (ChPT) [11], which describes the low-energy chiral symmetry broken phase of QCD in a model-independent framework where symmetry breaking is realized nonlinearly and pions are the only degrees of freedom in the Lagrangian. The previous current-algebra results are actually just the LO in the ChPT expansion in powers of a generic low-energy scale p, denoting pion momenta or temperature, relative, respectively, to $\Lambda_\chi \sim 1$ GeV and T_c. These are nothing but indicative natural upper limits for the chiral expansion in terms of scattering (typical resonance scale) and thermodynamics (critical phenomena), respectively, although both are treated on the same foot in the chiral expansion. In particular, the LO prediction for χ_P is temperature independent, so it is not obvious that it can be simply extrapolated as, say, $\langle \bar{q}q \rangle \to \langle \bar{q}q \rangle_T$. Actually, all the quantities involved change with temperature due to pion loop corrections, namely, $M_\pi(T)$, $F_\pi(T)$ and $\langle \bar{q}q \rangle(T)$ [12].

Similarly, from Eq. (1), one can relate χ_S with the propagator of a "σ-like state" such that it couples linearly to the external scalar source $s(x)$ in an explicit symmetry-breaking term $\mathcal{L}_{\mathrm{SB}} = 2B_0 F s(x)\sigma(x)$. Without further specification about its nature and its coupling to other physical states such as pions, one already gets $\chi_S \sim 4B_0^2F^2G_\sigma(p = 0)$, suggesting a growing behavior inversely proportional to M_σ^2 as the sigma state reduces its mass to become degenerate with the pion.

We also recall that the problem of $\chi_S - \chi_P$ degeneration has been studied in nuclear matter at $T = 0$ in [13], to linear order in nuclear density. In that work, current algebra is assumed to hold through PCAC in the operator representation and other low-energy theorems such as GOR, which as discussed in the previous paragraphs, leads to the pseudoscalar correlator $K_P(x)$ being directly proportional to the pion propagator. The authors in [13] work within low-energy models at finite density for which this PCAC realization holds, so that by including the proper finite-density corrections to G_π, which carries out all the density dependence of K_P through an in-medium mass, and to $\langle \bar{q}q \rangle$, the relation $\chi_P \sim -\langle \bar{q}q \rangle / m_q$ is found to hold in the nuclear medium. This result provides another supporting argument for the relation between the condensate and the pseudoscalar susceptibility and represents an additional motivation for our present ChPT analysis, where we do not need to make any assumption about the validity of current algebra.

II. STANDARD CHPT ANALYSIS OF THE PSEUDOSCALAR CORRELATOR AND SUSCEPTIBILITY

The next to leading order (NLO) corrections to χ_P can be obtained systematically and in a model-independent way within ChPT, where one can also calculate the scalar susceptibility χ_S to a given order only in terms of pion degrees of freedom. The price to pay is that we expect to reproduce only the behavior of $\chi_{S,P}(T)$ for low and moderate temperatures. However, since χ_P is dominated by pions, whose dynamics are well described through ChPT, we expect to obtain a reasonable qualitative description of its T behavior, whereas standard ChPT misses the peak structure of χ_S near the transition. We note in turn that the LO for χ_S vanishes, unlike that of χ_P. The ChPT NLO result for $\chi_S(T)$ can be found in [14,15].

For $\chi_P(T)$ we consider the effective Lagrangian $\mathcal{L}_2 + \mathcal{L}_4 + \cdots$, where $\mathcal{L}_{2n} = \mathcal{O}(p^{2n})$, including their dependence on the pseudoscalar source p^a as given in [11]. We follow similar steps as in [15,16], now for the pseudoscalar

correlator $K_P(x)$. The LO comes from $\mathcal{L}_2$ only and reproduces the current-algebra prediction. The NLO corrections to $K_P(x)$ are of the following types:

(i) the NLO corrections to the pion propagator $G_\pi^{\rm NLO}(x)$, which come both from $\mathcal{L}_2$ one-loop tadpolelike contributions $G_\pi^{\rm LO}(x=0)$ and from tree-level $\mathcal{L}_4$ constant terms,
(ii) pion self-interactions $\mathcal{O}(\pi p^a \times \pi^3 p^b)$ in $\mathcal{L}_2$ contributing as $G_\pi^{\rm LO}(x) G_\pi^{\rm LO}(x=0)$,
(iii) crossed terms $\mathcal{L}_2 = \mathcal{O}(p^a \pi) \times \mathcal{L}_4 = \mathcal{O}(p^b \pi)$ giving $G_\pi^{\rm LO}(x)$ multiplied by a NLO contribution,
(iv) $\mathcal{L}_4 = \mathcal{O}(p^a p^b)$ terms giving rise to a contact contribution proportional to $\delta^{(4)}(x)$.

The final result for the pseudoscalar correlator in momentum space for Euclidean four-momentum p can be written as

$$K_P(p) = a + 4B_0^2 F^2 G_\pi^{\rm NLO}(p,T) + c(T) G_\pi^{\rm LO}(p) + \mathcal{O}(F^{-2}), \tag{3}$$

where subleading terms are labeled by their F^2 dependence. The NLO propagator includes wave function and mass renormalization (at this order in ChPT there is no imaginary part for the self-energy):

$$G_\pi^{\rm NLO}(p,T) = -\frac{Z_\pi(T)}{p^2 - M_\pi^2(T)}, \tag{4}$$

where the LO propagator corresponds to $Z_\pi = 1$, $M_\pi = M$ and is temperature independent. F and M are the Lagrangian pion mass and decay constant, related to the vacuum ($T=0$) physical values $M_\pi(0) \equiv M_\pi \simeq 140$ MeV, $F_\pi(0) \equiv F_\pi \simeq 93$ MeV, by $\mathcal{O}(F^{-2})$ corrections [11].

The constant a in Eq. (3) is temperature independent and is a finite combination of low-energy constants (LECs) of $\mathcal{L}_4$ [11]. In the ChPT scheme, the divergent part of the $\mathcal{L}_4$ LEC cancels the loop divergences from $\mathcal{L}_2$ such that pion observables are finite and independent of the low-energy renormalization scale. To NLO in ChPT all the pion loop contributions in Eq. (3) are proportional to the tadpolelike contribution $G_\pi^{\rm LO}(x=0,T) = G_\pi^{\rm LO}(x=0,T=0) + g_1(M,T)$ with the thermal function:

$$g_1(M,T) = \frac{T^2}{2\pi^2} \int_{M/T}^{\infty} dx \frac{\sqrt{x^2 - (M/T)^2}}{e^x - 1}, \tag{5}$$

which is an increasing function of T for any mass. Thus, the pion thermal mass in the NLO propagator is given at this order by $M_\pi^2(T) = M_\pi^2(0)[1 + g_1(M,T)/2F^2]$ and is finite and scale independent. The same holds for $F_\pi^2(T) = F_\pi^2(0)[1 - 2g_1(M,T)/F^2]$ and for $\langle \bar{q}q \rangle_T = \langle \bar{q}q \rangle_0 \times [1 - 3g_1(M,T)/2F^2]$ [12]. Note that $M_\pi^{-2}(T)$ decreases with T a factor of 3 slower than the condensate $\langle \bar{q}q \rangle_T$. In addition, to this order it holds $F_\pi^2(T) M_\pi^2(T)/\langle \bar{q}q \rangle_T = F_\pi^2(0) M_\pi^2(0)/\langle \bar{q}q \rangle_0 \neq -m_q$. That is, the GOR relation is broken at finite temperature to NLO by the same $T=0$ terms, given in [11]. GOR holds to NLO only in the chiral limit, including temperature effects [17].

The constant $c(T)$ in Eq. (3) includes both LEC contributions and loop functions and the same happens with the wave function renormalization constant $Z_\pi(T)$. Both are divergent, but the combination $4B_0^2 F^2 Z_\pi(T) + c(T)$ turns out to be finite and scale independent. Note that if we replace $G_\pi^{\rm LO} = G_\pi^{\rm NLO}$ in the last term in Eq. (3), which is allowed at this order since $c(T) = \mathcal{O}(F^0)$ is of NLO, that combination is precisely the one multiplying the NLO propagator, i.e, it is the T-dependent residue at the $M_\pi^2(T)$ pole (when the Euclidean propagator is analytically continued to the retarded one). That finite residue, being finite, has to be then a combination of the finite observables involved. Actually, it happens to be

$$4B_0^2 F^2 Z_\pi(T) + c(T) = \frac{F_\pi^2(T) M_\pi^4(T)}{m_q^2} + \mathcal{O}(F^{-2}). \tag{6}$$

Thus, the expression in Eq. (6) represents the residue of the NLO K_P correlator (3) at the thermal pion pole. Note that by showing explicitly that the residue can be expressed as (6) we obtain that the thermal part of the pseudoscalar susceptibility $\chi_P(T)$ is the same as that in $-m_q \langle \bar{q}q \rangle_T$, since $F_\pi^2(T) M_\pi^2(T)/m_q^2 + \mathcal{O}(F^{-2}) = (\langle \bar{q}q \rangle_T / \langle \bar{q}q \rangle_0)(F_\pi^2 M_\pi^2/m_q^2) + \mathcal{O}(F^{-2})$, so that

$$\chi_P(T) = K_P(p=0,T) = K_P(p=0,T=0) + \frac{F_\pi^2 M_\pi^2}{m_q^2} \frac{\langle \bar{q}q \rangle_T - \langle \bar{q}q \rangle_0}{\langle \bar{q}q \rangle_0} + \mathcal{O}(F^{-2}). \tag{7}$$

Now, since $\langle \bar{q}q \rangle_T - \langle \bar{q}q \rangle_0 = \mathcal{O}(F^0)$, at the NLO order we are working, we can replace in Eq. (7) $F_\pi^2 M_\pi^2 = -m_q \langle \bar{q}q \rangle_0 + \mathcal{O}(F^0)$ so that we get $\chi_P(T) - \chi_P(0) = -m_q(\langle \bar{q}q \rangle_T - \langle \bar{q}q \rangle_0) + \mathcal{O}(F^{-2})$. Furthermore, the constant a appearing in Eq. (3) contains precisely the LEC combination that combines with that in the residue (6) to give the same scaling law, now including the $T=0$ part. Thus, our final result for the pseudoscalar susceptibility in ChPT to NLO (finite and scale independent) is

$$\chi_P^{\rm ChPT}(T) = 4B_0^2 \left[\frac{F^2}{M^2} + \frac{1}{32\pi^2}(4\bar{h}_1 - \bar{l}_3) - \frac{3}{2M^2} g_1(M,T) \right] + \mathcal{O}(F^{-2}) = -\frac{\langle \bar{q}q \rangle_T^{\rm ChPT}}{m_q} + \mathcal{O}(F^{-2}), \tag{8}$$

where the first term inside brackets is the LO current algebra $\mathcal{O}(F^2)$ and $\bar{l}_3$, $\bar{h}_1$ are renormalized scale-independent LECs [11].

Therefore, we have obtained the WI connecting $\langle \bar{q}q \rangle$ and χ_P to NLO in model-independent ChPT, including finite-T effects. Furthermore, the m_q dependence cancels in $\chi_P(T)/\chi_P(0) = \langle \bar{q}q \rangle_T / \langle \bar{q}q \rangle_0$, where only meson parameters show up. To this order, $\chi_P(T)/\chi_P(0) = 1 - 3g_1(M,T)/(2F^2)$ so that the LEC dependence also

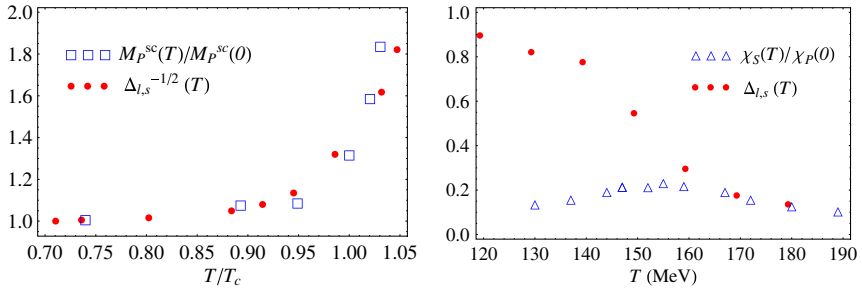

FIG. 1 (color online). Left: Comparison between the pseudoscalar screening mass ratio and $\Delta_{l,s}^{-1/2}$, where $\Delta_{l,s} = r(T)/r(0)$ with $r = \langle\bar{q}q\rangle - (2m_q/m_s)\langle\bar{s}s\rangle$, for the lattice data in [18] (masses) and [20] (condensate) with the same lattice action and resolution and $T_c \simeq 196$ MeV. Right: Scalar susceptibility versus $\Delta_{l,s} \sim \chi_P(T)/\chi_P(0)$ from the data in [1] for which $T_c \simeq 155$ MeV.

disappears. Recall that $\bar{h}_1$ comes from a contact term in $\mathcal{L}_4$ and is therefore another source of ambiguity in the NLO condensate [11].

Note also that, unlike the approach followed in [13], we have arrived to the result (8) without relying on the validity of current algebra, which actually holds only in ChPT to the lowest order. Actually, as explained, our result takes into account NLO corrections to $F_\pi(T)$, $M_\pi(T)$, $\langle\bar{q}q\rangle_T$ through GOR breaking terms, both at $T = 0$ and $T \neq 0$, which turn out to be crucial to obtain the correct scaling law given in Eq. (8).

III. LATTICE DATA ANALYSIS

We can draw some important conclusions from the previous results. First, $\chi_P(T)$ scales like the order parameter $\langle\bar{q}q\rangle$, instead of the much softer behavior $1/M_\pi^2(T)$. This scaling suggests a chiral-restoring nature for the pseudoscalar susceptibility, although we cannot draw any definitive conclusion about chiral restoration just from our standard ChPT analysis, which makes sense only at low T. Its behavior for higher T approaching the transition should be considered merely as indicative extrapolations, pretty much in the same way as the ChPT prediction for the vanishing point of the quark condensate is just a qualitative indication that the restoring behavior goes in the right direction. For this reason, in the following we will complement our standard ChPT calculation with a direct lattice data analysis, and later on with a unitarized study which, as we will see, incorporates the relevant degrees of freedom to achieve a more precise description near the transition point.

One can actually observe a clear signal of a critical chiral-restoring behavior for χ_P, consistent with our previous ChPT result, in the lattice analysis of Euclidean correlators, which determine their large-distance spacelike screening mass M^{sc} in different channels [18]. From Eq. (2) we expect $\chi_P = K_P(p=0) \sim (M_P^{pole})^{-2}$ with M_P^{pole} the pole mass associated to $K_P(p)$ in a general parametrization of the form $K_P^{-1}(\omega, \vec{p}) = -\omega^2 + A^2(T)|\vec{p}|^2 + M_P^{pole}(T)^2$ with $A(T) = M_P^{pole}(T)/M^{sc}(T)$ [19]. Here, $\omega = i\omega_n$ would correspond to the thermal Euclidean propagator and $\omega \in \mathbb{R} + i\epsilon$ to the retarded Minkowski one setting the dispersion relation. Assuming a soft temperature behavior for $A(T)$, which is plausible below T_c [for instance, $A = 1$ for the NLO ChPT propagator in Eq. (4)], we can then explain the sudden increase of $M_P^{sc}(T)/M_P^{sc}(0)$ observed in this channel [18] since we expect that ratio to scale like $[\chi_P(0)/\chi_P(T)]^{1/2} \sim [\langle\bar{q}q\rangle_0/\langle\bar{q}q\rangle_T]^{1/2}$. We show in Fig. 1 (left panel) these two quantities. The correlation between them is notorious, given the uncertainties involved, and the mentioned increase is clearly observed. Data are taken from the same lattice group and under the same lattice conditions [18,20]. Note that in the lattice works, $(2m_q/m_s)\langle\bar{s}s\rangle$ is subtracted from $\langle\bar{q}q\rangle_T$ in order to avoid renormalization ambiguities. Estimating the $T = 0$ condensates from NLO ChPT,[1] this subtraction gives a 6% correction and, from the lattice values, it is about a 15% correction near T_c. Apart from the screening versus pole mass and the strange condensate corrections, one should not forget about the typical lattice uncertainties, like resolution, choice of action, staggered taste breaking, and large pion masses [1,20].

Another important conclusion of our analysis is that the decrease of χ_P and the increase of χ_S as they approach the critical point, lead to scalar-pseudoscalar susceptibility partner degeneration, which in an ideal $O(4)$ pattern should take place near the χ_S peak. Once again, this behavior is observed in lattice data. In Fig. 1 (right panel) we plot the subtracted condensate, expected to scale as $\chi_P(T)/\chi_P(0)$ according to our previous ChPT and lattice analysis, versus $\chi_S(T)/\chi_P(0)$, both from the lattice analysis in [1]. The $T = 0$ values are taken from ChPT. The current degeneration is evident, not only at the critical point but also above it, where those two quantities remain very close to one another.

Recall that both the analysis of the correlation between screening masses and inverse rooted condensate and that of scalar versus pseudoscalar (condensate) susceptibilities,

[1]For standard ChPT we use the same LEC values as in [14,15]. Their influence is more important in χ_S, due to the vanishing of the LO, than in χ_P, $\langle\bar{q}q\rangle$.

although elaborated from available lattice data, have not been presented before, to the best of our knowledge. As commented above, this analysis has been motivated by our ChPT results in Sec. II and it gives strong support to the scalar-pseudoscalar degeneration pattern at the transition, as well as providing a natural explanation for the behavior of lattice masses in this channel.

IV. UNITARIZED CHPT AND RESULTS

A. Extracting the $f_0(500)$ thermal pole from unitarized ChPT

Since the scalar susceptibility is dominated by the $I = J = 0$ lightest state, which does not show up in the ChPT expansion, let us consider its unitarized extension given by the inverse amplitude method (IAM) [21] which generates dynamically in $SU(2)$ the $f_0(500)$ and $\rho(770)$ resonances and has been extended to finite temperature in [22–24]. Thus, before proceeding to derive the unitarized susceptibility in Sec. IV B, let us review briefly here, for the sake of completeness, some of the more relevant aspects of the thermal IAM, particularly in the scalar channel. We refer to [22–25] for a more detailed analysis.

The IAM scattering amplitude is constructed by demanding unitarity and matching with the low-energy expansion, for which all the ChPT scattering diagrams at finite temperature are included up to one-loop [22]. The different types of those diagrams are represented in Fig. 2. The T-dependent corrections to the scattering amplitude come from the internal loop Matsubara sums in the imaginary-time formalism of thermal field theory. The external pion lines correspond to asymptotic $T = 0$ states. The thermal amplitude is defined after the application of the $T = 0$ Lehmann-Symanzik-Zimmermann reduction formula, which allows us to deal just with thermal Green functions. After the Matsubara sums are evaluated, the external lines are analytically continued to real frequencies. The full result for the thermal amplitude to NLO in ChPT is given in [22].

The scattering amplitude can be projected into partial waves $t_{IJ}(s)$ in the reference frame $\vec{p}_1 = -\vec{p}_2$ where the incoming pions 1,2 are at rest with the thermal bath, so that

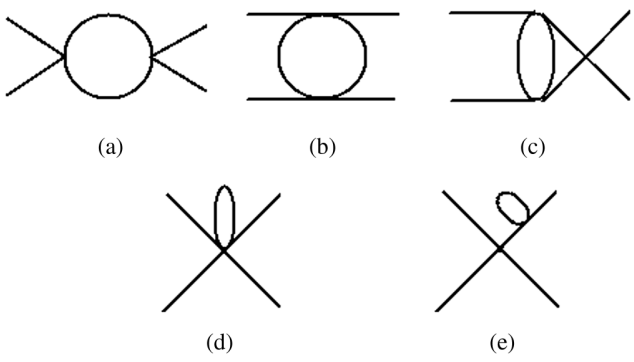

FIG. 2. One-loop diagrams for T-dependent pion scattering.

$s = (E_1 + E_2)^2$. The NLO partial waves have the generic form (we drop in the following the IJ indices for brevity) $t(s;T) = t_2(s) + t_4(s;T)$, where $t_2(s)$ is the $\mathcal{O}(p^2)$ tree-level T-independent scattering amplitude from $\mathcal{L}_2$ and t_4 is $\mathcal{O}(p^4)$ including the tree level from $\mathcal{L}_4$ plus the one-loop from the diagrams in Fig. 2. Each partial wave satisfies $\mathrm{Im}\, t_4(s + i\epsilon;T) = \sigma_T(s) t_2(s)^2$ for $s > 4M_\pi^2$ with $\sigma_T(s) = \sqrt{1 - 4M_\pi^2/s}[1 + 2n_B(\sqrt{s}/2;T)]$ and $n_B(x;T) = [\exp(x/T) - 1]^{-1}$, the Bose-Einstein distribution. This is the perturbative version of the unitarity relation for partial waves $\mathrm{Im}\, t(s + i\epsilon;T) = \sigma_T(s)|t(s;T)|^2$ and σ_T is the two-pion phase space, which at finite T receives the thermal enhancement proportional to n_B which has a neat interpretation in terms of the emission and absorption scattering processes allowed in the thermal bath [22,25]. Precisely imposing that the partial waves satisfy the above unitarity relation exactly while matching the ChPT series at low s and low T leads to the thermal unitarized IAM amplitude:

$$t^{\mathrm{IAM}}(s;T) = \frac{t_2(s)^2}{t_2(s) - t_4(s;T)}. \tag{9}$$

When the IAM amplitude is continued analytically to the s complex plane [23], it presents poles in the second Riemann sheet $t^{\mathrm{II}}(s;T) = t_2(s)^2/[t_2(s) - t_4^{\mathrm{II}}(s;T)]$ with $t_4^{\mathrm{II}}(s;T) = t_4(s;T) + 2i\sigma_T t_2(s)^2$ so that $\mathrm{Im}\, t^{\mathrm{II}}(s - i\epsilon) = \mathrm{Im}\, t^{\mathrm{IAM}}(s + i\epsilon)$ for $s > 4M_\pi^2$. Those poles correspond to the physical resonances, which in the case of pion scattering are the $f_0(500)$ ($I = J = 0$) and $\rho(770)$ ($I = J = 1$). The T-dependent poles can be extracted numerically by searching for zeros of $1/t^{\mathrm{II}}(s;T)$ in the s complex plane. We denote the pole position by $s_p(T) = [M_p(T) - i\Gamma_p(T)/2]^2$. The LEC for the IAM are chosen so that, within errors, they remain compatible with the standard ChPT ones and with the $T = 0$ pole values for the ρ and $f_0(500)$ listed in the PDG [6].

Let us comment now on the thermal evolution of the resonance poles, whose main features for this work are represented in Fig. 3. Since $t_2(s) = a(s - s_0)$ with real a and s_0, the thermal dependence $s_p(T)$ is governed by that of t_4^{II} at the pole.

In the vector-isovector channel, $\Gamma_p \ll M_p$ for all temperatures of interest here and therefore the ρ can be considered a narrow Breit-Wigner (BW) resonance with M_p and Γ_p its mass and width respectively. Actually, $M_p^2(T)$ decreases very slightly with T for the relevant temperature range. Hence, the T-dependent contribution of the real part of t_4^{II} is almost negligible compared to its $T = 0$ part, due to the large ρ mass value. The latter gives roughly the $T = 0$ rho mass, so the real part of the denominator of t^{II} behaves dominantly as $s - M_p^2(0)$. In particular, the tadpole contributions of diagrams (d) and (e) in Fig. 2 are suppressed in this channel typically by $\mathcal{O}(T^2/M_\rho^2)$. However, the thermal effect in $\Gamma_p(T)/\Gamma_p(0)$ is much more sizable, increasing with T. Its dominant contribution comes from

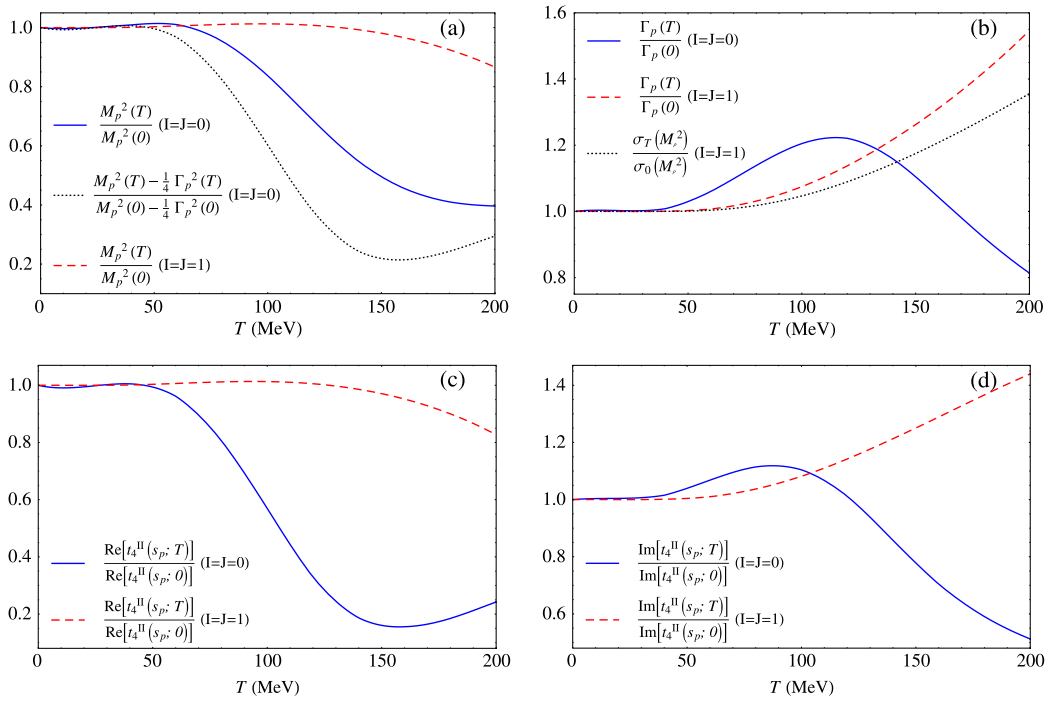

FIG. 3 (color online). Thermal pole evolution (a)–(b) and contributions from the second sheet amplitude (c)–(d) for the scalar-isoscalar ($I = J = 0$) and vector-isovector ($I = J = 1$) channels.

the imaginary part of the amplitude. The imaginary part of the t^{II} denominator at the pole behaves like $M_p\Gamma_p(T)$ and, up to $T \simeq 100$ MeV $\Gamma_p(T)/\Gamma_p(0) \sim \sigma_T/\sigma_0$, which for s_p near the real axis comes essentially from diagram (a) in Fig. 2 (which would give the only imaginary part for real $s > 4M_\pi^2$) so the broadening can be explained just by a thermal phase space increase up to that temperature. Note that, although this effect is formally $\mathcal{O}(e^{-M_\rho/T})$, it activates below the transition because of the relative small value of $\Gamma_p(0)$. Above that, there is an additional increase of the effective $\rho\pi\pi$ coupling with T [23], to which tadpoles contribute, which explains a further increase of the width. This behavior is represented in Fig. 3. Observe the softer behavior of the mass as compared to the width in this channel, and the correlation with the real and imaginary parts of the amplitude at the pole position.

In the scalar-isoscalar channel, the one we are interested in here, the behavior is remarkably different. We rather talk of a broad resonance pole, since M_p and Γ_p are comparable, so that the $f_0(500)$ pole is away from the real axis. As a consequence, all thermal contributions from diagrams (a)–(e) in Fig. 2 to t_4^{II} become complex at the pole and the real and imaginary parts of the pole equations do not have the simple form of a BW resonance. In addition, due to the lower value of $M_p^2(0)$ as compared to the ρ case, the thermal dependence is much more stronger, both for the real and imaginary parts, and all contributions from those diagrams become equally relevant. In particular, the tadpoles in diagrams (d) and (e) in Fig. 2 now come into play. The numerical solution of the pole equations show that $M_p^2(T)$ in this channel decreases significatively, while $\Gamma_p(T)$ increases up to $T \simeq 120$ MeV and decreases from that point onwards, as seen in Fig. 3. Note that this nonmonotonic behavior for Γ_p cannot be explained now just in terms of phase space or vertex increasing. On the other hand, a possible interpretation of the decreasing M_p^2 is a chiral-restoring behavior. Actually, in Fig. 3(a) we also represent $\mathrm{Re}\, s_p(T) = M_p^2(T) - \Gamma_p^2(T)/4 \equiv M_S^2(T)$, which would correspond to the self-energy real part of a scalar particle with energy squared s and $\vec{p} = \vec{0}$, exchanged between the incoming and outgoing pions. This σ-like squared mass not only drops faster but it develops a minimum at a certain temperature, which as we will see below corresponds to a maximum in the scalar susceptibility. In the ρ channel, there is almost no numerical difference between M_p^2 and $\mathrm{Re}\, s_p$. Thus, a qualitative explanation for the $\Gamma_p(T)$ change from a increasing to a decreasing behavior in the scalar channel would be the influence of the strong mass decreasing of the decaying state.

B. Unitarized scalar susceptibility and quark condensate

In order to establish a connection between the scalar susceptibility and the scalar pole, we construct a unitarized susceptibility by saturating the scalar propagator with the $f_0(500)$ thermal state and assuming that its $p = 0$ mass does not vary much with respect to the pole mass. Thus, we

identify the pole of a scalar state exchanged in pion scattering with the thermal pole in the scalar channel discussed in the previous section. Therefore, we have

$$\chi_S^U(T) = \frac{\chi_S^{\rm ChPT}(0) M_S^2(0)}{M_S^2(T)}, \qquad (10)$$

where we have normalized to the $T = 0$ ChPT value, since we are demanding that all our $T = 0$ results match the model-independent ChPT predictions. This normalization compensates partly the difference between the $p = 0$ and pole masses. Under this approximation, the self-energy real part is the squared scalar mass $M_S^2(T) = M_p^2(T) - \Gamma_p^2(T)/4$, as discussed in the previous section, and the self-energy imaginary part vanishes at $p = 0$.

The quark condensate cannot be extracted directly from the unitarized susceptibility. However, we can obtain an approximate description by assuming that the relevant temperature and mass dependence, as far as the critical behavior is concerned, comes from pion loop functions as $\delta\langle\bar{q}q\rangle^U(T, M) = B_0 T^2 g(T/M)$ and $\delta\chi_S = B_0^2 h(T/M)$, with $\delta f(T) = f(T) - f(0)$. This T/M dependence holds actually to NLO ChPT, as in Eq. (5). Then, from Eq. (1), since $\delta\chi_S = -\partial\delta\langle\bar{q}q\rangle/\partial m_q$, we get

$$g(x) = g(x_0) + \int_{x_0}^{x} \frac{h(y)}{y^3} dy \quad \text{for } x > x_0, \qquad (11)$$

with $T_0 = x_0 M \ll M$ a suitable low-T scale below which we use directly NLO ChPT, which has a better analytic behavior near $T = 0$. The h function is obtained from the T dependence of χ_S in Eq. (10).

C. Results

Our theoretical results based on effective theories are plotted in Fig. 4. First, ChPT to NLO gives an increasing $\chi_S(T)$, intersecting $\chi_P(T)$ at $T_d \simeq 0.9 T_c$, where $\langle\bar{q}q\rangle_T^{\rm ChPT} \times (T_c) = \chi_P^{\rm ChPT}(T_c) = 0$. Once again, this result should be considered just as an extrapolation of the model-independent expressions for $\chi_S(T)$ and $\chi_P(T)$ beyond their low-T applicability range. With this caution in mind, standard ChPT supports the idea of partner degeneration. Actually, near the chiral limit $M_\pi \ll T$, where critical effects are meant to be enhanced, the degeneration point $T_d = T_c - 3M_\pi/4\pi + \mathcal{O}(M_\pi^2/T_c)$, approaching the chiral restoration temperature in that limit.

We also plot $\chi_S^U(T)$ in Fig. 4. The result agrees with standard ChPT at low T and improves remarkably the behavior near the transition. It actually develops a maximum at $T_c \simeq 157$ MeV. We show for comparison the lattice data of [1]. Furthermore, approaching the chiral limit by taking the $M_\pi = 10$ MeV poles from [24] gives a vanishing $M_S(T)$ at $T_c \simeq 118$ MeV and hence a divergent χ_S^U from Eq. (10) at T_c. Thus, we get, at least qualitatively, the T_c reduction and stronger χ_S growth near the chiral limit expected from theoretical [26] and lattice [2,3] analysis.

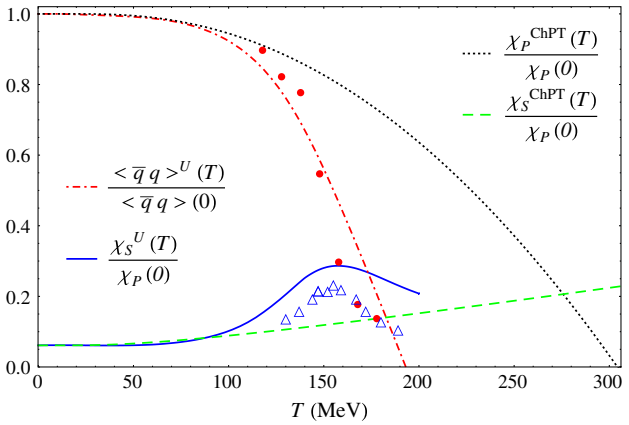

FIG. 4 (color online). Scalar versus pseudoscalar susceptibilities in ChPT and in our unitarized description. We show for comparison the lattice data of Fig. 1 (right).

The clear improvement of the unitarized approach with respect to the standard ChPT one for the scalar susceptibility is essentially due to the introduction of the thermal $f_0(500)$ state, whose importance in this case is clearly seen from the dependence $\chi_S \sim 1/M_S^2$, rather than to an enlargement of the applicability range in the unitarized approach. Actually, even within the unitarized description, we should be cautious when extrapolating it to near T_c since we may be strictly beyond the effective theory range.

The resulting $\langle\bar{q}q\rangle_T^U$ is plotted in Fig. 4 with $T_0 \simeq 12$ MeV.[2] The critical behavior is again nicely improved compared to the ChPT curves and is in better agreement with lattice data in that region. In addition, we obtain once more a scalar-pseudoscalar intersection near the χ_S peak and hence of chiral restoration. The corresponding $\langle\bar{q}q\rangle_T^U$ near the chiral limit ($M_\pi = 10$ MeV) is much more abrupt, vanishing and meeting χ_S at T_c as expected.

Recall that in the above unitarized analysis, we are not performing a fit to lattice points. We just use the same LECs which generate the $T = 0$ physical $f_0(500)$, ρ states [24] and then provide our results for the susceptibility and condensate. The theoretical uncertainties in the LEC, as well as the lattice errors already discussed, should be taken into account for a more precise comparison. Besides, our effective theory analysis is not expected to reproduce the chiral restoration pattern above T_c. In any case, apart from the important consistency obtained for chiral restoration properties, such as the χ_S peak and the χ_S/χ_P matching, an important point we want to stress is the crucial role of the $f_0(500)/\sigma$ state to describe the scalar susceptibility. Since $\chi_S \sim 1/M_S^2$, this observable is much more sensitive to this broad state, so that a physically realistic description, including its thermal effects, turns out to be essential.

[2]We find very small numerical differences changing T_0 between 10–60 MeV.

This may not be the case for other thermodynamical observables, for which other approaches may provide a much better description. For instance, the hadron resonance gas (HRG) framework gives very accurate results compared to lattice data [27,28] and particle distributions [29,30] below the transition, by including all known hadronic states as free particles in the partition function, often including small interaction corrections. Within the HRG approach, hadron interactions are generically encoded in the resonant states. This framework works for most thermodynamic quantities, which are obtained, by construction, as monotonic functions of T, and generally increase with the mass of the states considered. For instance, the scalar susceptibility within that approach would increase with T, as it happens for other quantities such as the trace anomaly. Thus, the effect of a properly included broad σ T-dependent state arising from pion scattering in order to describe chiral restoring properties such as the susceptibility peak, is once more highlighted. In fact, the σ state is just not included in many HRG works [28] or, at most, considered as a BW state [29,30] with its $T = 0$ mass and width, which, as we have commented above, does not provide an entirely adequate description. Finally, let us comment that apart from higher mass states, inclusion of higher order interactions may also be important for certain hadronic observables. For instance, including $\rho\pi$ interactions in the vector channel are essential to describe properly the dilepton spectra [5].

V. CONCLUSIONS

Summarizing, we have analyzed the scalar-pseudoscalar $O(4)$-like current degeneration pattern at chiral symmetry restoration, from lattice simulations and effective theory analysis. The pseudoscalar susceptibility scales as the quark condensate, which we have explicitly shown in ChPT to NLO at low temperature, and becomes degenerate with its ''chiral partner'' scalar susceptibility close to the scalar transition peak. The lattice data and the unitarized ChPT analysis support this picture and are well accounted for by the dominant physical states: pions and the $f_0(500)$ scalar resonance generated in pion scattering at finite temperature. In turn, we have provided a natural explanation for the sudden growth of lattice masses observed in the pseudoscalar channel. Although we have restricted here, for simplicity, to the $N_f = 2$ case, the analysis can be extended to $N_f = 3$, where the role of other scalar states such as the $a_0(980)$ can also be studied [31].

ACKNOWLEDGMENTS

Useful comments from F. Karsch, S. Mukherjee, and D. Cabrera are acknowledged. This work is partially supported by the EU FP7 HadronPhysics3 project, the Spanish project FPA2011-27853-C02-02, and FPI Programme (BES-2009-013672, R. T. A), and by the German DFG (SFB/TR 16, J. R. E.).

[1] Y. Aoki, S. Borsányi, S. Dürr, Z. Fodor, S. D. Katz, S. Krieg, and K. Szabo, J. High Energy Phys. 06 (2009) 088.
[2] A. Bazavov *et al.*, Phys. Rev. D **85**, 054503 (2012).
[3] S. Ejiri, F. Karsch, E. Laermann, C. Miao, S. Mukherjee, P. Petreczky, C. Schmidt, W. Soeldner, and W. Unger, Phys. Rev. D **80**, 094505 (2009).
[4] T. Hatsuda and T. Kunihiro, Phys. Rev. Lett. **55**, 158 (1985).
[5] R. Rapp and J. Wambach, Adv. Nucl. Phys. **25**, 1 (2002).
[6] J. Beringer *et al.* (Particle Data Group Collaboration), Phys. Rev. D **86**, 010001 (2012), and references therein.
[7] E. V. Shuryak, Phys. Rep. **115**, 151 (1984); **264**, 357 (1996).
[8] D. J. Broadhurst, Nucl. Phys. **B85**, 189 (1975).
[9] M. Bochicchio, L. Maiani, G. Martinelli, G. Rossi, and M. Testa, Nucl. Phys. **B262**, 331 (1985).
[10] Ph. Boucaud, J.-P. Leroy, A. Le Yaouanc, J. Micheli, O. Pène, and J. Rodríguez-Quintero, Phys. Rev. D **81**, 094504 (2010).
[11] J. Gasser and H. Leutwyler, Ann. Phys. (N.Y.) **158**, 142 (1984).
[12] J. Gasser and H. Leutwyler, Phys. Lett. B **184**, 83 (1987).
[13] G. Chanfray and M. Ericson, Eur. Phys. J. A **16**, 291 (2003).
[14] A. Gomez Nicola and R. Torres Andres, Phys. Rev. D **83**, 076005 (2011).
[15] A. Gomez Nicola, J. R. Pelaez, and J. Ruiz de Elvira, Phys. Rev. D **87**, 016001 (2013).
[16] A. Gomez Nicola, J. R. Pelaez, and J. Ruiz de Elvira, Phys. Rev. D **82**, 074012 (2010).
[17] D. Toublan, Phys. Rev. D **56**, 5629 (1997).
[18] M. Cheng *et al.*, Eur. Phys. J. C **71**, 1 (2011).
[19] F. Karsch and E. Laermann, in *Quark Gluon Plasma*, edited by R. C. Hwa (World Scientific, Singapore, 2004), pp. 1–59.
[20] A. Bazavov *et al.*, Phys. Rev. D **80**, 014504 (2009).
[21] T. N. Truong, Phys. Rev. Lett. **61**, 2526 (1988); A. Dobado, M. J. Herrero, and T. N. Truong, Phys. Lett. B **235**, 134 (1990); A. Dobado and J. R. Pelaez, Phys. Rev. D **56**, 3057 (1997).
[22] A. Gomez Nicola, F. J. Llanes-Estrada, and J. R. Pelaez, Phys. Lett. B **550**, 55 (2002).
[23] A. Dobado, A. Gomez Nicola, F. J. Llanes-Estrada, and J. R. Pelaez, Phys. Rev. C **66**, 055201 (2002).
[24] D. Fernandez-Fraile, A. Gomez Nicola, and E. T. Herruzo, Phys. Rev. D **76**, 085020 (2007).
[25] A. Gomez Nicola, J. R. Pelaez, A. Dobado, and F. J. Llanes-Estrada, AIP Conf. Proc. **660**, 156 (2003).

[26] A. V. Smilga and J. J. M. Verbaarschot, Phys. Rev. D **54**, 1087 (1996).
[27] F. Karsch, K. Redlich, and A. Tawfik, Eur. Phys. J. C **29**, 549 (2003).
[28] P. Huovinen and P. Petreczky, Nucl. Phys. **A837**, 26 (2010).
[29] A. Andronic, P. Braun-Munzinger, and J. Stachel, Phys. Lett. B **673**, 142 (2009); **678**, 516(E) (2009).
[30] A. Andronic, P. Braun-Munzinger, J. Stachel, and M. Winn, Phys. Lett. B **718**, 80 (2012).
[31] A. Gomez Nicola, J. Ruiz de Elvira, and R. Torres Andres (unpublished).

3

Intercambio de fotones virtuales y resonancias en el cálculo de la diferencia de auto-energías de piones cargados y neutros

Este capítulo está formado por los resultados 3.1.1 y la publicación 3.1.2, enraizados en una sola sección que tiene como objeto el estudio de la auto-energía de un gas de piones en equilibrio térmico, de modo complementario al análisis de los condensados y las susceptibilidades quirales que se hizo en la sección previa.

Los resultados que conforman 3.1.1 llevan a cabo un estudio de los efectos electromagnéticos debidos a la inclusión de fotones virtuales sobre la parte real e imaginaria de la auto-energía dentro de la Teoría Quiral de Perturbaciones a temperatura finita. Asimismo, con el fin de comprobar la robustez de estas predicciones frente a la incorporación de partículas más pesadas y estudiar la restauración de la simetría quiral hemos calculado las correcciones debidas a la incorporación de resonancias ligeras mediante un modelo [110] que implemente su intercambio a través de la saturación de los canales axial y vectorial por la $a_1(1260)$ y la $\rho(770)$, respectivamente.

La publicación 3.1.2 se corresponde con un trabajo previo que revisa los resultados para la parte real de la auto-energía de un gas de piones a temperatura cero

y anticipa algunas de las conclusiones de temperatura finita que aparecen en los resultados correspondientes al epígrafe 3.1.1. Debido a esto, tanto la introducción como la motivación —así como las conclusiones fundamentales— expuestas en la sección 3.1 son compartidas por las publicaciones 3.1.1 y 3.1.2.

Análisis de la diferencia de auto-energías para piones cargados y neutros a un loop en *ChPT*.

Los piones son las partículas más abundantes después de una Colisión Relativista de Iones Pesados y sus propiedades, desde el proceso de hadronización al *freeze-out* térmico, pueden ser descritas a través de *ChPT* de modo razonable debido a que —como se indicó en el capítulo 1—las temperaturas involucradas en estos procesos no están demasiado lejos de las temperaturas para las que la expansión perturbativa de la Teoría Quiral tiene sentido. De esta manera, las predicciones *model-independent* de *ChPT* sobre el gas de mesones permiten reproducir las características principales en los momentos posteriores a la colisión —como por ejemplo el comportamiento tendente a la restauración de la simetría quiral basado en el condensado de quarks [70]—.

Las modificaciones de las propiedades espectrales de las partículas que constituyen el baño térmico durante las Colisiones Relativistas de Iones Pesados pueden dar lugar a importantes correcciones, por ejemplo en el caso de la $\rho(770)$ y su influencia en el espectro de dileptones [50,157–159]. Por contra, el papel de las correcciones térmicas a la masa de los piones y otros mesones ligeros no se incluye, habitualmente, en los análisis fenomenológicos [160] a pesar de que la relación de dispersión de los mismos contribuye de forma directa a la distribución del número de partículas. Además, su estudio es importante para el cálculo de la presión y la ecuación de estado del gas de hadrones en expansión, como ha sido discutido en [161].

En [162] se muestra que el efecto que sobre los parámetros de *freeze-out* tienen las correcciones térmicas a la masa del pión es muy pequeño, toda vez que estas modificaciones se tomen directamente de los trabajos en *ChPT* a un *loop*. En efecto, a bajas temperaturas, la masa $M_\pi(T)$ sufre pequeños cambios y, según la temperatura se va haciendo mayor y los efectos térmicos suponen modificaciones importantes respecto al valor a temperatura cero, los momentos de los piones están distribuidos en la zona $p \sim T$, lo que hace que los términos de masa sean despreciables.

En este contexto, nuestro interés a la hora de estudiar este tema se centra en las posibles correcciones que tienen lugar en la auto-energía a *leading order* en *ChPT* de un gas de piones (tanto en la parte real como en la parte imaginaria) al incluir la posibilidad de intercambiar fotones virtuales. Además, estos efectos electromagnéticos dan lugar a una parte imaginaria procedente de un corte de Landau —y, por consiguiente, de carácter puramente térmico— que podría dar lugar a diferentes anchuras térmicas para piones cargados y neutros. Estos efectos podrían ser detectados experimentalmente a través de la observación de diferencias en los tiempos de termalización y en los recorridos libres medios para las dos distribuciones de partículas [163, 164]; o mediante la medida de coeficientes de transporte [98] ya que si las diferencias en la anchura térmica de piones cargados y neutros fueran significativas, podría haber correcciones importantes a la conductividad eléctrica, relacionada con el espectro de fotones [99] o con las viscosidades de cizalla y de volumen (necesarias para explicar observables como la anomalía de traza o el flujo elíptico) [98, 100, 101].

El estudio de las correcciones a la relación de dispersión en un baño térmico dentro del contexto de *ChPT* sin fotones virtuales ha sido analizado a un *loop* en [165], resultando sólo en una ligera modificación de la masa del pión a través de un diagrama de tipo *tadpole*; y a dos *loops* en [166], donde aparecen contribuciones a la parte imaginaria de la auto-energía que permite definir un recorrido libre medio [167] y que se incluye de modo natural en el cálculo de los coeficientes de transporte [98].

Los resultados que presentamos incluyen —como ya se ha dicho— efectos de ruptura de isoespín debida a fotones virtuales a un *loop* así como las modificaciones térmicas a la auto-energía para una masa de pión distinta de cero, con lo que se complementan tanto los resultados de *ChPT* que se mencionaron anteriormente, como aquéllos en los que se calculan las correcciones en el límite quiral a la masa del pión [168, 169] o usando un enfoque basado en la relación de Cottingham en el contexto de un modelo de intercambio de resonancias [170].

La consideración de un escenario fuera del límite quiral introduce la dependencia de la auto-energía en el tri-momento del pión externo y hace que las reglas de suma basadas en técnicas de tipo *soft-pion* dejen de ser válidas formalmente. Además nuestro enfoque resulta más realista para su descripción en el régimen de temperaturas bajas e intermedias. Esto es debido a dos razones fundamentales: a que el rango de temperaturas para el que el límite quiral se presupone una buena aproximación ($T >> M_\pi$) no se alcanza *de facto* en el gas de mesones; y debido al carácter *model-independent* de la Teoría Quiral, que lo distingue de otros tratamientos basados en modelos. Debido a que el gas de piones formado tras la colisión está en equilibrio térmico, los momentos de las partículas del gas siguen una distribución de Bose-Einstein, por lo que la descripción de las propiedades de la parte real de la auto-energía a través de la masa promediada

en momentos resulta más acertada a la hora de intentar explicar lo que sucede en este escenario. Esta distribución de tri-momentos varía con la temperatura de modo que, al tomar ésta un cierto valor, sólo una parte de los piones del baño térmico permanecen termalmente activos. Para bajas temperaturas, $T << M_\pi$, los momentos se distribuyen en torno a los valores $p \sim \sqrt{M_\pi T}$, mientras que para altas temperaturas, $T >> M_\pi$, lo hacen alrededor del valor $p \sim T$.

Aparte de las implicaciones fenomenológicas que acabamos de comentar, existen otras de carácter más formal relacionadas con la restauración de la simetría quiral y la saturación por resonancias. A temperatura cero y en el llamado *soft-pion limit* —consistente en tomar piones externos con masa y tri-momento nulos— y a *leading order* en la carga electromagnética, es posible conectar [61] la diferencia de masas electromagnética de los piones con las diferencias de funciones espectrales vectorial y axial a través de la siguiente regla de suma

$$\lim_{p\to 0} \Delta M_\pi^2 = \lim_{p\to 0}(M_{\pi^\pm}^2 - M_{\pi^0}^2) = -\frac{3e^2}{16\pi^2 F_\pi^2}\int_0^\infty ds\, \log\Big(s\left[\rho_V(s) - \rho_A(s)\right]\Big). \qquad (3.1)$$

resultado que —una vez saturados los canales axial y vectorial por las resonancias más ligeras del espectro hadrónico, *i.e.* a través de la $a_1(1260)$ y la $\rho(770)$, respectivamente— muestra que la diferencia de masas electromagnética de los piones está dominada en este régimen por el intercambio de resonancias.

Debido a que los canales axial y vectorial se degeneran durante la transición quiral, la diferencia de masas del pión cargado respecto al neutro podría funcionar como un parámetro de orden de la restauración de la simetría quiral. Esta es la razón por la que es importante extender la regla de suma (3.1) fuera del límite quiral y teniendo en cuenta efectos electromagnéticos. Sin embargo, como fue mostrado por primera vez en [166], la masa del pión cargado recibe siempre una contribución de apantallamiento de la forma $\sim e^2T^2$ que provoca que la diferencia crezca en lugar de disminuir. Cuando a la regla de suma (3.1) se le añaden correcciones puramente térmicas es necesario modificar las funciones espectrales a través de factores multiplicativos proporcionales, a *leading order* y en el límite quiral, a T^2 [158]. Estos cambios dan lugar a un término que se opone al de apantallamiento y que provocan un decrecimiento neto muy suave con la temperatura para la diferencia de masas de piones cargados y neutros en el límite quiral, resultado en perfecta consonancia con [168].

Con todo, las principales conclusiones de los resultados 3.1.1 y publicación 3.1.2 son los siguientes:

Parte real de la auto-energía

- Hemos calculado las correcciones a la parte real de la auto-energía de un gas de piones fuera del límite quiral debidas a la ruptura de isoespín exclusivamente procedentes del intercambio de fotones virtuales en el baño térmico.

Los resultados son finitos e independientes de la escala quiral, lo que los convierte en verdaderos observables.

La pérdida de invariancia Lorentz debida a la existencia de un sistema de referencia preferente (el asociado al baño térmico) introduce una dependencia en el tri-momento del pión externo. Definiendo, como suele hacerse, la masa como el valor de la parte real de la auto-energía en el límite estático ($\vec{p}_{\text{ext}} = \vec{0}$) observamos[1] que la parte real de las masas corregidas de piones cargados y neutros no muestran grandes correcciones debidas a temperatura, así como tampoco la diferencia de masas entre ambos. Esta diferencia es creciente con la temperatura para piones masivos (incluso asumiendo $m_u = m_d = 0$ y considerando las correcciones de carga a *nivel árbol*), llegando a ser un 24 % mayor que el valor de temperatura cero a unos ~ 150 MeV.

Este crecimiento observado fuera del límite quiral —más realista habida cuenta de las temperaturas de *freeze-out* que se manejan en los momentos posteriores de colisiones *RHIC*— es cualitativamente opuesto al obtenido en el límite quiral [168] donde, de hecho, la diferencia decrece. Hay varias comprobaciones que nos sirven para verificar nuestros resultados: por un lado nuestro cálculo para las masas de los piones cargados y neutros coinciden con los calculados en [168] si nos vamos al régimen en el que el límite quiral se presupone una buena descripción, *i.e.* $M_\pi/T \to 0$. Este hecho nos lleva a la segunda verificación: incluso en el caso de piones masivos, al subir suficientemente la temperatura encontramos que la diferencia de masas comienza a decrecer y se acerca al comportamiento esperado en el límite quiral. Desde luego el valor de temperatura para el que este decrecimiento se produce está muy lejos de considerarse dentro de los límites predictivos de *ChPT*, pero es importante recuperar este comportamiento desde un punto de vista teórico.

Una de las conclusiones más importantes de este trabajo es que el término de apantallamiento de Debye procedente de los diagramas con fotones virtuales, junto con los que proceden de considerar piones masivos en el resto de diagramas, es capaz de oponerse a la tendencia hacia la restauración quiral que se esperaría si la regla de suma (3.1) fuera aplicable en este régimen.

❧ Los resultados para las masas promediadas en tri-momentos son los siguientes: a bajas temperaturas, los promedios para la masa del pión cargado y para la diferencia de masas electromagnética, $\langle M_{\pi^\pm} - M_{\pi^0} \rangle$, indistinguibles respecto a los valores calculados en el límite estático. Al llegar al rango de temperaturas moderadas-altas ($\sim (100-150)$ MeV) la diferencia experimenta un crecimiento mucho más lento que su equivalente estática, lo que se

[1] Para este cálculo hemos usado masas físicas de piones en lugar de las correspondientes a *nivel árbol* debido a que la diferencia es de orden superior. Asimismo, donde ha sido necesario, hemos utilizado los mismo valores numéricos que en la publicación 2.1.1.

explica debido a dos razones: por un lado el hecho de que la sustracción en este observable de las contribuciones de temperatura cero provoca que las diferencias respecto al límite estático sean más perceptibles; y, por otro, la observación —ya comentada— de que la distribución de momentos tienen un pico en torno a valores $p \sim T$ cuando aumenta la temperatura, por lo que es de esperar que los efectos sobre el promedio aumenten con la temperatura.

El comportamiento creciente con la temperatura que encontrábamos para la diferencia de masas electromagnética de piones masivos a este orden se suaviza y acerca más al comportamiento en el límite quiral si se calcula el promedio en momentos en lugar de los observables directamente en el límite estático.

Parte imaginaria de la auto-energía

❧ El efecto más importante de este cálculo es la aparición de una parte absortiva directamente relacionada con el diagrama de *photon-exchange* a temperatura finita, aun a pesar de que el *bremmstrahlung* en el vacío para un escalar radiando un fotón es un proceso prohibido. La auto-energía, como función de la variable $p_0 \in \mathbb{C}$, se vuelve no-analítica en el eje real y da lugar a un corte al atravesar esta línea. La parte imaginaria está asociada a un corte de Landau, por lo que su naturaleza es puramente térmica, siendo nula a temperatura cero.

Suponiendo la existencia de un régimen de oscilaciones pequeñas en el plasma térmico, es posible desacoplar la relación de dispersión del gas de piones y asociar la parte imaginaria con la anchura térmica perturbativa, $\gamma(\vec{p}, T)$ como función del tri-momento externo del pión y la temperatura.

Es importante notar la sutileza de este cálculo puesto que —aunque hemos demostrado que el resultado no depende del *gauge* siempre que se usen *gauges* covariantes— encontramos resultados que no están físicamente bien definidos. En efecto, calculándolo en el *gauge* de Feynman llegamos a la conclusión —utilizando la prescripción habitual de usar el propagador retardado, *i.e.* una vez prolongada analíticamente la auto-energía calculada en el formalismo de tiempo imaginario hacia valores retardados de la variable p_0, es decir, $p_0 \to p_0 + i\epsilon$— de que la parte imaginaria es positiva. Este resultado provocaría la aparición de una anchura térmica negativa, resultado físicamente inaceptable.

Este mismo problema ha sido ya encontrado en el cálculo de la parte imaginaria de la auto-energía asociada a campos *gauge* [171, 172] trabajando en *gauges* covariantes. El problema puede evitarse trabajando en el *gauge* de Coulomb, donde uno sí encuentra resultados físicos [173].

El problema tiene que ver con el hecho de que el cálculo de la parte imaginaria a temperatura finita implica la consideración de que los fotones virtuales se hallan en la capa de masas, por lo que la elección de *gauges* covariantes implica suponer que grados de libertad que no son físicos se encuentran en equilibrio térmico. Esta es la razón por la que estos trabajos apuestan por la elección del *gauge* de Coulomb estricto, que sólo propaga los modos físicos del fotón.

Procediendo de este modo, hemos calculado en *ChPT* la anchura térmica fuera del límite quiral a orden $\mathcal{O}(p^4)$ en el *gauge* de Coulomb, y la hemos comparado con los resultados promediados en tri-momentos para la anchura térmica de carácter electromagnético procedente de nuestro cálculo con la obtenida a *next-to-leading order* en *ChPT* [166].

Llegados a este punto es necesario hacer notar que la parte real de la auto-energía que hemos obtenido, calculada originalmente en el *gauge* de Feynman, no se ve afectada por el uso de uno u otro *gauge* y da lugar al mismo resultado que ya se expuso.

Nuestro cálculo arroja un resultado finito, *model-independent* e independiente, también, de la escala quiral. La anchura térmica es lineal en la temperatura, anulándose para $|\vec{p}| := p \to 0$ y que tiende a $\gamma(T, p \to \infty) = {}^{e^2T}/_{4\pi}$. Esta dependencia en el tri-momento es similar a la que se muestra en [174] al calcular la parte transversal de la anchura térmica de un escalar en *QED* a temperatura finita[2].

La comparación de los valores promediados en tri-momentos con el valor promediado para la anchura de dispersión *next-to-leading order* [166, 167] indica que la contribución dominante hasta una temperatura de aproximadamente 50 MeV procede de la parte electromagnética $\mathcal{O}(p^4)$, pero a partir ese valor la contribución $\mathcal{O}(p^6)$ procedente de la dispersión de piones es claramente dominante (es aproximadamente ocho veces mayor que la electromagnética a una temperatura de 80 MeV).

Con objeto de estimar de manera fenomenológica esta contribución a la anchura —y a modo de aproximación— hemos usado el promedio en momentos para la anchura térmica para medir las correcciones sobre el cálculo de la conductividad eléctrica y las viscosidades de cizalla y volumen, estimadas en aproximadamente un 10 % para una temperatura de entre 80 y 100 MeV, rango de temperaturas para el que la expansión en el plasma relativista resultante de la Colisión de Iones Pesados cesa (*freeze-out* térmico). En un intento de mejorar numéricamente los resultados numéricos, hemos utilizado el valor unitarizado de [166] para la anchura térmica no electromagnética.

[2] Nótese que allí, debido a la presencia de divergencias infrarrojas asociadas al revestimiento del fotón, el resultado depende también del *cut-off* infrarrojo. En el esquema de cálculo que hemos usado, a este orden, no existen divergencias infrarrojas.

Asimismo, debido a que la interacción electromagnética sólo se acopla a corrientes cargadas, los recorridos libres medios para piones cargados y neutros calculados según este enfoque son distintos. Esto da lugar a diferentes temperaturas de *freeze-out* térmico para piones cargados y neutros, aunque los efectos son más pequeños que en el caso de los coeficientes de transporte: la diferencia entre las temperaturas de *freeze-out* térmico asociadas a las dos especies es de aproximadamente 2 MeV.

Resonancias, regla de suma y restauración de simetría quiral

El trabajo en este sentido sigue dos direcciones: por un lado se estudian las modificaciones a la regla de suma que relaciona las funciones espectrales asociadas a los canales vectorial y axial con la diferencia de masas electromagnética de los piones cuando se consideran piones fuera del límite quiral a temperatura finita. Por otro se analiza la robustez de las predicciones *model-independent* de *ChPT* para la parte real de la diferencia de auto-energía para el pión cargado y el neutro cuando se incluyen las partículas $a_1(1260)$ y $\rho(770)$ a través de un modelo con los canales vectorial y axial saturados por estas primeras resonancias ligeras.

Debido a la ausencia de un contaje formal en este modelo los resultados serán obtenidos sólo a *leading order*, es decir, considerando sólo correcciones a un *loop* para la diferencia de auto-energías de piones cargados y neutros.

Con todo:

- Encontramos que la regla de suma original no es aplicable en este régimen debido a que fue originalmente concebida en el llamado *soft pion limit*, que considera piones sin masa. Es posible, no obstante, añadir los términos necesarios para completarla a partir de la comparación con los resultados *model-independent* proporcionados por *ChPT*. Estos cambios se traducen en la incorporación de los resultados del diagrama de *photon exchange* con un pión masivo así como de las correcciones multiplicativas de las contribuciones $V-A$. Los resultados se han efectuado a *leading* y *next-to-leading order* en el parámetro $x \sim T^2/M_R^2 \sim M_\pi^2/M_R^2$, siendo M_R la masa genérica de las resonancias en cuestión ($\sim 1\,\mathrm{GeV}$).

- El efecto de la consideración de piones masivos contribuye a amplificar la diferencia electromagnética de las masas de los piones, es decir, a emborronar el comportamiento tendente a la restauración quiral que parecía predecir la estructura de la regla de suma $V-A$. No es posible, por tanto, reconocer un efecto de restauración quiral asociada a la diferencia de masas de los piones cargados y neutros fuera del límite quiral.

- Mediante el estudio de un modelo de intercambio de resonancias en el límite de saturación de las mismas, encontramos que las correcciones a la masa (definida como la parte real de la auto-energía en el límite estático) debidas a las resonancias son numéricamente pequeñas, siendo la contribución de la $\rho(770)$ mayor que la de la $a_1(1260)$ en el rango térmico considerado. Este resultado no debiera sorprender puesto que la masa de la a_1 hace que los efectos asociados a ella hagan su aparición a temperaturas considerablemente mayores que para la ρ.

- En general los efectos resonantes se activan a una temperatura de entre 170 y 200 MeV, por lo que las predicciones de *ChPT* pueden considerarse fiables para un rango térmico considerable, siempre por debajo de la transición quiral.

- Hemos comprobado que las partes imaginarias asociadas con algunos de los diagramas con resonancias que contribuyen a *leading order* a la diferencia de auto-energía están exponencialmente suprimidas a través de funciones de Boltzmann y, por tanto, son subdominantes en comparación con la anchura térmica electromagnética calculada con anterioridad.

- El término $-4Ze^2 g_1(T, M_\pi)$ y el correspondiente a la diferencia $g_1(T, M_\pi^\pm) - g_1(T, M_\pi^0)$ que se obtienen en *ChPT* a partir de diagramas de tipo *tadpole* de piones y que está directamente relacionado con la estructura $V - A$ de la regla de suma (y por tanto con la restauración de la simetría quiral) no puede reproducirse a partir de un análisis en el contexto del modelo de resonancias a *leading order*. Esto pone de manifiesto la inequivalencia entre los contajes en la Teoría Quiral y en el modelo de resonancias. De hecho este modelo carece de una expansión perturbativa controlable en los acoplos de piones con resonancias y sólo un esquema basado en gran N_C nos ha permitido clasificar los diagramas *leading order* de un modo fiable.

3.1.1 *Preprint:*
A. Gómez Nicola, R. Torres Andrés,
Electromagnetic effects in the pion dispersion relation at finite temperature,
arXiv:1404.2746

Electromagnetic effects in the pion dispersion relation at finite temperature

A. Gómez Nicola* and R. Torres Andrés†
Departamento de Física Teórica II. Univ. Complutense. 28040 Madrid. Spain.

We investigate the charged-neutral difference in the pion self-energy at finite temperature T. Within Chiral Perturbation Theory (ChPT) we extend a previous analysis performed in the chiral and soft pion limits. Our analysis with physical pion masses leads to additional non-negligible contributions for temperatures typical of a meson gas, including a momentum-dependent function for the self energy. In addition, a nonzero imaginary part arises to leading order, which we define consistently in the Coulomb gauge and comes from an infrared enhanced contribution due to thermal bath photons. For distributions typical of a heavy-ion meson gas, the charged and neutral pion masses and their difference depend on temperature through slowly increasing functions. Chiral symmetry restoration turns out to be ultimately responsible for keeping the charged-neutral mass difference smooth and compatible with the observed charged and neutral pion spectra. We study also phenomenological effects related to the thermal electromagnetic damping, which gives rise to corrections for transport coefficients and distinguishes between neutral and charged mean free times. An important part of the analysis is the connection with chiral symmetry restoration through the relation of the pion mass difference with the vector-axial spectral function difference, which holds at $T = 0$ due to a sum rule in the chiral and soft pion limits. We analyze the modifications of that sum rule including nonzero pion masses and temperature, up to $\mathcal{O}(T^2) \sim \mathcal{O}(M_\pi^2)$. Both effects produce terms making the pion mass difference grow against chiral-restoring decreasing contributions. Finally, we analyze the corrections to the previous ChPT and sum rule results within the resonance saturation framework at finite temperature, including explicitly ρ and a_1 exchanges. Our results show that the ChPT result is robust at low and intermediate temperatures, the leading resonance corrections within this framework being $\mathcal{O}(T^2 M_\pi^2/M_R^2)$ with M_R the involved resonance masses.

PACS numbers: 11.10.Wx, 12.39.Fe, 13.40.Dk, 11.30.Rd

* gomez@fis.ucm.es
† rtandres@fis.ucm.es

I. INTRODUCTION AND MOTIVATION

The study of hadronic properties at finite temperature T is one of the theoretical ingredients needed to understand the behaviour of matter created in Relativistic Heavy Ion Collision experiments, such as those in RHIC and LHC (ALICE), as it expands from the onset of local equilibrium to the final freeze-out regime [1, 2]. This is especially relevant for chiral symmetry restoration and deconfinement, for which the lattice groups have explored exhaustively the phase diagram and other thermodynamical properties [3–7]. For the case of vanishing baryon chemical potential, the QCD transition becomes a crossover for the physical case of 2+1 flavours, which makes it especially important to define observables which would behave as order parameters, since different quantities would point to different critical temperatures. Thus, the critical range from the latest lattice simulations lies within $T_c \sim$ 150-170 MeV.

Several hadron gas features have been studied in different approximations. The Hadron Resonance Gas (HRG) describes the system through the statistical ensemble of all free states thermally available and provides a good description both of lattice thermodynamical data and of experimental hadron yields, when some corrections due to interactions and lattice masses are accounted for [8, 9]. On the other hand, effective chiral models including explicitly vector and axial-vector resonances have been successfully used to describe several hadron thermal properties relevant for observables such as the dilepton and photon spectra and $\rho - a_1$ mixing/degeneration at the chiral transition [10–13].

A systematic and model-independent framework to take into account the relevant light meson degrees of freedom and their interactions is Chiral perturbation Theory (ChPT) [14, 15]. The effective ChPT lagrangian is constructed as an expansion of the form $\mathcal{L} = \mathcal{L}_{p^2} + \mathcal{L}_{p^4} + \ldots$ where p denotes a meson energy scale compared to the chiral scale $\Lambda_\chi \sim$ 1 GeV. Pions are actually the more copiously produced particles after a Heavy Ion Collision and their properties from hadronization to thermal freeze-out can be reasonably described within ChPT. The temperatures involved in that regime are not far from the ChPT applicability range and ChPT has the added value of providing model-independent results. Thus, the meson gas description based on ChPT reproduces fairly well the main qualitative features of the system, such as the chiral restoring behaviour given by the quark condensate [16]. The introduction of realistic (unitarized) pion interactions improves ChPT, providing a more accurate description of several effects of interest in a Heavy-Ion environment, such as thermal resonances and transport coefficients [17–21]. This approach has also given rise to a deeper understanding of the scalar-pseudoscalar degeneration pattern taking place at chiral restoration, in agreement with lattice data for meson masses and susceptibilities [22]. In addition, the virial expansion approach within ChPT, including unitarized corrections, allows to parametrize consistently the deviations from the HRG-like free gas contributions [23–25].

The modification of the pion dispersion relation in the thermal bath has been also analyzed within ChPT. Perturbatively, to one loop the only modification is a shift in the pion mass coming from a tadpole diagram, softly increasing with T [26]. At two loops, pions develop a more complicated dispersion relation [27] including an absorptive imaginary part, which defines a mean collision rate [28] responsible for the thermalization mean time and the mean free path of pions in the thermal bath. This rate is also essential to describe correctly the transport coefficients of the pion gas [19]. Corrections to the dispersion relation due to nonzero pion chemical potential during the chemical nonequilibrium phase have also been studied [29].

In this work we will continue with this program by studying the modifications of the pion dispersion relation due to electromagnetic (EM) isospin-breaking corrections, including virtual photon exchange, during the hadronic phase at finite temperature. We will work within ChPT but corrections due to resonance exchange will also be considered, within the framework of a sum rule connecting the self-energy difference with vector and axial spectral functions to evaluate the possible impact on chiral symmetry restoration, and explicitly in a resonance saturation model to estimate the range of validity of the ChPT analysis. Electromagnetic corrections are the main source of the charged-neutral mass (or more general, the self-energy) difference and can be consistently studied within ChPT by introducing the relevant lagrangian terms of orders $\mathcal{L}_{e^2}$, $\mathcal{L}_{e^2p^2}$ and so on, with e the electric charge considered formally in the chiral expansion as $e^2 = \mathcal{O}(p^2/F^2)$, with F the pion decay constant in the chiral limit.

Our analysis extends, on the one hand, the previously mentioned ChPT studies on the thermal pion dispersion relation and, on the other hand, previous partial analysis of the isospin breaking of such relation, namely, in the chiral and soft pion limit [30, 31] and using a Cottingham-like approach within resonance exchange in [32]. We will consider physical pion masses, which will give rise to new effects such as the momentum dependence of the self-energy (a pure thermal effect) and a nonzero imaginary part. In addition, the departure from soft-pion sum rules will complicate the connection with spectral functions. Our analysis provides more realistic results regarding heavy-ion and lattice phenomenology, since the chiral limit is intended to be valid only for temperatures $T \gg M_\pi$, which are not reached in the hadron gas. In addition, our ChPT analysis will ensure the model independency of the results at low and moderate temperatures taking into account all relevant thermal contributions, which is a benchmark when comparing to resonance exchange models. Besides, as we will explain here, the ChPT leading correction includes certain tadpole-like terms which are not present in the leading resonance saturation diagrams and play an important role at the

temperatures considered. We will concentrate first on the corrections to the real part of the self-energy, including its momentum dependence, but we will see that the nonzero pion mass also induces imaginary parts coming from Landau pure thermal cuts of diagrams both with photon and resonance exchange, the latter remaining as a subleading contribution. Our present work complements and extends also our previous studies of isospin-breaking corrections in the meson gas [33, 34].

Let us discuss some additional motivations to perform this analysis.

The spectral properties of the particles which constitute the thermal bath are in principle subject to modifications with respect to the vacuum, due to their mutual interactions. These modifications might lead to important observable effects, as it is indeed the case with the $\rho(770)$ meson and its influence in the dilepton spectrum[10–12, 17]. However, the temperature dependence of the masses of pions and other light mesons is usually not included in phenomenological analysis of hadron yields [8] despite the fact that the dispersion relation enters directly in the particle number distribution. In addition, the very same expansion dynamics is also in principle influenced by the thermal change in the pion dispersion relation.

The importance of the pion dispersion relation in the pressure and equation of state and thus in the hadron gas expansion has been discussed in [35]. On the other hand, a detailed analysis of the impact of the thermal pion mass shift in freeze-out parameters [36] shows a tiny effect from $M_\pi(T)$, taken as that predicted by one-loop ChPT and hence very soft and increasing. The reason is that at low temperatures the shift is negligible while at higher temperatures, when it becomes sizable, pion momenta are distributed near $p \sim T$ so that the mass terms become small in the dispersion relation. In [36] it is also pointed out that an increasing temperature-dependent pion mass is consistent with the existence of hadron-like states prior to hadronization, with a mass larger than their vacuum value, which could explain the experimentally observed quark number scaling in elliptic flow.

What we intend to address here in this phenomenological context is, first, how EM corrections modify the prediction of a slowly increasing pion mass, at leading order in ChPT. In addition, we want to examine possible sizable differences between neutral and charged self-energies with temperature and momentum, which could be of phenomenological interest when comparing charged and neutral pion distributions.

Neutral pion distributions have been measured experimentally in recent Heavy Ion Collisions experiments at RHIC in PHENIX [37, 38] and STAR [39] as well as in more recent ALICE (LHC) measurements [40, 41]. The comparison between neutral and charged pion spectra for STAR data [39] shows that, although they are compatible within errors, the central values for the π^0 lie systematically below the $\pi^\pm$ for low p_T in the central region. The difference is much larger when nuclear modification factors of neutral pions and total charged hadrons are compared in central events, which comes basically from the baryon excess of p/π in the intermediate momentum region 2 GeV $< p_T <$ 4 GeV, where different hadron production mechanisms such as recombination come into play [42, 43]. At high enough p_T, say above 4-5 GeV, hadron production comes mainly from fragmentation mechanisms and the neutral- charged hadron yields tend to be similar. The experimental difficulties of accessing the low momentum region are evident and hence, the lowest point to which the yields are compared is $p_T = 0.5$ GeV in the ALICE analysis [40]. At those lower momenta, the neutral-charged yields are compatible within errors, although the central π^0 value at $p_T = 0.5$ GeV is slightly above the charged one. Overall, the above phenomenological data indicate compatibility with isospin symmetry within errors for the observed pion spectrum.

In this experimental context, it makes sense to explore possible differences in the charged-neutral pion masses, or more generally in their dispersion relation, which can include momentum dependent corrections coming from thermal effects, as we will see. At the very least, this analysis should serve to confirm the very small charged-neutral deviations observed in particle distributions and would certainly be more useful to explore the low momentum region, where soft thermal pions are dominant, so that more precise experimental points at low p_T, as expected from ALICE data, would be welcome.

Moreover, the possible modifications in the imaginary part would give rise to differences in the thermal width between charged and neutral pions. These differences could in principle be observable at least in two phenomenological contexts. One could be differences in thermalization times and mean free path and hence in kinetic freeze-out temperatures for the charged and neutral pion components, estimating kinetic freeze-out as the temperature for which the mean free path becomes of the order of the system size, or equivalently for the mean collision time [29, 44]. The other one is in transport coefficients, for which the inverse thermal width of the internal lines enters in the integrals of the relevant loop diagrams [19]. If there are significative differences between charged and neutral thermal widths, there could be sizable corrections e.g. to the electrical conductivity, related to the photon spectrum [18] or to the shear and bulk viscosities needed to explain correctly observables such as the elliptic flow or the trace anomaly [19–21].

Besides the possible phenomenological implications, there are other, more theoretical, aspects of our analysis, mostly in connection with chiral symmetry restoration and resonance saturation. At $T = 0$, in the soft pion limit, i.e. vanishing external pion four-momentum p_π (consistent only in the chiral limit of vanishing pion masses), and to leading order in e^2, the following sum rule connects the EM pion mass difference with the vector-axial spectral

function difference [45]:

$$\lim_{p_\pi\to 0}\Delta M_\pi^2=\lim_{p_\pi\to 0}\left(M_{\pi^\pm}^2-M_{\pi^0}^2\right)=-\frac{e^2}{16\pi^2}\frac{3}{F_\pi^2}\int_0^\infty ds\ln s\left[\rho_V(s)-\rho_A(s)\right] \tag{1}$$

A natural question in this context is therefore the possible connection to chiral symmetry restoration at finite temperature. Since vector and axial channels (saturated by the ρ and a_1 resonances respectively) are meant to degenerate at the transition, the pion mass difference could then behave as an order parameter. However, as pointed out first in [31], at finite temperature, the charged pion mass always receives a contribution $\Delta M^2(T)\sim e^2T^2/4$, similarly to Debye screening for the longitudinal photon field, which actually would make the pion mass difference grow instead. That contribution alone would be comparable to the $T=0$ value near T_c. However, when the sum rule (1) is corrected at $T\neq 0$ one has to take into account also the modifications of the spectral functions $\rho_{V,A}\to\rho_{V,A}(T)$, which in the chiral limit and to leading T^2 order are given simply by a multiplicative T-dependent renormalization that mixes the vector and axial spectral functions, predicting that they become degenerate at $T\simeq\sqrt{3}F_\pi$ [46]. That term gives rise to a decreasing correction to $\Delta M^2(T)$ which added to the Debye-like one gives a net very soft decreasing behaviour for the pion mass difference, in agreement with the ChPT calculation in the chiral limit [30].

All these aspects already studied in the chiral limit are meant to change considerably when nonzero physical pion masses are considered. First of all, the soft pion limit will not be applicable because it only makes sense in the chiral limit. Second, for the relevant temperatures involved near chiral restoration and in heavy-ion collisions, T and M_π effects are comparable, so that new mass-dependent and momentum-dependent terms are expected, which could change the previous chiral restoring and not-restoring balance. One of our purposes in this work will be precisely to analyze those aspects related to the connection of the self-energy electromagnetic difference with the vector and axial spectral functions when the pion mass is taken at its physical value.

Moreover, since the previous sum rule arguments and their finite-T extensions are not directly applicable out of the chiral limit, we will find useful also to appeal to models based on resonance exchange, for which the pion mass difference has been calculated at $T=0$ [47], in order to identify the leading and subleading contributions for physical masses in the resonance saturation limit. Also within this framework we will establish the validity limit of our pure-ChPT calculation.

Taking all these considerations into account, the structure of this work is the following: In section II we will carry out the ChPT analysis of the self-energy, the real part contribution being discussed in section II A and the imaginary one in section II B. In both cases we will discuss several aspects such as the differences with the chiral limit, gauge invariance, the momentum dependence and possible phenomenological consequences. Section III will be devoted to the discussion of the extension of the sum rule connecting the pion electromagnetic self-energy difference with the vector-axial vector spectral function difference. We will review the main aspects of previous derivations, both at $T=0$ and $T\neq 0$ in the chiral limit and analyze the main differences arising for physical pion masses and the formal implications regarding chiral symmetry restoring and not-restoring terms. In section IV we will consider the pion self-energy calculation in a resonance saturation framework including the ρ and a_1 resonances explicitly and will examine the size of the different corrections within the context of the present work. In Appendices A and B we will clarify several properties, definitions and conventions used throughout this work regarding spectral functions and loop integrals.

II. CHPT ANALYSIS FOR PHYSICAL PION MASSES

The effective chiral lagrangian up to fourth order in p (a meson mass, momentum, temperature or derivative) including EM interactions proportional to e^2 is given schematically by $\mathcal{L}_{eff}=\mathcal{L}_{p^2+e^2}+\mathcal{L}_{p^4+e^2p^2+e^4}$. The second order lagrangian corresponds to the familiar non-linear sigma model plus the addition of the gauge coupling of mesons to the photon field via the covariant derivative, and an additional term proportional to a low-energy constant C compatible with the $e\neq 0$ symmetries of the QCD lagrangian [48–51].

$$\mathcal{L}_{p^2+e^2}=\frac{F^2}{4}\mathrm{tr}\left[D_\mu U^\dagger D^\mu U+2B_0\mathcal{M}\left(U+U^\dagger\right)\right]+C\mathrm{tr}\left[QUQU^\dagger\right]. \tag{2}$$

Since we are dealing only with pions, the Goldstone Boson field matrix takes the form $U(x)=\exp[i\Phi/F]\in SU(2)$, being

$$\Phi=\begin{pmatrix}\pi^0 & \sqrt{2}\pi^+\\ \sqrt{2}\pi^- & -\pi^0\end{pmatrix} \tag{3}$$

the pion field matrix.

The covariant derivative is $D_\mu = \partial_\mu + iA_\mu[Q,\cdot]$ with A_μ the EM field and $Q = (e/3)\mathrm{diag}(2,-1)$ and $\mathcal{M} = \hat{m}\mathbb{1}_2$ are respectively the quark charge and mass matrices, where we will take the QCD isospin limit $m_u = m_d = \hat{m}$, since as explained in the introduction, we are interested in the dominant EM isospin breaking effect in the pion masses. Thus, from the lagrangian (2) we read off the tree level neutral and charged pion masses, which we denote by a hat:

$$\begin{aligned} \hat{M}^2_{\pi^\pm} &= 2\hat{m}B_0 + 2C\frac{e^2}{F^2}, \\ \hat{M}^2_{\pi^0} &= 2\hat{m}B_0. \end{aligned} \tag{4}$$

The above squared tree level pion masses are then, consistently, $\mathcal{O}(p^2)$ quantities independent of temperature, which are related to the physical pion masses formally as $M^2_\pi = \hat{M}^2_\pi + \mathcal{O}(p^4)$. We will be interested here in the calculation of those p^4 corrections, since they include the leading temperature dependence coming from pion loops. Similarly, the pion decay constant $F^2_\pi = F^2 + \mathcal{O}(p^4)$ and the quark condensate $\langle\bar{q}q\rangle = 2B_0F^2[1+\mathcal{O}(p^2)]$.

Physical predictions are rendered UV finite by renormalization of the low-energy constants (LEC) multiplying the different terms of the lagrangian. Thus, the fourth order lagrangian consists of all possible terms compatible with the QCD symmetries to that order, including the EM ones, and can be found for SU(2)-ChPT, for instance, in [51]. It introduces a set of EM and non-EM LEC which appear in the calculation of the masses by instance of $\mathcal{L}_{p^4+e^2p^2+e^4}$, when renormalizing the $T=0$ divergences coming from the loops.

At finite temperature $T \neq 0$, we will work in the Imaginary Time (IT) formalism [1, 52] in which the correlators corresponding to propagators are obtained by replacing in the action $t \to -i\tau$, $i\int d^4x \to \int_T d^4x \equiv \int_0^\beta d\tau \int d^3\vec{x}$. The vertices remain the same as at $T=0$ and the Feynman rules are modified according to the replacements indicated in (B1). Once the internal loop sums over Matsubara frequencies ω_n are performed, the result for a given correlator can be analytically continued to external frequencies $\omega + i\epsilon$ to obtain the retarded propagator, which contains the information about the dispersion relation. The details and definitions of the various propagators and spectral functions are given in Appendix A while in Appendix B we collect the results for the typical thermal loop integrals that we will need throughout this work.

The dispersion relation is set up by the poles of the retarded propagator at $\omega = \pm\omega_p - i\gamma_p$ with γ_p the damping rate in the thermal bath. It is obtained from the self-energy Σ, which in imaginary time is defined in (A1). As we will work perturbatively within ChPT, $\Sigma = \mathcal{O}(p^4)$ so that the dispersion relation is perturbed around the vacuum value, i.e, $\omega_p^2 = E_p^2 + \mathrm{Re}\,\Sigma(E_p;|\vec{p}|;T)$ and $\gamma_p = -\mathrm{Im}\,\Sigma(E_p+i\epsilon;|\vec{p}|;T)/(2E_p)$ where $E_p^2 = |\vec{p}|^2 + \hat{M}^2$, $\hat{M}$ is the tree level mass and the T-dependent and $\vec{p}$ dependent self-energy has been analytically continued from the IT one as $i\omega_n \to \omega + i\epsilon$ to obtain the retarded propagator $G_R(\omega,|\vec{p}|)$ (see Appendix A for more details). Recall that at $T \neq 0$, $\Sigma(\omega,|\vec{p}|)$ depends separately on ω and $|\vec{p}|$ as a result of the Lorentz Symmetry breaking due to the choice of the reference system associated with the thermal bath.

If EM isospin breaking is considered, the dispersion relation is different for charged and neutral pions already at tree level, as indicated in (4). To one loop, the diagrams contributing to the charged pion self-energy in ChPT are showed in Fig.1. To the neutral pion self-energy, only diagrams of type (a) and (b) contribute. The numbers between brackets in those diagrams denote the momentum order of the lagrangian that gives the corresponding vertex. Diagrams (c) and (d) involve virtual photons. It is important to note that apart from the charged-neutral differences in the self-energy coming from diagrams (c) and (d), there are others contributing at the same chiral order from diagrams of tadpole type (a). Thus, on the one hand, a four-pion vertex coming from the F^2 term in (2) gives rise to a contribution of the type $G(\hat{M}_{\pi^\pm}) - G(\hat{M}_{\pi^0})$ to the self-energy charged-neutral difference, with G the tadpole function defined in (B2). On the other hand, a four-pion vertex coming from the C term in (2) only contributes to the charged pion self-energy proportionally to $CG(\hat{M}_{\pi^\pm})$.

We will discuss separately the real and imaginary contributions to the pion self-energy within our ChPT approach. We will refer to the Appendices for details of the calculation. All the $T=0$ contributions will be regularized in the dimensional regularization (DR) scheme throughout this work.

A. Real part of the dispersion relation. Pion mass difference and momentum dependence

As discussed above, the real part of the self-energy shifts the real part of the pion pole, introducing T and momentum dependence, perturbatively within ChPT through $\mathrm{Re}\,\Sigma(E_p,|\vec{p}|;T)$ with $E_p^2 = |\vec{p}|^2 + \hat{M}^2$ with $\hat{M}^2$ the corresponding tree level pion mass. As customary, we will define the pion masses in the static limit $\vec{p}=\vec{0}$.

The photon-tadpole diagram in Fig.1(c) defines the thermal Debye screening mass for longitudinal modes [1] and vanishes at $T=0$. It is UV finite as it should for a pure thermal contribution. The UV divergences coming from the

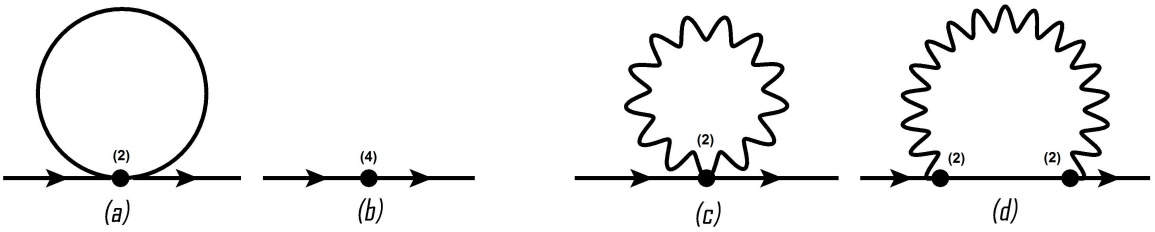

Figure 1. 1-PI diagrams contributing to the self-energy of a charged pion in SU(2)-ChPT to leading order. Diagrams for neutral pions are the same removing those in which photons are present.

tadpole diagrams (a) and the photon-exchange diagram (d) are the same as at $T = 0$ and are absorbed by the tree level diagrams (b), which include a particular combination of the fourth order LEC. The $T = 0$ result for the neutral and charged pion masses taking into account all these diagrams is given in [51].

For the neutral pion mass, the above mentioned tadpole diagrams give to this order:

$$M^2_{\pi^0}(T) = \hat{M}^2_{\pi^0}(T=0)\left[1 + \frac{1}{F^2}\left(g_1(\hat{M}_{\pi^\pm}, T) - \frac{1}{2}g_1(\hat{M}_{\pi^0}, T)\right)\right], \tag{5}$$

with the thermal g_1 function defined in (B3). The above thermal neutral pion mass is still increasing with temperature, as showed in Fig.2.

As for the charged pion self-energy, for the photon-tadpole contribution in Fig.1(c) and the photon-exchange diagram (d) we will work in the Feynman gauge $\alpha = 1$ (see our notation for thermal propagators in Appendix A) as in the $T = 0$ analysis [47, 51] and previous $T \neq 0$ ones [30–32]. In that gauge we have for diagram (c):

$$\Sigma_{\gamma T ad}(T) = 4e^2 T \sum_n \int \frac{d^3\,q}{(2\pi)^3}\frac{1}{\omega_n^2 + |\vec{q}|^2} = 4e^2 g_1(0;T) = \frac{e^2T^2}{3} \tag{6}$$

where $\omega_n = 2\pi n T$ is the internal Matsubara frequency and we have used (B3) and (B7). As commented above, this is the typical e^2T^2 screening or Debye mass behaviour appearing for longitudinal photon fields in the thermal bath [1, 53] which holds also for gluons with prefactor corrections. Note also that this is a growing term with T, behaving then against the naive arguments of chiral restoration mentioned in section I.

The photon exchange term corresponding to diagram (d) in Fig.1 is given in the Feynman gauge as:

$$\Sigma_{\gamma Ex}(i\omega_m, |\vec{p}|; T) = e^2 T \sum_n \int \frac{d^3\,q}{(2\pi)^3}\frac{(2p-q)^2}{q^2\left[(p-q)^2 - \hat{M}^2_{\pi^\pm}\right]} \tag{7}$$

where $p \equiv (i\omega_m, |\vec{p}|)$ and $q \equiv (i\omega_n, \vec{q})$ are the external and loop IT momenta respectively, with $\omega_k = 2\pi k T$.

Writing in (7), $2p\cdot q = -(p-q)^2 + q^2 + p^2$, we have in IT:

$$\Sigma_{\gamma Ex}(i\omega_m, |\vec{p}|; T) = e^2\left\{G(\hat{M}_{\pi^\pm}; T) - 2G(0;T) + 2\left[\hat{M}^2_{\pi^\pm} - \omega_m^2 - |\vec{p}|^2\right]J_T(0, \hat{M}_{\pi^\pm}; i\omega_m, |\vec{p}|)\right\} \tag{8}$$

where the G and J_T functions are defined in (B2) and (B9) respectively. Therefore, performing the analytical continuation $i\omega_m \to p_0 + i\epsilon$ and for on-shell pions $p^2 = \hat{M}^2_{\pi^\pm}$ (perturbative self-energy), this contribution can be cast as:

$$\Sigma_{\gamma Ex}(\omega + i\epsilon, \omega^2 = E_p^2; T) = e^2\left[G(\hat{M}_{\pi^\pm}; T) - 2G(0;T) + 4\hat{M}^2_{\pi^\pm}J_T(0, \hat{M}_{\pi^\pm}; \omega + i\epsilon, \omega^2 = E_p^2)\right] \tag{9}$$

Note that in the chiral limit ($\hat{m} = 0$) and neglecting $\mathcal{O}(e^4)$ we get $\Sigma_{\gamma T ad} + \Sigma_{\gamma Ex} = \frac{e^2T^2}{4}$ which is nothing but the scalar thermal mass squared obtained to one loop in Scalar QED (SQED) [53]. Note also that, according to our analysis in Appendix B, the above J_T function develops an imaginary part, which we will analyze in section II B.

At this point, let us discuss the gauge invariance of the previous result in a covariant gauge. The gauge parameter dependence is in the photon propagator and then it only affects diagrams (c) and (d) in Fig.1. If we add the contribution proportional to $(\alpha-1)$ of the gauge boson propagator (A9), we obtain the following additional contributions to those diagrams

$$\begin{aligned}\delta\Sigma_{\gamma Tad}(T) &= -e^2(\alpha-1)\frac{T^2}{12}\\ \delta\Sigma_{\gamma Ex}(i\omega_m,|\vec{p}|;T) &= e^2(\alpha-1)T\sum_n\int\frac{d^3\,q}{(2\pi)^3}\frac{\left[(2p-q)\cdot q\right]^2}{(q^2)^2\left[(p-q)^2-\hat{M}^2_{\pi^\pm}\right]}\end{aligned} \tag{10}$$

Now, let us concentrate on the on-shell point $p^2=M^2_{\pi^\pm}$ (which will hold after analytical continuation) so that with similar manipulations as before, we can write the numerator of $\delta\Sigma_{\gamma Ex}$ as $(2p\cdot q)\left[-(p-q)^2+M^2_{\pi^\pm}-q^2\right]+(q^2)^2=\left[-(p-q)^2+M^2_{\pi^\pm}\right]\left[2p\cdot q-q^2\right]$ so that we get $\delta\Sigma_{\gamma Ex}(\omega^2=E_p^2)=e^2(\alpha-1)\frac{T^2}{12}=-\delta\Sigma_{\gamma Tad}(T)$ since the sum and integration of $p\cdot q/(q^2)^2$ vanishes. Therefore, within our perturbative ChPT scheme, the dispersion relation is independent of the gauge parameter in covariant gauges. Note that it is crucial that we remain within the strict regime of perturbation theory to prove this result, since, consistently with that approach, we have taken the self-energy at the on-shell point.

Therefore, we get, after collecting all the pieces, for the real part of the self-energy difference at finite temperature:

$$\begin{aligned}\Delta\Sigma(|\vec{p}|;T) &= \Delta\Sigma(T=0)+\frac{\hat{M}^2_{\pi^0}}{F^2}\left[g_1(\hat{M}_{\pi^0},T)-g_1(\hat{M}_{\pi^\pm},T)\right]+(1-4Z)e^2g_1(\hat{M}_{\pi^\pm},T)\\ &+\frac{e^2T^2}{6}+4M^2_{\pi^\pm}\mathrm{Re}\,J_T(0,\hat{M}_{\pi^\pm};|\vec{p}|)+\mathcal{O}(p^6),\end{aligned} \tag{11}$$

where the explicit expression for $\mathrm{Re}\,J_T(0,\hat{M}_{\pi^\pm};|\vec{p}|)$ is given in (B14) and $Z=C/F^4$. We recover the $T=0$ result of [51] taking into account (B5) and (B15). On the other hand, in the chiral limit $\hat{m}=0$ and neglecting $\mathcal{O}(e^4)$, we reproduce the result of [30] for the EM mass difference, namely $M^2_{\pi^\pm}-M^2_{\pi^0}=(2Ce^2/F^2)\left(1-\frac{T^2}{6F^2}\right)+\frac{1}{4}e^2T^2$. Note the combination of a first decreasing term, coming from vector-axial mixing towards chiral restoration (as we will discuss in section III) plus the increasing thermal scalar mass term. The net result in the chiral limit is a slowly decreasing function as showed in Fig.2.

In our present work, we have additional mass and momentum dependence terms, which should play a relevant role for the physically realistic temperature regime, where the approach $T\gg M_\pi$ is not justified. In particular, if we define the mass in the static limit $\vec{p}=\vec{0}$, using (B16) in (11) we get:

$$\begin{aligned}\Delta M^2_\pi(T)\equiv\Delta\Sigma(|\vec{p}|=0;T) &= \Delta M^2_\pi(0)+\frac{\hat{M}^2_{\pi^0}}{F^2}\left[g_1(\hat{M}_{\pi^0},T)-g_1(\hat{M}_{\pi^\pm},T)\right]+(1-4Z)e^2g_1(\hat{M}_{\pi^\pm},T)\\ &+\frac{e^2T^2}{6}+4M^2_{\pi^\pm}g_2(M_{\pi^\pm};T)+\mathcal{O}(p^6)\\ &=\Delta M^2_\pi(0)+e^2\left[2(2+Z)\hat{M}^2_\pi g_2(\hat{M}_\pi;T)+(1-4Z)g_1(\hat{M}_\pi;T)+\frac{T^2}{6}\right]+\mathcal{O}(e^4)+\mathcal{O}(p^6)\end{aligned} \tag{12}$$

with g_2 defined in (B17). Note that, as it is written in the last line in (12), it is clear that all the terms give contributions increasing with T except for the term $-4Zg_1$ which, as we will show in section III carries out the chiral-restoring $V-A$ mixing. Note also that apart from the $g_1(M,T)$ terms which become $T^2/12$ in the chiral limit, there is also a g_2 term which was absent in the chiral limit and receives a contribution from the photon exchange diagram and another one from the tadpole difference of g_1 functions. Taking into account the typical asymptotic behaviours for these functions described in Appendix B, this new g_2 term is comparable to the others for the range of temperatures considered here, i.e., relevant for a Heavy Ion environment and actually, as we will just see, the net result for the pion mass difference is now an increasing function of T. Recall that both g_1 and g_2 are increasing functions of T.

The results for the charged and neutral masses separately and for their difference are displayed in Fig.2. For the numerical evaluation of our results we will take the same values for the low-energy constants as in [54]. We have used physical masses for the pions instead of the tree level masses for the numerical results since the difference is encoded in higher order corrections. In the thermal range considered, and despite the different sign of the various terms, the increasing terms turn out to dominate the pion mass difference, which is approximately 24% bigger at $T=150$ MeV than the zero temperature value and altogether the variation is quite soft with temperature. Also, when T grows

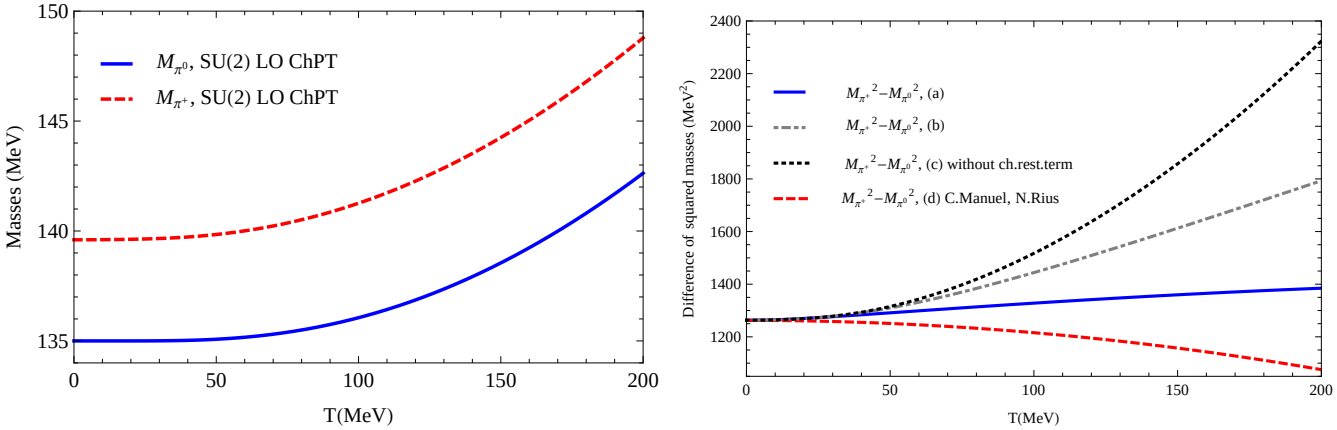

Figure 2. Left: Charged (red,dashed line) and neutral (blue,solid line) pion masses in the static limit to leading order in SU(2)-ChPT for non zero tree level pion masses. Right: Different results for the charged-neutral pion mass difference: (a, solid line) corresponds to our calculation in the chiral limit keeping corrections $e \neq 0$ for the tree level charged pion mass inside the loops; (b, dot-dashed line) corresponds to the same calculation with $m \neq 0$ and $e \neq 0$ also inside the loops; (c, dotted line) is the full result subtracting the chiral restoring term as explained in the text and (d, dashed line) is the result given in [30].

much above the applicability range of these ChPT calculations the mass difference starts to decrease. But this should be expected since expansions in $M_{\pi^\pm}/T \to 0$ should coincide with the T-decreasing chiral limit behaviour commented above. It is important to remark though that for low and moderate temperatures our result with physical masses differs qualitative and quantitatively from the chiral limit one. Finally, we have shown also in the right panel of Fig.2 the results in a modified chiral limit where we set $\hat{m} = 0$ but consider EM effects to be still turned on, i.e. $e \neq 0$, even inside the loops. In addition, in order to calibrate the importance of chiral symmetry restoration in the obtained behaviour, we have also plotted in Fig.2 the result for the EM (static) mass difference without including the chiral restoring term $-4Zg_1(M_\pi, T)$ in (12). The effect would be much larger then, giving rise to about a 9 MeV mass difference around $T = 200$ MeV, i.e. twice its $T = 0$ value.

One of the conclusions of this work is then that the scalar mass inherent to the thermal bath plus the massive pion effects overshadow the restoring terms coming from axial-vector degeneration leaving no trace of a chiral restoring behaviour as would have been inferred naively from (1). On the contrary, the net result is monotonically increasing. In section III we will present a more detailed discussion in connection with sum rules and resonance saturation.

Let us analyze now the momentum dependence in the real part of the dispersion relation. The pion gas formed after a relativistic heavy ion collision is in thermal equilibrium and hence momenta are weighted with the Bose-Einstein distribution function. Thus, we can define a momentum-averaged mass and compare with the static mass defined before. This is then a relevant observable when comparing with experimental pion distributions. The distribution function peaks around some three-momentum value which varies with temperature, in such a way that for a certain T there are only an effective number of pions with three-momenta around this value which are thermally active. Actually, for small $T \ll M_\pi$, momenta are distributed around $p \sim \sqrt{MT}$ while in the opposite regime $T \gg M$ they do around $p \sim T$.

For any $\vec{p}$-dependent observable, $\mathcal{A}(\vec{p}, T)$, we can associate a momentum average taking into account the neat effect of the thermal bath by weighting over the number of particles present at a given temperature and dividing by the total number of pions existing in the gas, i.e.

$$\langle \mathcal{A}(T) \rangle_p = \frac{\int d^3\vec{p}\, n_B(E_p, T) \mathcal{A}(\vec{p}, T)}{\int d^3p\, n_B(E_p, T)}. \tag{13}$$

In Fig.3 we show the results for the averaged charged pion mass (left panel) and for the charged-neutral difference (right panel) compared with the results in the static limit. Since eq.(5) does not depend on $\vec{p}$, neutral pions satisfy $\langle M_{\pi^0} \rangle = M_{\pi^0}$. As we see there, both pictures show that at very low temperatures the results are almost indistinguishable and, in the case of the charged mass, almost imperceptible, along the range of temperatures at which ChPT can be still predictive. The departure from the static limit is more perceptible in the mass difference since we are subtracting the main vacuum contribution to the neutral and charged masses. In that plot, note that even at moderate temperatures of about T =100 MeV, the effect of the thermal bath makes the averaged curve to grow

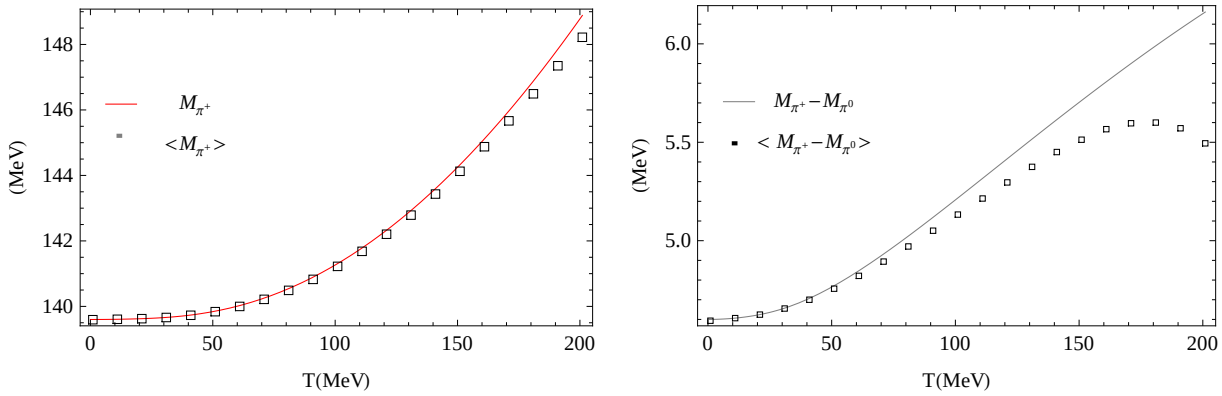

Figure 3. Leading order ChPT result for the static charged pion mass (left) and the charged-neutral pion mass difference (right) versus the mean value of those same observables over external momenta in the thermal bath.

slower than the static one and, for larger temperatures, we even see a qualitative decreasing, eventually approaching the chiral limit behaviour faster than in the static case. Since we expect the momentum distribution to be peaked around $p \sim T$ as T is increased, it is not surprise that the differences with the $p = 0$ case become more relevant for higher temperatures. Note also that from (B14), we obtain that the $\mathrm{Re}\, J_T$ term in (11) vanishes asymptotically for $p \to \infty$ as $\mathcal{O}(M_\pi^2/p^2)$, so that the importance of that p-dependent term becomes gradually smaller as T increases and therefore the total result gets closer to the chiral limit.

The main conclusion of this section is that the EM mass difference when physical pion masses are considered is a softly increasing function of T, pretty much as in the $e = 0$ case. This behaviour is even softer for the momentum averaged mass. This result is consistent with the experimental observations in the pion spectra commented in section I. In this respect, one can actually consider chiral symmetry restoration as being ultimately responsible for charged-neutral differences not being observed, in view of the results showed in Fig.2.

B. Imaginary part: bremsstrahlung-like IR enhanced contributions

To the order in ChPT that we are considering, the photon-exchange diagram (d) in Fig.1 leads to a nonzero imaginary part of the self-energy which, according with our previous discussion, allows to define perturbatively a damping rate for the pion as $\gamma_{EM}(|\vec{p}|) = -\mathrm{Im}\,\Sigma(E_p + i\epsilon, |\vec{p}|)/(2E_p)$. By the subscript EM we recall that this would be a pure EM correction felt only by the charged pions and therefore would introduce neutral-charged differences in the damping effects, as discussed below.

In a covariant gauge, for which we have just showed that the on-shell one-loop Σ is independent of the gauge parameter α, and according to (9), we would have $\gamma_{EM}(|\vec{p}|) = -\frac{2M_\pi^2}{E_p}\mathrm{Im}\, J_T(0, M_\pi; \omega = E_p, |\vec{p}|)$ with $\mathrm{Im}\, J_T$ the function given in (B18). Note that we get a nonzero answer despite the fact that the vacuum bremsstrahlung process of a scalar radiating a photon is forbidden. The reason is that, as discussed in Appendix B, the Landau and unitarity cuts in this case give a contribution for which, respectively, the conditions $E_p = |\vec{q}| \pm E_{|\vec{q}-\vec{p}|}$, with $|\vec{q}|$ and $|\vec{q}-\vec{p}|$ the photon and internal pion momentum respectively, are fulfilled for $|\vec{q}| = 0$. Thus, those terms correspond to the two possible processes $\pi \to \pi\gamma$ arising from cutting diagram (d) in Fig.1, with thermal photons (quasiparticle states) weighted by $n(|\vec{q}|) \sim T/|\vec{q}|$ which enhances this contribution so that $\int qn(q)\delta(q)$ remains finite according to the prescription for the δ function arising from the retarded propagator, as we explain in detail at the end of Appendix B.

However, the previous covariant gauge calculation of the damping rate is not well defined. In particular, one readily realizes that $\mathrm{Im}\,\Sigma$ thus obtained is positive, so that the damping rate would be negative and then unphysical, the corresponding retarded propagator not having the correct analytic behavior described in Appendix A. This sign problem is just a reflection of a deeper issue directly related to the gauge choice. For the imaginary part, we are putting the internal quasiparticles in the loop on their mass shell, weighted by the different thermal distributions. That means that in a covariant gauge, we are counting the additional nonphysical gauge degrees of freedom as being in thermal equilibrium and hence contributing to the damping rate. The problem of introducing the correct degrees of freedom in hot gauge theories has been actually treated extensively in the literature [1]. For instance, a strict loop calculation of the gauge field damping rate leads to a dependence on the gauge parameter α when working in covariant gauges, which may actually result in a wrong sign for the damping rate [55, 56]. This problem is avoided in physical

gauges such as the Coulomb gauge, where one gets physically meaningful answers [57]. To arrive to the same result in covariant gauges, alternative approaches have to be used [58, 59] which yield modifications of the naive gauge field propagator so as to ensure that only the physical gauge degrees of freedom remain thermally active. Actually, as it is well known in thermal field theory, these kind of difficulties with gauge invariance of the standard loop calculations was one of the motivations that led to the formulation of the Hard Thermal Loop (HTL) resummation scheme at high temperatures [60]. However, within the ChPT framework for physical pion masses, we are not in the regime where a HTL-based approach would be applicable since temperature, mass and momenta are all of the same order, so we have to ensure that the correct degrees of freedom for thermal quasiparticles are included. For that purpose, we will define the charged pion damping rate in the strict Coulomb gauge, which free propagator is given in (A10). It contains only longitudinal D^{00} and transverse D^{ij} components, the longitudinal one not propagating, since the corresponding free spectral function vanishes. Note that the previous arguments should not affect the real part calculation performed in section II A in covariant gauges and actually we have checked that the real part of the perturbative on-shell self-energy remains the same in the Coulomb gauge. We also point out that previous calculations of the charged scalar damping rate in SQED, formally similar to ours although within the HTL regime, are also carried out in the Coulomb gauge [61, 62]. In those works, similarly to QCD, it is found that the transverse part of the HTL-resummed damping rate is infrared divergent, while the longitudinal part remains finite.

It must be born in mind that the gauge problem mentioned above, as well as the existence of infrared singularities for the damping rate and a nonzero longitudinal contribution in SQED, are warnings that may indicate the necessity of considering higher terms also in our ChPT analysis, which is beyond the scope of this work. We consider then our results in this section as mere estimates of the possible size of this pion damping effect and its consequences, which have the advantage that, at least to the order considered, the results are guaranteed to be infrared finite, as well as model-independent. The inclusion of those higher orders could actually amplify some of the phenomenological consequences that we will just discuss.

Guided by the previous considerations, we will calculate the charged pion damping rate in the strict Coulomb gauge, with gauge propagator given by (A10). When this propagator is used in diagrams (c) and (d) of Fig.1, we obtain respectively, in dimensional regularization:

$$\Sigma^{CG}_{\gamma Tad}(T) = -e^2 T \sum_n \int \frac{d^3\,q}{(2\pi)^3} \frac{\delta_{ij} P_T^{ij}(q)}{q^2} = -2e^2 T \sum_n \int \frac{d^3\,q}{(2\pi)^3} \frac{1}{q^2} = \frac{e^2 T^2}{6} \tag{14}$$

$$\Sigma^{CG}_{\gamma Ex}(i\omega_m, |\vec{p}|; T) = e^2 T \sum_n \int \frac{d^3\,q}{(2\pi)^3} \frac{(2\omega_m - \omega_n)^2}{|\vec{q}|^2 \left[(p-q)^2 - \hat{M}^2_{\pi^\pm}\right]} - 4e^2 |\vec{p}|^2 T \sum_n \int \frac{d^3\,q}{(2\pi)^3} \frac{1-\cos^2\theta}{q^2 \left[(p-q)^2 - \hat{M}^2_{\pi^\pm}\right]} \tag{15}$$

where $\cos\theta = \frac{\vec{p}\cdot\vec{q}}{|\vec{p}||\vec{q}|}$. Of the above terms, only the second one in the r.h.s. of (15) contributes to the imaginary part when Σ is analytically continued and taken on the mass shell. This is precisely the transverse contribution, second term in (A10), to the photon exchange diagram. The longitudinal part does not contribute to the photon spectral function at this order, consistently with the idea that longitudinal free photons do not propagate.

As commented above, we have explicitly checked that $\Sigma^{CG}_{\gamma Tad}(T) + \mathrm{Re}\,\Sigma^{CG}_{\gamma Ex}(\omega^2 = E_p^2, |\vec{p}|; T)$ equals the result (11). As for the imaginary part, which as stated is only well defined in the Coulomb gauge, after analytic continuation and following the same steps as in Appendix B when analyzing $\mathrm{Im}\, J_T(0, M)$, we get:

$$\begin{aligned}\gamma_{EM}(p) &= \frac{e^2}{8\pi}\frac{p^2}{E_p^2}\int_0^\infty dqqn(q)\delta(q)\int_{-1}^1 dx(1-x^2)\left[\frac{1}{1-\frac{px}{E_p}} + \frac{1}{1+\frac{px}{E_p}}\right] \\ &= \frac{e^2 T}{4\pi}\left[1 - \frac{M_\pi^2}{2pE_p}\log\left(\frac{E_p+p}{E_p-p}\right)\right]\end{aligned} \tag{16}$$

where we have denoted $p \equiv |\vec{p}|$ and we have used the retarded prescription for the δ function discussed in Appendix B. Once more, the above contribution comes from processes radiating thermal (physical) photon degrees of freedom at vanishing spatial momentum.

The function $\gamma_{EM}(p)$ in (16) is plotted in Fig.4 (left panel). As it can be directly checked from (16), it is linearly proportional to T, it vanishes for $p \to 0^+$ for fixed pion mass M_π, and behaves asymptotically as $\gamma_{EM}(p \to \infty) \to \frac{e^2 T}{4\pi}$. This asymptotic value is also the result in the chiral limit $M \to 0^+$ or taking directly $M = 0$ from the start. This p dependence is indeed very similar to the one found in [61] for the transverse part of the damping, although in that work γ is logarithmically dependent on the infra-red cutoff, which we do not need to introduce at the order we are considering. In turn, we mention that we have checked that we arrive also to (16) by replacing in the general expressions in [61] the free spectral function in the Coulomb gauge.

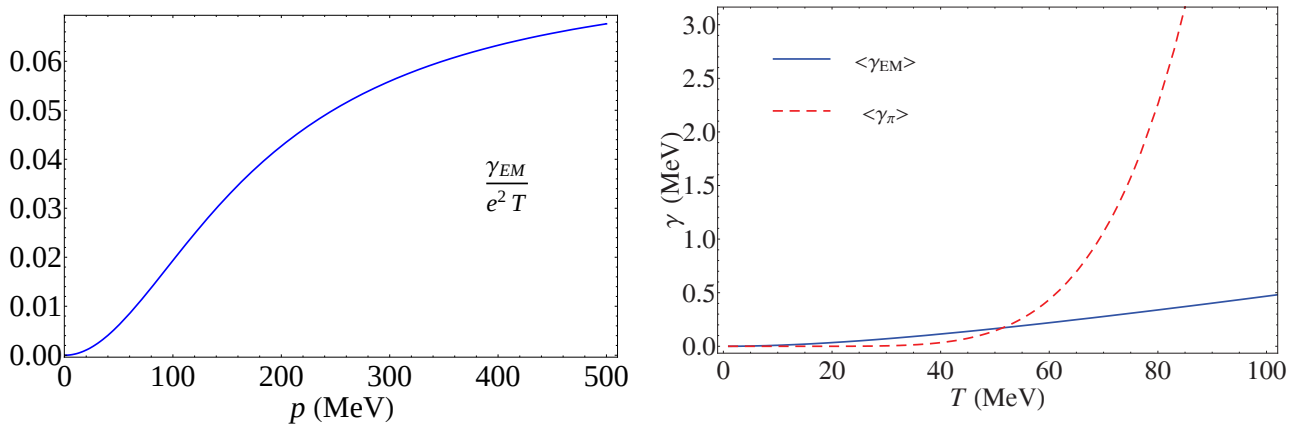

Figure 4. Left: The EM damping rate versus momentum. Right: The momentum averaged pion damping rate with $e = 0$ $\langle\gamma_\pi\rangle$ and the EM contribution $\langle\gamma_{EM}\rangle$.

In order to analyze the possible phenomenological effects of this EM contribution to the damping rate, we have plotted in Fig.4 (right panel) the average $\langle\gamma_{EM}\rangle$ according to (13), compared to the averaged damping rate in ChPT for $e = 0$, which we denote γ_π which comes from a two-loop sunset diagram [27] and can be obtained also from kinetic theory arguments [28]. The damping γ_π is the leading contribution to the inverse mean collision time and to the inverse mean free path for pions in the isospin limit, i.e., contributes equally for charged and neutral pions, whereas, as stated above, γ_{EM} would contribute only to the charged ones. We also recall that γ_π, within the dilute regime applicable here, depends linearly on the imaginary part of the $\pi\pi$ scattering forward amplitude and hence on the total cross section from the optical theorem, which allows to get a unitarized version whose average value grows much smoothly with temperature due to the unitarity bounds on the amplitude [27]. This unitarized damping is actually more realistic physically, since it describes scattering more accurately.

From the curve in Fig.4, we observe that, even though in principle γ_π is a higher order contribution with respect to γ_{EM} in the ChPT expansion, their numerical values are comparable for low and moderate temperatures and γ_π gets actually much larger as T increases further. This is due on the one hand to the small numerical size of EM contributions and on the other hand to the large growing with T of the nonunitarized damping discussed above, due to the strongly interacting character of pion scattering as energy increases. The second effect starts being significant from about $T \simeq 80$ MeV, although the unitarized curve still departs from the EM one above $T = 100$ MeV.

Thus, within a Heavy-Ion environment, we expect the maximum EM effects to be operative at the end of the expansion, i.e. around thermal freeze out $T \simeq 100$ MeV. As discussed in section I, the thermal damping $\gamma(p)$ enters inversely in transport coefficients, inside a p integral corresponding to the leading diagram for conserved current correlators [18–20]. It is not the purpose of this work to carry out a detailed evaluation of this effect, but in order to get a rough estimate of the size of the corrections, we can use just the thermal averaged values. In particular, in the electrical conductivity only the charged pion enters in the dominant loop [18] so that an estimate of the correction to that coefficient with respect to the isospin limit would be of order $1 - \gamma_\pi/(\gamma_\pi + \gamma_{EM})$, which gives, for averaged values, 0.07 for $T = 100$ MeV (taking the unitarized value for $\langle\gamma_\pi\rangle$) and 0.13 for $T = 80$ MeV so in that region the expected correction to the electrical conductivity is around 10%. Regarding other transport coefficients, such as the shear and bulk viscosities, since all pion species enter the loop of energy-momentum correlators [19], the correction will be of order $1 - [1 + 2\gamma_\pi/(\gamma_\pi + \gamma_{EM})]/3$ which gives 0.05 for $T = 100$ MeV and 0.09 for $T = 80$ MeV.

Another consequence of the EM damping effect is that the mean free time $\tau = 1/\gamma$ and the mean free path $\lambda = p/(E_p\gamma)$ for charged pions are smaller than for the neutral component. Thus, for neutral pions $\tau_0 = 1/\gamma_\pi$ while for charged ones $\tau_{ch} = 1/(\gamma_\pi + \gamma_{EM})$. This implies for instance a reduction in the thermal or kinetic freeze-out temperature of the charged pion component with respect to the neutral one, defined as $\tau(T_{FO}) \simeq 10$ fm/c, the typical plasma lifetime. This effect is much smaller: we get around 2 MeV reduction in T_{FO} between the neutral and charged components, using again the unitarized $\langle\gamma_\pi\rangle$.

III. SUM RULE, RESONANCES AND CHIRAL RESTORATION

The study of sum rules regarding spectral functions in the vector and axial-vector channels and their in-medium or thermal bath modifications has been the subject of thorough investigation up to very recently [63–65]. We will be interested here in the sum rule related to the EM pion mass difference and its extension to finite pion masses and finite temperature. That sum rule was originally derived in [45] and analyzed at finite temperature in the chiral limit in [30, 31].

The traditional derivation of Das sum rule [30, 45, 47] starts from the $\mathcal{O}(e^2)$ correction to the pion mass given in terms of a EM current-current correlator:

$$\begin{aligned}\Delta\Sigma(|\vec{p}|;T) &= \frac{e^2}{2}\int_T d^4x \langle\pi^+(p)|\mathcal{T}J_\mu(x)J_\nu(0)|\pi^+(p)\rangle_T D_0^{\mu\nu}(x) \\ &= \frac{e^2}{2}T\sum_n\int\frac{d^3\vec{q}}{(2\pi)^3}\frac{g^{\mu\nu}T_{\mu\nu}(q,p;T)}{\omega_n^2+|\vec{q}|^2}\end{aligned} \tag{17}$$

Here, we have allowed for a $\vec{p}$ dependence on the self-energy, from the loss of Lorentz covariance. The $|\pi\rangle$ states are meant to be $T=0$ free ones with dispersion relation $p^2=M_\pi^2(e=0)$. The current J_μ is the EM current, whose QCD representation is $J_\mu=\bar{q}Q\gamma_\mu q$ and time ordering is along the imaginary time axis. The subscript T in the matrix element indicates that the corresponding IT correlators obtained after LSZ reduction formulas are to be averaged in the thermal bath. After all the Matsubara sums are performed, the result for the self-energy defined in (17) is meant to be analytically continued to the external $p=(\omega+i\epsilon,\vec{p})$ with $\omega\in\mathbb{R}$, so that this corresponds to the retarded self-energy, which encodes properly the spectral properties, as discussed in Appendix A.

Since this is just the leading order correction in e^2, we can take $D_0^{\mu\nu}$ as the free photon propagator, which we consider in the Feynman gauge $\alpha=1$. $T_{\mu\nu}(q,p)$ is the Fourier transform of the pion matrix element in the first equation above and corresponds to Compton scattering. It is useful to split this amplitude into contact and non-contact terms $T_{\mu\nu}=T_{\mu\nu}^{(C)}+T_{\mu\nu}^{(NC)}$ so that the contact contribution corresponds to two photons interacting in the same vertex (seagull diagram (c) in Fig.1 in our previous ChPT calculation), i.e, $T_{\mu\nu}^{(C)}=2g_{\mu\nu}$.

A. $T=0$ sum rule in the Soft Pion Limit

In order to relate (17) with vector and axial-vector thermal averages, suitable to connect with chiral restoration, one possible approach is to take the Soft Pion Limit (SPL) $p\to 0$ for the pion states and use Current Algebra (CA) for the current commutators involved. Note that using the SPL implies automatically to work in the chiral limit of vanishing quark masses $\hat{m}=0$ so that the π^0 is massless. Let us first analyze the $T=0$ case in the SPL.

In the SPL+CA approach the NC part of the Compton amplitude satisfies:

$$\lim_{p\to 0}T_{\mu\nu}^{(NC)}(q,p)=\frac{2}{F_\pi^2}\left[\Pi_{\mu\nu}^V(q)-\Pi_{\mu\nu}^A(q)\right] \tag{18}$$

where $\Pi_{\mu\nu}^{V,A}(q)$ are respectively the Fourier transforms of the vector and axial-vector vacuum expectation values $\langle 0|V_\mu^3(x)V_\nu^3(0)|0\rangle$ and $\langle 0|A_\mu^3(x)A_\nu^3(0)|0\rangle$ with $V_\mu^a(x)$ and $A_\mu^a(x)$ the vector and axial-vector currents. Note that here we do not make any distinction between the physical F_π and the tree level F appearing in the lowest order chiral lagrangian (2) since they coincide in the regime of validity of CA, equivalent to the lowest order in the chiral expansion.

For the non-contact contribution we use the standard $T=0$ decomposition (see Appendix A):

$$\begin{aligned}\Pi_{\mu\nu}^V &= \left(\frac{q_\mu q_\nu}{q^2}-g_{\mu\nu}\right)\Pi^V(q^2) \\ \Pi_{\mu\nu}^A &= \left(\frac{q_\mu q_\nu}{q^2}-g_{\mu\nu}\right)\Pi_t^A(q^2)+\frac{q_\mu q_\nu}{q^2}\Pi_l^A(q^2)\end{aligned} \tag{19}$$

Note that for the axial-vector case, we have added a four-dimensional longitudinal piece, which arises from the partial conservation of axial current (PCAC) in QCD. We use T,L to denote three-dimensional transverse and longitudinal contributions (both four-dimensionally transverse) and t,l to denote four-dimensional transverse and longitudinal ones.

On the other hand, as customary, we can write for the correlators Π^V and Π_t^A their spectral function representation at $T=0$:

$$\Pi^V(q^2) = q^2 \int_0^\infty ds \frac{\hat{\rho}^V(s)}{q^2-s}$$
$$\Pi_t^A(q^2) = q^2 \int_0^\infty ds \frac{\hat{\rho}^A(s)}{q^2-s} \tag{20}$$

since at $T=0$ they only depend on q^2 and there are no cuts for $s<0$ (see Appendix A).

To leading order in the low-energy expansion, or equivalently using CA, in the chiral limit and for $T=0$ one has $\Pi_l^A(q) = F_\pi^2 q^2 G_\pi(q)$ with G_π the leading order pion propagator, since the axial-vector current in the low-energy representation from is just $A_\mu^a = F_\pi \partial_\mu \pi^a + \ldots$, the dots denoting higher terms in the chiral expansion (labeled formally by the $1/F$ in the lagrangian). This is consistent also with the PCAC theorem, valid within CA, $\langle 0|\partial^\mu A_\mu^a|\pi^b\rangle = \delta^{ab} F_\pi M_\pi^2$.

Thus, for $T=0$ and in the chiral limit one has:

$$\Delta M_\pi^2\big|_{SPL,T=0} = \frac{3e^2}{F_\pi^2} i \int \frac{d^4q}{(2\pi)^4} \frac{q^2}{q^2+i\epsilon} \left[\frac{F_\pi^2}{q^2+i\epsilon} - \int_0^\infty ds \frac{\rho^V(s)-\rho^A(s)}{q^2-s+i\epsilon} \right] \tag{21}$$

where the momentum integral is in Minkowski space-time. The first term inside the brackets in the above expression comes from the sum of the contact term $T_{\mu\nu}^C$ plus the Π_l^A term contribution. Even though that first term would vanish in DR, we keep it to track more easily the UV behaviour in terms of a cutoff $\Lambda \to \infty$, since in that way one can check the consistency of the different versions of the sum rule. Actually, and this is an important point, the finiteness of the result for $\Lambda \to \infty$ is directly connected with the well-known Weinberg sum rules [66] (at $T=0$ in the chiral limit):

$$\int_0^\infty ds \left[\rho^V(s) - \rho^A(s)\right] = F_\pi^2 \tag{22}$$
$$\int_0^\infty ds\ s \left[\rho^V(s) - \rho^A(s)\right] = 0 \tag{23}$$

Hence, consider the dominant quadratic $\int d^4q (1/q^2) \sim \Lambda^2$ divergent UV part in the s integral in (21), which is given just by the leading order in the expansion $q^2 \gg s$ (formally $Q^2 \gg s$ after Wick rotating the integral so that the Minkowskian $q_0 \to -iq_0$ and $Q^2 = q_0^2 + |\vec{q}|^2$). That leading contribution cancels then exactly with the first term inside the brackets if (22) holds. The next to leading UV divergence is of order $\int d^4q (1/q^4) \sim \log\Lambda$ and cancels also once (23) is used. Once $\Delta M_\pi^2\big|_{SPL,T=0}$ in (21) is shown to be finite, the Q^2 Euclidean integral can be performed, giving rise to the original sum rule in [45]:

$$\Delta M_\pi^2\big|_{SPL,T=0} = -\frac{3e^2}{16\pi^2 F_\pi^2} \int_0^\infty ds s (\ln s) \left[\rho_V(s) - \rho_A(s)\right] \tag{24}$$

Thus, at $T=0$ and in the chiral limit one gets the typical $\rho_V - \rho_A$ contribution which naively would vanish if chiral symmetry is restored.

For practical purposes, it would be useful to assume that the vector and axial spectral functions are saturated, respectively, by the $\rho(770)$ and $a_1(1260)$ resonances, consistently with Vector Meson Dominance and Resonance Saturation (RS) [47, 48, 67]. See also our comments in section IV. In this section, this will only used for power counting arguments regarding the sum rule, rather than to get a numerically accurate prediction. In addition, at least for a rough estimate, we can in principle neglect the width of those resonances with respect to their mass, so that at zero temperature $\rho_{V,A} \sim F_{V,A}^2 \delta\left(s - M_{V,A}^2\right)$ where F_V^2 and F_A^2 are the constant residues of the current correlators. They correspond respectively to $\rho\gamma\pi^{2n}$ and $a_1\gamma\pi^{2n+1}$ ($n \geq 0$) couplings in the spin-1 resonance lagrangian [67]. Recall that, in that limit, (22) and (23) would give respectively $F_V^2 - F_A^2 = F_\pi^2$ and $F_V^2 M_V^2 = F_A^2 M_A^2$, which are reasonably fulfilled by the physical values of those constants [47, 48]. When this narrow RS limit is used in (24), one gets $\Delta M_\pi^2\big|_{SPL,T=0} \simeq \frac{3e^2 F_V^2 M_V^2}{16\pi^2 F_\pi^2} \log(M_A^2/M_V^2)$ which gives $M_{\pi^\pm} - M_{\pi^0} \simeq 4.7$ MeV, reasonably close to the experimental value of 4.594±0.001 MeV.

In general, the vector and axial-vector spectral functions should be more elaborated, including nonzero widths, continuum and excited states contributions, in order to comply with phenomenology data such as τ-decay data (see [64] for a recent update). This level of precision will not be necessary for our present work.

An important point in our analysis will be to classify the different contributions to the pion mass difference according to a power counting in terms of typical resonance masses. Thus, we consider a formal expansion parameter:

$$x \sim M_\pi^2/M_R^2 \sim T^2/M_R^2$$

where $M_R = \mathcal{O}(M_{V,A})$. $F_{V,A}$ and F_π are treated as parameters of the same order in this expansion. Note that we treat the pion mass and the temperature as being of the same order, which is the main difference of the present work with [30]. This counting is basically equivalent to the chiral expansion. However, working within the framework of resonance models will help better to understand the modifications to the sum rule (24) as well as to make numerical estimates of the accuracy of ChPT, which will be carried out in section IV.

Thus, according to our previous discussion, we can think of the SPL result (24) as the leading $\mathcal{O}(M_R^2)$ order, which actually gives the numerically dominant contribution to the constant C in (4), whereas NLO corrections of $\mathcal{O}(xM_R^2) \sim \mathcal{O}(M_\pi^2, T^2)$ arise from the ChPT pion loops discussed in section II.

B. $T \neq 0$ sum rule in the SPL

Let us now still keep the SPL (and therefore the chiral limit) but allow $T \neq 0$, as in the analysis performed in [30]. One can then assume that the soft pion and current algebra theorems relating the pion expectation value of (17) with current correlation functions, as in (18) still holds. However, a crucial point is that now $\Pi_{\mu\nu}^{V,A}(q;T)$ are T-dependent correlation functions corresponding to $\langle \mathcal{T} V_\mu^3(x) V_\nu^3(0)\rangle_T$ and $\langle \mathcal{T} A_\mu^3(x) A_\nu^3(0)\rangle_T$.

Those correlators, apart from carrying on T-dependent corrections to the spectral functions, will give rise to a more complicated tensor structure, as discussed in Appendix A. Thus, the steps leading to the thermal version of (18) are only valid in the SPL and up to $\mathcal{O}(T^2)$ corrections. For instance, $F_\pi^2(T)$ defined through the residue of the axial correlator at the pion pole gives rise to two independent pion decay constants, corresponding to the space and time components of the axial current, from $\mathcal{O}(T^4)$ onwards [68], even in the chiral limit.

Keeping only the leading $\mathcal{O}(T^2)$ corrections in the chiral limit, it is well known that the only thermal correction to axial and vector spectral functions is a multiplicative renormalization with respect to the $T = 0$ ones, namely [46]:

$$\begin{aligned}\Pi_{\mu\nu}^V(q;T) &= [1-\epsilon(T)]\,\Pi_{\mu\nu}^V(q;0) + \epsilon(T)\Pi_{\mu\nu}^A(q;0)\\ \Pi_{\mu\nu}^A(q;T) &= [1-\epsilon(T)]\,\Pi_{\mu\nu}^A(q;0) + \epsilon(T)\Pi_{\mu\nu}^V(q;0)\end{aligned} \tag{25}$$

where $\epsilon(T) = \frac{T^2}{6F^2} = 2g_1(0,T)/F^2$ comes from pion tadpole corrections. Note that this SPL mixing predicts chiral restoration, in the sense of axial-vector current degeneration, at $\epsilon = 1/2$, i.e, at $T \simeq \sqrt{3}F$, before the value for which the quark condensate vanishes in the chiral limit, $T \simeq \sqrt{8}F$ [26]. Thus, to this order the only modification is the residue of the correlators, not their poles. Actually, the temperature corrections to the ρ,a_1 meson masses and widths are expected to be of order $\mathcal{O}(e^{-M_R/T}) = \mathcal{O}(e^{-1/\sqrt{x}})$ [11, 12, 17, 69].

Therefore, using in (17), the thermal version of (18) with $F_\pi^2 \to F_\pi^2(T)$ and the VA correlators replaced by (25), we can write now:

$$\begin{aligned}\Delta M_\pi^2\big|_{SPL,T\neq 0} = 4e^2 T\sum_n \int \frac{d^3\vec{q}}{(2\pi)^3}\frac{1}{\omega_n^2+|\vec{q}|^2} - \frac{e^2\,[1-2\epsilon(T)]\,F_\pi^2}{F_\pi^2(T)} T\sum_n \int \frac{d^3\vec{q}}{(2\pi)^3}\frac{1}{\omega_n^2+|\vec{q}|^2}\\ -\frac{3e^2\,[1-2\epsilon(T)]}{F_\pi^2(T)} T\sum_n \int \frac{d^3\vec{q}}{(2\pi)^3}\int_0^\infty ds \frac{\rho^V(s;0)-\rho^A(s;0)}{\omega_n^2+|\vec{q}|^2 - s + i\epsilon}\end{aligned} \tag{26}$$

where $F_\pi^2(T) = F^2\,[1-\epsilon(T)]$ in the chiral limit [26].

The first term above comes from the contact term (photon tadpole in Fig.1) and is the Debye screening mass of the longitudinal photons which will contribute also to the charged thermal mass. In DR, from (B2), is given by $4e^2 g_1(0,T) = \frac{e^2T^2}{3}$, the $T = 0$ term vanishing identically for a massless particle (in this case the photon) as discussed already in section II A.

The second term in (26) comes from the $\Pi_l^A(q^2;T=0)$ part of the $T=0$ axial correlator when using the mixing (25). Note that to the order T^2 that we are keeping, in the SPL the first and second term in (26) add together giving a net T^2 contribution.

Finally, the last term in (26) is the reminder of the $V-A$ correlator coming from the non-contact part. Now the relevant T^2 contribution arises from the multiplicative factor in front of the integrals. The rest of the thermal contributions coming from that term are the result of evaluating the Matsubara sum, and are essentially of the order of $g_1(M_R;T)\sim e^{-M_R/T}$ if the spectral functions are taken as saturated by the vector and axial-vector lightest resonances, i.e, those contributions are exponentially suppressed in the x counting that we have introduced in section III A.

Note also that the formal expression (26) is finite up to $\mathcal{O}(T^2)$ in the UV cutoff Λ, by the same reason than for $T=0$, i.e, using the sum rules (22)-(23), taking into account that the infinities are contained only in the $T=0$ part of the integrals and that the $\mathcal{O}(\Lambda^2)$ is formally $\mathcal{O}(xM_R^2)$ so that when extracting that contribution one should not consider the $\epsilon(T)$ corrections in (26), which would be of higher order, since we are relying on the mixing (25) which is valid only up to $\mathcal{O}(xM_R^2)=\mathcal{O}(T^2)$. On the other hand, the $\log\Lambda$ is $\mathcal{O}(M_R^2)$ and then, for that logarithmic divergence those $\epsilon(T)$ corrections have to be kept in both the second and third terms in (26). Alternatively, before using the mixing (25), it can be proven that the expression remains finite, since the Weinberg sum rules hold also at finite temperature by replacing the s integrals of spectral functions by energy ones at fixed spatial momentum [63], which is the correct representation for the thermal correlators, as discussed in Appendix A. Recall that in [63], these sum rules are derived for the full axial spectral function, i.e, including the longitudinal part.

Thus, in the chiral and SPL limits and to $\mathcal{O}(T^2)$, using DR one has:

$$\Delta M_\pi^2\big|_{SPL,T\neq 0}=\frac{e^2T^2}{4}+\frac{2Cf(T)e^2}{F^2} \tag{27}$$

where $f(T)=\left(1-\frac{T^2}{6F^2}\right)$ and C given by the leading order (24), i.e., $C=\frac{F^2}{2e^2}\,\Delta M_\pi^2\big|_{SPL,T=0}=\mathcal{O}(M_R^2)$. Recall that (27) includes the corrections of $\mathcal{O}(xM_R^2)$ to the leading $\mathcal{O}(M_R^2)$ order, which in the SPL amount either to $\mathcal{O}(T^2)$ or $\mathcal{O}(\epsilon(T)M_R^2)$. Further corrections would include either $\mathcal{O}(\exp(-1/\sqrt{x}))$ or $\mathcal{O}(x^2M_R^2)$, the latter entering proportionally to T^4 in the chiral limit. The above result was obtained in [30] and gives the same answer as taking the chiral and SPL limits in our general ChPT expression (11) as we have actually shown in section II A.

It is actually instructive at this point to compare the origin of the different terms from the viewpoint of the role of resonances and possible remnants of the naive chiral-restoring $V-A$ behaviour of the $T=0$ expression (24). Thus, the first term in (26), the Debye screening term, is the one coming from diagram (c) in Fig. 1 as given in (6). The second term in (26) is nothing but the chiral limit and SPL version of $\Sigma_{\gamma Ex}$ in (9) from diagram (d) in Fig.1. Thus, when setting $\vec{p}=\vec{0}$ and $M=0$, that contribution becomes proportional to the tadpole T^2, as discussed in section II A. These two terms combine into the T^2 first term in the r.h.s of (27), the thermal scalar mass. The remaining bit, i.e, the last term in (26), proportional to the integrated difference of spectral functions, is a tadpole correction coming from diagrams of type (a) in Fig.1, namely the $-4Ze^2g_1$ term in (11). This term gives rise to the second contribution in the r.h.s of (27) since in the chiral limit, the additional tadpole contribution in (11) vanishes exactly.

Therefore, the chiral restoration $V-A$ behaviour of the mass difference, driven by the function $f(T)$ in (27), which in principle makes the EM pion mass difference decrease, is compensated now by the increasing behaviour of the combined Debye+Photon exchange first term in (27). The numerical size of these two terms are indeed comparable, and the net result is an almost constant T behaviour which masks then the chiral restoring. This was already noticed in [30]. Our purpose here is to show that this behaviour remains and is even more pronounced for physically realistic pion masses, coming from two different sources: the naive extension of the SPL sum rule using now $M_\pi\neq 0$ thermal functions, plus the $\mathcal{O}(M_\pi^2)$ deviations from that sum rule. As discussed above, the chiral limit is nothing but the leading asymptotic term for $T\gg M_\pi$. However, for realistic masses, the corrections are important and actually their analysis allows to understand better the obtained T-dependent behaviour.

C. $T\neq 0$ analysis for nonzero pion masses and momenta

Most of our previous discussion deals with the SPL $p_\mu\to 0$ with p the external pion four-momentum. In that limit it is mandatory to take the chiral limit, i.e, massless pions for $e=0$ or vanishing quark masses. However, for realistic temperatures such as those being reached in Heavy Ion experiments, this is not a good approximation, since T and M_π are parameters of the same order, and so they are in the chiral expansion.

If the SPL is abandoned and the quark masses are nonzero, some of the previous arguments in this section have certainly to be revisited. We can start from the general equation (17), from which we separate the connected part of

the current correlator. However, for the non-connected part, the relation with the thermal correlators $\Pi^{V,A}_{\mu\nu}$ through the thermal extension of (18) does not necessarily hold for $p_\mu \neq 0$. It is also unclear that the $V-A$ mixing effect (25) is also the dominant one when replacing $\epsilon(T) \to 2g_1(M_\pi;T)/F^2$, as it is often considered [64], since the original mixing theorem [46] was derived precisely assuming the SPL in the connection between pion expectation values and thermal correlators. Note that this replacement would come just from changing the free pion propagator form the massless case to the massive one.

One could then wonder whether the thermal SPL sum rule could be naively extended just by changing the free pion propagator. One way to see that such sum rule extension does not hold, is to look again at the UV behaviour with a cutoff Λ. Consider then the extension of (26) replacing just $(\omega_n^2 + |\vec{q}|^2) \to (\omega_n^2 + |\vec{q}|^2 + M_\pi^2)$ in the second integral, to comply with PCAC at $M_\pi \neq 0$, $\epsilon(T) \to 2g_1(M_\pi;T)/F^2$ and the finite mass correction to $F_\pi^2(T)$ which is just $F_\pi^2(T) = F_\pi^2(0)\left[1 - 2g_1(M_\pi;T)/F^2\right]$ [26]. Note that $F_\pi^2(0)$ receives now corrections of order $x \sim M_\pi^2/\Lambda_\chi^2$. Taking now the leading UV terms, as we did in section III A, the infinities do not cancel, since the WSR (22)-(23) are known to receive $\mathcal{O}(M_\pi^2)$ corrections. In particular, (22) remains the same, but (23) changes to [64, 70]:

$$\int_0^\infty ds\; s\left[\rho^V(s) - \rho^A(s)\right] = F_\pi^2 M_\pi^2 \tag{28}$$

Thus, the leading UV Λ^2 term corresponding to take $s = 0$ in the denominator would still cancel with the Debye term, by the same reasons as discussed in the massless case in the previous section. Note that for this leading term it is irrelevant to put $M_\pi \neq 0$ in the propagator inside the second integral. However, when the NLO $\log\Lambda$ is considered, there is no cancelation, since the last integral gives an extra factor of 3 when using (28), with respect to the M_π^2 term in the expansion of the second integral. Thus, we expect additional $\mathcal{O}(M_\pi^2)$ and $\mathcal{O}(|\vec{p}|^2)$ corrections. Actually, as we did in the chiral and SPL limits, we can read off the full result for the pion mass difference up to order $\mathcal{O}(e^2 x M_R^2)$ from our previous ChPT analysis in section II since this has to be the model-independent answer to that order. However, the sum rule analysis presented here will still be useful to keep track of the fate of the chiral-restoring terms, associated to the $V-A$ spectral function differences in the thermal bath, and of the main differences with the chiral limit.

Thus, let us consider the different thermal contributions to the mass difference obtained in our previous ChPT analysis, now for $M_\pi \neq 0$. The Debye term of diagram (c) in Fig.1 is given in (6) and is directly identified with the $T^{(C)}_{\mu\nu}$ contact term as in the SPL/chiral limit. The remaining contributions are of three different types, which we discuss in connection with our analysis in this section:

1. The term with no F^2 dependence, namely the pion-photon exchange contribution $\Sigma_{\gamma Ex}(|\vec{p}|;T)$ given in (7) and (9), which comes from the photon exchange diagram (d) in Fig.1. We can think of this term as the proper extension of the second contribution in (26) which, apart from the modification of the pion propagator to the massive case, includes the insertion of $\dfrac{(2p-q)^2}{(p-q)^2+M_\pi^2}$, which takes into account that the pion-photon vertex also receives p corrections. Now this term is not simply proportional to T^2 as in the SPL. As discussed in section II A, its on-shell contribution splits as indicated in eq.(9), giving rise to a T^2 term which adds to the Debye one to give the positive T^2 term in (11) plus the $e^2 g_1$ and $4M_\pi^2 \mathrm{Re}\, J_T$ terms in (11), which are both increasing functions of T, as it is clear from the discussion in Appendix B.

2. The $-4Ze^2 g_1$ term in (11), which comes from tadpoles (a) in Fig.1 and is therefore proportional to the leading-order EM mass difference as $-2g_1(M_\pi,T)\Delta M_\pi^2/F^2$. Therefore, this term gives the direct $M_\pi \neq 0$ extension of the T^2 term in $f(T)$ in (27) and thus inherits the $V-A$ chiral restoring behaviour.

3. The remaining term, i.e, the second one in (11), coming also from tadpoles (a) in Fig.1. It has no counterpart in the SPL and therefore it is an $\mathcal{O}(M_\pi^2)$ modification of the SPL sum rule that has to be taken into account also to this order. Recall that, as indicated in section II A, this term can be written, to $\mathcal{O}(e^2)$ and $\mathcal{O}(xM_R^2)$ as $\frac{M_\pi^2}{F^2}\Delta M_\pi^2 g_2(M_\pi,T) + \mathcal{O}(e^4, x^2 M_R^2)$ with g_2 in (B17).

With the above structure, let us consider again the formal cutoff Λ dependence in order to arrive to a consistent modification of the thermal sum rule. For that purpose, recall the large q^2 expansion of the $T=0$ part (which contains the UV divergences) of the pion-photon exchange contribution:

$$\int d^4q \frac{1}{q^2}\frac{(2p-q)^2}{(p-q)^2-M_\pi^2} = \int d^4q \frac{1}{q^2}\left[1 + \frac{4M_\pi^2}{q^2} - 2\frac{p\cdot q}{q^2} - 4\frac{(p\cdot q)^2}{(q^2)^2} + \mathcal{O}(q^{-3})\right] \tag{29}$$

where the on-shell condition $p^2 = M_\pi^2$ has been used. Now, taking into account that, at $T = 0$:

$$\int d^4q \frac{1}{q^2} \frac{p \cdot q}{q^2} = 0$$

by parity, and

$$\int d^4q \frac{1}{q^2} \frac{(p \cdot q)^2}{(q^2)^2} = p_\mu p_\nu \int d^4q \frac{1}{q^2} \frac{q^\mu q^\nu}{(q^2)^2} = \frac{1}{4} p_\mu p_\nu g^{\mu\nu} \int d^4q \frac{1}{q^2} \frac{q^2}{(q^2)^2} = \frac{M_\pi^2}{4} \int d^4q \frac{1}{(q^2)^2}$$

we find that the $\log \Lambda$ contribution in the photon exchange term (29) equals

$$3M_\pi^2 \int d^4q \frac{1}{(q^2)^2}$$

and therefore cancels with the $\log \Lambda$ part of the $\rho_V - \rho_A$ contribution

$$\frac{3}{F_\pi^2} \int d^4q \frac{1}{(q^2)^2} \int_0^\infty ds \; s \left[\rho^V(s) - \rho^A(s)\right]$$

when using the corresponding $\mathcal{O}(M_\pi^2)$ extension (28) of the WSR. Recall that, as we commented before in the SPL case, when considering the $\log \Lambda$ correction one has to keep the T-dependent function multiplying both the pion-photon exchange and the $\rho_V - \rho_A$ contributions.

Therefore, at least at the order considered here, we find that the thermal part of the sum rule (26)-(27) can be consistently modified at $M_\pi \neq 0$ by a) Replacing the sum and integral in the second term in the r.h.s. of (26) by the pion-photon exchange contribution (7) and b) Modifying the T-dependent function multiplying the $V - A$ vacuum spectral function difference, i.e $f(T)$ in (27), by:

$$f(T) \to 1 - 2\frac{g_1(M_\pi, T)}{F^2} + \frac{M_\pi^2}{F^2} g_2(M_\pi, T) \tag{30}$$

Such modification is consistent with ChPT (model independent) and with the required UV behaviour at this order, i.e up to $\mathcal{O}(xM_R^2)$ as explained. We then see, as anticipated in section II, that the "chiral restoring" function f is modified by the T-increasing term g_2 in (30) which typically for $T \gg M_\pi$ behaves as TM_π instead of the T^2 decreasing behaviour (restoring) coming from the g_1 part, but which for physically realistic masses and temperatures $T \sim M_\pi$ can be of the same numerical order as the restoring term. In addition, the nontrivial modification of the pion-photon exchange introduces a p-dependence, a nonzero imaginary part at this order and an additional T-increasing term for the real part. Recall that the scalar thermal mass coming from the Debye term plus the chiral limit of pion-photon exchange, is also growing with T against the chiral behaviour, so that our analysis in this section of the structure of the sum rule shows that introducing $M_\pi \neq 0$ corrections amplifies even further this shadowing effect and there is finally no trace of a recognizable chiral-restoring effect in the EM pion mass difference. Put in different words, and as recalled in section II A, chiral symmetry is ultimately responsible for keeping the EM pion mass difference almost unchanged and softly increasing with T.

The analysis we have just shown clarifies the structure of the sum rule and the formal role of the resonance contributions, to the order considered, equivalent to that in our previous ChPT calculation. Our next step will be to explore to what extent we can trust this order for numerically relevant masses and temperatures. For that purpose, we will consider explicitly a model in which ρ and a_1 resonances are coupled explicitly to pion and photon fields, which allows to estimate the typical size of the corrections to our previous ChPT and sum-rule analysis of the EM self-energy difference.

IV. EXPLICIT RESONANCE ANALYSIS

In order to estimate the size of the corrections to the ChPT $\mathcal{O}(p^4)$ result for the EM pion self-energy difference and also to contrast the previous sum rule analysis of the role of resonances and chiral restoration, we will consider the self-energy calculation in a model where ρ and a_1 resonances are explicitly included in the lagrangian, within the

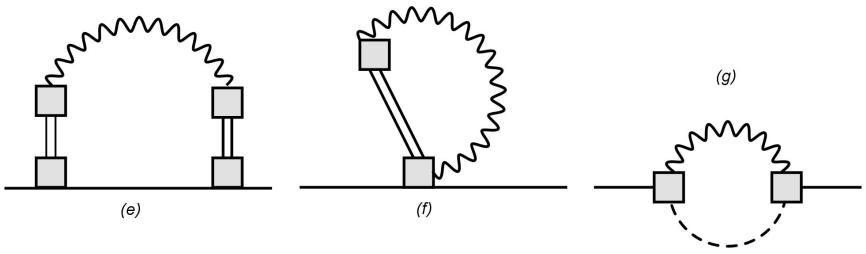

Figure 5. Resonance Saturation 1-PI diagrams contributing at leading one-loop order to the charged-neutral pion self-energy difference. ρ and a_1 particles are represented by double and dashed lines, respectively. The relevant vertices including charged pions, resonances and photons are drawn as grey boxes.

RS approach. In particular, we will take the resonance lagrangian in [48] where resonances are coupled to pions in the chiral lagrangian. Without electromagnetic contributions, the resonance couplings produce $\mathcal{O}(p^4)$ contributions to the non-EM LEC when those resonances are integrated out, saturating completely those LEC in the RS limit. Actually, we will consider the RS limit for narrow resonances, which is formally well understood in the large-N_c limit [71] since resonance masses are $\mathcal{O}(1)$ but resonance widths as well as pion loops are $\mathcal{O}(1/N_c)$ [15, 72]. Actually, we will formally rely on the large-N_c limit to classify the resonance diagrammatic contributions. We shall see that a consistent matching with ChPT would require formally higher order diagrams, although RS to leading order would be enough to estimate the corrections to the ChPT result and hence its validity range. With EM interactions, resonances contribute already to the C constant in (2), saturating it almost completely [48, 73], which is actually what we have discussed in section III A in the context of Das sum rule [45]. Therefore, within the RS hypothesis, we start from the lagrangian in (2) with $C = 0$ plus the resonance lagrangian in [48], whose relevant propagators and vertices can also be found in that paper. We consider in this model the diagrams contributing to the EM pion mass self-energy difference. Alternatively, as done for instance in [32, 47], one can start from (17) and write down the relevant Compton scattering diagrams. Thus, to leading order in RS and to $\mathcal{O}(e^2)$, we consider the one-loop diagrams shown in Fig.5 for the charged-neutral pion self-energy difference, to be added to diagram (c) in Fig.1. We do not need to consider tadpole contributions (diagram (a) in Fig.1) since, as we have just explained, the tree level charged and neutral pion masses are the same to leading order in RS. In that sense, note that pion loops carry also additional factors $F^{-2} = \mathcal{O}(N_c^{-1})$. Diagram (b) in Fig.1 has to be considered formally to absorb the loop divergences in the corresponding EM LEC [73], which is a $T = 0$ contribution not altering our finite T analysis. Actually, by the RS procedure, one finds also the finite resonance contribution to those LEC [73]. Note also that diagram (e) in Fig.5 represents the extension of diagram (d) in Fig. 1 when the $\pi\pi\gamma$ vertex is corrected by a form factor coming from ρ exchange.

Let us then consider the contribution to the neutral-charged self-energy difference of the finite temperature integrals corresponding to the diagrams in Fig.5. After some algebraic manipulations, similar to those performed in section II, we can write them in terms of the G and J_T functions described in Appendix B as follows:

$$\begin{aligned}\Delta\Sigma^{(e)} &= -4e^2M_\rho^4 T\sum_n\int\frac{d^3\vec{q}}{(2\pi)^3}\frac{(p\cdot q)^2-p^2q^2}{q^2\left(M_\rho^2-q^2\right)^2\left((p-q)^2-M_\pi^2\right)}+e^2T\sum_n\int\frac{d^3\vec{q}}{(2\pi)^3}\frac{1}{q^2}\\ &= \Sigma_{\gamma Ex}(\omega+i\epsilon,\omega^2=E_p^2;T)+e^2\left[1-M_\rho^2\frac{\partial}{\partial M_\rho^2}\right][G(M_\rho,T)-G(M_\pi,T)\\ &- (4M_\pi^2-M_\rho^2)J_T(M_\rho,M_\pi;\omega+i\epsilon,\omega^2=E_p^2)]\end{aligned} \tag{31}$$

$$\Delta\Sigma^{(f)} = -3e^2\left(\frac{F_V}{F_\pi}\right)^2 T\sum_n\int\frac{d^3\vec{q}}{(2\pi)^3}\frac{1}{M_\rho^2-q^2} = -3e^2\left(\frac{F_V}{F_\pi}\right)^2 G(M_\rho,T) \tag{32}$$

$$\Delta\Sigma^{(g)} = 3e^2\left(\frac{F_A}{F_\pi}\right)^2 T\sum_n\int\frac{d^3\vec{q}}{(2\pi)^3}\frac{1}{M_{a_1}^2-q^2}$$
$$+\,2e^2\left(\frac{F_A}{F_\pi}\right)^2 T\sum_n\int\frac{d^3\vec{q}}{(2\pi)^3}\frac{1}{M_{a_1}^2\left(M_{a_1}^2-(p-q)^2\right)}\left(\frac{(p\cdot q)^2}{q^2}-p^2\right)$$
$$=\frac{1}{2}e^2\left(\frac{F_A}{F_\pi M_{a_1}}\right)^2\left[\left(5M_{a_1}^2-M_\pi^2\right)G(M_{a_1},T)+(M_{a_1}^2-M_\pi^2)G(0,T)\right.$$
$$\left.-\,(M_{a_1}^2-M_\pi^2)^2 J_T(0,M_{a_1};\omega+i\epsilon,\omega^2=E_p^2)\right] \tag{33}$$

with $\Sigma_{\gamma Ex}(\omega+i\epsilon,\omega^2=E_p^2;T)$ the ChPT contribution in eq.(9), $E_p^2=|\vec{p}|^2+M_\pi^2$ and we have taken $F_VG_V=F^2$ in the (e) contribution, where G_V is the coupling constant entering the $\rho\pi\pi$ vertex [67, 73]. The $T=0$ contributions of the above diagrams, which include the UV divergent part to be absorbed in the low-energy constants, can be found in [73].

In connection with our discussion in previous chapters, let us discuss the x-expansion (defined in section III A) of the different contributions. The leading order $\mathcal{O}(M_R^2)$ to the self-energy difference comes from the $T=0$ part of diagrams (f) and (g) and one can check that its UV λ-pole contribution in DR cancels precisely using the leading part of the WSR (28), i.e, $F_V^2M_V^2=F_A^2M_A^2+\mathcal{O}(xM_R^2)$. Recall that within the RS approach, we are taking the resonance spectral functions as completely saturated by the ρ and a_1 poles. On the other hand, its finite part gives precisely the narrow resonance limit of (24), i.e, the value for $C=\frac{3F_V^2M_V^2}{32\pi^2}\log(M_A^2/M_V^2)$ [45] in (4), which saturates the pion mass difference at $T=0$, accordingly with the RS hypothesis and with our discussion in Section III A. In turn, note that the form factor contribution (f) in (31) is UV finite as can be checked from direct power counting and by the cancelation of the λ pole in the expression given in (31) in terms of G and J_T, recalling the pole contribution of these two functions given in Appendix B.

To $\mathcal{O}(xM_R^2)$, the form factor contribution (e) in (31) reduces to the first term $\Sigma_{\gamma ex}$, which is the ChPT result of diagram (d) analyzed in section II. We have checked that the remaining terms in (31), once their $T=0$ par is separated, do not contribute to this order, expanding the J_T term in inverse powers of M_ρ^2. On the other hand, diagrams (f) and (g) both contribute with a zero temperature $M_\pi^2\lambda$ pole. In the case of diagram (f), that pole comes from including the M_π^2 correction in the WSR, i.e, $F_V^2M_V^2=F_A^2M_A^2+F_\pi^2M_\pi^2$ according to (28). The T-dependent part of (32) is exponentially suppressed as $\mathcal{O}\left(e^{-M_\rho/T}\right)=\mathcal{O}\left(e^{-1/\sqrt{x}}\right)$ according to (B8), while in (33) we have also checked that the $\mathcal{O}(T^2)$ contributions coming from the $M_{a_1}^2G(0,T)$ and $M_{a_1}^4J_T$ terms cancel each other, once the J_T is expanded in inverse powers of $M_{a_1}^2$.

An important comment at this point is that one does not recover from the leading order RS approach the full result of the ChPT calculation given in (11). The second term and the $-4Zg_1$ contribution in the r.h.s of (11), both coming from tadpole diagrams of the type (a) in Fig.1, appear in higher order diagrams in the RS expansion. For instance, diagrams of type (a) in Fig.1 in which one of the internal charged lines is dressed with the resonance diagrams in Fig.5 will contribute to the second term in the r.h.s of (11). Also, diagrams in Fig.5 in which a pion tadpole is attached to the $\rho\gamma\pi\pi$ or to the $a_1\gamma\pi$ vertices, would contribute as Zg_1. In addition, vector and axial vector propagators are modified by loop diagrams beyond RS. Their residues are meant to contribute also at $\mathcal{O}(T^2)\sim\mathcal{O}(xM_R^2)$ via the $\rho-a_1$ mixing effect discussed in section III [10, 46, 74], while the mass and width modifications of the spectral functions are expected to be of $\mathcal{O}\left(e^{-1/\sqrt{x}}\right)$[10–12, 17]. The $\rho\gamma$ coupling can also receive finite T corrections [11]. Some of those corrections to the EM self-energy difference, but clearly not all of them, could be parametrized in a T-dependent form factor as considered in [32].

In any case, what is relevant for our present discussion is that all these higher order diagrams come with prefactors coming from the vertices, which are formally subleading in the $1/N_c$ counting, for instance those coming with inverse powers of F^2 in (11), as compared to those considered in Fig.5. This is the formal way to keep track of the leading RS contributions. As emphasized above, we will stick here to the strict RS limit, which is consistent with considering free resonance spectral functions with zero widths, in order to estimate the size of the corrections to the ChPT analysis. Actually, we recall that due to the model independency of the ChPT framework, we are sure that the final answer to $\mathcal{O}(xM_R^2)$ is that given by (11). Therefore, we estimate the corrections as the result of evaluating the thermal contributions (31)-(33) once the $T=0$ and the $\mathcal{O}(xM_R^2)$ given by the first term in the r.h.s of (31) are subtracted. In doing so, we note that the next order of correction is actually $\mathcal{O}(x^2M_R^2)$. In particular, there are $\mathcal{O}(g_1(M_\pi,T)M_\pi^2/M_\rho^2)$ and $\mathcal{O}(T^2M_\pi^2/M_{a_1}^2)$ terms arising, respectively, from (31) and (33). Note that these terms are not present in the chiral limit. As commented above, the contribution (32) is exponentially suppressed, and, we have also checked that the

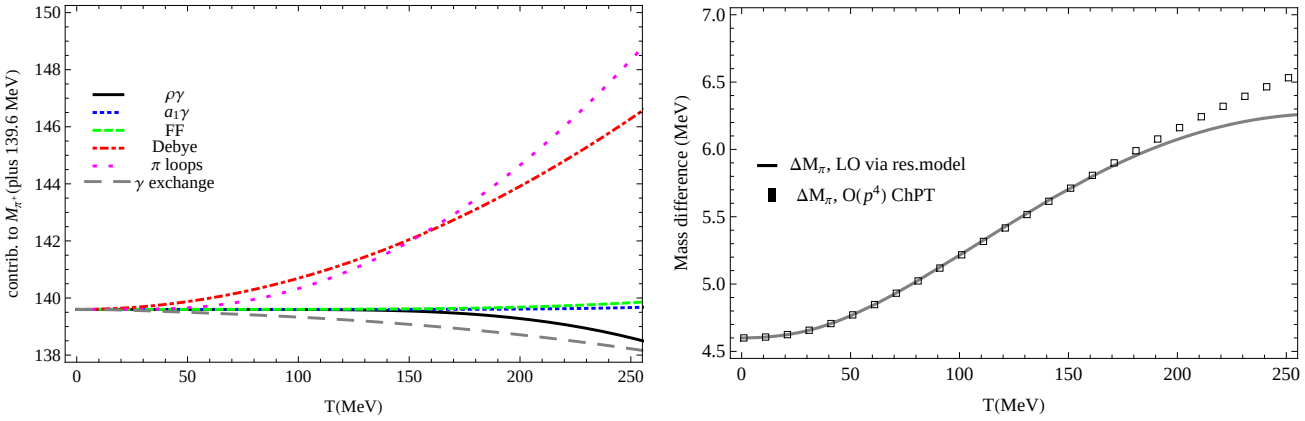

Figure 6. Left: The different thermal contributions to the charged pion mass, including the resonance model ones, as explained in the main text. Right: Comparison between the EM mass difference obtained with just ChPT and that including the Resonance Saturation leading order contributions.

imaginary part contributions coming from (31) and (33) are also exponentially suppressed with respect to the ChPT result arising from the first term in (31) and analyzed in section II B.

We have evaluated numerically the resonance contributions to the real part of the self-energy in the static limit, in order to get an approximate idea of the expected size of the corrections to the ChPT result. The results are showed in Fig.6. In the left panel of that figure, we show the different thermal contributions to the charged pion mass given by the diagrams in Figs.1 and 5, all shifted to the $T = 0$ mass, and discussed here and in section II. Namely, the pion tadpole loops given generically by diagram (a) in Fig.1, the Debye term from diagram (c) in Fig.1, the photon exchange term from diagram (d) in Fig.1, the form factor (FF) contribution of diagram (e) in Fig.5 excluding the ChPT photon exchange term, the $\rho\gamma$ photon loop of diagram (f) in Fig.5 and the $a_1\gamma$ exchange of diagram (g) in Fig.5. In the right panel we show the deviations of the charged-neutral mass difference calculated within the resonance model with respect to the same ChPT calculation. The numerical values of F_V, F_A and G_V are those of [48], compatible with $F_V G_V = F^2$. There are no significant changes when using values coming from more recent fits like [75, 76]. We have used the physical masses for the resonances, namely $M_{a_1} = 1260$ MeV and $M_\rho = 770$ MeV.

From this plot, we observe that resonant contributions additional to the ChPT result activate thermally around 170-200 MeV, which leaves big room for the validity range of the ChPT result. We recall that those resonant contributions do not include $\rho - a_1$ mixing to leading order, which is accounted for already in the ChPT result, as discussed above. Therefore, the ChPT calculation for this observable is dominant and robust throughout its own applicability range, i.e, below the chiral phase transition. It must be pointed out that, in addition to the size of the absolute value of those resonant corrections, there is an approximate numerical cancelation between the FF and $\rho\gamma$ terms, as can be seen in the left panel of Fig.6.

V. CONCLUSIONS

In this work we have performed a thorough analysis of the electromagnetic effects in the pion self-energy at finite temperature, within Chiral Perturbation Theory to one loop, which allows to obtain model-independent results, and also including the effect of vector and axial-vector resonant states. The latter have been studied within the context of sum rules and in a explicit resonance saturation approach and allows to understand in a clearer way which contributions come from chiral restoration via $V - A$ mixing. Apart from the link with chiral symmetry restoration, particular attention has been paid to discuss phenomenological effects and gauge invariance.

Within one-loop ChPT we have provided the full expressions for the charged and neutral pion self-energy for physical pion masses and external momenta. There are important differences with respect to a previous calculation in the chiral limit and vanishing external momentum. The real part of the self-energy and hence the dispersion relation is momentum dependent. That dependence is rather soft for the relevant range of temperatures, which we have studied by comparing the momentum-averaged self-energy, weighted by pion thermal distributions, with the mass defined in the static limit. Including the physical pion mass gives rise to new terms making the EM pion mass difference increase with temperature. The net result is a soft increasing behaviour for that difference, which makes it presumably undetectable in the neutral-charged pion spectra observed in Heavy ion Collisions, as it seems to be the case with

the measurements performed so far. The increasing is softer for the momentum averaged mass than for the static one. The important formal point here is that chiral symmetry restoration via vector-axial vector mixing plays an important role for keeping that difference small, which follows from our combined ChPT and resonance analysis.

Another important conclusion of our present work is the analysis of the EM damping rate for charged pions from the imaginary part of the self-energy. Here it is crucial to work in a physical gauge, we choose the strict Coulomb gauge, to get a meaningful answer, since only physical photon degrees of freedom are in thermal equilibrium. Thus, the contributions to the imaginary part come from bremsstrahlung-like processes with physical quasiparticle thermal photons at vanishing spatial momentum, whose contribution is thermally enhanced, giving rise to an infrared finite result at this order for the imaginary part of the retarded self-energy. The result for the EM damping rate comes only from the transverse modes, it is linearly increasing with temperature, vanishes at zero pion momentum and behaves asymptotically as a constant for large momentum. We have analyzed possible phenomenological consequences of this result. The electromagnetic damping is added to the standard ChPT one so that mean free paths and free times of charged and neutral pions become different. The electromagnetic corrections are comparable in size to the neutral ones up to $T \sim 60$ MeV. Transport coefficients are expected to be reduced by this effect around a 10% near the kinetic freeze-out region, with a larger effect in the electrical conductivity than in viscosities. The freeze-out temperatures for charged and neutral components would also be different, although the expected effect is only about 2 MeV.

We have also studied in detail how the sum rule relating the electromagnetic pion mass difference in the soft and chiral limits with the $V-A$ spectral function difference, is modified by the inclusion of a finite pion mass and nonzero momentum. The standard derivation of the sum rule is no longer applicable and we have found the required modifications in order to match the ChPT model-independent result at finite temperature. These are the modification of the photon-exchange contribution to account for the mass and momentum dependence, as well as the multiplicative function in the $V-A$ spectral function difference, which acquires an additional mass-dependent T-dependent increasing term. This analysis has been performed to leading and next to leading order in the expansion in $x \sim T^2/M_R^2 \sim M_\pi^2/M_R^2$ with M_R the resonance masses, i.e, including $\mathcal{O}(M_R^2)$ and $\mathcal{O}(xM_R^2)$, equivalent to the ChPT analysis.

In order to confirm the ChPT and sum-rule analysis and also to estimate the next order corrections, we have carried out a explicit calculation of the corrections to the electromagnetic pion self-energy difference at finite temperature within a resonance saturation approach. Thus, we have been able to estimate next to next to leading order corrections, which show up at $\mathcal{O}(x^2M_R^2)$. Those corrections remain numerically small for the range of temperatures relevant within Heavy Ion Collisions, which results in a rather large applicability range of our ChPT analysis.

ACKNOWLEDGMENTS

Work partially supported by the Spanish Research contract FPA2011-27853-C02-02 and the FPI programme (BES-2009-013672). We acknowledge the support of the EU FP7 HadronPhysics3 project.

Appendix A: General definitions and properties of spectral functions and dispersion relations

Throughout this work we follow closely [1] and [52] regarding the finite-temperature formalism. We summarize in these Appendices the most relevant results for our purposes in this work.

For a scalar field or current, the time-ordered version of the propagator in the Euclidean IT Formalism is given by:

$$G(\vec{x},\tau) = \langle \mathcal{T}\phi(\vec{x},-i\tau)\phi(0)\rangle_T$$

where the subscript T indicates a thermal average, $\omega_n = 2\pi nT$ is the bosonic Matsubara frequency with $n \in \mathbb{Z}$ and time-ordering $\mathcal{T}$ is along $t = -i\tau$ with $\tau \in [-\beta,\beta]$ (time differences). Its Fourier representation can be written as:

$$G(i\omega_n,|\vec{p}|) = \int_T d^4x G(\vec{x},\tau)e^{-i\omega_n\tau}e^{-i\vec{p}\cdot\vec{x}} = \frac{1}{\omega_n^2+E_p^2+\Sigma(i\omega_n,|\vec{p}|;T)} \tag{A1}$$

where $\int_T d^4x \equiv \int_0^\beta d\tau \int d^3\vec{x}$, $E_p^2 = |\vec{p}|^2 + M_0^2$ and M_0^2 is the tree level mass. We will keep the $(+,-,-,-)$ metric with the Euclidean $p_0^E \equiv i\omega_n$ so that we write for instance $p^2 = (i\omega_n)^2 - E_p^2$ which will become the Minkowski p^2 after analytic continuation (see below). In the above equation, Σ is the IT self-energy function, which in the thermal case depends independently on frequency and three-momentum and explicitly on T.

The analytical continuation from external discrete frequencies to continuous ones can be carried out once all the internal Matsubara sums have been performed and gives rise to the retarded and advanced propagators defined as:

$$G_{R,A}(\omega,|\vec{p}|) = \mp iG(i\omega_n = \omega \pm i\epsilon, |\vec{p}|) \tag{A2}$$

with $\omega \in \mathbb{R}$ and $\epsilon > 0$ and we define from these propagators the spectral function as $\rho(\omega,|\vec{p}|) = 2\mathrm{Im}\, iG_R(\omega,|\vec{p}|;T)$ whose main properties we discuss below. The spectral function is odd in ω and in the free case, for which $\Sigma = 0$, it reads $\rho_0(\omega,|\vec{p}|) = 2\pi \mathrm{sgn}(\omega)\delta(\omega^2 - E_p^2)$.

In the interacting case and in the perturbative regime considered in this paper (see comments below), the self-energy contributions come from loop diagrams which generate cuts for $\mathrm{Im}\,\Sigma$ along the real axis, so that we write $\mathrm{Im}\,\Sigma(\omega \pm i\epsilon, |\vec{p}|) = \mp 2\omega\Gamma(\omega,|\vec{p}|)$ with $\Gamma > 0$ along the cuts.

The dispersion relation is determined by the poles of $G_R(\omega,|\vec{p}|)$, which lie below the real axis, or equivalently by the spectral function. If we denote the position of the poles by $z_{pole} = \omega_p - i\gamma_p$, with $\gamma_p > 0$ the thermal damping rate, we have then $z_{pole}^2 = E_p^2 + \mathrm{Re}\,\Sigma(z_{pole},|\vec{p}|;T) - 2iz_{pole}\Gamma(z_{pole},|\vec{p}|;T)$.

In this work we will work within the perturbative regime: $\Sigma \ll E_p^2$, $\omega_p^2 = E_p^2(1 + \mathcal{O}(\Sigma/E_p^2))$, $\Gamma_p = \mathcal{O}(\Sigma/E_p)$ so that the perturbative solution of the pole equations reads $\omega_p^2 = E_p^2 + \mathrm{Re}\,\Sigma(E_p,|\vec{p}|;T)$, $\gamma_p = \Gamma(E_p,|\vec{p}|;T) = -\mathrm{Im}\,\Sigma(E_p + i\epsilon,|\vec{p}|)/2E_p$, where we have made use of the fact that $\mathrm{Re}\,\Sigma(\omega,|\vec{p}|)$ and $\Gamma(\omega,|\vec{p}|)$ are even functions of ω. Thus, there are two perturbative poles at $\pm\omega_p - i\gamma_p$.

From the previous properties, one can define a complex function $G(z,|\vec{p}|)$ for complex z analytic for z off the real axis and such that the IT propagator is $G(z = i\omega_n,|\vec{p}|)$ and the retarded/advanced propagators are $G_{R,A}(\omega,|\vec{p}|) = \mp iG(z = \omega \pm i\epsilon,|\vec{p}|)$ with $\omega \in \mathbb{R}$, i,e,

$$G(z,|\vec{p}|) = \frac{-1}{z^2 - E_p^2 - \Sigma(z,|\vec{p}|;T)} \tag{A3}$$

In particular, in the perturbative regime described above, it is easy to check that the above function does not have (perturbative) poles and has the same cuts as $\Sigma(\omega)$ along the real axis.

Let us comment also on the spectral function representation of the different propagators. Applying Cauchy's theorem to $G(z)$ in (A3), with its analytical structure discussed above, on a suitable contour surrounding the real axis from above and from below, one arrives to a dispersion relation valid for the retarde/advanced propagators and for the IT one, from the same spectral function, namely:

$$G(z,|\vec{p}|) = \int_{\infty}^{\infty} \frac{d\omega'}{2\pi} \frac{\rho(\omega',|\vec{p}|;T)}{\omega' - z} \qquad (z \notin \mathbb{R}) \tag{A4}$$

Thus, $z = i\omega_n$ correspond to the IT propagator and $z = \omega \pm i\epsilon$ to the retarded/advanced ones.

The above frequency representation is the more adequate one when working at finite temperature. As commented, the analytical continuation of the IT propagator yields naturally the retarded propagator, which has the correct analytic structure in terms of the physical states. In addition, it is valid for any cut structure of G along the real axis, including possible Landau-like purely thermal cuts (see below). It is possible also to define thermal expectation values of T-ordered products along $t \in \mathbb{R}$, within the so-called real-time formalism of Thermal Field Theory [52]. However, those real-time T-ordered products do not have a representation like (A4), not even in the free case, nor they describe the spectral properties of the theory in the general interacting case. The problem of how to obtain the retarded correlator from the RT one is discussed in [77].

It is instructive to relate the above "energy" spectral representation with the usual s-representation used customarily at $T = 0$. First, let us write (A4) as:

$$G(z,|\vec{p}|) = \int_{0}^{\infty} \frac{d\omega'}{2\pi} \frac{2\omega'\rho(\omega',|\vec{p}|;T)}{(\omega')^2 - z^2} \qquad (z \notin \mathbb{R}) \tag{A5}$$

Now, denoting $s = z^2 - |\vec{p}|^2$ and $s' = (\omega')^2 - |\vec{p}|^2$ and assuming that the following two conditions hold: i) $\rho(\omega' > 0, |\vec{p}|)$ is a function only of s', so that G is only a function of s and ii) $G(s)$ is analytic for $0 > s \in \mathbb{R}$, the lower limit of integration in (A5) can be extended to $-|\vec{p}|$ so that by changing variables from ω' to s' on ends up at $T = 0$ with:

$$G(s) = \int_{0}^{\infty} ds' \frac{\hat{\rho}(s')}{s - s'} \qquad (s \notin \mathbb{R}) \tag{A6}$$

with $\hat{\rho}(s') = (-1/\pi)\mathrm{Im}\, G(s'+i\epsilon)$ for $\omega' > 0$. Note also the 2π factor conventionally included in the normalization of the spectral function at $T = 0$. Alternatively, one can arrive to (A6) directly from the analytic properties of G in the s complex plane. It is important to remark that none of the conditions i) and ii) above are met at $T \neq 0$ since Lorentz covariance is broken and Landau cuts may be present. At $T = 0$, the representation (A6) allows to define the T-ordered product $-iG(s+i\epsilon)$ with $s \in \mathbb{R}$.

For the case of conserved vector and axial-vector current propagators at finite temperature, there are two independent tensor structures $P_T^{\mu\nu}$, $P_L^{\mu\nu}$ which are four-dimensionally transverse [1], P_T being also three-dimensional transverse:

$$P_T^{ij}(q) = \delta^{ij} - \frac{q^i q^j}{|\vec{q}|^2}; \qquad P_T^{00} = P_T^{0i} = P_T^{i0} = 0$$
$$P_L^{\mu\nu}(q) = \frac{q^\mu q^\nu}{q^2} - g^{\mu\nu} - P_T^{\mu\nu} \tag{A7}$$

where $q^0 = i\omega_n$. We remind that the metric signature here is $(+---)$.

Therefore, any correlator of conserved vector or axial-vector currents can be written as

$$\Pi^{\mu\nu}(i\omega_n, \vec{q}) = \Pi^T(q) P_T^{\mu\nu}(q) + \Pi^L(q) P_L^{\mu\nu}(q) \tag{A8}$$

At $T = 0$, one has simply $\Pi^T = \Pi^L \equiv \Pi$ so that $\Pi^{\mu\nu}(q) = \left(\frac{q^\mu q^\nu}{q^2} - g^{\mu\nu}\right)\Pi(q)$. [1]

For the photon case, its Euclidean propagator in an arbitrary covariant gauge reads:

$$D^{\mu\nu}(i\omega_n, \vec{q}) = \frac{1}{\omega_n^2 + |\vec{q}|^2 + \Sigma_T(i\omega_n, \vec{q})} P_T^{\mu\nu}(q) + \frac{1}{\omega_n^2 + |\vec{q}|^2 + \Sigma_L(i\omega_n, \vec{q})} P_L^{\mu\nu}(q) + \alpha \frac{q^\mu q^\nu}{(q^2)^2}$$

$$\Sigma^{\mu\nu} = \Sigma_T P_T^{\mu\nu} + \Sigma_L P_L^{\mu\nu}$$

so that the free ($\Sigma = 0$) Euclidean photon propagator is:

$$D_0^{\mu\nu}(i\omega_n, \vec{q}) = \frac{g^{\mu\nu}}{q^2} + (\alpha - 1)\frac{q^\mu q^\nu}{(q^2)^2} \tag{A9}$$

As explained in the text, we will also need the free photon propagator in the strict ($\alpha = 0$) Coulomb gauge, which reads [1]:

$$D_0^{\mu\nu}(i\omega_n, \vec{q}) = -\frac{g^{\mu 0} g^{\nu 0}}{|\vec{q}|^2} - \frac{P_T^{\mu\nu}}{q^2} \tag{A10}$$

Appendix B: Thermal loop functions for self-energies

We describe here the main properties of the typical thermal loop integrals appearing throughout this work. They come from the corresponding $T = 0$ one through the replacements

$$q_0 \to i\omega_n = i2\pi n T \quad , \quad \int \frac{d^4p}{(2\pi)^4} \to iT \sum_n \int \frac{d^3\vec{p}}{(2\pi)^3} \tag{B1}$$

in the IT formalism, with $n \in \mathbb{Z}$.

First, consider the tadpole integral of the free propagator:

---

[1] Our convention for vector and axial-vector current correlators corresponds to that in [45, 63–65] but differs from [30, 47]. The latter authors include an additional q^2 multiplying the $\Pi(q)$ functions.

$$G(M,T) = T\sum_{n=-\infty}^{\infty}\int\frac{d^3\vec{q}}{(2\pi)^3}\frac{1}{\omega_n^2+E_q^2} = G(M,0) + g_1(M,T) \tag{B2}$$

with:

$$g_1(M,T) = \frac{1}{2\pi^2}\int_0^\infty dq\frac{q^2}{E_q}n_B(E_q), \tag{B3}$$

with $E_q \equiv \sqrt{q^2+M^2}$,

$$n_B(x) = \frac{1}{e^{\beta x}-1} \tag{B4}$$

and the $T=0$ part containing the UV divergence ($T\neq 0$ UV divergences are always contained in the $T=0$ part) is given in dimensional regularization $D=4-\epsilon$ by:

$$G(M,0) = 2M^2\lambda + \frac{M^2}{16\pi^2}\log\frac{M^2}{\mu_\chi^2} \tag{B5}$$

with

$$\lambda = \frac{1}{2}(4\pi)^{-D/2}\Gamma\left(1-\frac{D}{2}\right)\mu_\chi^{D-4} \tag{B6}$$

being μ_χ the renormalization ChPT scale and Γ the Euler gamma function. For the $T=0$ part we follow the same notation as in [14, 15].

The $g_1(M,T)$ function has the following asymptotic behaviours:

$$T\gg M:\ g_1(M,T) = \frac{T^2}{12}\left[1-6\frac{M}{T}+\mathcal{O}(\frac{M^2}{T^2}\log\frac{M}{T})\right] \tag{B7}$$

$$T\ll M:\ g_1(M,T) = (2\pi)^{-3/2}\left(\frac{M}{T}\right)^{1/2}e^{-M/T}\left[1+\mathcal{O}(T/M)\right]+\mathcal{O}(e^{-2M/T}) \tag{B8}$$

Second, we analyze the one-loop integral appearing in self-energy diagrams:

$$J_T(m_1,m_2;i\omega_m,|\vec{p}|) = T\sum_{n=-\infty}^{\infty}\int\frac{d^3\vec{q}}{(2\pi)^3}\frac{1}{q^2-m_1^2}\frac{1}{(q-p)^2-m_2^2} \tag{B9}$$

for arbitrary masses m_1 and m_2.

As discussed above, we are interested in the analytic continuation of the above integral $i\omega_m\to z$ for complex z off the real axis. In particular for $z=\omega+i\epsilon$ with $\omega\in\mathbb{R}$, that would give rise to the retarded function appearing in the retarded self-energy and hence describing the dispersion relation as explained in Appendix A. The analytic continuation is performed after evaluating the internal Matsubara sum in n, which can be carried out using standard finite-temperature methods. In fact, inserting the spectral representation (A4) for the two IT propagators inside the integral and using the formula:

$$T\sum_n\frac{1}{\omega_1-i\omega_n}\frac{1}{\omega_2-i(\omega_m-\omega_n)} = \frac{n_B(\omega_1)-n_B(-\omega_2)}{\omega_1+\omega_2-i\omega_m} \tag{B10}$$

we arrive to the retarded continuation of J_T:

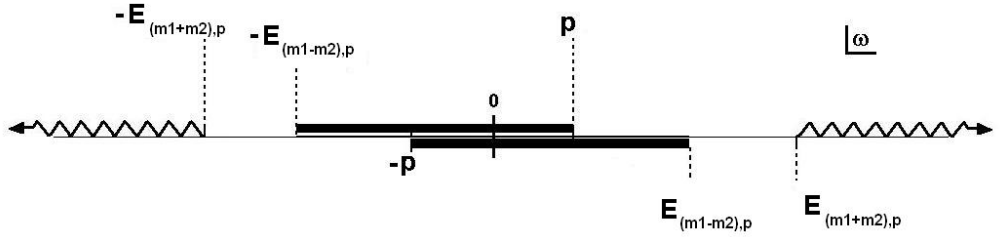

Figure 7. Cut structure of the loop integral $J_T(m_1, m_2; \omega, |\vec{p}|)$ in the ω complex plane with $E_{(m_1 \pm m_2),p} \equiv \sqrt{|\vec{p}|^2 + (m_1 \pm m_2)^2}$ and $p \equiv |\vec{p}|$.

$$J_T(m_1, m_2; z, |\vec{p}|) = -\int \frac{d^3\vec{q}}{(2\pi)^3} \frac{1}{4E_1E_2} \left\{ [1 + n_B(E_1) + n_B(E_2)] \left[\frac{1}{z - E_1 - E_2} - \frac{1}{z + E_1 + E_2} \right] \right.$$
$$\left. + \, [n_B(E_1) - n_B(E_2)] \left[\frac{1}{z + E_1 - E_2} - \frac{1}{z - E_1 + E_2} \right] \right\} \tag{B11}$$

where we have used $n_B(x) + n_B(-x) + 1 = 0$ and, for simplicity, we denote $E_1 = \sqrt{|\vec{q}|^2 + m_1^2}$, $E_2 = \sqrt{|\vec{q} - \vec{p}|^2 + m_2^2}$.

Thus, setting $z = \omega + i\epsilon$ with $\omega \in \mathbb{R}$ and separating the real and imaginary parts gives:

$$\mathrm{Re}\, J_T(m_1, m_2; \omega, |\vec{p}|) = \mathrm{Re}\, J_{T=0}(m_1, m_2; \omega, |\vec{p}|) - \frac{1}{2}\mathcal{P} \int \frac{d^3\vec{q}}{(2\pi)^3} \left\{ \frac{n_B(E_1)}{E_1} \left[\frac{1}{(E_1 - \omega)^2 - E_2^2} + \frac{1}{(E_1 + \omega)^2 - E_2^2} \right] \right.$$
$$\left. + \, \frac{n_B(E_2)}{E_2} \left[\frac{1}{(E_2 - \omega)^2 - E_1^2} + \frac{1}{(E_2 + \omega)^2 - E_1^2} \right] \right\} \tag{B12}$$

$$\mathrm{Im}\, J_T(m_1, m_2; \omega + i\epsilon, |\vec{p}|) = \pi \int \frac{d^3\vec{q}}{(2\pi)^3} \frac{1}{4E_1E_2} \left\{ [1 + n_B(E_1) + n_B(E_2)] \, [\delta(\omega - E_1 - E_2) - \delta(\omega + E_1 + E_2)] \right.$$
$$\left. + \, [n_B(E_1) - n_B(E_2)] \, [\delta(\omega + E_1 - E_2) - \delta(\omega - E_1 + E_2)] \right\} \tag{B13}$$

where $\mathcal{P}$ denotes Cauchy's principal value. Note that $\mathrm{Re}\, J$ is even in ω whereas $\mathrm{Im}\, J$ is odd in ω as it corresponds to a spectral function.

The $T = 0$ part of the above functions corresponds to take all n_B functions as vanishing and is equal to $J(s)$ in the notation of [15], with $s = \omega^2 - |\vec{p}|^2$. The explicit expression for $T = 0$ is given in that paper and we do not reproduce it here. The DR UV pole proportional to λ in (B6) is contained in $J(s = 0) = -2\lambda +$ finite terms.

In the general $T \neq 0$ case, the J_T function depends on ω and $|\vec{p}|$ separately due to the breaking of Lorentz covariance in the heat bath. For the case of equal masses $m_1 = m_2$, J_T reduces to the J_0 function analyzed in [78] for thermal pion scattering.

The imaginary part in (B13) is nonzero along the cuts depicted in Fig.7 in the ω complex plane. A detailed account of the contributions to the imaginary part for every cut can be found for instance in [79]. The $\delta(\omega - E_1 - E_2)$ and $\delta(\omega + E_1 + E_2)$ terms in (B13) require $\omega^2 \geq |\vec{p}|^2 + (m_1 + m_2)^2$ to be nonzero, for $\omega > 0$ and $\omega < 0$ respectively. Those two terms account physically for the decay of a particle P with energy and momentum $(\omega, \vec{p})$ into a pair $P \to 12$ and the inverse process $12 \to P$, or equivalently to the direct and inverse scattering processes with intermediate states 12 and $s = \omega^2 - |\vec{p}|^2$ the Mandelstam variable. Therefore, this is the usual $T = 0$ cut giving rise to unitarity, where the factor $n_B(E_1) + n_B(E_2)$ enhance the contribution of the imaginary part due to the presence of 1 and 2 particles in the thermal bath. On the other hand, the terms proportional to $n_B(E_1) - n_B(E_2)$ give rise to the so called Landau cuts, which are purely thermal, and require $\omega^2 \leq |\vec{p}|^2 + (m_1 - m_2)^2$. These Landau cuts arise from processes like $1 \to P2$ and $2 \to P1$ from thermally distributed states 1 and 2. Thus, the $\delta(\omega - E_1 + E_2)$ term produces two contributions, one for $\omega \geq \sqrt{(m_1 + m_2)^2 + |\vec{p}|^2}$ and another one for $-|\vec{p}| \leq \omega \leq |\vec{p}|$, which are depicted as two overlapping cuts in Fig.7. The same happens for the $\delta(\omega - E_1 + E_2)$ term, giving rise to the remaining cuts.

An important case for this paper is $m_1 = 0$, $m_2 = M$, $\omega^2 = |\vec{p}|^2 + M^2$ (on-shell) for which we find, from (B12):

$$\mathrm{Re}\, J_T(0, M; |\vec{p}|) = \mathrm{Re}\, J_{T=0}(0, M) + \frac{1}{16\pi^2} \frac{1}{|\vec{p}|} \mathcal{P} \int_0^\infty dq q \frac{n_B(E_q)}{E_q} \log \left(\frac{|\vec{p}| + q}{|\vec{p}| - q} \right)^2 \tag{B14}$$

where the $T=0$ part can be obtained from the expressions for J in [15] and reads:

$$\mathrm{Re}\, J_{T=0}(0,M) = -2\lambda + \frac{1}{16\pi^2}\left(1 - \log\frac{M^2}{\mu_\chi^2}\right) \tag{B15}$$

Note that in passing from (B12) to (B14), the $n_B(E_1) = n_B(q)$ term, which contained an integrable singularity at $q=0$, vanishes exactly and in the $n_B(E_2)$ term, the change of variable $\vec{q} \to \vec{q} + \vec{p}$ has been performed, so that the integrable singularity at $q=0$ moves to $q = |\vec{p}|$.

A particularly interesting limit is the static one $\vec{p} = \vec{0}$. Taking this limit in our previous expression (B14) yields:

$$\mathrm{Re}\, J_T(0,M;|\vec{p}|\to 0^+) = \mathrm{Re}\, J_{T=0}(0,M) + g_2(M,T) \tag{B16}$$

with:

$$g_2(M,T) = \frac{1}{4\pi^2}\int_0^\infty dq \frac{n_B(E_q)}{E_q} = -\frac{dg_1(M,T)}{M^2} \tag{B17}$$

which behaves asymptotically as $g_2(M,T) \simeq \frac{T}{8\pi M}$ for $T \gg M$ and $g_2(M,T) \simeq (1/2M^2)(2\pi)^{-3/2}(M/T)^{3/2}e^{-M/T}$ for $T \ll M$.

The analysis of the imaginary part for the case of one vanishing mass and on-shell external line is relevant for our discussion in section II B. In this case, the Landau and unitarity cuts in Fig.7 meet at the branch points $\omega^2 = |\vec{p}|^2 + M^2$ ($\omega = \pm E_p$) i.e. precisely at the physical on-shell point. Starting from the general expression (B13), the first δ function requires in that case $E_p = q + \sqrt{|\vec{q}-\vec{p}|^2 + M^2}$. That condition holds only for $q=0$, provided $M>0$ (so that the other solution at $\frac{\vec{p}\cdot\vec{q}}{|\vec{p}|q} \equiv \cos\theta = E_p/|\vec{p}| > 1$ is discarded). Hence, $\delta(E_p - q - E_2) = \frac{E_p\delta(q)}{E_p - |\vec{p}|\cos\theta}$ so that the angular integration in θ can be easily performed, and so on for $\omega = -E_p$ in the second δ contribution in (B13). The third and fourth δ contribution for this case require also $q=0$, with $\omega = E_p$ for the third one and $\omega = -E_p$ for the fourth. Now, because of the $\delta(q)$, in all these terms the only surviving contributions are those proportional to $n_B(q)$, for which the integrand behaves near $q \to 0^+$ as $q^2\frac{n_B(q)}{q} \sim T$. In particular, the $T=0$ contribution vanishes, as it corresponds to the absence of bremsstrahlung for a charged scalar particle in vacuum. In addition, we should take into account that our δ-functions come from the separation in (B11) $\frac{1}{x+i\epsilon} = \mathcal{P}\frac{1}{x} - i\pi\delta(x)$ so that $\delta(x) = \frac{1}{\pi}\frac{\epsilon}{\epsilon^2+x^2}$ and therefore:

$$\int_0^\infty \delta(x) = \lim_{\epsilon\to 0^+}\int_0^\infty \frac{1}{\pi}\frac{\epsilon}{\epsilon^2+x^2} = \lim_{\epsilon\to 0^+}\frac{1}{\pi}\arctan\left(\frac{x}{\epsilon}\right)\Big|_0^\infty = \frac{1}{2}$$

Altogether, we find:

$$\mathrm{Im}\, J_T(0,M;\omega = E_p,|\vec{p}|) = \frac{1}{16\pi}\frac{T}{p}\log\left(\frac{E_p+|\vec{p}|}{E_p-|\vec{p}|}\right) \tag{B18}$$

which in the $|\vec{p}|\to 0^+$ limit becomes $\mathrm{Im}\, J_T(0,M;|\vec{p}|\to 0^+) = \frac{T}{8\pi M}$.

An alternative way to arrive to the result (B18) is to calculate $\mathrm{Im}\, J_T(0,M;\omega+i\epsilon,|\vec{p}|)$ for arbitrary ω off the on-shell point. Taking then the limit $\omega \to E_p^+$ one can then check that (B18) is recovered.

[1] J.I. Kapusta and C.Gale, "Finite temperature field theory. Principles and Applications". Cambridge University Press 2006.
[2] Proceedings of "Quark Matter 2012", Nucl. Phys. A **904-905** (2013).
[3] Y. Aoki, S. Borsanyi, S. Durr, Z. Fodor, S. D. Katz, S. Krieg and K. K. Szabo, JHEP **0906**, 088 (2009).
[4] M. Cheng *et al.*, Phys. Rev. D **81**, 054504 (2010).
[5] S. Borsanyi, Z. Fodor, C. Hoelbling, S. D. Katz, S. Krieg, C. Ratti and K. K. Szabo [Wuppertal-Budapest Collaboration], JHEP **1009**, 073 (2010).
[6] M. Cheng, S. Datta, A. Francis, J. van der Heide, C. Jung, O. Kaczmarek, F. Karsch and E. Laermann *et al.*, Eur. Phys. J. C **71**, 1564 (2011)
[7] A. Bazavov, T. Bhattacharya, M. Cheng, C. DeTar, H. T. Ding, S. Gottlieb, R. Gupta and P. Hegde *et al.*, Phys. Rev. D **85**, 054503 (2012)

[8] A. Andronic, P. Braun-Munzinger and J. Stachel, Phys. Lett. B **673**, 142 (2009) [Erratum-ibid. B **678**, 516 (2009)].
[9] P. Huovinen and P. Petreczky, Nucl. Phys. A **837**, 26 (2010).
[10] C. Song, Phys. Rev. D **53**, 3962 (1996)
[11] C. Song and V. Koch, Phys. Rev. C **54**, 3218 (1996)
[12] R. Rapp and J. Wambach, Adv. Nucl. Phys. **25**, 1 (2000)
[13] S. Turbide, R. Rapp and C. Gale, Phys. Rev. C **69**, 014903 (2004).
[14] J. Gasser and H. Leutwyler, Annals Phys. **158**, 142 (1984).
[15] J. Gasser and H. Leutwyler, Nucl. Phys. B **250**, 465 (1985).
[16] P. Gerber and H. Leutwyler, Nucl. Phys. B **321**, 387 (1989).
[17] A. Dobado, A. Gomez Nicola, F. J. Llanes-Estrada and J. R. Pelaez, Phys. Rev. C **66**, 055201 (2002).
[18] D. Fernandez-Fraile and A. Gomez Nicola, Phys. Rev. D **73**, 045025 (2006).
[19] D. Fernandez-Fraile and A. Gomez Nicola, Eur. Phys. J. C **62**, 37 (2009).
[20] D. Fernandez-Fraile and A. Gomez Nicola, Phys. Rev. Lett. **102**, 121601 (2009).
[21] A. Dobado, F. J. Llanes-Estrada and J. M. Torres-Rincon, Phys. Rev. D **79**, 014002 (2009).
[22] A. Gomez Nicola, J. Ruiz de Elvira and R. Torres Andres, Phys. Rev. D **88**, 076007 (2013).
[23] A. Dobado, J. R. Pelaez, Phys. Rev. **D59**, 034004 (1999).
[24] J. R. Pelaez, Phys. Rev. D **66**, 096007 (2002).
[25] A. Gomez Nicola, J. R. Pelaez and J. Ruiz de Elvira, Phys. Rev. D **87**, 016001 (2013).
[26] J. Gasser and H. Leutwyler, Phys. Lett. B **184**, 83 (1987).
[27] A. Schenk, Phys. Rev. D **47**, 5138 (1993).
[28] J. L. Goity and H. Leutwyler, Phys. Lett. B **228**, 517 (1989).
[29] D. Fernandez-Fraile and A. Gomez Nicola, Phys. Rev. D **80**, 056003 (2009).
[30] C. Manuel and N. Rius, Phys. Rev. D **59**, 054002 (1999).
[31] J. I. Kapusta and V. Visnjic, Phys. Lett. B **147**, 181 (1984).
[32] M. Ladisa, G. Nardulli and S. Stramaglia, Phys. Lett. B **465**, 241 (1999).
[33] A. Gomez Nicola and R. Torres Andres, Phys. Rev. D **83**, 076005 (2011).
[34] R. Torres Andres and A. Gomez Nicola, Prog. Part. Nucl. Phys. **67**, 337 (2012).
[35] R. Rapp and J. Wambach, Phys. Rev. C **53**, 3057 (1996).
[36] S. Zschocke and L. P. Csernai, Eur. Phys. J. A **39**, 349 (2009).
[37] K. Adcox *et al.* [PHENIX Collaboration], Phys. Rev. Lett. **88**, 022301 (2002).
[38] S. S. Adler *et al.* [PHENIX Collaboration], Phys. Rev. Lett. **91**, 072301 (2003).
[39] B. I. Abelev *et al.* [STAR Collaboration], Phys. Rev. C **80**, 044905 (2009)
[40] G. Conesa Balbastre, J. Phys. G **38**, 124117 (2011).
[41] Y. Kharlov [ALICE Collaboration], Nuclear Physics A **910-911** (2013) 335.
[42] S. S. Adler *et al.* [PHENIX Collaboration], Phys. Rev. C **69**, 034910 (2004).
[43] R. J. Fries, B. Muller, C. Nonaka and S. A. Bass, Phys. Rev. C **68**, 044902 (2003).
[44] M. Kataja and P. V. Ruuskanen, Phys. Lett. B **243**, 181 (1990).
[45] T. Das, G. S. Guralnik, V. S. Mathur, F. E. Low and J. E. Young, Phys. Rev. Lett. **18**, 759 (1967).
[46] M. Dey, V. L. Eletsky and B. L. Ioffe, Phys. Lett. B **252**, 620 (1990).
[47] J. F. Donoghue and A. F. Perez, Phys. Rev. D **55**, 7075 (1997) [hep-ph/9611331].
[48] G. Ecker, J. Gasser, A. Pich and E. de Rafael, Nucl. Phys. B **321**, 311 (1989).
[49] R. Urech, Nucl. Phys. B **433**, 234 (1995).
[50] U. G. Meissner, G. Muller and S. Steininger, Phys. Lett. B **406**, 154 (1997) [Erratum-ibid. B **407**, 454 (1997)].
[51] M. Knecht and R. Urech, Nucl. Phys. B **519**, 329 (1998).
[52] M.Le Bellac, *Thermal Field Theory* (Cambridge University Press, 1996).
[53] U. Kraemmer, A. K. Rebhan and H. Schulz, Annals Phys. **238**, 286 (1995).
[54] A. Gomez Nicola and R. Torres Andres, J. Phys. G **39**, 015004 (2012).
[55] S. -Y. Wang, Phys. Rev. D **70**, 065011 (2004).
[56] E. Mottola and Z. Szep, Phys. Rev. D **81**, 025014 (2010).
[57] A. Rebhan, Lect. Notes Phys. **583**, 161 (2002) [hep-ph/0105183].
[58] P. V. Landshoff and A. Rebhan, Nucl. Phys. B **383**, 607 (1992) [Erratum-ibid. B **406**, 517 (1993)]
[59] U. Kraemmer and A. Rebhan, Rept. Prog. Phys. **67**, 351 (2004).
[60] E. Braaten and R. D. Pisarski, Nucl. Phys. B **337**, 569 (1990). Phys. Rev. D **46**, 1829 (1992).
[61] M. H. Thoma and C. T. Traxler, Phys. Lett. B **378**, 233 (1996) [hep-ph/9601254].
[62] A. Abada and K. Bouakaz, JHEP **0601**, 161 (2006).
[63] J. I. Kapusta and E. V. Shuryak, Phys. Rev. D **49**, 4694 (1994).
[64] P. M. Hohler and R. Rapp, Nucl. Phys. A **892**, 58 (2012)
[65] N. P. M. Holt, P. M. Hohler and R. Rapp, Phys. Rev. D **87**, 076010 (2013)
[66] S. Weinberg, Phys. Rev. Lett. **18** (1967) 507.
[67] G. Ecker, J. Gasser, H. Leutwyler, A. Pich and E. de Rafael, Phys. Lett. B **223**, 425 (1989).
[68] R. D. Pisarski and M. Tytgat, Phys. Rev. D **54**, 2989 (1996)
[69] R. Rapp and C. Gale, Phys. Rev. C **60**, 024903 (1999).
[70] P. Pascual and E. de Rafael, Z. Phys. C **12**, 127 (1982). S. Narison, Z. Phys. C **14**, 263 (1982).
[71] P. Masjuan and S. Peris, JHEP **0705**, 040 (2007).

[72] G. 't Hooft, Nucl. Phys. B **72**, 461 (1974). ; E. Witten, Nucl. Phys. B **160**, 57 (1979).
[73] R. Baur and R. Urech, Phys. Rev. D **53** (1996) 6552.
[74] S. Mallik and S. Sarkar, Eur. Phys. J. C **25**, 445 (2002).
[75] S. Leupold, Eur. Phys. J. A **18** (2003) 219.
[76] Z. -H. Guo and J. A. Oller, Phys. Rev. D **84** (2011) 034005.
[77] R. Kobes, Phys. Rev. D **42**, 562 (1990). Phys. Rev. D **43**, 1269 (1991).
[78] A. Gomez Nicola, F. J. Llanes-Estrada and J. R. Pelaez, Phys. Lett. B **550**, 55 (2002).
[79] S. Ghosh, S. Sarkar and S. Mallik, Eur. Phys. J. C **70**, 251 (2010).

3.1.2 Publicación:
A. Gómez Nicola, R. Torres Andrés,
Scalar susceptibilities and electromagnetic thermal mass differences in Chiral Perturbation Theory,
Prog. Part. Nucl. Phys. **67** (2012) 337

Progress in Particle and Nuclear Physics 67 (2012) 337–342

Contents lists available at SciVerse ScienceDirect

Progress in Particle and Nuclear Physics

journal homepage: www.elsevier.com/locate/ppnp

Review

Scalar susceptibilities and electromagnetic thermal mass differences in chiral perturbation theory

R. Torres Andrés *, A. Gómez Nicola

Departamento de Fısica Teórica II, Universidad Complutense de Madrid, Spain

ARTICLE INFO

Keywords:
Chiral symmetry
Chiral perturbation theory
Isospin breaking
Finite-temperature field theory

ABSTRACT

We make a thermal analysis of the light scalar susceptibilities using SU(3)-chiral perturbation theory to one-loop order, taking into account the QCD source of isospin breaking (IB), i.e. corrections coming from $m_u \neq m_d$. The value of the connected scalar susceptibility in the infrared regime, the one relevant when approaching chiral symmetry restoration, and below the critical temperature is found to be entirely dominated by the π^0–η mixing, which leads to model-independent $\mathcal{O}(\epsilon^0)$ corrections, where $\epsilon \sim m_d - m_u$, in the combination $\chi_{uu} - \chi_{ud}$ of flavour breaking susceptibilities. We also present preliminary results for the corrections to the real part of the pion self-energy at next-to-leading order in SU(2)-chiral perturbation theory, taking into account electromagnetic interaction. The results for zero and finite temperature for the charged and neutral pions are given in terms of the 3-momentum of the external pion, and their difference is calculated to this order, stressing the fact that, at low and moderate temperature, the mass splitting $M_{\pi^\pm} - M_{\pi^0}$ grows with temperature for, at least, non-zero charged pion mass running inside the loops.

1. Introduction

The low energy sector of QCD has been successfully described over recent years within the chiral Lagrangian framework. Chiral perturbation theory (ChPT) is based on the spontaneous breaking of the chiral symmetry $SU_V(N_f) \times SU_A(N_f) \to SU_V(N_f)$ with $N_f = 2, 3$ light flavours and provides a consistent, systematic and model-independent scheme for calculating low energy observables [1–3]. The effective ChPT Lagrangian is constructed as an expansion of the form $\mathcal{L} = \mathcal{L}_{p^2} + \mathcal{L}_{p^4} + \cdots$ where p denotes a meson energy scale compared to the chiral scale $\Lambda_\chi \sim 1$ GeV. The formalism can also be extended to finite temperature T, in order to describe meson gases and their evolution towards chiral symmetry restoration for T below the critical temperature T_c [4,5], where $T_c \simeq 180$–200 MeV from lattice simulations [6–8]. The use of ChPT in this context is important for providing model-independent results for the evolution of the different observables with T, supporting the original predictions for chiral restoration [9], also confirmed by lattice simulations, which are consistent with a crossover-like transition for $N_f = 3$ ($2 + 1$ flavours in the physical case), a second-order one for $N_f = 2$ in the $O(4)$ universality class and a first-order one in the degenerate case of three equal flavours.

The invariance under the $SU_V(2)$ vector group is the isospin symmetry, which is a very good approximation to Nature. However, there are several processes where isospin breaking corrections are phenomenologically relevant, for example those of sum rules for quark condensates [3], meson masses [10] or pion scattering [11,12]. There are two possible sources of isospin breaking: the QCD $m_d - m_u$ light quark mass difference and electromagnetic interactions. Both can be accommodated within the ChPT framework. From the first source we expect corrections of order $(m_d - m_u)/m_s$, encoded in the quark mass matrix, which generates also a π^0–η mixing term in the SU(3) Lagrangian [3]. On the other hand, the electromagnetic

* Corresponding author.
E-mail address: rtandres@fis.ucm.es (R.T. Andrés).

0146-6410/$ – see front matter © 2012 Elsevier B.V. All rights reserved.
doi:10.1016/j.ppnp.2011.12.040

interactions are included in the ChPT effective Lagrangian via the external source method and give rise to new terms [10–13] of order $\mathcal{L}_{e^2}$, $\mathcal{L}_{e^2p^2}$ and so on, e being the electric charge. It is possible to accommodate these terms into the ChPT power counting scheme by considering formally $e^2 = \mathcal{O}(p^2/F^2)$, with F the pion decay constant in the chiral limit.

The purpose of this paper is to calculate the leading thermal contributions to the connected and disconnected scalar susceptibilities, taking into account isospin breaking, and to show our preliminary results concerning the thermal evolution of the masses of the charged and neutral pions.

2. Light scalar susceptibilities and the role of the π^0–η mixing

Calculations for light quark condensates, $\langle\bar{u}u\rangle$ and $\langle\bar{d}d\rangle$, at zero and finite temperature have been made to one-loop in [14,15], respectively, within the framework of SU(3)-ChPT taking into account both sources of IB. The main feature that we want to stress is that there is a π^0–η mixing term appearing through the tree level mixing angle ε defined by $\tan 2\varepsilon = \frac{\sqrt{3}}{2}\frac{m_d-m_u}{m_s-\hat{m}}$.

Different light quark masses allow us to consider three independent light scalar susceptibilities defined as

$$\chi_{ij} = -\frac{\partial}{\partial m_i}\langle\bar{q}_j q_j\rangle = \frac{\partial^2}{\partial m_i \partial m_j}\log Z(m_u \neq m_d). \tag{1}$$

From now on in this section, we will neglect the electromagnetic corrections because they are small and not relevant for our present discussion, so we will put $e = 0$. Then, to leading order in the mixing angle, the contribution of the π^0–η mixing in the quark condensate sum is of order ϵ^2, whereas for the difference it goes like ε. The thermal functions $g_i(T, M_i)$, $i = \pi^0, \eta$, defined as $g_i(T) = \frac{1}{4\pi^2F^2}\int_0^\infty dp \frac{p^2}{E_p}\frac{1}{e^{\beta E_p}-1}$, with $E_p^2 = p^2 + M_i^2$ and $\beta = T^{-1}$, are suppressed by those coefficients and the quark condensates do not receive important corrections. The important point is that differentiating with respect to a light quark mass is essentially the same as differentiating with respect to $\varepsilon \sim \frac{m_d-m_u}{m_s}$, so the suppression of the thermal functions is smaller in the case of the susceptibilities than in the quark condensate case.

Because of the linearity in ε in $\langle uu - dd\rangle$ for a small mixing angle, the combinations $\chi_{uu} - \chi_{ud}$ and $\chi_{dd} - \chi_{du}$ receive an $\mathcal{O}(1)$ IB correction due to π^0–η mixing, which would not be found if $m_u = m_d$ was taken from the beginning. The analysis of the ε-dependence of $\langle uu - dd\rangle$ shows that, up to $\mathcal{O}(\epsilon)$, $\chi_{uu} \simeq \chi_{dd}$, so combinations like $\chi_{uu} - \chi_{dd}$, which also vanish with $m_u = m_d$, are less sensitive to IB.

One can also relate these flavour breaking susceptibilities to the connected and disconnected ones [16], often used in lattice analysis [17,18]: $\chi_{\rm dis} = \chi_{ud}$, and $\chi_{\rm con} = \frac{1}{2}(\chi_{uu} + \chi_{dd} - 2\chi_{ud})$. From the previous analysis, we get $\chi_{\rm con} \simeq \chi_{uu} - \chi_{ud}$.

Therefore, our model-independent analysis including IB effects provides the leading non-zero contribution for the connected susceptibility which arises partially from π^0–η mixing. This is particularly interesting for the lattice, where artefacts such as taste breaking mask the behaviour of $\chi_{\rm con}$ with the quark mass and T when approaching the continuum limit [18]. In fact, our ChPT approach is useful for exploring the chiral limit ($m_{u,d} \to 0$) or infrared (IR) regime, which gives a qualitative picture of the behaviour near chiral symmetry restoration. In this regime $M_\pi \ll T \ll M_K$, and therefore we can neglect thermal heavy particles, which are exponentially suppressed.

The leading order results for the connected and disconnected susceptibilities at zero temperature are the following:

$$\chi_{\rm con}^{\rm IR}(T=0) = 8B_0^2[2L_8^r(\mu) + H_2^r(\mu)] - \frac{B_0^2}{16\pi^2}\left(1 + \log\frac{M_K^2}{\mu^2}\right) - \frac{B_0^2}{24\pi^2}\log\frac{M_\eta^2}{\mu^2} + \mathcal{O}(\epsilon^2), \tag{2}$$

$$\chi_{\rm dis}^{\rm IR}(T=0) = 32B_0^2L_6^r(\mu) - \frac{3B_0^2}{32\pi^2}\left(1 + \log\frac{M_\pi^2}{\mu^2}\right) + \frac{B_0^2}{288\pi^2}\left(5\log\frac{M_\eta^2}{\mu^2} - 1\right) + \mathcal{O}(\epsilon^2), \tag{3}$$

where B_0 is the parameter which relates masses and quark condensates at tree level via the Gell-Mann–Oakes–Renner formula, and L_6, L_8, H_2 are low energy constants.

The log term in Eq. (3) is the dominant one at $T = 0$ and can be found in [16], but the connected IR susceptibility (2) is not zero at $T = 0$, because it receives contributions of order $\mathcal{O}(1)$ in the mixing angle.

If we consider the pion gas in a thermal bath, then expressions (2)–(3) are modified according to

$$[\chi_{\rm con}(T) - \chi_{\rm con}(0)]^{\rm IR} = \frac{B_0^2}{18}\frac{T^2}{M_\eta^2} + \mathcal{O}\left(\epsilon^2 B_0^4\frac{T^4}{M_\eta^4}\right) + \mathcal{O}\left(\exp\left[-\frac{M_{\eta,K}}{T}\right]\right), \tag{4}$$

$$[\chi_{\rm dis}(T) - \chi_{\rm dis}(0)]^{\rm IR} = \frac{3B_0^2}{16\pi}\frac{T}{M_\pi} + \mathcal{O}\left(\epsilon^2 B_0^4\frac{T^4}{M_\eta^4}\right) + \mathcal{O}\left(\exp\left[-\frac{M_{\eta,K}}{T}\right]\right). \tag{5}$$

Note that, as we have already mentioned, the eta mass term in Eq. (4) and in the subleading corrections in the mixing angle comes from the ϵ-analysis and the IR expansion of the $g_1(M_\pi)$, and does not have anything to do with thermal etas.

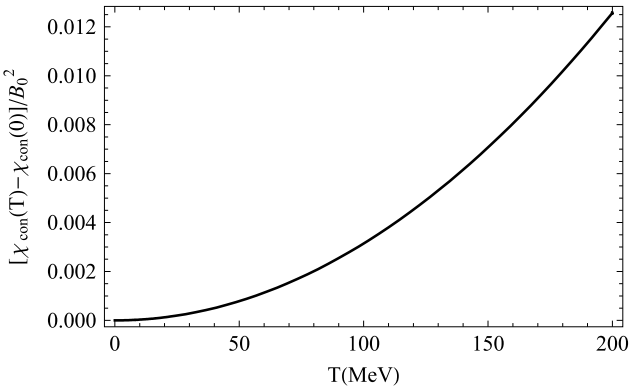

Fig. 1. Connected IR susceptibility normalized to B_0^2, for fixed tree level eta mass and $m_s = 80$ MeV.

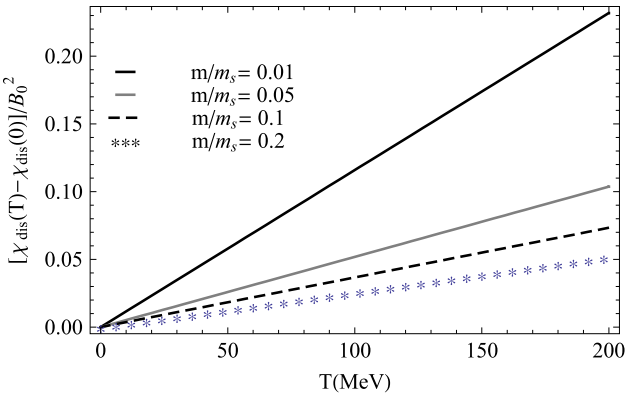

Fig. 2. Disconnected IR susceptibility normalized to B_0^2, for several light quark mass ratios and fixed tree level eta mass ($m/m_s = 0.05$ is the physical case).

Figs. 1 and 2 show, respectively, the connected susceptibility (4) for fixed tree level eta mass (proportional to $\sqrt{B_0 m_s}$ in the IR regime), and the disconnected one (5) for several values of the light quark mass ratio m/m_s, and also with fixed tree level eta mass. The leading scaling with T and the light quark mass in this regime for the disconnected piece goes like $\frac{T}{\sqrt{m}}$, i.e. with the same scaling as was calculated in [16,17], whereas the connected susceptibility grows quadratically in T over a mass scale much greater than the SU(2) Goldstone boson's one. Therefore, in the continuum limit, we only expect $\chi_{\rm dis}$ to peak near the transition, as the $m \to 0^+$ limit in Fig. 2 clearly shows.

3. Charged and neutral thermal pion masses in SU(2)-ChPT at $\mathcal{O}(p^4)$

If we consider virtual photons in the calculation of the real part of the self-energy in the mass shell, there are four relevant diagrams that correct the masses at order $\mathcal{O}(p^4)$: there are pion tadpoles, diagram (a) in Fig. 3, and the tree level NLO diagram needed for renormalization, (b), where both charged and neutral pions participate; and diagrams with virtual photons, (c) and (d), which only modify the charged pion mass.

The photon tadpole diagram (c) is proportional to the photon mass and therefore vanishes at zero temperature, while pion tadpoles (a) and the photon exchange diagram (d) are finite and chiral scale independent once regularized and combined with diagram (b). The LO corrections to the masses of the SU(2) NGB are calculated as $M^2 = \hat{M}^2 + \Sigma(\hat{M}^2)$, where $\hat{M}$ is the respective tree level mass. At zero temperature the neutral and charged pion masses are [11]

$$M^2_{\pi^0} = \hat{M}^2_{\pi^0}\left(1 + 2\mu_\pm - \mu_0 + e^2\mathcal{K}_{\pi^0} + 2l_3^r\frac{\hat{M}^2_{\pi^0}}{F^2}\right) - 2\frac{B^2}{F^2}l_7^r(m_d - m_u)^2 - \frac{4}{3}Be^2k_7(m_d - m_u), \tag{6}$$

where $\mu_{\pm,0} = \frac{M^2_{\pi^\pm,\pi^0}}{32\pi^2F^2}\log\frac{M^2_{\pi^\pm,\pi^0}}{\mu_\chi^2}$, and $\mathcal{K}_{\pi^0} = -\frac{20}{9}\left[k_1^r + k_2^r - \frac{9}{10}(2k_3^r - k_4^r) - k_5^r - k_6^r - \frac{1}{5}k_7^r\right]$, with k_i being electromagnetic low energy constants, Z the parameter that corrects the leading order charged pion mass, and

$$M^2_{\pi^\pm} = \hat{M}^2_{\pi^0}\left[1 + \frac{e^2}{4\pi} + \mu_0 + e^2\mathcal{K}^A_{\pi^\pm} + 2l_3^r\frac{\hat{M}^2_{\pi^0}}{F^2}\right]$$
$$+ 2e^2F^2\left[Z\left(1 + \frac{e^2}{4\pi}\right) + e^2\mathcal{K}^B_{\pi^\pm} - (3 + 4Z)\mu_\pm\right] - \frac{4}{3}Be^2k_7(m_d - m_u), \tag{7}$$

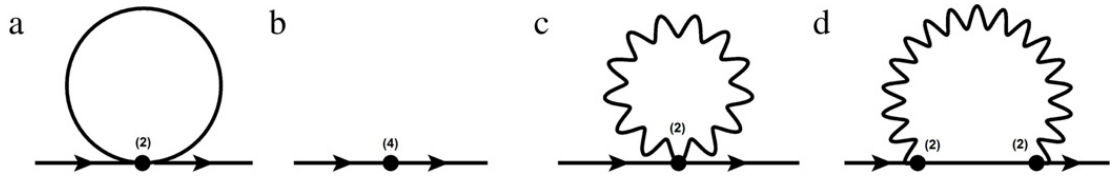

Fig. 3. Diagrams for the pion self-energy at order $\mathcal{O}(p^4)$. (a) and (b) represent pion tadpole contributions and the tree level NLO diagram which renormalizes the loops, respectively. (c) (photon tadpole) and (d) (one-photon exchange) only correct the charged pion self-energy.

with the definitions

$$\mathcal{K}^A_{\pi^\pm} = -\frac{20}{9}\left[k^r_1 + k^r_2 - k_5 - \frac{1}{5}(23k^r_6 + 18k^r_8 + k^r_7)\right],$$

and

$$\mathcal{K}^B_{\pi^\pm} = -\frac{10}{9}\left[2Z(k^r_1 + k^r_2) - \frac{1}{2}k_{13} - k_{14}\right].$$

There is a factor 1/2 in the coefficient of k_7 for both masses which does not appear in [11], and that was also noted by [19]. At this point the total mass difference between charged and neutral pions becomes

$$M^2_{\pi^\pm} - M^2_{\pi^0} = 2\hat{M}^2_{\pi^0}(\mu_0 - \mu_\pm) + 2\frac{B^2}{F^2}l^r_7(m_d - m_u)^2 + 2e^2F^2\left[Z\left(1 + \frac{e^2}{4\pi}\right) + e^2\mathcal{K}^B_\pm\right] + \hat{M}^2_{\pi^0}e^2\left[\frac{1}{4\pi} + \mathcal{K}^A_\pm - \mathcal{K}_{\pi^0}\right] - 2e^2F^2(3 + 4Z)\mu_\pm, \tag{8}$$

which has pure strong, pure EM and mixed EM–strong contributions.

If the pions are immersed in a thermal bath, there appear new contributions with no UV divergences, since these only appear in the zero-temperature part and they have already been renormalized. The pion tadpoles, charged or not, give rise to $g_1(M, T)$ thermal functions. For the neutral pion mass we get

$$M^2_{\pi^0} = \hat{M}^2_{\pi^0}(T = 0)\left[1 + \frac{1}{F^2}\left(g_1(M^2_{\pi^\pm}, T) - \frac{1}{2}g_1(M^2_{\pi^0}, T)\right)\right], \tag{9}$$

where it is worth noting that the neutral pion mass decreases with T, contrary to what happens if we do not consider electromagnetic effects, as can be seen if we put $M^2_{\pi^\pm} = M^2_{\pi^0}$ in the last expression.

As for the charged pion, we can separate the contributions coming from pion tadpoles, $M^2_{\pi\ \text{tadpoles}}$, and the two different contributions from the virtual photon diagrams: one coming from the photon tadpole which is not zero at finite temperature and gives a typical thermal screening contribution, $M^2_{\text{Ph. tadpole}}$; and the other due to the one-photon exchange, $M^2_{\text{Ph. Exchange}}$.

For the first two ones we get $M^2_{\pi\ \text{Tadpoles}} = \frac{\hat{M}^2_{\pi^0}}{2F^2} - 4Ze^2g_1(M^2_{\pi^\pm}, T)$ and $M^2_{\text{Ph. Tadpole}} = \frac{1}{3}e^2T^2$. The latter has the typical form of a Debye or screening mass of the electric field in a thermal bath [20], which always grows with T.

The one-photon exchange diagram is more complex and its contributions to the real part depend, in general, on the 3-momentum of the external pion, which is a direct consequence of the Lorentz symmetry breaking in the thermal bath. The Matsubara sums can be performed in the standard way, before performing the analytic continuation to external continuous frequencies:

$$\text{Re}\left(\Sigma_{\text{Ph. Exchange}}\right) = e^2\left(\int\frac{d^3k}{(2\pi)^3}\frac{n(\omega)}{2\omega}\frac{(2q-k)^2|_{k_0=\omega}}{(q_0-\omega)^2-\omega'^2} + \int\frac{d^3k}{(2\pi)^3}\frac{n(\omega)}{2\omega}\frac{(2q-k)^2|_{k_0=-\omega}}{(q_0+\omega)^2-\omega'^2} + \int\frac{d^3k}{(2\pi)^3}\frac{n(\omega')}{2\omega'}\frac{(2q-k)^2|_{k_0=q_0-\omega'}}{(q_0-\omega')^2-\omega^2} + \int\frac{d^3k}{(2\pi)^3}\frac{n(\omega')}{2\omega'}\frac{(2q-k)^2|_{k_0=q_0+\omega'}}{(q_0+\omega')^2-\omega^2}\right),$$

with $\omega^2 = \vec{k}^2$ the photon energy squared inside the loop and $\omega'^2 = (\vec{q}-\vec{k})^2 + M^2_{\pi^\pm}$ the pion energy squared, also inside the loop; here k is the virtual photon 4-momentum. The above 3-momentum integrals can be written as

$$\text{Re}\left(\Sigma_{\text{Ph. Exchange}}\right) = \frac{e^2}{2\pi^2}\int_0^\infty dk\int_0^\pi d\phi\, n(k)\sin\phi \times\frac{M^2_{\pi^\pm}\sqrt{E^2 - M^2_{\pi^\pm}}\cos\phi - k(E^2\sin^2\phi + M^2_{\pi^\pm}\cos^2\phi)}{E^2\sin^2\phi + M^2_{\pi^\pm}\cos^2\phi} + \frac{e^2}{4\pi^2}\int_0^\infty dk\int_0^\pi d\phi\,\frac{n(\omega')}{\omega'} \times\sin\phi\frac{k^2(M^2_{\pi^\pm}\cos^2\phi + E^2\sin^2\phi) + 2M^2_{\pi^\pm}(E^2 - k\sqrt{E^2 - M^2_{\pi^\pm}}\cos\phi)}{E^2\sin^2\phi + M^2_{\pi^\pm}\cos^2\phi}. \tag{10}$$

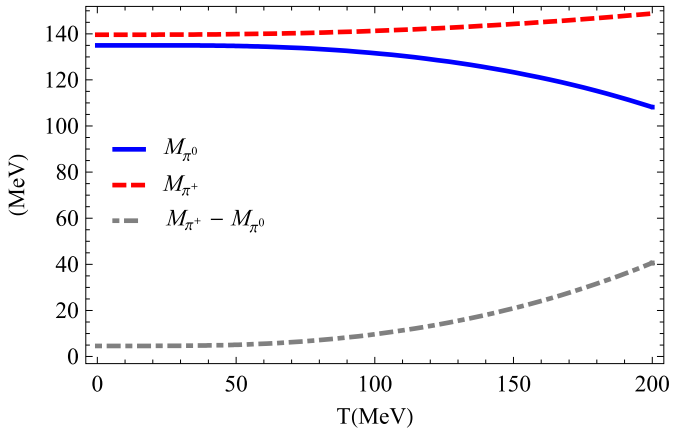

Fig. 4. Preliminary results for the charged (dashed line) and neutral (solid line) masses and their difference (dot–dashed line) at LO in the static limit.

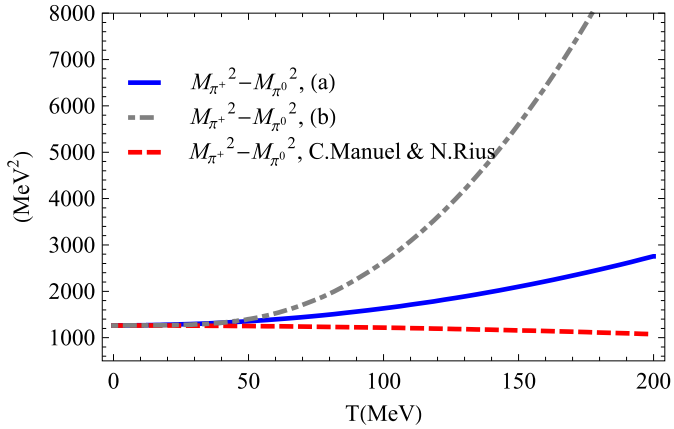

Fig. 5. Different results for the charged–neutral pion mass difference: (a) (solid line) corresponds to our preliminary results in the chiral limit keeping corrections $e \neq 0$ for the tree level charged pion mass inside the loops; (b) (dot–dashed line) corresponds to the same preliminary calculation with $m_u = m_d \neq 0$ and $e \neq 0$ also inside the loops; and the full dashed line is the result given in [21].

It is clear now that the charged pion real part of the self-energy depends on the energy of the external pion $E^2 = |\vec{q}|^2 + M^2_{\pi^\pm}$, and, therefore, on the external 3-momentum.

The final result will take the form $M^2_{\pi^\pm} = \hat{M}^2_{\pi^\pm}(T=0) + M^2_{\pi\ \text{Tadpoles}} + M^2_{\text{Ph. Tadpole}} + \text{Re}\left(\Sigma_{\text{Ph. Exchange}}\right)$. In Fig. 4 we have plotted our preliminary results for the neutral and charged pion real masses as a function of the temperature of the thermal bath, taking physical values for the pion masses and calculating $M^2_{\text{Ph. Exchange}}$ in the static limit, i.e., for $E = M_{\pi^\pm}$. Once we have the thermal and isospin breaking corrections to the masses separately for any value of the external momentum, we can calculate it in the limit where temperatures are (i) much greater than the masses and the external momenta (which means that we have to set the masses inside the loops to zero), and (ii) sizable with respect to the momenta running inside the loops, $T \sim k \gg m, q$. With these assumptions, we are led to the HTL result given in [21], $M^2_{\pi^\pm} - M^2_{\pi^0} = \hat{M}^2_{\pi^\pm}\left(1 - \frac{T^2}{6}\right) + \frac{1}{4}e^2T^2$, which serves as a consistency check.

Moreover, our low temperature analysis allows us to assume a slightly different chiral limit, in the sense that we can still assume $m_u = m_d = 0$ and consider $e \neq 0$ inside the loops. In Fig. 5 we show the plot of our preliminary calculation both in this latter limit, and also considering $m_u = m_d \neq 0$, $e \neq 0$, to be compared with those appearing in the HTL result [21] where the contributions from the screening-like term, always increasing with T and inherent to the thermal bath, are responsible for the final growth of the mass difference, contrary to what one would expect naively from the sum rule relating the axial and vector spectral functions [20] applying chiral symmetry restoration arguments.

References

[1] S. Weinberg, Physica A 96 (1979) 327.
[2] J. Gasser, H. Leutwyler, Ann. Phys. 158 (1984) 142.
[3] J. Gasser, H. Leutwyler, Nuclear Phys. B 250 (1985) 465.
[4] J. Gasser, H. Leutwyler, Phys. Lett. B 184 (1987) 83.
[5] P. Gerber, H. Leutwyler, Nuclear Phys. B 321 (1989) 387.
[6] [MILC Collaboration], C. Bernard, et al., Phys. Rev. D 71 (2005) 034504.
[7] Y. Aoki, S. Borsanyi, S. Durr, Z. Fodor, S.D. Katz, S. Krieg, K.K. Szabo, J. High Energy Phys. 0906 (2009) 088.
[8] M. Cheng, et al., Phys. Rev. D 81 (2010) 054504.

[9] R.D. Pisarski, F. Wilczek, Phys. Rev. D 29 (1984) 338.
[10] R. Urech, Nuclear Phys. B 433 (1995) 234.
[11] M. Knecht, R. Urech, Nuclear Phys. B 519 (1998) 329.
[12] U.G. Meissner, G. Muller, S. Steininger, Phys. Lett. B 406 (1997) 154. (erratum);
U.G. Meissner, G. Muller, S. Steininger, Phys. Lett. B 407 (1997) 454.
[13] G. Ecker, J. Gasser, A. Pich, E. de Rafael, Nuclear Phys. B 321 (1989) 311.
[14] A.G. Nicola, R.T. Andres, J. Phys. G: Nucl. Part. Phys. 39 (2012) 015004.
[15] A.G. Nicola, R.T. Andres, Phys. Rev. D 83 (2011) 076005.
[16] A.V. Smilga, J.J.M. Verbaarschot, Phys. Rev. D 54 (1996) 1087.
[17] S. Ejiri, et al., Phys. Rev. D 80 (2009) 094505.
[18] C.E. DeTar, PoS (2008) 001. LATTICE2008.
[19] J. Schweizer, J. High Energy Phys. 0302 (2003) 007.
[20] Kraemmer, Rebhan, Ann. Phys. 238 (1995) 286–332.
[21] C. Manuel, N. Rius, Phys. Rev. D 59 (1999) 054002. arXiv:hep-ph/9806385.

4

Conclusiones

La investigación que he llevado a cabo ha tenido como objetivo principal el estudio de ciertas propiedades térmicas de gases de bosones de Goldstone a través del enfoque efectivo provisto por la Teoría Quiral de Perturbaciones, extendida puntualmente a través de métodos de unitarización y modelos auxiliares con el fin de incorporar a sus predicciones el efecto de la inclusión de resonancias ligeras en diversos canales.

A continuación expondremos de modo resumido las principales conclusiones que ya han sido mostradas de modo detallado a lo largo de los capítulos 2 y 3.

En las dos primeras secciones del capítulo 2 de esta tesis se han estudiado los efectos de la inclusión de términos de ruptura de la simetría de isoespín —intrínseca y electromagnética— sobre los parámetros de orden asociados a la restauración de la simetría quiral, en concreto sobre los condensados escalares de quarks ligeros y sobre el condensado *strange* en la teoría de tres sabores.

A temperatura cero nuestros resultados muestran que el cálculo de estos efectos de modo sistemático, partiendo de la Teoría Quiral para tres sabores, se diferencia —respecto al esquema de cálculo de [121] basado en la inclusión de efectos de ruptura a través de términos que violan el Teorema de Dashen para las masas de mesones— en un 2 %, en el caso del condensado de quarks ligeros y hasta un 4 % para el *strange*. Esto muestra que, aunque relativamente pequeña, la diferencia entre considerar todas las constantes de baja energía a través de un enfoque

efectivo basado en el lagrangiano quiral es importante si uno tiene en cuenta la precisión con la que se dan los resultados en [121].

Nuestra asunción de la hipótesis de respuesta ferromagnética para el vacío —junto con la especificación de la prescripción para la separación de la parte electromagnética de la no electromagnética en el cálculo de los condensados consistente en tomar directamente el límite $e = 0$— es el origen de distintas cotas inferiores para las combinaciones de *EM LECs* que aparecen en el cálculo del condensado total tanto en $SU(2)-ChPT$ como en $SU(3)-ChPT$. Hemos comprobado que estas condiciones son satisfechas por todos y cada uno de los valores de las *EM LECs* relevantes que hemos consultado en la literatura especializada (obtenidas a partir de diversos métodos); y son más restrictivas para tres sabores que para dos, pero menos confiables debido a la presencia de la masa del quark *strange* en la serie perturbativa quiral.

El conocimiento general de las constantes de baja energía electromagnética en la literatura es —hasta donde hemos podido consultar [130–134]— bastante limitado, particularmente para el caso de la teoría de dos sabores. A través de un proceso de desacoplo del quark *strange*— hemos relacionado las combinaciones de constantes de baja energía en las teorías de dos y tres sabores a costa de introducir una dependencia explícita a través de masas de mesones. Sin embargo, debido a que la separación de las contribuciones electromagnéticas e intrínsecas en cualquier observable es siempre ambigüa [108, 131, 133, 139], no existe una prescripción única y general que permita —para todo orden en *ChPT*— separar *EM LECs* de las *LECs* de naturaleza no electromagnética.

A temperatura finita, el condensado total recibe, tanto en $SU(2)$ como en $SU(3)$, pequeñas correcciones a causa de la violación de la simetría de isoespín. Éstas se traducen en un aumento de la temperatura crítica respecto al límite de isoespín de menos de un 1 %. De esta manera —aunque represente una modificación pequeña— sí se presenta en la dirección correcta y de forma consistente con la hipótesis de respuesta ferromagnética asumida en la obtención de ligaduras para las *EM LECs*.

En cuanto al parámetro de orden de la ruptura de la simetría de isoespín —relacionado, como ya dije, con la asimetría de vacío— hemos mostrado que no recibe correcciones térmicas para dos sabores, mientras que en $SU(3)-ChPT$ se amplifica suavemente a través de una dependencia cuadrática en la temperatura de la forma $(m_u - m_d)\frac{T^2}{M_\eta^2}$. Nótese que, aunque la dependencia con la temperatura es cuadrática, es $O(\epsilon)$ en el ángulo de mezcla y está controlada por una escala de energía mucho mayor que la dependencia característica $1/F_\pi^2$ —asociada al parámetro de orden de la restauración quiral—.

Las diferencias ($\sim 1\,\%$) entre considerar o no efectos de ruptura de isoespín a

temperatura cero en el condensado ligero y el *strange* son tales que pueden ser despreciadas en comparación con las incertidumbres asociadas a los cálculos que se obtienen mediante simulación en el retículo [125].

Pese a esto, existen observables para los que este tipo de correcciones son importantes, tanto desde un punto de vista formal como desde una perspectiva numérica. Es el caso de cantidades que se anulan en el límite de isoespín, como por ejemplo el parámetro de orden de la ruptura de isoespín $<\bar{u}u> - <\bar{d}d>$, o la llamada asimetría de vacío que se define a partir de este último y que arroja correcciones —a temperatura cero— que van desde un 15% hasta un 24% dependiendo de que se use la cota inferior o superior de valores naturales para las constantes de baja energía electromagnéticas—. Existen también modificaciones importantes a la regla de suma [31] que conecta los cocientes $<\bar{d}d>/<\bar{u}u>$ y $<\bar{s}s>/<\bar{u}u>$ —libre de términos de contacto— puesto que los efectos de ruptura electromagnética (calculados en este trabajo por vez primera) son formal y numéricamente comparables a los de ruptura intrínseca.

Esta regla de suma puede ser extendida de forma natural a temperatura finita manteniendo su carácter independiente de términos de contacto. Debido a que las correcciones que experimenta el cociente $<\bar{u}u>/<\bar{d}d>$ son grandes para temperaturas moderadas, las modificaciones a esta regla de suma asociadas a la presencia del baño térmico son significativas en este rango de temperaturas (*e.g.*: de aproximadamente un 20% para $T \sim 100$ MeV respecto al valor a temperatura cero), llegando incluso —y siendo conscientes de que se trata de una extrapolación de los resultados de *ChPT*— a ser formalmente comparables al valor de temperatura cero en el rango de temperaturas altas.

Hemos relacionado, además, las correcciones electromagnéticas al condensado total de quarks en la teoría de dos sabores con la diferencia $\chi(T)^{SU(2)} - \chi(0)^{SU(2)}$ —directamente medible en el retículo [86,147]— para la susceptibilidad escalar total a través de una regla de suma. La extrapolación cualitativa de los resultados proporcionados por esta regla de suma hacia temperaturas cercanas al valor crítico permite inferir un crecimiento importante de los efectos debidos a la ruptura electromagnética sobre el condensado total, habida cuenta del comportamiento que se presupone para la susceptibilidad escalar cerca de la transición.

Para la Teoría Quiral con tres sabores es posible concluir que —pese a que la interpretación ahora no es tan clara como en el caso anterior— las correcciones sobre el condensado total también se hallan dominadas por la susceptibilidad escalar sustraída debido a la supresión Boltzmann de los grados de libertad asociados al quark *strange*.

Esta regla de suma ha llevado a conectar nuestros resultados con aquéllos obtenidos a través del formalismo *staggered* en el retículo. En efecto, debido a que la masa de las copias se corrige [86, 89, 148] con el espaciado de la red

de forma similar a como entran las correcciones electromagnéticas a *nivel árbol* en la masa de los bosones de Goldstone, la regla de suma permite comparar las diferencias entre nuestros resultados para los condensados en el límite del continuo y los obtenidos mediante simulación en el retículo usando acciones de tipo *staggered*. Además, a partir de este la extrapolación de los resultados se colige que las correcciones debidas a efectos de *taste-breaking* son susceptibles de verse amplificadas en un entorno de la temperatura crítica de restauración.

El cálculo de las susceptibilidades quirales escalares a un *loop* en $SU(3)$–$ChPT$ permite la obtención de las llamadas susceptibilidades conexa y disconexa, cantidades que —junto a la susceptibilidad escalar total— son de uso habitual en las simulaciones en el retículo.

En este trabajo se ha mostrado cómo la consideración de un escenario que incluya la ruptura de isoespín consistentemente es fundamental para la obtención de las contribuciones dominantes de cada una de las partes de la susceptibilidad. Estos resultados permiten obtener el *scaling* de estos observables en relación con los parámetros de masa quark y temperatura desde un punto de vista *model-independent* en el continuo, importantes para explicar ciertos comportamientos anómalos que aparecen en el formalismo *staggered* del retículo. En relación a esto, es vital la advertencia de que considerar un sólo sabor puede dar lugar a una interpretación demasiado simplista del problema, puesto que asumir la existencia de una sola susceptibilidad asociada a un sólo sabor ligero —tomando el límite de isoespín desde el principio del cálculo— no permite obtener las contribuciones dominantes para la susceptibilidad conexa y da lugar, también, a importantes diferencias a la hora de calcular el valor numérico de la susceptibilidad total (cuantificadas en un 30 % a temperatura cero, y en hasta un 10 % en la diferencia relativa para su valor térmico sustraído).

El análisis de lo que sucede en el llamado régimen infrarrojo ($\hat{m}<<m_s, M_\pi<<T<<M_{K,\eta}$) es verdaderamente útil para el estudiar los *scalings* de las susceptibilidades con la masa de los quarks ligeros y la temperatura.

El cálculo en el continuo que hemos realizado satisface las predicciones de cálculos anteriores [145] para las partes divergentes de la susceptibilidad conexa y disconexa, y las complementa indicando que la parte finita de $\chi_{\rm con}(T)$ no es nula en el límite de isoespín, lo que nos ha permitido interpretar las propiedades de *scaling* a temperatura finita de la susceptibilidad conexa cerca del límite quiral a través de su relación con la mezcla π^0–η.

Los resultados en el régimen infrarrojo nos permiten afirmar que el comportamiento crítico que se espera en el caso de la parte disconexa de la susceptibildiad escalar sea mucho más acusado que el de la parte conexa. Al hilo de todo lo que hemos dicho, es natural asociar este comportamiento a la naturaleza de cada observable. En efecto, la susceptibilidad conexa puede asociarse con efectos

de ruptura intrínseca a través de las fluctuaciones del parámetro de orden de la ruptura de isoespín, mientras que la disconexa representa una medida de las fluctuaciones del parámetro de orden asociado a la restauración quiral, *vid.* el condensado total de quarks.

Pese a su indudable utilidad formal a la hora de describir los *scalings* de las susceptibilidades —y debido al orden de las correcciones que se desprecian— los cálculos de la investigación que defiendo muestran que los términos dominantes en el régimen infrarrojo no son una buena aproximación numérica en el caso de que se usen masas físicas para los mesones. Es por esto que un análisis sistemático fuera del límite quiral como el que aquí se ha realizado aporta una información especialmente útil al problema.

En la tercera sección del capítulo 2 se amplia el estudio acerca de las susceptibilidades incluyendo el análisis en *ChPT* de la susceptibilidad pseudoescalar, así como su relación con el condensado de quarks y con la susceptibilidad escalar. El estudio conjunto de estos dos correladores lugar a un posible escenario de restauración quiral en *ChPT* manifestado a través de la degeneración de ambas susceptibilidades, lo que resulta respaldado también por nuestros cálculos en *UChPT* y por datos procedentes de simulaciones en el retículo.

A través del análisis del patrón de degeneración de las susceptibilidades escalar y pseudoescalar en el contexto de la Teoría Quiral de Perturbaciones de dos sabores en el límite de isoespín, hemos mostrado la existencia de un posible escenario de restauración de simetría quiral a una temperatura ligeramente inferior $(0{,}9T_C)$ a la temperatura crítica proporcionada por la anulación del condensado de quarks. Debido a que, a bajas energías, es razonable suponer que el comportamiento de estos correladores está saturado por las partículas asociadas a los números cuánticos del canal correspondiente, este comportamiento conduce a un escenario de degeneración de los correladores de dos campos asociados a los compañeros quirales $f_0(500)/\sigma$ y pión.

Además, también hemos comprobado —en *ChPT* a *next-to-leading-order* y a temperatura finita— que la susceptibilidad pseudoescalar es proporcional al condensado de quarks, y tiende a reproducir de modo mucho más parecido el comportamiento *crítico* predicho por las simulaciones en el retículo que el que se obtendría si se asume la saturación del correlador pseudoescalar por el inverso de la parte real de la auto-energía para el pión calculada a través de *ChPT* ($\chi_P \sim 1/M_\pi^2(T)$).

Para comprobar este patrón en un contexto más amplio que el de la Teoría Quiral efectiva, hemos procedido a a través de dos medios distintos. Por un lado, hemos recopilado datos para las masas de apantallamiento en el canal pseudoescalar y el condensado de quarks sustraído, procedentes de simulaciones en el retículo bajo las mismas condiciones [126, 127]. Asumiendo que estas masas de

apantallamiento se comportan —por debajo del valor de temperatura crítico de restauración quiral— como las masas asociadas al polo del correlador pseudoescalar comprobamos que la relación entre la susceptibilidad pseudoescalar y el condensado se cumple de modo satisfactorio también para estos resultados en el retículo.

Este resultado explica también también el rápido crecimiento observado [126] para el cociente $M_P^{sc}(T)/M_P^{sc}(0)$ de las *masas de apantallamiento* asociadas al canal pseudoescalar (puesto que éste es inversamente proporcional al cociente $\langle\bar{q}q\rangle_0/\langle\bar{q}q\rangle_T$); y permite reproducir el escenario de degeneración para las dos susceptibilidades estudiadas. Este enfoque permite además ver que ambas susceptibilidades, a diferencia de lo que sucedía en el cálculo en *ChPT*, permanecen degeneradas incluso para temperaturas mayores a la temperatura crítica en [126].

El segundo método que hemos aplicado consiste en la utilización de *UChPT* y, por tanto, en la implementación de los efectos asociados a las resonancias más ligeras. Asumiendo que la partícula escalar intercambiada en la dispersión de piones a momento nulo (tal y como exige la definición de susceptibilidad) corresponde exclusivamente a la $f_0(500)$, y que su masa queda absolutamente determinada por la parte real del polo térmico del canal escalar —calculado a través del *IAM* a un *loop*—, obtenemos un máximo para la susceptibilidad escalar a una temperatura de 157 MeV, compatible con las predicciones del retículo y que está íntimamente relacionado con el carácter no estrecho de la $\sigma/f_0(500)$.

Para encontrar la degeneración entre las susceptibilidades escalar y pseudoescalar, necesitamos asumir que la relación entre ésta última y el condensado se sigue cumpliendo en la Teoría Unitarizada. Además —debido a que no disponemos de información que nos dé una idea del comportamiento crítico del condensado en el límite quiral— es necesario asumir que la variación térmica del mismo es —a este orden, y tal y como sucede, por ejemplo, a un *loop* en *ChPT*— proporcional al cociente T/M. El resultado es que la intersección entre ambas susceptibilidades se produce unos 20 MeV por encima de la temperatura asociada al máximo de la susceptibilidad escalar unitarizada, aunque en este caso no permanecen iguales por encima de esta temperatura, donde nuestras extrapolaciones son ya demasiado extremas.

Respecto al capítulo 3: hemos calculado, participando del mismo enfoque efectivo que en el resto de esta memoria, las correcciones a la auto-energía de un gas de piones fuera del límite quiral a temperatura finita debidas al intercambio de fotones virtuales. Los resultados para la parte real e imaginaria son finitos, independientes de la escala y dependientes en el tri-momento externo como resultado de la existencia de un sistema de referencia privilegiado solidario con el baño térmico.

Usando, para los cálculos, los mismos valores numéricos que en la publicación

2.1.1, y definiendo la masa del pión a *leading order* como la parte real de la auto-energía en el límite estático (tri-momento externo nulo) hallamos que la masa de los piones cargados y neutros, así como la diferencia entre ellos, sufre pequeñas modificaciones térmicas respecto al valor su temperatura cero. La diferencia de masas electromagnética es suavemente creciente para piones fuera del límite quiral (incluso asumiendo límite quiral intrínseco y conservando correcciones de carga a *nivel árbol*), y llega a ser hasta un 24 % mayor que el valor a temperatura cero para $T \sim 150$ MeV.

Este crecimiento para la diferencia de masas es cualitativamente opuesto al obtenido en otras publicaciones en el límite quiral [168], donde de hecho tiene carácter decreciente con la temperatura. La inclusión de piones masivos da lugar a un escenario más realista que el límite quiral en cuanto a la descripción del gas de piones que se forma en las Colisiones Relativistas de Iones Pesados, debido a que la temperatura del sistema no llega a cumplir nunca la condición $T >> M_\pi$, que determina la región térmica en la que el límite quiral tiene capacidad predictiva.

Una de las conclusiones más importantes de este trabajo ha sido comprobar que el término de apantallamiento de tipo Debye —típico término de revestimiento electromagnético de un escalar— es capaz de oponerse a la tendencia hacia la restauración quiral que se esperaría si la regla de suma (3.1) que conecta la diferencia de masa electromagnética de piones con la diferencia entre las funciones espectrales de los canales vectorial y axial fuera aplicable.

La diferencia de masas, promediada a tri-momentos, aunque indistinguible de la diferencia calculada en el límite estático, experimenta un crecimiento más suave al llegar a los $100 - 150$ MeV, y comienza incluso a decrecer —si se extrapolan los resultados hacia regiones térmicas fuera del alcance predictivo de *ChPT*—, acercándose más rápido al comportamiento esperado en el límite de altas temperaturas, M_π/T, donde el límite quiral proporciona una descripción adecuada.

La parte imaginaria presenta un comportamiento mucho más interesante puesto que nuestros cálculos dan lugar a una nueva contribución absortiva que no ha sido presentada antes a este orden en el contexto de la Teoría Quiral. En efecto, al calcular la parte imaginaria de la auto-energía en el régimen de pequeñas oscilaciones del plasma para piones fuera del límite quiral, encontramos una contribución puramente térmica procedente del diagrama de *photon-exchange*. Esta contribución es lineal en la temperatura, nula para $p \to 0$ y tiende asintóticamente al valor $\gamma(p \to \infty, T) = e^2 T/4\pi$.

Es importante notar que el resultado ha sido obtenido a partir de un cálculo en el *gauge* de Coulomb, para el que sólo los grados de libertad físicos del fotón contribuyen y están, por tanto, en equilibrio térmico. Aunque hemos demostra-

do que la parte imaginaria es invariante bajo cambios de *gauge* covariantes, el resultado para la anchura en estos *gauges* no está bien definido, como ya ha sido descrito en otros trabajos [171,172].

La comparación de la anchura térmica promediada en tri-momentos con la anchura obtenida en *ChPT* al orden siguiente (y procedente exclusivamente de procesos de dispersión en el baño térmico [166]) indica que esta nueva contribución es dominante hasta temperaturas de hasta unos 50 MeV. A partir de esta temperatura la anchura debida a dispersión de piones es manifiestamente mayor, llegando a ser hasta ocho veces mayor a unos 80 MeV.

Esta contribución a la anchura podría inducir correcciones sobre el cálculo de la conductividad eléctrica y las viscosidades de cizalla y volumen. Utilizando los valores unitarizados [166] para los promedios en tri-momentos de la anchura térmica en *ChPT* y usando nuestros números para la anchura electromagnética encontramos diferencias de alrededor de un 10 % para una temperatura de entre 80 y 100 MeV, rango de temperaturas para el que la expansión en el plasma relativista resultante de la Colisión de Iones Pesados cesa (*freeze-out* térmico). Respecto a la variación en los tiempos de *freeze-out* térmico: nuestras estimaciones dan lugar a una diferencia de temperaturas de unos 2 MeV para las distribuciones de piones cargados y neutros.

Asimismo hemos estudiado la validez de la extensión *simplista* fuera del límite quiral y a temperatura finita de la regla de suma $V-A$ que relaciona (en el límite quiral y a temperatura cero) la diferencia de masas electromagnética de los piones con la diferencia entre las funciones espectrales asociadas a los canales vectorial y axial. El resultado al que hemos llegado es que esta regla de suma, *per se*, no es directamente aplicable cuando se consideran piones masivos y efectos de temperatura finita. Sin embargo sí puede modificarse para dar cuenta de estas correcciones a través de la incorporación de los términos a que da lugar el diagrama de *photon exchange* y unas correcciones térmicas multiplicativas para las contribuciones de tipo $V-A$.

El efecto de la consideración de piones masivos contribuye a la amplificación de la diferencia electromagnética de las masas de los piones, por lo que el comportamiento tendente a la restauración quiral que se observaba en el límite quiral queda emborronado. No es posible, por tanto, reconocer un efecto de restauración quiral asociada a la diferencia de masas de los piones cargados y neutros a temperatura finita para piones masivos.

Finalmente, con el fin de comprobar la robustez de los resultados de *ChPT* para la diferencia de auto-energías de los piones cargados y neutros hemos calculado este observable utilizando un modelo de intercambio de resonancias y asumiendo saturados los canales axial y vectorial por la $a_1(1260)$ y la $\rho(770)$, respectivamente. En este contexto encontramos que las contribuciones resonantes

se activan a una temperatura de unos $170 - 200$ MeV y son numéricamente pequeñas comparados con los valores obtenidos mediante *ChPT*. Esto indica que los resultados *model-independent* de la Teoría Quiral son estables frente a la incorporación de resonancias, lo que permite pensar en una validez mayor y más contrastada de los resultados de *ChPT*.

Además, hemos comprobado que las partes imaginarias asociadas a algunos de los diagramas resonantes que contribuyen a la diferencia de auto-energía están exponencialmente suprimidas y son subdominantes frente a la anchura térmica electromagnética que ya calculamos previamente.

Por último: el término $-4Ze^2 g_1(T, M_\pi)$ y el correspondiente a la diferencia $g_1(T, M_\pi^\pm) - g_1(T, M_\pi^0)$, que se obtienen en *ChPT* a partir de diagramas de tipo *tadpole* que involucran piones y que están directamente relacionados con la restauración de la simetría quiral, no pueden conseguirse exclusivamente a partir de usar el modelo de resonancias a *leading order*, lo que pone de manifiesto la inequivalencia de los contajes asociados a la Teoría Quiral de Perturbaciones y al modelo de resonancias, donde de hecho el único contaje que nos ha permitido clasificar formalmente los diagramas se basa en gran N_C.

5

Resumen en inglés

The fundamental aim of this research has been the study of the thermal properties of Goldstone Boson's gases through the effective approach provided by Chiral Perturbation Theory, extended —wherever needed— via unitarization methods and auxiliar models in order to accomodate to their predictions the effect of the inclusion of the lightest resonances in diverse channels.

In the first part of this thesis (chapter 2) we have studied the effects of the inclusion of isospin symmetry breaking terms —both intrinsic and electromagnetic— on the order parameters associated to chiral symmetry restoration, specially on the light quark condensates and on the strange condensate —when considering the non vanishing strangeness sector—.

At zero temperature our results show that comparing the systematic calculation of these effects in $SU(3) - ChPT$ and in the scheme used in [121] —which includes the symmetry breaking via mass terms violating Dashen's Theorem— results into differences of 2 % in the case of light quark condensates, and up to 4 % in the strange one. This shows that, although relatively small, the differences between considering properly all the low energy constants through an effective approach based on the chiral lagrangian is important if one takes into account the precision of the results given in that work [121].

Our assumption of the ferromagnetic-like response hypothesis for the vacuum —in addition to a suitable specification of the splitting prescription between the EM and non-EM parts in the calculation of the quark condensates—

is the origin of the diverse lower bounds we have found for the combination of electromagnetic low energy constants (*EM LECs*) appearing in the calculation of the total quark condensate, both in $SU(2) - ChPT$ and $SU(3) - ChPT$.

We have checked that these bounds are satisfied for each and every value of the relevant *EM LECs* we have found on the specialized literature (obtained by the use of different theoretical tools); and are more restrictive in the case of three flavours than in the two-flavour sector, but also less reliable due to the distortion caused in the chiral series by the presence of the strange quark mass.

The state-of-the-art concerning the low energy constants in the literature is —to the best of our knowledge [130–134]– scarce, specially in the two-flavour sector.

Integrating out the strange quark by means of an expansion in inverse powers of its mass, we have related the combination of low energy constants in both the theory of two and three flavours at the expense of introducing an explicit dependence in terms with Goldstone boson masses. Nevertheless —due to the fact that the separation of the contributions from electromagnetic and non electromagnetic contribution in any observable is always ambiguous [108,131,133,139]— it doesn't exist one unique and general prescription that allows to disentangle— to any order in *ChPT*— the contributions of the *EM LECs* from the *non-EM LECs*.

At finite temperature the total condensate receives —in $SU(2)$ as well as in $SU(3)$— little corrections because of the violation of the isospin simmetry. These give rise to a larger critical temperature, about a 1% more, with respect to the isospin limit one. Although this is a small modification, it is produced in the expected direction, in the sense that it is consistent with the ferromagnetic response hypothesis assumed in the calculation of the bounds relating the *EM LECs* relevant in this calculation.

With respect to the order parameter of the isospin symmetry breaking — related with the vacuum asymmetry— we have shown that it doesn't receive thermal corrections for two-flavour *ChPT*, while in $SU(3) - ChPT$ it suffers from a soft enhancement through a cuadratical dependence in the temperature over the eta mass, *vid.* $(m_u - m_d)\frac{T^2}{M_\eta^2}$. Although these corrections are significant at high enough temperatures, they are controlled by a mass scale much bigger than that caracteristic scale of the chiral symmetry breaking order parameter, $1/F_\pi^2$.

The differences ($\sim 1\%$) between consider or not isospin breaking effects at zero temperature in the light quark condensate and also in the strange one indicate that they can be ignored, since they are small when comparing with the uncertainties associated to lattice calculations [125].

In spite of this, there exist observables for which isospin breaking corrections are important, from a formal point of view as well as regarding a numerical perspective. This is indeed the case of quantities vanishing in the isospin limit like, for example, the isospin breaking order parameter, $<\bar{u}u - \bar{d}d>$, or the vacuum asymmetry defined from the latter and that gives corrections, at zero temperature, that go from 15% up to 24%, depending on which bound —upper or lower— we use for the natural approximation of the *EM LECs* values.

There exist also important modifications to the sum rule [31] relating the ratios $<\bar{d}d>/<\bar{u}u>$ and $<\bar{s}s>/<\bar{u}u>$ —both free of contact terms—, for the electromagnetic breaking effects (calculated in this work for the first time) are formal and numerically sizeable with those of the intrinsic breaking.

This sum rule can be extended in a natural way to finite temperature. Because of the fact that the corrections to the ratio $<\bar{u}u> / <\bar{d}d>$ are important for intermediate temperatures, the modifications to this sum rule are also significant in the very same thermal range (for example, they are of about 20% at $T \sim 100$ MeV, with respect to the zero temperature value) and become formally sizeable to the zero temperature value for larger temperatures —although we are not allowed to extent our *ChPT* calculation in such a manner and these results must be taken as qualitative extrapolations—.

We have also related the electromagnetic corrections to the total quark condensate in the two-flavour theory with the difference $\chi(T)^{SU(2)} - \chi(0)^{SU(2)}$ for the total scalar susceptibility through a sum rule measurable directly in lattice [86, 147]. The qualitative extrapolation of the results provided by this sum rule towards temperatures near the critical restoration value allow to infer an important growth of the effects due to electromagnetic breaking on the condensate, bearing in mind the behaviour supposed for the scalar susceptibility near the transition. For the three-flavour theory it is also possible to conclude that —although the interpretation is not as clear as in the latter case— the corrections to the total condensate are also dominated by the scalar susceptibility. This is due to the thermal suppresion of the strange quark effects by means of Boltzmann exponentials.

This sum rule also connects our results with those obtained via the staggered formalism in lattice calculations. Since the mass of the spureous copies of Goldstone bosons produced there are corrected with the lattice spacing in the same manner as electromagnetic corrections enter at tree level in the mass of the pions and etas in *ChPT*, our sum rule allows to compare our results for the condensates in the continuum with the ones obtained in lattice using staggered actions. Furthermore, the extrapolation of our results indicates that the corrections of taste-breaking effects are susceptible of being enhanced in the neighbourhood of the critical restoration temperature.

The calculation of the chiral scalar susceptibilities to one loop in $SU(3)$–$ChPT$ leads to the obtention of the so-called connected and disconnectes susceptibilities, quantities that —with the total scalar susceptibility— are of common use in lattice simulations.

In this work, we have shown that the consideration of a scenario that includes isospin breaking in a consistent way is fundamental for the obtention of the dominant contributions of the connected and disconnected susceptibilities. These results allow to find their scaling with the light quark mass and the temperature, which turns out to be very important in order to explain certain anomalous behaviours of these quantities when using staggered actions. It is, then, essential to warn about the fact that considering just one flavour could lead to an oversimplified interpretation of the problem. Indeed, assuming just one susceptibility associated to a just one light quark —*i.e.* taking the isospin limit from the very beginning— does not give the dominant contribution for the connected susceptibility and, also, leads to important differences when calculating the numerical value of the total susceptiblity (quantified as a 30 % at zero temperature, and up to a 10 % in the relative difference with respect to its thermal substracted value).

The analysis of the infrared regime ($\hat{m}<<m_s, M_\pi<<T<<M_{K,\eta}$) turns out to be very useful for the study of the scalings of the different susceptibilities with the light quark mass and the temperature.

The continuum calculation we have made satisfies previous predictions [145] for the divergent part of the connected and disconnected susceptibilities in the chiral limit, and complement them with non vanishing meson masses, indicating that the finite part of $\chi_{\text{con}}(T)$ doesn't vanish in the isospin limit. This has allowed us to make an interpretion of its scaling properties at finite temperature and near the chiral limit by means of its relation to the π^0–η mixing.

The results in the infrared regime have allowed us to infer that the critical behaviour we would expect for the disconnected piece of the susceptibility should be more pronounced than that of the connected one. Along these same lines, it is natural to associate this behaviour to the nature of each observable. Indeed, the connected susceptibility measures fluctuations of the order parameter of the isospin symmetry breaking, while the disconnected piece measures the fluctuations of the chiral restoration order parameter, *vid.* the total quark condensate.

In spite of its undoubted formal usefulness when it comes time to describe the scaling of the different susceptibilities, our calculations show that the dominant terms in the infrared regime are not a good numerical approximation when using physical masses for the different mesons due to the order of the corrections

neglected. This is why we think our sistematic analysis out of the chiral limit gives a very useful information about this issue.

In the third section of chapter 2, we have gone in detail about the study of chiral susceptibilities, specially about the scalar —previously defined— and the pseudoscalar ones.

Through the analysis of the degeneration pattern of the latter in the context of two-flavour *ChPT* in the isospin symmetric limit, we have shown the existence of a possible chiral restoration scenario at a temperature slightly lower $(0{,}9T_C)$ than the critical temperature at which the chiral condensate vanishes. At low temperatures and energies, it is reasonable to suppose the behaviour of those correlators to be saturated by the particles with the quantum numbers of the corresponding channel; so this scenario leads to a mass degeneration of the $f_0(500)/\sigma$ and the pion.

Moreover, we have also confirmed that —up to next-to-leading-order *ChPT* , and at finite temperature— the pseudoscalar susceptibility is proportional to the quark condensate, and tends to reproduce lattice critical results in a manner more satisfactory than that consisting in saturating the pseudoscalar correlator by a pion state $(\chi_P \sim 1/M_\pi^2)$.

To check this relation in a wider context, we have proceed in two different ways. First, we have compiled data for screening masses in the pseudoscalar channel and substracted quark condensates from the same lattice calculations [126, 127]. Assuming this screening mass to behave —below the critical restoration temperature— as the pseudoscalar pole mass (and assuming also that this one is saturated by a pion state), we have checked that the relation between the pseudoscalar susceptibility and the quark condensate is well fulfilled also for these lattice data.

This result explains, too, the fast growth observed in the pseudoscalar screening mass quotient $M_P^{sc}(T)/M_P^{sc}(0)$, and allows to reproduce the degeneration scenario for scalar and pseudoscalar susceptibilities. Furthermore, this approach shows that —contrary to what happened in the *ChPT* calculation— both susceptibilities remain degenerated even for temperatures greater than the critical temperature given in [126].

The second way we have choosen to check our results, is the use of *UChPT* and, therefore, the dynamic implementation of the effects associated with the lightest hadron resonances. Assuming the scalar particle exchanged in pion scattering at zero momentum (such as the definition requires) to be the $f_0(500)$, and that its mass is completely fixed by the real part of the thermal pole in the scalar channel calculated via one-loop *IAM*, we have obtained a maximum for the scalar unitarized susceptibility at 157 MeV, completely compatible with the pre-

dictions provided by lattice calculation and essentially due to the non-narrow character of the $f_0(500)/\sigma$.

To find the degeneration pattern in this context, we have to assume that the relation between the pseudoscalar and the scalar susceptibilities is also satisfied in the Unitarized Theory. Furthermore —because we do not have information about the critical behaviour of the quark condensate in the chiral limit— we have to assume, in addition, that the thermal variation of the condensate goes proportional to T/M —which is indeed fulfilled in one-loop $ChPT$—. With these assumptions in mind, the result we get is that the intersection between the susceptibilities occurs at a temperature 20 MeV greater than the temperature associated to the unitarized scalar susceptibility maximum, although in this case they do not remain degenerated above the critical temperature, where our extrapolations are not so reliable.

With respect to the conclusiones of chapter 3: we have calculated, within the same effective approach followed in the previous sections of this memory, the correction to the self-energy of a pion gas out of the chiral limit and at finite temperature due to the exchange of virtual photons with the thermal bath. The results for the real and the imaginary part are all finite, independent of the chiral renormalization scale and do depend on the external tri-momentum as a result of the existence of a special reference frame associated with the thermal bath.

Using, for numerical purposes, the very same numerical values as in publication 2.1.1, and defining the pion mass at leading order as the real part of the self-energy in the static limit, we found that neutral and charged pion masses, as well as the difference between them, suffer from little thermal modifications with respect to their zero temperature value. The difference grows smoothly with temperature for massive pions, being a 24 % greater than the zero temperature value at $T \sim 150$ MeV.

This growing behaviour for the mass difference is qualitatively opposite to that obtained in other chiral-limit calculations [168], where it decreases with temperature. The inclusion of massive pions gives rise to a more realistic scenario than the chiral limit in the context of RHIC, since the temperature of such a system is never reaching the condition $T >> M_\pi$, which determines the thermal region where the chiral limit is supposed to be predictive.

One of the main conclusions of this work has been to check that the Debye-screening-like term for the mass —a typical EM dressing mass of a scalar— is able to face the tendency towards chiral symmetry restoration one would expect if the sum rule (3.1) —connecting the electromagnetic mass difference of pions with the difference of the spectral functions associated with the axial and vector channels— were suitable to be applied also at finite temperature and out the chiral limit.

The tri-momentum-averaged mass diference, although indistinguisable from the difference calculated in the static limit, develops a smoother growth at a temperature of about $100-150$ MeV, and even starts to decrease —if results are extrapolated to thermal regions far away from the predictive power of *ChPT*— , reaching quicker the behaviour expected in the high temperature regime ($M_\pi/T \to 0$), where the chiral limit is believed to be a good description.

The imaginary part presents a much more interesting behaviour since our calculations give rise to a new absortive part, which —to the best of our knowledge— has never been published yet in the context of *ChPT*. Indeed, when calculating the imaginary part of the self-energy in the small oscillations limit of the plasma for pions out of the chiral limit, we find a pure thermal contribution coming from the photon-exchange diagram. This contribution goes like $\sim T$, vanishes for vanishing external pion tri-momentum and goes like $\gamma(p \to \infty) \to {}^{e^2T}/_{4\pi}$, when p goes to infinity.

It is important here to note that our result has been obtained in the Coulomb gauge, in which only the physical degrees of freedom of the photon are taken into account and, therefore, assumed in thermal equilibrium. Although we have demonstrated that this imaginary part is covariant-gauge invariant, the result in these kind of gauges is sometimes ill-defined, as already described in other previous works [171, 172].

The comparation of the thermal width averaged in tri-momenta with respect to the next-to-leading-order width obtained in *ChPT* indicates that this new EM contribution is dominant up to temperatures of about 50 MeV. From there, the width associated with pion scattering in the thermal bath starts to dominate, becoming approximately eight times greater at a temperature of about 80 MeV.

This EM contribution to the thermal width may induce corrections on the calculation of the electrical conductivity and the sehar and bulk viscosities. Using the unitarized values [166] for the tri-momentum averaged thermal widths and our results for the EM width we find differences of about 10 % for a temperature of $80-100$ MeV, thermal range for which the expansion of the relativistic plasma produced in the RHIC ceases (thermal freeze-out). Our estimations also show up thtat a difference of 2 MeV in the thermalisation time (thermal freeze-out temperatures) for charged and neutral pions must be expected.

Moreover, we have studied the validity of the naive extension out of the chiral limite and at finite temperature of the $V-A$ sum rule relating (in the chiral limit and at zero temperature) the electromagnetic mass difference of piones with the difference of the spectral functions associated to the vectorial and axial channels. The result we show is that this sum rule, *per se*, is no longer valid when considering massive pions and must be modificated.

The effect of including massive piones contributes to the enhancement of the electromagnetic mass difference of the pions, so the chiral restoring behaviour we observe in the chiral limit turns out to be smeared. It is not possible, then, to recognize any chiral restoration effect in the charged-neutral pion mass difference at finite temperature when considering massive pions.

We have also used a resonance exchange model coupling the lightest resonances in the axial and vector channels (*i.e.* the a_1 and the ρ, respectively) with photons and pions in order to check if there are important resonant corrections in the regime of applicability of *ChPT*. It is important to stress that all the calculations in this model have been carried out to leading order because of the lack of a numerically reliable counting scheme besides large-N_C-based arguments that allow us to separate formally the different diagrams.

We have found that altough resonant corrections do exist, they activate thermally at a temperature of about $170-200$ MeV and are numerically smaller than the *ChPT* results. The model-independent results provided by *ChPT* are, then, stable with respect to the inclusion of resonances in the sense that there are no important modifications within its applicability thermal range.

Finally, we have checked that the imaginary part associated to some of the resonant diagrams contributing to the mass difference are exponentially suppressed and subdominant with respect to the electromagnetic thermal width calculated before.

Fe de errores y erratas

Se hacen constar las siguientes erratas y errores:

- En la publicación 2.2.1, página 8; donde dice

$$r(T)^{SU(3)} - r(0)^{SU(3)} = 1 + \frac{Ce^2}{F^4}\Big(2g_2(M_{\pi^\pm}, T) + g_2(M_{K^\pm}, T)\Big) + O(e^4),$$

  debe decir

$$r(T)^{SU(3)} - r(0)^{SU(3)} = \frac{Ce^2}{F^4}\Big(2g_2(M_{\pi^\pm}, T) + g_2(M_{K^\pm}, T)\Big) + O(e^4).$$

- En la publicación 3.1.2, página 340, penúltimo párrafo; donde dice

  For the first two ones we get $M^2_{\pi,\text{Tadpoles}} = \frac{\hat{M}^2_{\pi^0}}{2F^2} - 4Ze^2 g1(M^2_{\pi^\pm}, T)$ *and* (...)

  debe decir

  For the first two ones we get $M^2_{\pi,\text{Tadpoles}} = \left(\frac{\hat{M}^2_{\pi^0}}{2F^2} - 4Ze^2\right) g1(M^2_{\pi^\pm}, T)$ *and* (...)

- En la misma publicación 3.1.2, las figuras 4 y 5 no se corresponden con las expresiones analíticas para las masas de los piones cargados y neutros. Estas últimas, no obstante, sí son correctas. Las gráficas correctas pueden encontrarse, por ejemplo, en la figura 2 de [175].

Bibliografía

[1] M. Gell-Mann, *Broken Symmetries*, *Phys. Lett.* **8** (1964) 214.

[2] G. Zweig, *An SU(3) model for strong interaction symmetry and its breaking. Version 1*, .

[3] T. Appelquist and J. Carazzone, *Infrared Singularities and Massive Fields*, *Phys.Rev.* **D11** (1975) 2856.

[4] S. Weinberg, *Nonabelian Gauge Theories of the Strong Interactions*, *Phys.Rev.Lett.* **31** (1973) 494–497.

[5] H. Fritzsch, M. Gell-Mann, and H. Leutwyler, *Advantages of the Color Octet Gluon Picture*, *Phys.Lett.* **B47** (1973) 365–368.

[6] D. Gross and F. Wilczek, *Asymptotically Free Gauge Theories. 1*, *Phys.Rev.* **D8** (1973) 3633–3652.

[7] D. J. Gross and F. Wilczek, *Ultraviolet Behavior of Nonabelian Gauge Theories*, *Phys.Rev.Lett.* **30** (1973) 1343–1346.

[8] H. D. Politzer, *Reliable Perturbative Results for Strong Interactions?*, *Phys.Rev.Lett.* **30** (1973) 1346–1349.

[9] N. Nielsen, *Asymptotic freedom as a spin effect*, *Am.J.Phys.* **49** (1981) 1171.

[10] A. Di Giacomo, *Confinement of color: A Review*, hep-lat/0310023.

[11] A. M. Jaffe and E. Witten, *Quantum Yang-Mills theory*, 2000.

[12] S. R. Coleman and D. J. Gross, *Price of asymptotic freedom*, *Phys.Rev.Lett.* **31** (1973) 851–854.

[13] A. Zee, *Study of the renormalization group for small coupling constants*, *Phys.Rev.* **D7** (1973) 3630–3636.

[14] **Particle Data Group** Collaboration, J. Beringer *et. al.*, *Review of Particle Physics (RPP)*, *Phys.Rev.* **D86** (2012) 010001.

[15] Eidelman, *Review of Particle Physics, 2004-2005. Review of Particle Properties*, *Phys. Lett. B* **592** (2004) 1–5.

[16] S. L. Adler, *Axial vector vertex in spinor electrodynamics*, *Phys.Rev.* **177** (1969) 2426–2438.

[17] S. L. Adler and W. A. Bardeen, *Absence of higher order corrections in the anomalous axial vector divergence equation*, *Phys.Rev.* **182** (1969) 1517–1536.

[18] W. A. Bardeen, *Anomalous Ward identities in spinor field theories*, *Phys.Rev.* **184** (1969) 1848–1857.

[19] J. Bell and R. Jackiw, *A PCAC puzzle: $\pi^0 \to \gamma\gamma$ in the sigma model*, *Nuovo Cim.* **A60** (1969) 47–61.

[20] C. Vafa and E. Witten, *Restrictions on Symmetry Breaking in Vector-Like Gauge Theories*, *Nucl.Phys.* **B234** (1984) 173.

[21] L. Montanet, *The Positive Parity Mesons*, *Rept.Prog.Phys.* **46** (1983) 337.

[22] D. Morgan and M. Pennington, *The scalar meson enigma*, *Nucl.Phys.Proc.Suppl.* **21** (1991) 37–42.

[23] J. Nebreda, J. Pelaez, and G. Rios, *Enhanced non-quark-antiquark and non-glueball Nc behavior of light scalar mesons*, *Phys.Rev.* **D84** (2011) 074003, [arXiv:1107.4200].

[24] Y. Nambu, *Axial vector current conservation in weak interactions*, *Phys.Rev.Lett.* **4** (1960) 380–382.

[25] Y. Nambu and G. Jona-Lasinio, *Dynamical model of elementary particles based on an analogy with superconductivity. II*, *Phys. Rev.* **124** (Oct, 1961) 246–254.

[26] Y. Nambu and G. Jona-Lasinio, *Dynamical model of elementary particles based on an analogy with superconductivity. I*, *Phys. Rev.* **122** (Apr, 1961) 345–358.

[27] J. Goldstone, *Field Theories with Superconductor Solutions*, *Nuovo Cim.* **19** (1961) 154–164.

[28] J. Goldstone, A. Salam, and S. Weinberg, *Broken Symmetries*, *Phys.Rev.* **127** (1962) 965–970.

[29] S. Weinberg, *Phenomenological Lagrangians*, *Physica* **A96** (1979) 327.

[30] J. Gasser and H. Leutwyler, *Chiral Perturbation Theory to One Loop*, *Annals Phys.* **158** (1984) 142.

[31] J. Gasser and H. Leutwyler, *Chiral Perturbation Theory: Expansions in the Mass of the Strange Quark*, *Nucl.Phys.* **B250** (1985) 465.

[32] G. Ecker, J. Gasser, A. Pich, and E. de Rafael, *The Role of Resonances in Chiral Perturbation Theory*, *Nucl.Phys.* **B321** (1989) 311.

[33] H. Leutwyler, *On the foundations of chiral perturbation theory*, *Annals Phys.* **235** (1994) 165–203, [hep-ph/9311274].

[34] M. Knecht and A. Nyffeler, *Resonance estimates of $O(p^6)$ low-energy constants and QCD short distance constraints*, *Eur.Phys.J.* **C21** (2001) 659–678, [hep-ph/0106034].

[35] V. Cirigliano, G. Ecker, M. Eidemuller, R. Kaiser, A. Pich, *et. al.*, *Towards a consistent estimate of the chiral low-energy constants*, *Nucl.Phys.* **B753** (2006) 139–177, [hep-ph/0603205].

[36] M. Golterman and S. Peris, *Relation between low-energy constants and resonance saturation*, *Phys. Rev. D* **74** (Nov, 2006) 096002.

[37] E. D'Hoker and S. Weinberg, *General effective actions*, *Phys. Rev. D* **50** (Nov, 1994) R6050–R6053.

[38] U.-G. Meissner, G. Muller, and S. Steininger, *Virtual photons in SU(2) chiral perturbation theory and electromagnetic corrections to $\pi\pi$ scattering*, *Phys.Lett.* **B406** (1997) 154–160, [hep-ph/9704377].

[39] M. Knecht and R. Urech, *Virtual photons in low-energy $\pi\pi$ scattering*, *Nucl.Phys.* **B519** (1998) 329–360, [hep-ph/9709348].

[40] R. Urech, *Virtual photons in chiral perturbation theory*, *Nucl.Phys.* **B433** (1995) 234–254, [hep-ph/9405341].

[41] H. Neufeld and H. Rupertsberger, *The Electromagnetic interaction in chiral perturbation theory*, *Z.Phys.* **C71** (1996) 131–138, [hep-ph/9506448].

[42] T. N. Truong, *Chiral Perturbation Theory and Final State Theorem*, *Phys.Rev.Lett.* **61** (1988) 2526.

[43] A. Dobado, M. J. Herrero, and T. N. Truong, *Unitarized Chiral Perturbation Theory for Elastic Pion-Pion Scattering*, *Phys.Lett.* **B235** (1990) 134.

[44] A. Dobado and J. Pelaez, *The Inverse amplitude method in chiral perturbation theory*, *Phys.Rev.* **D56** (1997) 3057–3073, [hep-ph/9604416].

[45] J. Oller, E. Oset, and J. Pelaez, *Nonperturbative approach to effective chiral Lagrangians and meson interactions*, *Phys.Rev.Lett.* **80** (1998) 3452–3455, [hep-ph/9803242].

[46] J. Nieves and E. Ruiz Arriola, *Bethe-Salpeter approach for meson meson scattering in chiral perturbation theory*, *Phys.Lett.* **B455** (1999) 30–38, [nucl-th/9807035].

[47] J. Nieves and E. Ruiz Arriola, *Bethe-Salpeter approach for unitarized chiral perturbation theory*, *Nucl.Phys.* **A679** (2000) 57–117, [hep-ph/9907469].

[48] A. Gomez Nicola, J. Nieves, J. Pelaez, and E. Ruiz Arriola, *Improved unitarized heavy baryon chiral perturbation theory for $\pi - N$ scattering*, *Phys.Lett.* **B486** (2000) 77–85, [hep-ph/0006043].

[49] A. Gomez Nicola and J. Pelaez, *Meson meson scattering within one loop chiral perturbation theory and its unitarization*, *Phys.Rev.* **D65** (2002) 054009, [hep-ph/0109056].

[50] A. Dobado, A. Gomez Nicola, F. J. Llanes-Estrada, and J. Pelaez, *Thermal rho and sigma mesons from chiral symmetry and unitarity*, *Phys.Rev.* **C66** (2002) 055201, [hep-ph/0206238].

[51] D. Cabrera, E. Oset, and M. Vicente Vacas, *Chiral approach to the rho meson in nuclear matter*, *Nucl.Phys.* **A705** (2002) 90–118, [nucl-th/0011037].

[52] D. Cabrera, E. Oset, and M. Vicente Vacas, *Evaluation of the $\pi\pi$ scattering amplitude in the σ-channel at finite density*, *Phys.Rev.* **C72** (2005) 025207, [nucl-th/0503014].

[53] L. Tolos, D. Cabrera, and A. Ramos, *Strange mesons in nuclear matter at finite temperature*, *Phys.Rev.* **C78** (2008) 045205, [arXiv:0807.2947].

[54] J. R. Taylor, *Scattering Theory: The quantum Theory on Nonrelativistic Collisions*. Wiley, New York, 1972.

[55] G. Ecker, J. Gasser, H. Leutwyler, A. Pich, and E. de Rafael, *Chiral Lagrangians for Massive Spin 1 Fields*, *Phys.Lett.* **B223** (1989) 425.

[56] S. Weinberg, *Precise relations between the spectra of vector and axial vector mesons*, *Phys.Rev.Lett.* **18** (1967) 507–509.

[57] J. Sakurai, *Theory of strong interactions*, *Annals of Physics* **11** (1960), no. 1 1 – 48.

[58] K. Kawarabayashi and M. Suzuki, *Partially conserved axial vector current and the decays of vector mesons*, *Phys.Rev.Lett.* **16** (1966) 255.

[59] Riazuddin and Fayyazuddin, *Algebra of current components and decay widths of rho and K* mesons*, *Phys.Rev.* **147** (1966) 1071–1073.

[60] J. F. Donoghue, C. Ramirez, and G. Valencia, *The Spectrum of QCD and Chiral Lagrangians of the Strong and Weak Interactions*, *Phys.Rev.* **D39** (1989) 1947.

[61] T. Das, G. S. Guralnik, V. S. Mathur, F. E. Low, and J. E. Young, *Electromagnetic mass difference of pions*, *Phys. Rev. Lett.* **18** (May, 1967) 759–761.

[62] J. Bijnens and J. Prades, *Electromagnetic corrections for pions and kaons: masses and polarizabilities*, *Nuclear Physics B* **490** (1997), no. 1–2 239 – 271.

[63] R. Baur and R. Urech, *Resonance contributions to the electromagnetic low energy constants of chiral perturbation theory*, *Nuclear Physics B* **499** (1997), no. 1–2 319 – 348.

[64] B. Moussallam, *A sum rule approach to the violation of dashen's theorem*, *Nuclear Physics B* **504** (1997), no. 1–2 381 – 414.

[65] B. Ananthanarayan and B. Moussallam, *Four-point correlator constraints on electromagnetic chiral parameters and resonance effective lagrangians*, *Journal of High Energy Physics* **2004** (2004), no. 06 047.

[66] T. Matsubara, *A new approach to quantum-statistical mechanics*, *Progress of Theoretical Physics* **14** (Oct., 1955) 351–378.

[67] N. Landsman and C. van Weert, *Real and Imaginary Time Field Theory at Finite Temperature and Density*, *Phys.Rept.* **145** (1987) 141.

[68] **HotQCD Collaboration** Collaboration, A. Bazavov *et. al.*, *Chiral and deconfinement aspects of the QCD transition*, *Phys. Rev. D* **85** (Mar, 2012) 054503.

[69] Y. Aoki, S. Borsanyi, S. Durr, Z. Fodor, S. Katz, *et. al.*, *QCD transition temperature: Approaching the continuum on the lattice*, *Nucl.Phys.* **A830** (2009) 805C–808C.

[70] P. Gerber and H. Leutwyler, *Hadrons Below the Chiral Phase Transition*, *Nucl.Phys.* **B321** (1989) 387.

[71] T. K. Herbst, M. Mitter, J. M. Pawlowski, B.-J. Schaefer, and R. Stiele, *Exploring the Phase Structure and Thermodynamics of QCD*, arXiv:1401.1735.

[72] K. Yagi, T. Hatsuda, and Y. Miake, *Quark-gluon plasma*, .

[73] C. Pajares, *Deconfinement*, *AIP Conf.Proc.* **892** (2007) 134–142, [hep-ph/0612054].

[74] **PHENIX Collaboration** Collaboration, J. Burward-Hoy, *Source parameters from identified hadron spectra and NBT radii for Au - Au collisions at* $\sqrt{s(NN)} = 200$ *GeV in PHENIX*, *Nucl.Phys.* **A715** (2003) 498–501, [nucl-ex/0210001].

[75] **STAR Collaboration** Collaboration, J. Adams *et. al.*, *Identified particle distributions in pp and Au+Au collisions at* $\sqrt{s(NN)} = 200$ *GeV*, *Phys.Rev.Lett.* **92** (2004) 112301, [nucl-ex/0310004].

[76] **BRAHMS Collaboration** Collaboration, I. Arsene *et. al.*, *Centrality dependent particle production at y=0 and y 1 in Au + Au collisions at* $\sqrt{s(NN)} = 200$ *GeV*, *Phys.Rev.* **C72** (2005) 014908, [nucl-ex/0503010].

[77] B. C. Barrois, *Superconducting quark matter*, *Nuclear Physics B* **129** (1977), no. 3, 390 – 396.

[78] D. Bailin and A. Love, *Superfluidity and superconductivity in relativistic fermion systems*, *Physics Reports* **107** (1984), no. 6 325 – 385.

[79] L. D. McLerran, *The Color glass condensate and small x physics: Four lectures*, *Lect.Notes Phys.* **583** (2002) 291–334, [hep-ph/0104285].

[80] N. Armesto, M. Braun, E. Ferreiro, and C. Pajares, *Percolation approach to quark - gluon plasma and J/ψ suppression*, *Phys.Rev.Lett.* **77** (1996) 3736–3738, [hep-ph/9607239].

[81] J. Albacete, A. Dumitru, and C. Marquet, *The initial state of heavy ion collisions*, *International Journal of Modern Physics A* **28** (2013), no. 11 1340010.

[82] R. D. Pisarski and F. Wilczek, *Remarks on the chiral phase transition in chromodynamics*, *Phys. Rev. D* **29** (Jan, 1984) 338–341.

[83] Y. Aoki, G. Endrodi, Z. Fodor, S. Katz, and K. Szabo, *The Order of the quantum chromodynamics transition predicted by the standard model of particle physics*, *Nature* **443** (2006) 675–678, [hep-lat/0611014].

[84] F. R. Brown, F. P. Butler, H. Chen, N. H. Christ, Z. Dong, W. Schaffer, L. I. Unger, and A. Vaccarino, *On the existence of a phase transition for qcd with three light quarks*, *Phys. Rev. Lett.* **65** (Nov, 1990) 2491–2494.

[85] M. Cheng, N. Christ, S. Datta, J. van der Heide, C. Jung, *et. al.*, *The QCD equation of state with almost physical quark masses*, *Phys.Rev.* **D77** (2008) 014511, [arXiv:0710.0354].

[86] Y. Aoki, S. Borsanyi, S. Durr, Z. Fodor, S. D. Katz, *et. al.*, *The QCD transition temperature: results with physical masses in the continuum limit II.*, *JHEP* **0906** (2009) 088, [arXiv:0903.4155].

[87] J. B. Kogut and L. Susskind, *Hamiltonian Formulation of Wilson's Lattice Gauge Theories*, *Phys.Rev.* **D11** (1975) 395.

[88] H. B. Nielsen and M. Ninomiya, *No Go Theorem for Regularizing Chiral Fermions*, *Phys.Lett.* **B105** (1981) 219.

[89] C. DeTar and U. Heller, *QCD Thermodynamics from the Lattice*, *Eur.Phys.J.* **A41** (2009) 405–437, [arXiv:0905.2949].

[90] R. Narayanan and H. Neuberger, *Chiral fermions on the lattice*, *Phys.Rev.Lett.* **71** (1993) 3251–3254, [hep-lat/9308011].

[91] V. Furman and Y. Shamir, *Axial symmetries in lattice QCD with Kaplan fermions*, *Nucl.Phys.* **B439** (1995) 54–78, [hep-lat/9405004].

[92] W. Lee and S. R. Sharpe, *Partial flavor symmetry restoration for chiral staggered fermions*, *Phys. Rev. D* **60** (Nov, 1999) 114503.

[93] J. I. Kapusta, *Finite-Temperature Field Theory*. Cambridge University Press, Jan., 1994.

[94] M. Le Bellac, *Thermal Field Theory*. Cambridge University Press, 1st.paperback ed., 1996.

[95] R. Kubo, *Statistical-mechanical theory of irreversible processes. I. General theory and simple applications to magnetic and conduction problems*, *Journal of the Physical Society of Japan* **12** (June, 1957) 570–586.

[96] P. C. Martin and J. Schwinger, *Theory of many-particle systems. I*, *Phys. Rev.* **115** (Sep, 1959) 1342–1373.

[97] C. W. Bernard, *Feynman rules for gauge theories at finite temperature*, *Phys. Rev. D* **9** (Jun, 1974) 3312–3320.

[98] D. Fernandez-Fraile and A. Gomez Nicola, *Transport coefficients and resonances for a meson gas in Chiral Perturbation Theory*, *Eur.Phys.J.* **C62** (2009) 37–54, [arXiv:0902.4829].

[99] D. Fernandez-Fraile and A. Gomez Nicola, *The Electrical conductivity of a pion gas*, *Phys.Rev.* **D73** (2006) 045025, [hep-ph/0512283].

[100] D. Fernandez-Fraile and A. Gomez Nicola, *Bulk viscosity and the conformal anomaly in the pion gas*, *Phys.Rev.Lett.* **102** (2009) 121601, [arXiv:0809.4663].

[101] A. Dobado, F. J. Llanes-Estrada, and J. M. Torres-Rincon, *eta/s and phase transitions*, *Phys.Rev.* **D79** (2009) 014002, [arXiv:0803.3275].

[102] A. Dobado and J. Pelaez, *Chiral symmetry and the pion gas virial expansion*, *Phys.Rev.* **D59** (1999) 034004, [hep-ph/9806416].

[103] J. Pelaez, *The SU(2) and SU(3) chiral phase transitions within chiral perturbation theory*, *Phys.Rev.* **D66** (2002) 096007, [hep-ph/0202265].

[104] A. Gomez Nicola, J. Pelaez, and J. Ruiz de Elvira, *Scalar susceptibilities and four-quark condensates in the meson gas within Chiral Perturbation Theory*, *Phys.Rev.* **D87** (2013) 016001, [arXiv:1210.7977].

[105] A. Gomez Nicola, F. J. Llanes-Estrada, and J. Pelaez, *Finite temperature pion scattering to one loop in chiral perturbation theory*, *Phys.Lett.* **B550** (2002) 55–64, [hep-ph/0203134].

[106] R. F. Dashen, *Chiral SU(3) x SU(3) as a symmetry of the strong interactions*, *Phys.Rev.* **183** (1969) 1245–1260.

[107] J. F. Donoghue, B. R. Holstein, and D. Wyler, *Electromagnetic selfenergies of pseudoscalar mesons and Dashen's theorem*, *Phys.Rev.* **D47** (1993) 2089–2097.

[108] J. Bijnens, *Violations of Dashen's theorem*, *Phys.Lett.* **B306** (1993) 343–349, [hep-ph/9302217].

[109] D.-N. Gao, M.-L. Yan, and B.-A. Li, *Electromagnetic mass splittings of π, a_1, K, $K_1(1400)$ and $K^*(892)$*, *Phys.Rev.* **D56** (1997) 4115–4132, [hep-ph/9611297].

[110] J. F. Donoghue and A. F. Perez, *The Electromagnetic mass differences of pions and kaons*, *Phys.Rev.* **D55** (1997) 7075–7092, [hep-ph/9611331].

[111] A. Nehme and P. Talavera, *Isospin breaking corrections to low-energy $\pi - K$ scattering*, *Phys.Rev.* **D65** (2002) 054023, [hep-ph/0107299].

[112] B. Kubis and U.-G. Meissner, *Isospin violation in low-energy charged pion kaon scattering*, *Phys.Lett.* **B529** (2002) 69–76, [hep-ph/0112154].

[113] B. Kubis and U.-G. Meissner, *Isospin violation in pion kaon scattering*, *Nucl.Phys.* **A699** (2002) 709–731, [hep-ph/0107199].

[114] G. Ecker, G. Muller, H. Neufeld, and A. Pich, *$\pi^0 - \eta$ mixing and CP violation*, *Phys.Lett.* **B477** (2000) 88–92, [hep-ph/9912264].

[115] C. Hanhart, B. Kubis, and J. R. Pelaez, *Investigation of $a_0 - f_0$ mixing*, *Phys.Rev.* **D76** (2007) 074028, [arXiv:0707.0262].

[116] A. Nehme, *Virtual photon correction to the $K^+ \to \pi^+\pi^0\pi^0$ decay*, *Phys.Rev.* **D70** (2004) 094025, [hep-ph/0406209].

[117] G. Colangelo, J. Gasser, and A. Rusetsky, *Isospin breaking in K(l4) decays*, *Eur.Phys.J.* **C59** (2009) 777–793, [arXiv:0811.0775].

[118] A. Nehme, *Splitting strong and electromagnetic interactions in K(l4) decays*, *Phys.Rev.* **D69** (2004) 094012, [hep-ph/0402007].

[119] A. Rusetsky, *Isospin symmetry breaking*, *PoS* **CD09** (2009) 071, [arXiv:0910.5151].

[120] G. Amoros, J. Bijnens, and P. Talavera, *K(lepton 4) form-factors and ππ scattering*, *Nucl.Phys.* **B585** (2000) 293–352, [hep-ph/0003258].

[121] G. Amoros, J. Bijnens, and P. Talavera, *QCD isospin breaking in meson masses, decay constants and quark mass ratios*, *Nucl.Phys.* **B602** (2001) 87–108, [hep-ph/0101127].

[122] J. Bijnens and I. Jemos, *A new global fit of the L_i^r at next-to-next-to-leading order in Chiral Perturbation Theory*, *Nucl.Phys.* **B854** (2012) 631–665, [arXiv:1103.5945].

[123] S. Narison, *Light and heavy quark masses, flavor breaking of chiral condensates, meson weak leptonic decay constants in QCD*, hep-ph/0202200.

[124] B. Ioffe, *QCD at low energies*, *Prog.Part.Nucl.Phys.* **56** (2006) 232–277, [hep-ph/0502148].

[125] G. Colangelo, S. Durr, A. Juttner, L. Lellouch, H. Leutwyler, *et. al.*, *Review of lattice results concerning low energy particle physics*, *Eur.Phys.J.* **C71** (2011) 1695, [arXiv:1011.4408].

[126] M. Cheng, S. Datta, A. Francis, J. van der Heide, C. Jung, *et. al.*, *Meson screening masses from lattice QCD with two light and the strange quark*, *Eur.Phys.J.* **C71** (2011) 1564, [arXiv:1010.1216].

[127] A. Bazavov, T. Bhattacharya, M. Cheng, N. Christ, C. DeTar, *et. al.*, *Equation of state and QCD transition at finite temperature*, *Phys.Rev.* **D80** (2009) 014504, [arXiv:0903.4379].

[128] M. Cheng, S. Ejiri, P. Hegde, F. Karsch, O. Kaczmarek, *et. al.*, *Equation of State for physical quark masses*, *Phys.Rev.* **D81** (2010) 054504, [arXiv:0911.2215].

[129] S. Durr, Z. Fodor, C. Hoelbling, S. Krieg, T. Kurth, *et. al.*, *Lattice QCD at the physical point meets SU(2) chiral perturbation theory*, arXiv:1310.3626.

[130] R. Baur and R. Urech, *Resonance contributions to the electromagnetic low-energy constants of chiral perturbation theory*, *Nucl.Phys.* **B499** (1997) 319–348, [hep-ph/9612328].

[131] J. Bijnens and J. Prades, *Electromagnetic corrections for pions and kaons: Masses and polarizabilities*, *Nucl.Phys.* **B490** (1997) 239–271, [hep-ph/9610360].

[132] A. Pinzke, *Estimating the electromagnetic chiral Lagrangian coefficients*, hep-ph/0406107.

[133] B. Moussallam, *A Sum rule approach to the violation of Dashen's theorem*, *Nucl.Phys.* **B504** (1997) 381–414, [hep-ph/9701400].

[134] B. Ananthanarayan and B. Moussallam, *Four-point correlator constraints on electromagnetic chiral parameters and resonance effective Lagrangians*, *JHEP* **0406** (2004) 047, [hep-ph/0405206].

[135] J. Gasser, V. E. Lyubovitskij, A. Rusetsky, and A. Gall, *Decays of the $\pi^+\pi^-$ atom*, *Phys.Rev.* **D64** (2001) 016008, [hep-ph/0103157].

[136] M. Knecht and A. Nehme, *Electromagnetic corrections to charged pion scattering at low-energies*, *Phys.Lett.* **B532** (2002) 55–62, [hep-ph/0201033].

[137] H. Jallouli and H. Sazdjian, *Relativistic effects in the pionium lifetime*, *Phys.Rev.* **D58** (1998) 014011, [hep-ph/9706450].

[138] C. Haefeli, M. A. Ivanov, and M. Schmid, *Electromagnetic low-energy constants in ChPT*, *Eur.Phys.J.* **C53** (2008) 549–557, [arXiv:0710.5432].

[139] J. Gasser, A. Rusetsky, and I. Scimemi, *Electromagnetic corrections in hadronic processes*, *Eur.Phys.J.* **C32** (2003) 97–114, [hep-ph/0305260].

[140] S. Descotes-Genon and J. Stern, *Vacuum fluctuations of $\bar{q}q$ and values of low-energy constants*, *Phys.Lett.* **B488** (2000) 274–282, [hep-ph/0007082].

[141] B. Moussallam, *$N(f)$ dependence of the quark condensate from a chiral sum rule*, *Eur.Phys.J.* **C14** (2000) 111–122, [hep-ph/9909292].

[142] B. Moussallam, *Flavor stability of the chiral vacuum and scalar meson dynamics*, *JHEP* **0008** (2000) 005, [hep-ph/0005245].

[143] R. D. Pisarski and F. Wilczek, *Remarks on the Chiral Phase Transition in Chromodynamics*, *Phys.Rev.* **D29** (1984) 338–341.

[144] **MILC Collaboration** Collaboration, C. Bernard *et. al.*, *QCD thermodynamics with three flavors of improved staggered quarks*, *Phys.Rev.* **D71** (2005) 034504, [hep-lat/0405029].

[145] A. V. Smilga and J. Verbaarschot, *Scalar susceptibility in QCD and the multiflavor Schwinger model*, *Phys.Rev.* **D54** (1996) 1087–1093, [hep-ph/9511471].

[146] A. Juttner and M. Della Morte, *New ideas for $g-2$ on the lattice*, *PoS* **LAT2009** (2009) 143, [arXiv:0910.3755].

[147] **Wuppertal-Budapest Collaboration** Collaboration, S. Borsanyi *et. al.*, *Is there still any T_c mystery in lattice QCD? Results with physical masses in the continuum limit III*, *JHEP* **1009** (2010) 073, [arXiv:1005.3508].

[148] W.-J. Lee and S. R. Sharpe, *Partial flavor symmetry restoration for chiral staggered fermions*, *Phys.Rev.* **D60** (1999) 114503, [hep-lat/9905023].

[149] S. Ejiri, F. Karsch, E. Laermann, C. Miao, S. Mukherjee, *et. al.*, *On the magnetic equation of state in $(2+1)$-flavor QCD*, *Phys.Rev.* **D80** (2009) 094505, [arXiv:0909.5122].

[150] **RBC-Bielefeld Collaboration** Collaboration, W. Unger, *The chiral transition in QCD: On the quark mass dependence of Goldstone fluctuations*, *PoS* **LAT2009** (2009) 180.

[151] T. Hatsuda and T. Kunihiro, *Fluctuation Effects in Hot Quark Matter: Precursors of Chiral Transition at Finite Temperature*, *Phys.Rev.Lett.* **55** (1985) 158–161.

[152] G. Chanfray and M. Ericson, *Critical fluctuations of the quark density in nuclei*, *Eur.Phys.J.* **A16** (2003) 291–297, [nucl-th/0106069].

[153] D. J. Broadhurst, *A Strong Constraint on Chiral Symmetry Breaking at Short Distances*, *Nucl.Phys.* **B85** (1975) 189.

[154] P. Boucaud, J. Leroy, A. L. Yaouanc, J. Micheli, O. Pene, *et. al.*, *Quark pseudoscalar vertex and quark mass function with clover fermions: spontaneous symmetry breaking, OPE, symmetry restoration at small volume*, *Phys.Rev.* **D81** (2010) 094504, [arXiv:0912.3173].

[155] M. Bochicchio, L. Maiani, G. Martinelli, G. C. Rossi, and M. Testa, *Chiral Symmetry on the Lattice with Wilson Fermions*, *Nucl.Phys.* **B262** (1985) 331.

[156] D. Fernandez-Fraile, A. Gomez Nicola, and E. Herruzo, *Pion scattering poles and chiral symmetry restoration*, *Phys.Rev.* **D76** (2007) 085020, [arXiv:0707.1424].

[157] C. Song, *Properties of vector mesons at finite temperature: Effective lagrangian approach*, *Phys. Rev. D* **53** (Apr, 1996) 3962–3966.

[158] C. Song and V. Koch, *Pion electromagnetic form-factor at finite temperature*, *Phys.Rev.* **C54** (1996) 3218–3231, [nucl-th/9608010].

[159] R. Rapp and J. Wambach, *Chiral symmetry restoration and dileptons in relativistic heavy ion collisions*, *Adv.Nucl.Phys.* **25** (2000) 1, [hep-ph/9909229].

[160] A. Andronic, P. Braun-Munzinger, and J. Stachel, *Thermal hadron production in relativistic nuclear collisions: The hadron mass spectrum, the horn, and the QCD phase transition*, *Physics Letters B* **673** (2009), no. 2 142 – 145.

[161] R. Rapp and J. Wambach, *Equation of state of an interacting pion gas with realistic $\pi - \pi$ interactions*, *Phys. Rev. C* **53** (Jun, 1996) 3057–3068.

[162] S. Zschocke and L. P. Csernai, *Pion Mass Shift and the Kinetic Freeze Out Process*, *Eur.Phys.J.* **A39** (2009) 349–363, [arXiv:0901.0499].

[163] D. Fernandez-Fraile and A. Gomez Nicola, *Chemical nonequilibrium for interacting bosons: Applications to the pion gas*, *Phys.Rev.* **D80** (2009) 056003, [arXiv:0903.0982].

[164] M. Kataja and P. Ruuskanen, *Nonzero Chemical Potential and the Shape of the p_T Distribution of Hadrons in Heavy Ion Collisions*, *Phys.Lett.* **B243** (1990) 181–184.

[165] J. Gasser and H. Leutwyler, *Light Quarks at Low Temperatures*, *Phys.Lett.* **B184** (1987) 83.

[166] A. Schenk, *Pion propagation at finite temperature*, *Phys. Rev. D* **47** (Jun, 1993) 5138–5155.

[167] J. Goity and H. Leutwyler, *On the Mean Free Path of Pions in Hot Matter*, *Phys.Lett.* **B228** (1989) 517.

[168] C. Manuel and N. Rius, *The Electromagnetic mass difference of pions at low temperature*, *Phys.Rev.* **D59** (1999) 054002, [hep-ph/9806385].

[169] J. I. Kapusta and V. Visnjic, *$\pi^+\pi^0$ mass difference at finite temperature*, *Phys.Lett.* **B147** (1984) 181.

[170] M. Ladisa, G. Nardulli, and S. Stramaglia, *Cottingham formula and the pion electromagnetic mass difference at finite temperature*, *Physics Letters B* **465** (1999), no. 1–4 241 – 248.

[171] S.-Y. Wang, *Gauge dependence of the fermion quasiparticle poles in hot gauge theories*, *Phys.Rev.* **D70** (2004) 065011, [hep-ph/0406002].

[172] E. Mottola and Z. Szép, *Systematics of high temperature perturbation theory: The two-loop electron self-energy in QED*, *Phys. Rev. D* **81** (Jan, 2010) 025014.

[173] A. Rebhan, *Thermal gauge field theories*, *Lect.Notes Phys.* **583** (2002) 161–208, [hep-ph/0105183].

[174] M. H. Thoma and C. T. Traxler, *Damping rate of a scalar particle in hot scalar QED*, *Phys.Lett.* **B378** (1996) 233–237, [hep-ph/9601254].

[175] R. Torres Andres and A. Gomez Nicola, *Pion masses at finite temperature*, *Proceedings of Science* **ConfinementX** (2012) 190, [arXiv:1303.6328].